

REPUBLIC DU CAMEROUN
Paix-Travail-Patrie

UNIVERSITE DE YAOUNDE I

FACULTE DE MEDECINE ET DES
SCIENCES BIOMEDICALES

CENTRE DE RECHERCHE ET DE
FORMATION DOCTORALE EN
SCIENCE DE LA VIE, SANTE ET
ENVIRONNEMENT

UNITE DE RECHERCHE ET DE
FORMATION DOCTORALE EN
SANTE ET ENVIRONNEMENT



REPUBLIC OF CAMEROON
Peace-Work-Fatherland

THE UNIVERSITY OF YAOUNDE I

FACULTY OF MEDICINE AND
BIOMEDICAL SCIENCES

RESEARCH AND DOCTORAL
TRAINING CENTER IN
LIFE SCIENCE, HEALTH AND
ENVIRONMENT

RESEARCH AND DOCTORAL
TRAINING UNIT IN HEALTH AND
ENVIRONMENT

NEUROSCIENCE LABORATORY (FMBS-UYI)
LABORATOIRE DE NEUROSCIENCES (FMSB-UYI)

Studies on the impact of diet and menopause on the course of cerebral toxoplasmosis and therapeutic potential of *Garcinia kola* (Clusiaceae) in Wistar rats

Thesis presented and publicly defended in partial fulfilment of the requirements for the award
of a PhD in Neuropharmacology

By:

NENE AHIDJO

Pharm-D, MSc in Neuroscience

Matricula: 09M120

DIRECTOR

Pr. NJAMNSHI Alfred K.

Professor of Neurology and Clinical
Neurophysiology/Neuroscience
FMBS, The University of Yaoundé I

CO-DIRECTORS

Pr. NGADJUI TCHALEU Bonaventure

Professor of Organic Chemistry, Faculty of Science,
The University of Yaoundé I

Pr. SEKE ETET Paul F.

Associate Professor of Medical Physiology and
Neuroscience, FMBS, University of Garoua

Academic Year: 2023-2024



LIST OF ADMINISTRATIVE AND ACADEMIC STAFF

(By Department and Rank)

1. ADMINISTRATIVE STAFF

Dean: **Pr Meka née Ngo Um Esther**

Vice- Dean in charge of academic Affairs: **Pr. NTSAMA ESSOMBA Claudine Mireille**

Vice-Dean in charge of Student Affairs and student follow-up: **Pr NGANOU Christ Nadège**

Vice-Dean in charge of Co-operation and Research: **Pr. ZEH Odile Fernande**

Director of Student Affairs, academic affairs and Research: **Dr VOUNDI VOUNDI Esther**

Director of Administrative and Financial affairs: **Mme ESSONO ENFA Muriel G. ép. MBIA**

General Coordinator of Specialization Cycle: **Pr NJAMNSHI Alfred K.**

Chief of Service, Finance: **Mme NGAMALI NGOU Mireille Albertine ép. WAH**

Chief of Service, Finance assistant: **Mme MANDA BANA Marie M. ép. ENGUENE ATANGA**

Chief of Service, Administration and Personnel: **Pr SAMBA Odette NGANO ép. TCHOUAWOU**

Chief of Service, Certificates: **Mrs ASSAKO Anne DOOBA**

Chief of Service, Certificates, Assistant: **Dr NGONO AKAM MARGA Vanina**

Chief of Service, Student Affairs and Statistics: **Mme BIENZA Aline**

Chief of Service, Student Affairs, Assistant: **Mrs FAGNI MBOUOMBO AMINA ép. ONANA.**

Chief of Service; Materials and Maintenance: **Mrs. HAWA OUMAROU**

Chief of Service; Materials, Assistant: **Dr NDONGO née MPONO EMENGUELE**

Interim Librarian-in-chief: **Mrs FROUSSISET née MAME Marie-Claire S**

Stores accountant: **M. MOUMEMIE NJOUNDIYIMOUN MAZOU**

2. COORDINATORS OF SPECIALISATION CYCLES

Coordinator of Dentistry: **Pr. BENGONDO MESSANGA Charles**

Coordinator of Pharmacy: **Pr. NTSAMA ESSOMBA Claudine**

Coordinator of Intern Cycle: **Pr. ONGOLO ZOGO Pierre**

Coordinator of Specialization Cycle of Morbid Anatomy: **Pr. SANDO Zacharie**

Coordinator of Specialization Cycle of Anaesthesiology: **Pr. ZE MINKANDE Jacqueline**

Coordinator of Specialization Cycle of General Surgery: **Pr. NGO NONGA Bernadette**

Coordinator of Specialization Cycle of Gynaecology-Obstetrics: **Pr. DOHBIT Julius SAMA**

Coordinator of Specialization Cycle of Internal medicine: **Pr. NGANDEU Madeleine**

Coordinator of Specialization Cycle of Paediatrics: **Pr. MAH Evelyn MUNGYEH**

Coordinator of Specialization in Clinical Biology: **Pr. KAMGA FOUAMNO Henri Lucien**

Coordinator of Specialization Cycle of Radiology: **Pr. ONGOLO ZOGO Pierre**

Coordinator of Specialization Cycle of Public Health: **Pr. TAKOUGANG Innocent**

Coordinator in charge of continuous training: **Pr. KASIA Jean Marie**

Project focal point: **Pr NGOUPAYO Joseph**

Pedagogic Instructor CESSI : **Pr. ANKOUANE ANDOULO Firmin**

HONORARY DIRECTORS OF CUSS (University Centre for Health Sciences)

Pr. MONEKOSSO Gottlieb (1969-1978)

Pr. EBEN MOUSSI Emmanuel (1978-1983)

Pr. NGU LIFANJI Jacob (1983-1985)

Pr. CARTERET Pierre (1985-1993)

HONORARY DEANS OF FMBS (Faculty of Medicine and Biomedical Sciences)

Pr. SOSSO Maurice Aurélien (1993-1999)

Pr. NDUMBE Peter (1999-2006)

Pr. TETANYE EKOÉ Bonaventure (2006-2012)

Pr. EBANA MVOGO Côme (2012-2015)

Pr. ZE MINKANDE Jacqueline (2015-2024)

3. THE TEACHING STAFF

NAME	GRADE	FIELD
DEPARTMENT OF SURGERY AND SPECIALTIES		
SOSSO Maurice Aurélien (HOD)	P	General Surgery
DJIENTCHEU Vincent de Paul	P	Neurosurgery
ESSOMBA Arthur (Intérim HOD)	P	General Surgery
HANDY EONE Daniel	P	Orthopedic Surgery
MOUAFO TAMBO Faustin	P	Pediatric Surgery
NGO NONGA Bernadette	P	General Surgery
NGOWE NGOWE Marcellin	P	General Surgery
ZE MINKANDE Jacqueline	P	Anesthesiology- Intensive care
BAHEBECK Jean	AP	Orthopedic surgery
BEYIHA Gérard	AP	Anesthesiology- Intensive care
ESIENE Agnès	AP	Anesthesiology- Intensive care
EYENGA Victor Claude	AP	Surgery/Neurosurgery
FARIKOU Ibrahima	AP	Orthopedic surgery
GUIFO Marc Leroy	AP	General Surgery
FOSSI KAMGA Gacelle	AP	Pediatric surgery
OWONO ETOUNDI Paul	AP	Anesthesiology- Intensive care
BANG GUY Aristide	AP	General Surgery
BENGONO BENGONO Roddy Stéphan	AP	Anesthesiology- Intensive care
JEMEA Bonaventure	AP	Anesthesiology- Intensive care
NGO YAMBEN Marie Ange	SL	Orthopedic surgery
AHANDA ASSIGA	SL	General Surgery
AMENGLÉ Albert Ludovic	SL	Anesthesiology- Intensive care
BIWOLE BIWOLE Daniel Claude Patrick	SL	General Surgery
BWELE Georges	SL	General Surgery
FONKOUÉ Loïc	SL	Orthopedic surgery
MBOUCHE Landry Oriole	SL	Urology

MEKEME MEKEME Junior Barthelemy	SL	Urology
TSIAGADIGI Jean Gustave	SL	Orthopedic surgery
SAVOM Eric Patrick	SL	General Surgery
BELLO FIGUIM	SL	Neurosurgery
BIKONO ATANGANA Ernestine Renée	SL	Neurosurgery
EPOUPA NGALLE Frantz Guy	SL	Urology
FOUDA Jean Cedrick	SL	Urology
IROUME C. R. B. ép. NYO'O NKOU MOU	SL	Anesthesiology- Intensive care
KONA NGONDO François Stéphane	SL	Anesthesiology- Intensive care
MOHAMADOU GUEMSE Emmanuel	SL	Orthopedic surgery
MULUEM Olivier Kennedy	SL	Orthopedic/Traumatology
NWAHA MAKON Axel Stéphane	SL	Urology
NDIKONTAR KWINJI Raymond	SL	Anesthesiology- Intensive care
FOLA KOPONG Olivier	L	Surgery
NGOUATNA DJEUMAKOU Serge Rawlings	L	Anesthesiology- Intensive care
NYANIT BOB Dorcas	L	Pediatric surgery
OUMAROU HAMAN NASSOU ROU	L	Neurosurgery
MBELE Richard II	L	Thoracic Surgery
MFOUAPON EWANE Herve Blaise	L	Neurosurgery
NYANKOUE MEBOUINZ Ferdinand	L	Orthopedic Surgery/Traumatology
ARROYE BETOU Fabrice Stéphane	L	Orthopedic /Cardiovascular Surgery

DEPARTMENT OF INTERNAL MEDICINE AND SPECIALTIES

SINGWE Madeleine ép. NGANDEU (HOD)

AFANE ZE Emmanuel	P	Internal Medicine/Rhumatology
ANKOUANE ANDOULO	P	Internal Medicine/Pulmonology
ASHUNTANTANG Gloria Enow	P	Int. Medicine/Hepato-Gastroenterology
BISSEK Anne Cécile	P	Internal Medicine/Nephrology
KAZE FOLEFACK François	P	Internal Medicine/Dermatology
KINGUE Samuel	P	Internal Medicine/Nephrology
KUATE TEGUEU Calixte	P	Internal Medicine/Cardiology
MBANYA Jean Claude	P	Internal Medicine/Nephrology
NDJITOYAP NDAM Elie Claude	P	Internal Medicine/Endocrinology
NDOM Paul	P	Int. Medicine/Hepato-Gastroenterology.
NJAMNSHI Alfred K.	P	Internal Medicine/Oncology
NOUEDOUI Christophe	P	Internal Medicine/Neurology
SINGWE Madeleine ép. NGANDEU	P	Internal Medicine/Endocrinology
SOBNGWI Eugène	P	Internal Medicine/rheumatology
PEFURA YONE Eric Walter	P	Internal Medicine/Endocrinology
HAMADOU BA	P	Internal Medicine/Pulmonology
KOUOTOU Emmanuel Armand	P	Internal Medicine/Cardiology
MENANGA Alain Patrick	AP	Internal Medicine/Dermatology
FOUDA MENYE Hermine Danielle	AP	Internal Medicine/Cardiology
KOWO Mathurin Pierre	AP	Internal Medicine/Nephrology
BOOMBHI Jérôme	AP	Int.Medicine/ Hepato- Gastroenterology
NGANOU Chris Nadège	AP	Internal Medicine/Cardiology
NDONGO AMOUGOU Sylvie	AP	Internal Medicine/Cardiology
KUATE née MFEUKEU KWA Liliane Claudine	AP	Internal Medicine/Cardiology
ATENGUENA OBALEMBA Etienne	SL	Internal Medicine/Medical Cancerology
ETOA NDZIE ép. ETOGA Martine Claude	SL	Internal Medicine/Endocrinology
KAMGA OLEN Jean Pierre Olivier	SL	Internal Medicine/Psychiatry

MBONDA CHIMI Paul-Cédric	SL	Internal Medicine/Nephrology
NDJITOYAP NDAM Antonin Wilson	SL	Int. Medicine/Hepato- Gastroenterology
NTONE ENYIME Félicien	SL	Internal Medicine/Psychiatry
DEHAYEM YEFOU Mesmin	SL	Internal Medicine/Endocrinology
ESSON MAPOKO Berthe S. ép. PAAMBOG	SL	Internal Medicine/Oncology
MAÏMOUNA MAHAMAT	SL	Nephrology
MASSONGO MASSONGO	SL	Internal Medicine/Pulmonology
MENDANE MEKOBE Francine ép. EKOBENA	SL	Internal Medicine/Endocrinology
MINTOM MEDJO Pierre Didier	SL	Internal Medicine/Cardiology
NDOBO ép. KOE Juliette Valérie Danielle	SL	Internal Medicine/Cardiology
NGAH KOMO Elisabeth	SL	Internal Medicine/Pulmonology
NGARKA Léonard	SL	Internal Medicine/Nephrology
NKORO OMBEDE Grâce Anita	SL	Internal Medicine/Dermatology
NTSAMA ESSOMBA Marie Josiane ép. EBODE	SL	Internal Medicine/Geriatrics
NZANA Victorine Bandolo ép. FORKWA M.	SL	Internal Medicine/Nephrology
OWONO NGABEDE Amalia Ariane	SL	Int. Medicine/Interventional Cardiology
ANABA MELINGUI Victor Yves	L	Internal Medicine/Rheumatology
FOJO TALONGONG Baudelaire	L	Internal Medicine/Rheumatology
EBENE MANON Guillaume	L	Internal Medicine/Cardiology
ELIMBY NGANDE Lionel Patrick Joel	L	Internal Medicine/Nephrology
KUABAN Alain	L	Internal Medicine/Pulmonology
NKECK Jan René	L	Internal Medicine/Rhumatology
NSOUNFON ABDOU WOUOLIYOU	L	Internal Medicine/Pneumonology
NTYO’O NKOU莫 MOU Arnaud Laurel	L	Internal Medicine/Pneumonology
TCHOUankeu KOUNGA Fabiola	L	Internal Medicine/Psychaitry

DEPARTMENT OF MEDICAL IMAGING AND RADIOLOGY

ZEH Odile Fernande (HOD)	P	Radiology/Medical Imagery
MOUELLE SONE	P	Radiotherapy
NKO'O AMVENE Samuel	P	Radiology/Medical Imagery
GUEGANG GOUJOU. E.	P	Radiology/Neuroradiology
MOIFO Boniface	P	Radiology/Medical Imagery
ONGOLO ZOGO Pierre	AP	Radiology/Medical Imagery
SAMBA Odette NGANO	AP	Biophysics /Medical Physics
MBEDE Maggy ép. ENDEGUE MANGA	SL	Radiology/Medical Imagery
MEKA'H MAPENYA Ruth-Rosine	SL	Radiotherapy
NWATSOCK Joseph Francis	SL	Radiology/Med. Imagery/Nuclear Med.
SEME ENGOUMOU Ambroise Merci	SL	Radiology/Medical Imagery
ABO’O MELOM Adèle Tatiana	L	Radiology/Medical Imagery

DEPARTMENT OF GYNAECOLOGY AND OBSTETRICS

NGO UM Esther Juliette ép. MEKA (HOD)	AP	Gynaecology/Obstetrics
BELLEY PRISO Eugène	P	Gynaecology/Obstetrics
FOUMANE Pascal	P	Gynaecology/Obstetrics
MBOUDOU Émile	P	Gynaecology/Obstetrics
MBU ENOW Robinson	P	Gynaecology/Obstetrics
NKWABONG Elie	P	Gynaecology/Obstetrics
TEBEU Pierre Marie	P	Gynaecology/Obstetrics
KEMFANG NGOWA J.D.	P	Gynaecology/Obstetrics
DOHBIT Julius SAMA	AP	Gynaecology/Obstetrics
FOUEDJIO Jeanne H.	AP	Gynaecology/Obstetrics
MVE KOH Valère Salomon	AP	Gynaecology/Obstetrics

NOA NDOUA Claude Cyrille	AP	Gynaecology/Obstetrics
BELINGA Etienne	AP	Gynaecology/Obstetrics
ESSIBEN Félix	AP	Gynaecology/Obstetrics
METO GO NTSAMA Junie Annick	SL	Gynaecology/Obstetrics
EBONG Cliford EBONTANE	SL	Gynaecology/Obstetrics
MBOUA BATOUM Véronique Sophie	SL	Gynaecology/Obstetrics
MENDOUA Michèle Florence ép. NKODO	SL	Gynaecology/Obstetrics
NSAHLAI Christiane JIVIR FOMU	SL	Gynaecology/Obstetrics
NYADA Serge Robert	SL	Gynaecology/Obstetrics
TOMPEEN Isidore	SL	Gynaecology/Obstetrics
MPONO EMENGUELE Pascale ép. NDONGO	L	Gynaecology/Obstetrics
NGONO AKAM Marga Vanina	L	Gynaecology/Obstetrics

DEPARTMENT OF OPHTHALMOLOGY/ ENT

DJOMOU François (HOD)	P	ENT
BELLA Assumpta Lucienne	P	Ophthalmology
EBANA MVOGO Côme	P	Ophthalmology
NDJOLO Alexis	P	ENT
NJOCK Richard	P	ENT
OMGBWA EBALE André	P	Ophthalmology
ÉPÉE Émilienne	P	Ophthalmology
KAGMENI Gilles	P	Ophthalmology
BILLONG Yannick	AP	Ophthalmology
DOHVOMA ANDIN Viola	AP	Ophthalmology
EBANA MVOGO Stève Robert	AP	Ophthalmology
KOKI Godefroy	AP	Ophthalmology
MINDJA EKO David	AP	ENT/ Maxilo-facial surgery
NGABA Olive	AP	ENT
ANDJOCK NKOUO Yves Christian	SL	ENT
ASMAOU BOUBA Dalil	SL	ENT
BOLA SIAFA Antoine	SL	ENT
MVILONGO TSIMI ép. BENGONO Caroline	SL	Ophthalmology
AKONO ZOUA ép. ETEME Marie Evodie	SL	Ophthalmology
ATANGA Léonel Christophe	SL	ENT/CFS
MEVA'A BIOUELE Roger Christian	SL	ENT/CFS
MOSSUS Yannick	SL	ENT/CFS
NANFACK NGOUNE Chantal	SL	Ophthalmology
NGO NYEKI Adèle-Rose ép. MOUAHA-BELL	SL	ENT/CFS
NOMO Arlette Francine	SL	Ophthalmology

DEPARTMENT OF PAEDIATRICS

ONGOTSOYI Angèle ép. PONDY (HOD)	P	Paediatrics
KOKI NDOMBO Paul	P	Paediatrics
ABENA OBAMA Marie Thérèse	P	Paediatrics
CHIABI Andreas	P	Paediatrics
CHELO David	P	Paediatrics
NGUEFACK Séraphin	P	Paediatrics
MAH Evelyn	P	Paediatrics
NGUEFACK ép. DONGMO Félicitée	P	Paediatrics
MBASSI AWA	AP	Paediatrics
NGO UM KINJEL Suzanne ép. SAP	AP	Paediatrics

KALLA Ginette Claude ép. MBOPI KEOU	AP	Paediatrics
NOUBI N. ép. KAMGAING M.	SL	Paediatrics
MEKONE NKWELE Isabelle	SL	Paediatrics
EPEE ép. NGOUE Jeannette	SL	Paediatrics
MEGUIEZE Claude-Audrey	SL	Paediatrics
TONY NENGOM Jocelyn	SL	Paediatrics
KAGO TAGUE Daniel Armand	L	Paediatrics

DEPARTMENT OF MICROBIOLOGY, PARASITOLOGY, HAEMATOLOGY AND INFECTIOUS DISEASES

MBOPI KEOU François-Xavier (HOD)	P	Bacteriology/Virology
ADIOGO Dieudonné	P	Bacteriology/Virology
GONSU née KAMGA Hortense	P	Bacteriology
LUMA Henry	P	Bacteriology/Virology
MBANYA Dora	P	Haematology
OKOMO ASSOUMOU Marie Claire	P	Bacteriology/Virology
TAYOU TAGNY Claude	P	Microbiology/Haematology
TOUKAM Michel	AP	Microbiology
LYONGA Emilia ENJEMA	AP	Medical Microbiology
CHETCHA CHEMEGNI Bernard	SL	Microbiology/Haematology
KINGE Thomson NJIE	SL	Infectious Diseases
NDOUMBA NKENGUE Annick ép. MINTYA	SL	Haematology
NGANDO Laure ép. MOUDOUTE	SL	Parasitology
VOUNDI VOUNDI Esther	SL	Virology
BOUM II YAP	SL	Microbiology
ESSOMBA Réné Ghislain	SL	Immunology and Infectious Diseases
MEDI SIKE Christiane Ingrid	SL	Clinical Biology
NGOGANG Marie Paule	SL	Clinical Biology
ANGANDJI TIPANE Prisca ép. ELLA	L	Clinical Biology and Haematology
BEYELA Frédérique	L	Infectious Diseases
Georges MONDINDE IKOMEY	L	Immunology
MBOUYAP Pretty Rosereine	L	Pharmacology

DEPARTMENT OF PUBLIC HEALTH

KAMGNO Joseph (HOD)	P	Public Health /Epidemiology
ESSI Marie Josée	P	Public Health /Medical Anthropology
BEDIANG Georges Wylfred	AP	Medical Information Technology/
NGUEFACK TSAGUE	AP	Public Health
TAKOUGANG Innocent	AP	Public Health
TANYA née NGUTI K. A.	AP	Nutrition
BILLONG Serges Clotaire	SL	Public Health
KEMBE ASSAH Félix	SL	Epidemiology
KWEDI JIPPE Anne Sylvie	SL	Epidemiology
MOSSUS Tatiana née ETOUNOU AKONO	SL	Health promotion
NJOUMEMI ZAKARIAOU	SL	Public Health /Health Economics
EYEBE EYEBE Serge Bertrand	SL	Public Health /Epidemiology
MBA MAADJHOU Berjauline Camille	SL	Public Health /Epidemiology/Nutrition
ABBA-KABIR HAAMIT-M	L	Pharmacy
AMANI ADIDJA	L	Public Health
ESSO ENDALLE Lovet Linda Augustine Julia	L	Public Health

DEPARTMENT OF MORPHOLOGIC-ANATOMOPATHOLOGIC SCIENCES

MENDIMI NKODO Joseph (HOD)	P	Anatomy Pathology
-----------------------------------	---	-------------------

ESSAME OYONO	P	Anatomy Pathology
FEWOU Amadou	P	Anatomy Pathology
SANDO Zacharie	P	Anatomy Pathology
BISSOU MAHOP	AP	Sports Medicine
KABEYENE OKONO Angèle	AP	Histology/Embryology
AKABA Désiré	AP	Human Anatomy
NSEME Eric	AP	Legal Medicine
NGONGANG Gilbert Frank Olivier	SL	Legal Medicine
MENDOUGA MENYE C. R. B. ép. KOUOTOU	SL	Anatomy Pathology
ESSAME Eric Fabrice	L	Anatomy Pathology

DEPARTMENT OF BIOCHEMISTRY

NDONGO EMBOLA ép. TORIMIRO J. (HOD)	P	Molecular Biology
PIEME Constant Anatole	P	Biochemistry
AMA MOOR Vicky Joceline	P	Clinical Biology/Biochemistry
EUSTACE BONGHAN BERINYUY	SL	Biochemistry
GUEWO FOKENG Magellan	SL	Biochemistry
MBONO SAMBA ELOUMBA Esther Astrid	L	Biochemistry

DEPARTMENT OF PHYSIOLOGY

ETOUNDI NGOA Laurent Serges (HOD)	P	Physiology
ASSOMO NDEMBA Peguy Brice	AP	Physiology
David Emery TSALA	AP	Physiology
DZUDIE TAMDJIA Anastase	AP	Physiology
AZABJI KENFACK Marcel	SL	Physiology
EBELL'A DALLE Ernest Remy Hervé	L	Human Physiology

DEPARTMENT OF PHARMACOLOGY AND TRADITIONAL MEDICINE

NGONO MBALLA Rose ABONDO (HOD)	AP	African Pharmaco-therapeutics
NDIKUM Valentine	SL	Pharmacology
ONDOWUA NGUELE Marc Olivier	L	Pharmacology

DEPARTMENT OF ORAL AND MAXILLO-FACIAL SURGERY AND PERIODONTOLOGY

BENGONDO MESSANGA Charles (HOD)	P	Stomatology
NOKAM TAGUEMNE M.E.	SL	Dental medicine
EDOUMA BOHIMBO Jacques Gérard	SL	Surgery / stomatology
LOWE NANTCHOUANG J. M. ép. ABISSEGUE	SL	Paediatric dentistry
Jules Julien NDJOH	SL	Dental Surgery
MBEDE NGA MVONDO Rose	SL	Dental medicine
MENGONG ép. MONEBOULOU Hortense	SL	Paediatric dentistry
BITHA BEYIDI Thècle Rose Claire	L	Maxillo-Facial Surgery
GAMGNE GUIADEM Catherine M	L	Dental Surgery
KWEDI Karl Guy Grégoire	L	Dental Surgery
NKOLO TOLO Francis Daniel	L	Dental Surgery

DEPARTMENT OF PHARMACOGNOSY AND PHARMACEUTICAL CHEMISTRY

NTSAMA ESSOMBA Claudine (HOD)	P	Pharmacognosy /Pharma. Chemistry
NGAMENI Bathélémy	P	Phytochemistry/Organic Chemistry
NGOUPAYO Joseph	P	Phytochemistry/pharmacognosy
GUEDJE Nicole Marie	AP	Ethnopharmacology/Plant Biology
BAYAGA Hervé Narcisse	L	Pharmacy

DEPARTMENT OF PHARMACOTOXICOLOGY AND PHARMACOKINETICS

ZINGUE Stéphane (HOD)	AP	Physiology and Pharmacology
------------------------------	----	-----------------------------

FOKUNANG Charles	P	Molecular Biology
MPONDO MPONDO Emmanuel	P	Pharmacy
TEMBE Estella ép. FOKUNANG	AP	Clinical pharmacology
TABI OMGBA	SL	Pharmacy
NENE AHIDJO ép. NJITUNG TEM	L	Neuro-pharmacology
ANGO Yves Patrick	L	Chemistry of natural substances

DEPARTMENT OF GALENICAL PHARMACY AND PHARMACEUTICAL LEGISLATION

NNANGA NGA Emmanuel (HOD)	P	Galenic Pharmacy
MBOLE Jeanne Mauricette ép. MVONDO M.	SL	Quality Control of Drugs and Food
SOPPO LOBE Charlotte Vanessa	SL	Quality Control of Drugs
NYANGONO NDONGO Martin	SL	Pharmacy
MINYEM NGOMBI Aude Périne ép. AFUH	L	Pharmaceutical Regulations
ABA'A Marthe Dereine	L	Drug Analysis
FOUMANE MANIEPI NGOUOPIHO Jacqueline Saurelle	L	Pharmacology

KEY

HOD = Head of Department / **P**= Professor / **AP**= Associate Professor / **SL**= Senior Lecturer / **L**= Lecturer

TABLE OF CONTENTS

DEDICATION	xii
ACKNOWLEDGEMENTS	xiii
LIST OF ABBREVIATIONS	xv
LIST OF FIGURES.....	xvi
LIST OF TABLES	xix
LIST OF ANNEXES.....	xxi
ABSTRACT	xxii
RÉSUMÉ.....	xxiii
INTRODUCTION.....	1
Research questions	3
Research hypothesis	3
Research objectives	3
CHAPTER I: LITERATURE REVIEW	4
1.1 Description and life cycle of <i>T. gondii</i>	5
1.2 Brain disorders in <i>T. gondii</i> -mediated immunocompetent hosts.....	6
1.2.1 Emerging mechanisms of host resistance to toxoplasmosis.....	6
1.2.2 Infection by <i>T. gondii</i> and neurologic and psychiatric disorders	7
1.2.3 Controversy on the link between <i>T. gondii</i> infection and epilepsy	9
1.2.4 Pathophysiological lessons from epilepsy.....	10
1.3 New insights into the neuroimmunology of <i>T. gondii</i> infection	12
1.3.1 Diet, menopause and the immune response	12
1.3.2 Innate immunity, sleep, motor, cognitive functions.....	13
1.3.3 Adaptive immunity.....	15
1.3.4 Neuronal involvement	17
1.4 Advances in diagnosis, vaccine and drug antitoxoplasmosis development	18
1.4.1 Parasite detection and typing.....	18
1.4.2 Parasite detection for infection staging	18
1.4.3 Parasite typing	19
1.4.4 Vaccine development	20
1.4.5 New drug development	20
1.5 The medicinal plant <i>Garcinia kola</i> Heckel	25
1.6 Plant secondary metabolites	27
1.6.1 Alkaloids	28
1.6.2 Phenolic compounds	29
1.6.3 Terpenes	31
1.7 Treatment of toxoplasmosis	33
1.7.1 Macrolides	33
1.7.2 Folic acid synthesis inhibitors	34

CHAPTER II: MATERIALS AND METHODS	35
2.1 Characteristics of the study	36
2.1.1 Type of study	36
2.1.2 Place of study	36
2.1.3 Study period	36
2.1.4 Animals	36
2.2 Experimental procedures	36
2.2.1 Objective 1 tasks	36
2.2.2 Objective 2 tasks	37
2.2.3 Objective 3 tasks	38
2.3 Plant material processing and phytochemical screening	38
2.3.1 Plant material processing	38
2.3.2 Qualitative phytochemical screening	39
2.3.3 Quantitative phytochemical screening	42
2.4 Ovariectomy	44
2.5 Behavioural tests	44
2.5.1 Open field test (OFT)	44
2.5.2 Elevated plus maze paradigm (EPM)	45
2.5.3 Footprint analysis (FPA)	46
2.6 Histopathological analyses	46
2.6.1 Blood sample processing	46
2.6.2 Tissue processing	47
2.7 Data analysis	51
CHAPTER III: RESULTS	52
3.1 Cognitive disorders associated with chronic <i>T. gondii</i> infection in rats	53
3.1.1 Body weight, temperature, and blood glucose	53
3.1.2 Long-term infection effects on gait	54
3.1.3 Long-term infection effects on organ weight	55
3.1.4 Long-term infection effects on OFT cognitive and motor indicators	56
3.1.5 Long-term infection effects on EPM cognitive and motor indicators	61
3.2 Diet, ovariectomy and <i>T. gondii</i> infection course in rats	67
3.2.1 Physiological parameters and gait	67
3.2.2 OFT changes	75
3.2.3 EPM changes	84
3.2.4 Sex differences in OFT and EPM cognitive indicators	94
3.2.5 Parasite and immune cell count in the blood	104
3.2.6 Brain neuronal density	107
3.3 Phytochemical screening and therapeutic potential of <i>G. kola</i> in infected rats	119
3.3.1 Plant extraction and phytochemical screening	119

3.3.2 Body weight, temperature and blood glucose level	120
3.3.3 Gait quality indicators	122
3.3.4 Organ weight	124
3.3.5 OFT	126
3.3.6 EPM.....	138
3.3.7 Parasite and immune cell count in the blood.....	150
3.3.8 Brain neuronal density.....	152
3.3.9 Histopathological analysis.....	164
3.3.10 Summary of <i>G. kola</i> potential therapeutic activities in neurotoxoplasmosis	167
CHAPTER IV: DISCUSSION	168
4.1 Chronic <i>T. gondii</i> infection in immune-competent rats	169
4.1.1 Physiological parameters.....	169
4.1.2 Motor function indicators.....	169
4.1.3 Cognitive function indicators	170
4.2 Abilities of diet and ovariectomy to accelerate the infection course	171
4.2.1 Physiological parameters.....	172
4.2.2 Cognitive and motor function indicators.....	172
4.2.3 Parasite and WBC count in the blood	173
4.2.4 Brain neuronal density.....	174
4.3 Phytochemical screening and therapeutic potential of <i>G. kola</i>	175
4.3.1 Phytochemical screening of the extracts tested.....	175
4.3.2 Effects of extracts on physiological parameters and gait	176
4.3.3 Effects of extracts on cognitive and motor indicators	176
4.3.4 Effects of extracts on brain, spleen and liver tissues.....	177
CHAPTER V: CONCLUSION AND PERSPECTIVES	178
5.1 Conclusion.....	179
5.2 Perspectives	180
REFERENCES	181
ANNEXES	200

DEDICATION

*To God almighty for His unending love
and grace that has permitted me to be
where I am today in life.*

To my sons and darling husband

ACKNOWLEDGEMENTS

I heartily thank the Lord God almighty for saving and giving me a direction and a reason for living.

Special thanks to:

- Prof Alfred K. Njamnshi, for not only being the director of this work but also being a father, an inspiration and a mentor. From the lower sixth form in secondary school, you gave me an inspiration and I feel honoured to finally become what you had declared over 16 years ago. Without your sacrifice and commitment to see us achieve this work, we would have been nowhere. You introduced me to research, to project writing and so much more. I am forever grateful.
- Prof Ngadjui T. Bonaventure, for accepting to co-direct this work and the inspiration you have been to me since my early years in the school of pharmacy in our faculty. Thanks for your continuous sacrifice in seeing us carry out this work till its end.
- Prof Seke Etet Paul F, for accepting to co-direct this work. Thank you for your immense sacrifice and constant availability in the day- to- day coordination of our work in the laboratory and for being a positive example to us in the domain of research. Thanks for your constant encouragements and support.
- Prof Pr Meka née Ngo Um Esther, current Dean of the Faculty of Medicine and Biomedical Sciences, during the period of my research. Thank you for leading a team of qualified teachers and administrators who taught me throughout my PhD research period.
- My beloved God-sent husband, for his constant financial, moral, spiritual support and for his constant encouragements, I'm for ever grateful to you darling.
- Pr Lorella Seke, for reading through our work and for letting your husband stay out long just to see that our work is completed. Thank you.
- Dr Sanga Dieudonne for his constant encouragements, financial and moral support.
- Mr Kennedy Tetzo for his constant encouragements, financial and moral support.
- My kids, Njitung Caleb Tem Junior and Joshua Njamnshi Njitung Tem, for coping without me at home in their tender age.
- Dr Munang Yvonne, for her constant encouragements, financial and moral support.
- Prof Zingue Stephane for your material support, reading through our work and for encouraging us in doing quality research.

- Dr Ango Yves for reading through our work and for encouraging us to carry the work to its end.
- Dr Nnennaya Nwasike Caroline for reading through our work and for your unconditional care, support and assistance throughout our work. Thanks for being a colleague, sister and friend to me and above all a daughter.
- The members of the Neuroscience Lab, in particular Mr Meka'a Zang Luc Yvan who was constantly present in the lab to help and encourage us carry out our PhD project to the end, and to Dr Wominong Ethel Ndianteng, Kemmo Christelle, Maidawa Frederic, Yonkeu Floriane G., Eyenga Aude L. for their infinite support throughout our PhD project.
- Dr Nzometia Crysantus for his encouragements and unending prayers.
- My entire extended family: my siblings Sanga Dieudonne, Abdoulai Ahidjo, Adamou Ahidjo.
- The leaders of Lead International Chapel, thank you for your prayers and constant encouragements.

LIST OF ABBREVIATIONS

ATCC 40050	Clinically-relevant cytogenic sub-strain of <i>Toxoplasma gondii</i> strain TS-4
CNS	Central nervous system
DCM	Dichloromethane
DPI	Day post-infection
EA	Ethyl acetate
EPM	Elevated plus maze
FMSB	Faculty of Medicine and Biomedical Sciences
FPA	Footprint Analysis
Hex.	Hexane
HFD	High-fat diet
HaE	Haematoxylin and Eosine
IL	Interleukin
INF.	Infected
IP	Intra-peritoneal
LMICs	Low- and middle-income countries
LPD	Low-protein diet
OFT	Open field test
OVX	Ovariectomised
PBS	Phosphate buffer solution
PWE	People with epilepsy
ROS	Reactive oxygen species
SAP	Strech attend posture
WBC	White blood cell
WHO	World health organisation

LIST OF FIGURES

Figure 1. Developmental stages of <i>T. gondii</i>	5
Figure 2. Pathways of transmission of <i>Toxoplasma gondii</i>	6
Figure 3. Pathogenetic interference of <i>T. gondii</i> with the anti-parasite immune response	16
Figure 4. <i>Garcinia kola</i> tree (A) and its seeds (B).	26
Figure 5. Biochemical mechanisms of beneficial properties of <i>G. kola</i> biflavonoids	27
Figure 6. Structure of quinine	28
Figure 7. The different classes of polyphenols	30
Figure 8. Structure of polyphenols	30
Figure 9. Structure of limonene.....	32
Figure 10. Rat in the open field arena	45
Figure 11. Elevated plus maze	46
Figure 12. Method for cell counting in the blood	47
Figure 13. RGB image to obtain a 16-bit image	49
Figure 14. Binary image for automatic counts	50
Figure 15. Body weight, temperature and blood glucose at 90 dpi.....	53
Figure 16. Gait quality indicators in the terminal stage	55
Figure 17. Organ weight relative to body weight in the terminal stage	56
Figure 18. Locomotion and grooming-related parameters in the terminal stage	58
Figure 19. Rearing activities and arena angle time in the terminal stage.....	59
Figure 20. Arena centre and close to wall activities in the terminal stage	61
Figure 21. EPM motor indicators in the terminal stage	62
Figure 22. EPM arm latency and time in the terminal stage	63
Figure 23. Head dipping and rearing in the maze in the terminal stage.....	65
Figure 24. Central platform entries and attend posture in the maze in the terminal stage	66
Figure 25. Body weight, temperature and blood glucose 17 days post-infection	67
Figure 26. Gait quality indicator changes	71
Figure 27. Organ weight relative to body weight at day 17 post-infection.....	73
Figure 28. Locomotion and grooming-related parameters at 17 days post-infection	75
Figure 29. Rearing activities and arena angle time at 17 days post-infection.....	79
Figure 30. Arena centre and close to wall activities at 17 days post-infection	82
Figure 31. EPM motor indicators at 17 days post-infection	85
Figure 32. EPM arm latency and time at 17 days post-infection	88
Figure 33. Head dipping and rearing in the maze at 17 days post-infection.....	90
Figure 34. Centre entries and attend posture in the maze at 17 days post-infection	93

Figure 35. Locomotion and grooming-related parameters of rats fed LPD	95
Figure 36. Arena centre and close to wall activities of rats fed LPD	97
Figure 37. Rearing activities and arena angle time of rats fed LPD	98
Figure 38. EPM motor indicators of rats fed LPD	99
Figure 39. Head dipping and rearing in the maze of rats fed LPD	101
Figure 40. EPM arm latency and time of rats fed LPD	102
Figure 41. Centre entries and attend posture in the maze of rats fed LPD.....	104
Figure 42. Blood smears of representative animals	105
Figure 43. Blood parasite and immune cell counts	105
Figure 44. Micrographs of anterior cingulate cortices of representative animals	107
Figure 45. Micrographs of medial septal nuclei of representative animals.....	108
Figure 46. Average counts in brain anterior areas	109
Figure 47. Micrographs of posterior parietal cortices of representative animals	111
Figure 48. Micrographs of lateral hypothalamic area of representative animals	112
Figure 49. Average counts in brain posterior areas.....	113
Figure 50. Molecular layer of cerebellar cortices of representative animals	115
Figure 51. Micrographs of cerebellar dentate nuclei of representative animals	116
Figure 52. Average counts in cerebellar areas	117
Figure 53. Body weight, temperature and blood glucose after treatment	120
Figure 54. Gait quality indicators after treatment	123
Figure 55. Organ weight relative to body weight after treatment	125
Figure 56. Locomotion and grooming-related parameters after treatment	128
Figure 57. Rearing activities and arena angle time at 17 days post-infection.....	131
Figure 58. Arena centre and close to wall activities after treatment	134
Figure 59. EPM motor indicators after treatment.....	138
Figure 60. EPM arm latency and time after treatment	142
Figure 61. Head dipping and rearing in the maze after treatment.....	146
Figure 62. Centre entries and attend posture in the maze after treatment	149
Figure 63. Blood smears of <i>G. kola</i> -treated representative treated animals.....	151
Figure 64. Blood parasite and immune cell counts of treated animals	151
Figure 65. Anterior cingulate cortices of representative treated animals.....	153
Figure 66. Medial septal nuclei of representative treated animals	154
Figure 67. Average counts in brain anterior areas of treated animals	154
Figure 68. Posterior parietal cortices of representative treated animals.....	156
Figure 69. Lateral hypothalamic area of representative treated animals.....	157
Figure 70. Average counts in brain posterior areas of treated animals	158

Figure 71. Molecular layer of cerebellar cortices of representative treated animals	160
Figure 72. Micrographs of cerebellar dentate nuclei of representative animals	161
Figure 73. Average counts in cerebellar areas	162
Figure 74. Micrographs of H&E stained brain sections.....	164
Figure 75. Micrographs of H&E stained spleen sections.....	166
Figure 76. Micrographs of H&E stained liver sections.....	166
Figure 77. <i>Garcinia kola</i> therapeutic potential against neurotoxoplasmosis	167

LIST OF TABLES

Table I. Emerging therapeutic targets against <i>T. gondii</i> infection	21
Table II. Drugs approved for other diseases recently reported anti- <i>T. gondii</i> activities	23
Table III. Natural products-derived compounds recently reported anti- <i>T. gondii</i> activities.....	24
Table IV. Other compounds recently reported anti- <i>T. gondii</i> activities.....	25
Table V. Taxonomy and classification of <i>G. kola</i>	26
Table VI. Body weight changes in infected rats over 90 days	54
Table VII. Physiological parameter and gait quality indicators changes	56
Table VIII. OFT motor function indicators of infected rats in the terminal stage	57
Table IX. Rearing and arena angle entries in the terminal stage.....	60
Table X. Centre activities and stretched-attend posture in the terminal stage	60
Table XI. EPM motor function indicators of infected rats in the terminal stage	62
Table XII. Arm entry time and latency of infected rats in the terminal stage.....	64
Table XIII. Head dipping and thigmotaxis indicators in the terminal stage	66
Table XIV. Body weight changes in infected rats over 17 days	68
Table XV. Physiological parameter changes in infected rats at 17 dpi.....	69
Table XVI. Gait quality indicator changes.....	72
Table XVII. Inter-group differences in organ weight at 17 dpi	74
Table XVIII. OFT motor function indicators of infected rats at 17 dpi.....	76
Table XIX. Rearing and arena angle entries at 17 dpi	80
Table XX. Centre activities and stretched-attend posture at 17 dpi	83
Table XXI. Motor function indicators of infected rats at 17 dpi.....	86
Table XXII. Arm entry time and latency of infected rats at 17 dpi	89
Table XXIII. Head dipping and thigmotaxis indicators after 17 of infection	91
Table XXIV. Activities around maze central platform at 17 dpi of infection	94
Table XXV. Sex comparisons in OFT indicators of rats fed LPD.....	96
Table XXVI. Sex comparisons of EPM cognitive indicators of rats fed LPD.....	100
Table XXVII. Sex comparisons of EPM arm visits by rats fed LPD.....	103
Table XXVIII. Blood cell count comparisons.....	106
Table XXIX. cell count comparisons in brain anterior areas	110
Table XXX. Cell count comparisons in the brain posterior areas.....	114
Table XXXI. Cell count comparisons in the cerebellar areas	118
Table XXXII. Qualitative analysis of total phenolic content.....	119
Table XXXIII. Results of quantitative phytochemistry	120
Table XXXIV. Body weight changes in infected rats after treatment	121

Table XXXV. Physiological parameter changes after treatment	122
Table XXXVI. Gait quality indicator differences after treatment.....	124
Table XXXVII. Inter-group differences in organ weight after treatment	126
Table XXXVIII. OFT motor function indicators of infected rats after treatment.....	129
Table XXXIX. Rearing and arena angle entries after treatment	132
Table XL. Centre activities and stretched-attend posture after treatment.....	135
Table XLI Motor function indicators of infected rats after treatment.....	140
Table XLII. Arm entry time and latency of infected rats after treatment	144
Table XLIII. Head dipping and thigmotaxis indicators after treatment	147
Table XLIV. Activities around maze central platform after treatment	149
Table XLV. Blood cell count comparisons of treated animals	152
Table XLVI. Brain anterior area cell count comparisons of treated animals.....	155
Table XLVII. Cell count comparisons in the brain posterior areas	159
Table XLVIII. Count comparisons in cerebellar areas of treated rats.....	163

LIST OF ANNEXES

Annex 1: Wistar rats in their cages (source: present work)	201
Annex 2: Preparation of Wistar rats feed (source: present work)	201
Annex 3: Ethological test setting (source: present work)	202
Annex 4: Plant extraction (source: present work)	203
Annex 5: Phytochemical screening (source: present work)	204
Annex 6: Animal treatment by gavage (source: present work).....	205
Annex 7: Rat sacrifice, blood and organ collection (source: present work)	205
Annex 8: Histopathological analysis (source: present work).....	206
Annex 9: Standard curve for flavonoid compounds.....	207
Annex 10: Standard curve for polyphenolic compounds (gallic acid).....	207
Annex 11: Standard curve for total flavanol content (quercetin).....	208
Annex 12: Standard curve for total tannin content	208
Annex 13. Reactant calibration for flavonoid quantification	209
Annex 14. Reactant calibration for flavanol quantification	209
Annex 15. Reactant calibration for polyphenolic compounds' quantification.....	209

ABSTRACT

Background. Epidemiological evidence associates latent *Toxoplasma gondii* infection with the development of neuropsychiatric diseases. Furthermore, physiopathological and environmental factors can alter the host immune response which may appear to play a key role in the disease course.

Rationale. We assessed the cognitive and motor alterations occurring in the late stage of *T. gondii* infection in rats and the occurrence of these alterations in early-stage infected animals exposed to a low-protein diet (LPD), a high-fat diet (HFD) or ovariectomy. We also evaluated the therapeutic potential of *Garcinia kola* in the reversal of these alterations.

Methods. 8-10 weeks old Wistar rats (157.5 ± 4.3 g, N = 72) were obtained in three waves for three series of *in vivo* experiments. In a first series, rats were infected with *T. gondii* (ATCC 40050 strain) and monitored up to the terminal stage of the disease. Open-field test (OFT), elevated plus maze (EPM) behavioural tests and footprint analysis (FPA) were performed to characterize cognitive and motor alterations. In the second series, rats fed on low-protein diet (LPD), high-fat diet (HFD) or ovariectomised rats were infected with *T. gondii* and processed as described before to determine which of these factors could accelerate the infection course in its early stage. In the last series, LPD-fed infected rats were treated for ten days with hexane, dichloromethane and ethyl acetate fractions of the methanolic extract of *Garcinia kola* seeds to assess the therapeutic potential of this medicinal plant against experimental neurotoxoplasmosis. Then, organs of all these animals were processed for histopathological analysis, neurons were counted in brains using stereology and parasites were counted in the blood.

Results. The late-stage infected rats showed significantly decreased body weight and blood glucose levels ($P < 0.05$). Increased body temperature and signs of alterations in cognitive and motor functions including decreased time spent in the central area of the OFT and in the open arms of the EPM compared to the non-infected group. LPD-fed infected animals displayed comparable alterations in the time frame of early-stage infection. Treatment of LPD-fed infected animals with *G. kola* ethyl acetate fraction either improved or prevented these alterations.

Conclusion. Low-protein diet accelerated neurotoxoplasmosis development in *T. gondii* infected rats, suggesting that undernutrition is a potential factor for the development of active toxoplasmosis in non-susceptible immunocompetent animals. *G. kola* ethyl acetate fraction appears to have therapeutic properties against neurotoxoplasmosis. Future studies aimed at developing anti-toxoplasma therapeutics from *G. kola* should be performed using the aqueous extraction of *Garcinia kola* seeds, to avoid eventual toxicity, probably present in organic solvents used in this series of studies.

Keywords: *Toxoplasma gondii*; low protein diet; *Garcinia kola*; cognitive alterations; neuroprotection.

RÉSUMÉ

Contexte : Les données épidémiologiques associent l'infection latente à *Toxoplasma gondii* au développement de maladies neuropsychiatriques. En outre, des facteurs physiopathologiques et environnementaux peuvent altérer la réponse immunitaire de l'hôte, ce qui semble jouer un rôle clé dans l'évolution de la maladie.

Justification de l'étude : Nous avons évalué les altérations cognitives et motrices survenant au stade chronique chez les rats infectés à *T. gondii*, mais aussi l'apparition de ces altérations au stade aigu chez les animaux infectés nourris avec une diète pauvre en protéines (LPD), riche en graisses (HFD) et ovariectomisées. Nous avons également évalué le potentiel thérapeutique de *Garcinia kola* contre ces altérations.

Méthodes : Des rats Wistar âgés de 8 à 10 semaines ($157,5 \pm 4,3$ g, N = 72) ont été inclus dans trois séries d'expériences *in vivo*. Dans la première série, les rats ont été infectés à *T. gondii* (souche ATCC 40050) et suivis jusqu'au stade chronique de la maladie, où des tests comportementaux dont le test de l'arène ouvert (OFT) et le labyrinthe en croix surélevé (EPM) ainsi que des analyses d'empreintes ont été réalisés pour caractériser les altérations cognitives et motrices. Dans la deuxième série, des rats nourris avec un régime pauvre en protéines (RPP), un régime riche en graisses et des rattenas ovariectomisées ont été infectés à *T. gondii* et traités comme décrit précédemment afin de déterminer lequel de ces facteurs pouvait accélérer le mieux l'évolution de l'infection. Dans la dernière série, des rats infectés nourris au RPP ont été traités pendant dix jours avec des fractions d'hexane, de dichlorométhane et d'acétate d'éthyle de l'extrait méthanolique de graines de *Garcinia kola* afin d'évaluer le potentiel thérapeutique de cette plante médicinale contre la neurotoxoplasmose expérimentale. Les organes de tous ces animaux ont ensuite été soumis à des analyses histopathologique, les neurones ont été comptés dans les cerveaux en utilisant la technique de stéréologie et les parasites ont été comptés dans le sang.

Résultats : Les rats infectés à un stade chronique ont présenté une diminution significative de leur poids corporel et de la glycémie ($P < 0,05$), la température corporelle a augmenté et des signes d'altération des fonctions cognitives et motrices ont été observés, notamment une diminution du temps passé dans la zone centrale de l'OFT et dans les bras ouverts de l'EPM par rapport au groupe non infecté. Les animaux infectés nourris au RPP ont présenté des altérations comparables au cours des premiers stades de l'infection. Le traitement des animaux infectés nourris au RPP avec la fraction d'acétate d'éthyle de *G. kola* a amélioré ou empêché ces altérations.

Conclusion : La diète pauvre en protéines a accéléré le développement de la neurotoxoplasmose chez des rats infectés à *T. gondii*, suggérant que la sous-alimentation est un facteur potentiel pour le développement de la toxoplasmose active chez des animaux immunocompétents. La fraction d'acétate d'éthyle de *G. kola* semble avoir des propriétés thérapeutiques contre la neurotoxoplasmose. Des études futures visant à développer des traitements anti-toxoplasmiques à partir de *G. kola* devraient être réalisées en utilisant l'extraction aqueuse moins toxique des graines de *Garcinia kola*.

Mot clé : *Toxoplasma gondii*; *diète pauvre en protéines*; altération cognitives ; *Garcinia kola* ; *neuroprotection*.

INTRODUCTION

The apicomplexan parasite *Toxoplasma gondii* is a serious public health problem in low- and middle-income countries (LMICs) such as Cameroon, partly due to the high burden of HIV/AIDS cases and poverty-related healthcare challenges that heavily affect pregnant women and infants (1, 2). Traditionally, *T. gondii* is known to be problematic in immunocompromised humans. The cat is the definite host, but this ubiquitous intracellular parasite can use a wide range of vertebrates, including humans, domestic and wild animals, as intermediate hosts (3, 4). Thus, the parasite has infected one third of the worlds' population without raising alarms as infections are mostly latent and seem asymptomatic in immunocompetent individuals. For decades, the symptomatic disease induced by *T. gondii* infection was almost uniquely associated with immunodeficiency and pregnancy. Notably, the parasite caused an opportunistic disease in HIV/AIDS patients with common brain involvement as well as neonatal complications such as chorioretinitis, cerebral calcification, hydrocephalus, foetal death in the third trimester of pregnancy, and miscarriage (5-7). With the implementation of corrective policies and scientific progress, the incidence of *T. gondii* affections in HIV/AIDS patients and pregnant women has been decreasing in developed countries (8, 9), but such measures are still needed in LMICs (10, 11).

A growing number of studies have reported links between *T. gondii* infection and the development of various neurologic and psychiatric disorders in immunocompetent individuals and cases of toxoplasmosis in immunocompetent individuals are increasingly reported (12-14). *T. gondii* has developed various strategies to adapt to its host, including the ability to: (i) evade host immune responses, including by hiding in host brain starting from early infection stages; and (ii) to switch between its replicative (tachyzoite) and latent drug-resistant tissue cyst (bradyzoites) (15, 16). The persistence of tachyzoites in neurons and cysts in brains of immunocompetent hosts results in brain tissue responses to parasite antigens, which were associated with behavioural changes in rodents (17-19), and more recently, to the risk for developing neurologic and psychiatric disorders (20-22) and brain tumours in humans (23, 24).

Various physiological and environmental factors able to affect the immune response may have contributed to the global success of *T. gondii* infection, notably: (i) undernutrition, particularly diets low in proteins which are common in low- and middle-income countries and negatively impact the metabolism and functions of immune cells (25, 26); (ii) overnutrition, which is common in high income countries and is associated with a dysregulation of the immune system (27, 28); and (iii) menopause, where aging-associated immune function decline is worsened by oestrogen deprivation (29, 30).

We discuss in this work, the current understanding of the pathogenesis of acquired neurotoxoplasmosis in immunocompetent hosts and the progress in anti-toxoplasmosis vaccine

and drug development, with an emphasis on the potential of *Garcinia kola*, a medicinal plant with reported neuroprotective (31-33) and antimalarial (34, 35) properties.

Research questions

- 1) Can a low-protein diet and menopause favour the development of *T. gondii* infection into a clinically relevant neurotoxoplasmosis in an immunocompetent intermediate host?
- 2) Do *Garcinia kola* extracts have therapeutic properties against the clinically relevant toxoplasmosis developed?

Research hypothesis

A Low-protein diet and menopause favour the development of *T. gondii* infection into a clinically-relevant toxoplasmosis in immunocompetent intermediate host and *G. kola* extracts have a therapeutic potential against neurotoxoplasmosis.

Research objectives

The general objective of this work was to evaluate the therapeutic efficacy of extracts of *Garcinia Kola* on the pathophysiology-pathogenesis of neurotoxoplasmosis.

Specifically, we sought to:

- 1- Evaluate the cognitive disorders associated with chronic *T. gondii* infection in the immune-competent and non-susceptible rat strain Wistar;
- 2- Assess the abilities of a low-protein (LPD) diet, a high-fat diet (HFD) and ovariectomy to accelerate *T. gondii* infection course in Wistar rats;
- 3- Perform a phytochemical study of *G. kola* extracts and use this to assess its therapeutic potential in *T. gondii*-infected rats fed LPD.

CHAPTER I: LITERATURE REVIEW

1.1 Description and life cycle of *T. gondii*

In 1908 parasitologists Charles Jules Henry Nicolle and Luis Herbert Manceaux isolated the *Toxoplasma* parasitic protozoan (tachyzoites) from the tissues of the North African rodent *Ctenodactylus gondii*. They then named it using the Greek words *toxo* ("arc") and *plasma* ("essence") referring to the arched shape of the vegetative form of this parasite and the Latin name of the host where it was isolated (36). *T. gondii* is an obligate intracellular protozoan parasite that belongs to the phylum Apicomplexa, which consists of intracellular parasites that have a characteristically polarized cell structure and a complex cytoskeletal and organelar arrangement at their apical end. This ubiquitous and cosmopolitan parasite can infect a variety of mammals and bird species worldwide (3). *T. gondii* infects hosts that are aquatic, terrestrial mammals and birds which are all intermediate hosts since only the asexual reproductive phases occur in them, while the sexual phase occurs only in the members of the family Felidae (domestic cat, leopard, lion, tiger, cheetah, puma...) that are the definite host (3, 36).

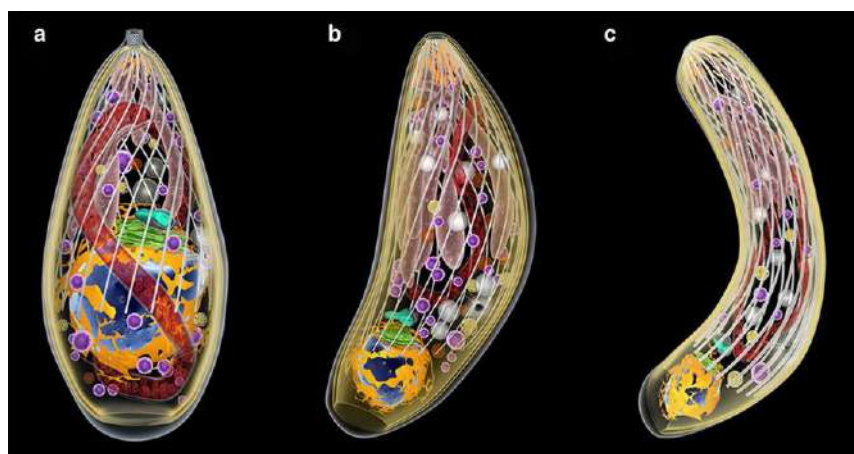


Figure 1. Developmental stages of *T. gondii*

Tachyzoite (a), bradyzoite (b), and sporozoite (c). Source: (3).

The *T. gondii* life cycle has three different developmental stages and all have the potential to infect cells (37):

- The tachyzoites, which cause an acute infection, and have a rapid multiplication rate;
- The bradyzoites, which cause a chronic infection, are the tissue cyst form and are characterized by a slow multiplication rate; and
- The sporozoites, which cause a latent infection, are produced in the definitive host cells during the sexual reproduction phase. Unlike tachyzoites and bradyzoites, they undergo asexual development in the intermediate host cells (3).

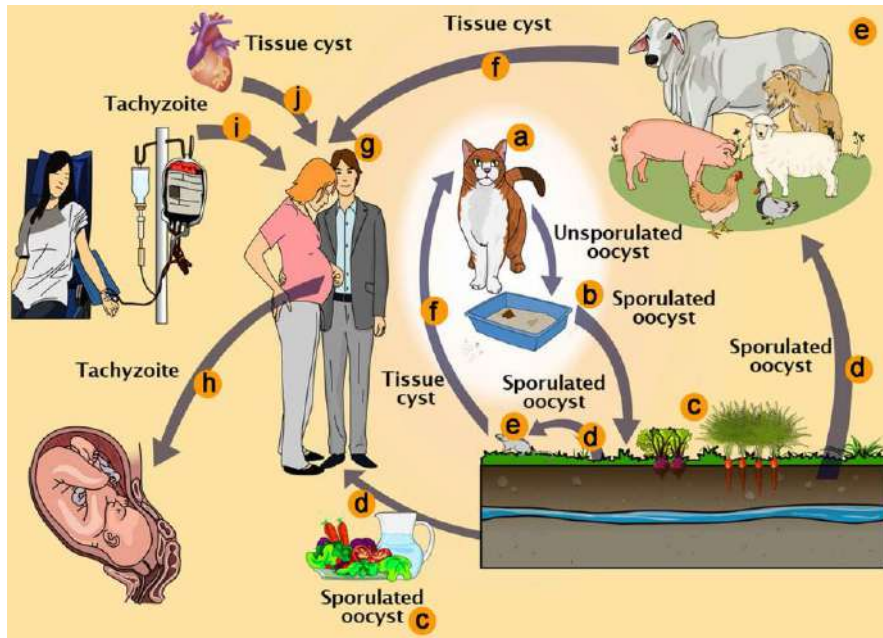


Figure 2. Pathways of transmission of *Toxoplasma gondii*

Definitive hosts, felines (a) emit unsporulated oocysts in their faeces (b) that become sporulated in the environment and contaminate water and raw vegetables (c), which will be ingested during their meal (d) by intermediate hosts (e.g. humans, cattle, sheep, poultry, and swine). (e) Cats ingest tissue cysts by eating raw contaminated meat (f). Furthermore, in humans (g) tachyzoite transmission may through the placenta (h), by blood transfusion (i) and organ transplant (j). Source: (3).

1.2 Brain disorders in *T. gondii*-mediated immunocompetent hosts

1.2.1 Emerging mechanisms of host resistance to toxoplasmosis

Toxoplasma gondii causes neurotoxoplasmosis or cerebral toxoplasmosis, a focal central nervous system (CNS) disease with intracranial lesions, nonspecific neurological deficits including epilepsy, delirium, ocular abnormalities, Wernicke encephalopathy, focal dystonia, facial paralysis, hemiparesis, and monoplegia in HIV/AIDS patients and susceptible immunocompetent individuals (6, 7, 38). Mechanisms through which *T. gondii*, an agent of opportunistic disease, can affect immunocompetent individuals are puzzling. Many investigators to date are addressing the puzzle on what confers resistance to toxoplasmosis in non-susceptible immunocompetent hosts, to unravel predictors of individual resistance (39). Many of these studies were performed in susceptible immunocompetent murine model, where *T. gondii* hypervirulence seems to parallel human infection (40). For example, RNA sequencing analysis of the *T. gondii*-resistant Lewis (LEW) rat versus the infection-susceptible Brown Norway (BN) rat revealed higher transcript levels of cytochrome enzymes such as Cyp2d3, Cyp2d5, and Cybrd1, and higher levels of reactive oxygen species (ROS) in LEW rat, suggesting a role for oxidative stress level in LEW resistance to toxoplasmosis (41). At the same time, *T. gondii* type 3 facilitates its growth and survival in unstimulated human fibroblasts

and murine macrophages through Rhopty Protein 16 (ROP16) -mediated activation of STAT6, which suppresses host cell ROS production (42). Other mechanisms of resistance of the LEW rat to *T. gondii* were reported, including a bone marrow-derived cells-dependent mechanism partially abrogated by neutralization of endogenous interferon-gamma (IFN- γ) (43) and a small GTPase Immunity-Associated Proteins (GIMAPs) -based mechanism (44). This corroborates the observation that host cells lacking the Immunity-Related GTPases (IRGs) family of molecules (Irgm1, Irgm2, and Irgm3), key elements of the resistance system for immunity against pathogens in mouse, do not have cell-autonomous immunity to *T. gondii*, as they fail to load IFN- γ -inducible guanylate-binding proteins (Gbps), and to recruit ubiquitin-binding proteins and ubiquitin ligases, thus, to prompt parasitophorous vacuole lysis and subsequent parasite destruction (45).

Intriguingly, Lee and colleagues (2019) reported that *T. gondii* infection was prevented by previous infection with the apicomplexan parasite *Plasmodium berghei* (ANKA) with which it shares 33% of amino acid sequences of inner membrane complex. Body weight loss was observed as well as reduced number and size of *T. gondii* cysts in brains of mice (34). This finding suggests that infections with other apicomplexan parasites such as malaria causative agents may confer *T. gondii* infection resistance to mice. This raises the question of the impact of *T. gondii* and *Plasmodium* spp. co-infections in humans and indicates that studies evaluating the molecular mechanisms of interactions between these parasites may unravel ways to reduce or abrogate *T. gondii* virulence. Moreover, a study assessing the role of P2X7 in murine cerebral toxoplasmosis, a purinergic receptor that protects against *Plasmodium chabaudi* malaria (46), revealed that: (i) P2X7 signalling would confer resistance to cerebral toxoplasmosis through various inflammatory events, such as the promotion of inflammatory infiltrates and of the production of ROS (Reactive oxygen species) and proinflammatory cytokines in the brain; and that (ii) disruptions of P2X7 signalling resulting in increased susceptibility to the disease (47).

1.2.2 Infection by *T. gondii* and neurologic and psychiatric disorders

The causal relationship between *T. gondii* infection and neuropsychiatric disorders in immunocompetent humans was proposed but is still debated, while data from experimentally-infected immunocompetent animals and *in vitro* studies using human brain cells seem to support such a link. For instance, *T. gondii* can induce the downregulation of the central noradrenergic system in chronically infected rodents, with altered noradrenergic-associated behaviours of sociability and arousal, through downregulation of the expression of dopamine β -hydroxylase (DBH) gene, which encodes the enzyme that synthesizes noradrenaline from dopamine (48). The study of the metabolomic signature of mouse cerebral cortex following *T.*

gondii infection supported the parasite ability to cause brain metabolism dysregulations able to fuel neurobehavioural and neuropathologic changes, such as upregulations of metabolites of the unsaturated fatty acid biosynthesis pathway, promoting parasite growth and survival, and downregulation of metabolites of steroid arachidonic acid metabolism and hormone biosynthesis pathways (18). In addition, *T. gondii* Chinese I genotype Wh6 strain infection induced a neurofibrillary pathology through a GSK3 β -dependent mechanism causing tau phosphorylation and hippocampal neuron apoptosis (49) and circular RNA expression alterations comparable with changes observed in neurodegenerative disorders were reported in mouse brain during cerebral toxoplasmosis development (50).

Interestingly, emerging data support a relative association of Alzheimer's disease with toxoplasmosis, due to the increase in amyloid- β (A β) peptide production in brain areas involved in memory processing, together with increased neuroinflammation and neurotransmitter imbalance in infected animals (51, 52). New evidence has been also provided by studies addressing the impact of *T. gondii* infection on brain extracellular matrix. A study in chronically infected mice demonstrated that cerebral toxoplasmosis leads to neurochemical alterations of perineuronal nets, specialized extracellular matrix structures accounting for synaptic stabilization, possibly resulting from the persistence of tissue cysts and subsequent activation of immune response in the host brains. Intriguingly, such alterations in the brain of *T. gondii*-infected hosts, are observed concomitantly with changes in host behaviour and other neuropsychiatric signs (19). The parasite may also fuel neuropsychiatric disorders through sleep-wake alterations, mainly persistently reduced sleep and increased wakefulness (20). Likewise, maternal exposure to *T. gondii* infection during pregnancy may increase offspring risk for mood disorders (21), which may be part of the strategy of the parasite to enhance dissemination through host predation. Notably, an early study suggesting a potential link between recurrent headaches and cerebral toxoplasmosis reported behavioural disturbances, attention deficit, and ocular and motor disorders in toxoplasmosis paediatric patients (53). However, only susceptible animal strains or "genetically vulnerable animals" would develop marked behavioural alterations (54), explaining at least partly the discrepancy in the literature on the occurrence and types of behavioural alterations induced by *T. gondii* infection in rodents.

Futhermore, a study evaluating the association between *T. gondii* infection and schizophrenia reported anti-*T. gondii* IgG in 25 schizophrenic patients (55.6%) against 13 normal healthy controls (28.9%), and increased serum dopamine level among schizophrenic patients (22), suggesting that chronic *T. gondii* infection causes high dopamine levels that may contribute to the development of schizophrenia. Also supporting *T. gondii* pathogenic involvement in schizophrenia and bipolar disorder, chronic infection of C57Bl/6 mice with the

T. gondii cystogenic strain ME-49 resulted in impaired startle reflex and reduced glutamate and D-serine levels in prefrontal cortical and hippocampal tissue homogenates suggestive of glutamate and D-serine imbalance (17). Similarly, a study evaluating the specific response of primary brain cells to long-term *T. gondii* infection revealed strong disruptions of GABA and glutamatergic signalling pathways, including schizophrenia-like downregulation of both metabotropic and ionotropic glutamate receptors (55). These observations in animals and in *vitro* strongly support a link between *T. gondii* infection and the development of neuropsychiatric disorders. However, they are only indicative for human disease, considering notably, the implications on the reliability of animal models which emerge from studies in patients supporting that: (i) certain strains of *T. gondii* infection induce an inflammation which can be neuroprotective in the context of a secondary insult like stroke or beta-amyloid accumulation (56); and that (ii) aging is associated with *T. gondii* clearance, resolution of neuroinflammation, and reduction of consequences to learning and memory (57).

1.2.3 Controversy on the link between *T. gondii* infection and epilepsy

Epilepsy is among the most common brain disorders in the world, but has no distinguishable cause in about 60% of patients. The suspicion that *T. gondii* may play a potential role as a causative agent, is built on the consideration that it is a neurotropic pathogen which has infected one-third of the world's population. Recent evidence has shown that *T. gondii* is the main cause of cerebral encephalitis and brain abscesses in immunodeficient patients (5, 58). Controversy on the link between *T. gondii* infection and epilepsy mainly emerged from epidemiological studies. Supporting this link, an early meta-analysis of case-controlled studies reported a strong association between seroprevalence rates for toxoplasmosis and prevalence rates of epilepsy (59). A serological investigation on *T. gondii* infection in China revealed a higher infection rate in immunocompetent patients with unknown CNS diseases (19.81%, N = 207 patients) than in healthy participants (5.42%, N = 203 healthy participants) (60). In two comparable studies performed in Egypt, anti-*Toxoplasma* IgG seropositivity was observed: (i) in 34.7% of cases with cryptogenic epilepsy, 2.5% of cases with non-cryptogenic epilepsy, and in 20.3% of depression patients, against only 11.7% among healthy controls (61); and (ii) more in children with cryptogenic epilepsy (20%) than in healthy children (0%) (62).

On the other hand, in a few other studies, anti-*T. gondii* IgG seroprevalences were comparable between people with epilepsy (PWE) and healthy individuals. For instance, a study in Iran reported anti-*T. gondii* IgG seroprevalences of 35.3 % in people with epilepsy (N = 414), 34.7 % in non-epileptic patients with other neurologic disorders (N = 150), and 38.1 % in healthy individuals (N = 63) (63). Similar results were reported from a study performed in

Turkey with 100 cryptogenic epilepsy patients and 50 healthy participants (64). However, key methodological aspects of the latter study were questioned, notably the small sample size that failed to provide statistical power to show inter-group differences (65). Meta-analysis of data from prospective and experimental studies also underlined the need for large studies (66-68). Sadeghi and colleagues (2019) found only 16 eligible studies for their meta-analysis, with a total of 7897 participants of which 3771 epileptic patients and 4026 healthy individuals. These authors hypothesized that the link between chronic *T. gondii* infection and cryptogenic epilepsy may remain controversial due the limited number of studies available and a lack of high-quality data, raising the need for more and better studies (68).

In addition, latent *T. gondii* infection could be linked with specific types of epilepsy. In a matched case-control study performed in a public hospital in northern Mexico, no link was observed between infection and epilepsy as a whole, while instead, there was a strong association between IgG seropositivity to *T. gondii* and ICD-10-CM Diagnosis Code G40.1 (“Localization-related (focal) (partial) symptomatic epilepsy and epileptic syndromes with simple partial seizures”) (69). These findings sustain that *T. gondii* infection is a causative agent of at least specific types of epilepsy and partly explain the origin of the controversy, as inter-study discrepancies may actually only reflect differences in the more common types of epilepsy in the cohorts of patients considered. Future studies assessing the concomitant occurrences of *T. gondii* infections in the different subtypes of other neuropsychiatric disorders are needed, as they may also provide insights into the origin of controversy on the causative role of *T. gondii* infections in these diseases.

1.2.4 Pathophysiological lessons from epilepsy

In a comprehensive system analysis of infected brains in congenital toxoplasmosis patients, Ngô and colleagues (2017) provided strong mechanistic evidence on *T. gondii* infection and epileptogenesis (70). In this study, *T. gondii* modulated the transcriptomes and proteomes of stem cells isolated and expanded from human hippocampus following temporal lobectomy for intractable epilepsy. Susceptibility genes expressed in brains of persons with congenital toxoplasmosis and their families were identified, namely *ABCA4*, *ALOX12*, *COL2A1*, *ERAP 1*, *HLA Class I and II*, *IRAK4*, *P2RX7*, *NALP1* genes. Correlations between *T. gondii* infection and top-ranked canonical signalling pathways’ genes of neurological diseases were found, including brain malignancy (1,188 genes), movement disorders (162 genes), Alzheimer’s disease (101 genes), and epilepsy (81 genes), supporting the ability of the parasite to modulate the genes involved in the pathogenic processes of these diseases. Network analysis of protein-protein interactions revealed parasite’s ability to hijack the cell cycle, cell motility and migration, ATP production by mitochondrial oxidative phosphorylation, lipid metabolism,

protein synthesis, and olfactory response in the host brain. Moreover, *T. gondii* affected the cell cycle and the protein degradation, and serum biomarkers reflected the severity of the infection and of the neuronal damage in congenitally infected children displaying epilepsy and motor abnormalities (70). Other studies confirmed these findings (71, 72), providing mechanistic insights on how *T. gondii* may cause neuropsychiatric diseases, as well as a substantial number of biologically relevant mechanisms to investigate for unravelling new therapeutic targets for cerebral toxoplasmosis.

Furthermore, recent studies in animal models reported that *T. gondii* hijacking of some neurotransmitters' signalling is part of the pathogenic mechanisms leading to neuropsychiatric diseases, including cryptogenic epilepsy. For instance, cannabinoid signalling, which is normally activated following brain insults to protect neurons from the deleterious effects of neuroinflammation and excitotoxicity is hijacked during cerebral toxoplasmosis, resulting in proconvulsant effects (73, 74). Agonists of cannabinoid CB1 and CB2 receptors, which are well-known neurotransmitter modulators involved in epilepsy, inhibited the proconvulsant effect of toxoplasmosis, while their antagonists intensified these effects in immunocompetent mice experimentally infected with *T. gondii* (74). In another study in the same model, disturbances of cannabinoid signalling pathways were observed, including the modulation of mRNA expressions of cannabinoid receptor-1, monoacylglycerol lipase, and diacylglycerol lipase in brains of infected animals (73). In addition, a study in mice experimentally infected with *T. gondii* reported the ability of antagonists of dopamine D1 and D2 receptors to inhibit proconvulsant effects of toxoplasmosis, suggesting that dopaminergic neurotransmission participate in *T. gondii* proconvulsant effect (75). Also supporting this hypothesis, a more recent study showed that *T. gondii* tachyzoites use their tyrosine hydroxylase to hijack the dopaminergic neurotransmission in the host brain (76). Interestingly, still in this study, *T. gondii* tachyzoites tyrosine hydroxylase showed a potent antigenic activity with increases in IgG1, IgG2a, but also IFN- γ , IL-4, and IL17 during animal challenge experiments, pointing out the potential of *T. gondii* tyrosine hydroxylase as a vaccine candidate antigen to mediate cell-mediated and humoral immunity.

Moreover, both acute or chronic *T. gondii* infections can accelerate the acquisition of epilepsy in rats undergoing pentylenetetrazole-induced kindling (77); speech disorders appeared after epileptic seizures, resulting later in full extent Landau-Kleffner syndrome, in immunocompetent children infected with *T. gondii* (78, 79); and a 15 year old immunocompetent traveller returning from Africa with an acute infection with *T. gondii* presented with lymphadenopathy and recurrent seizures (80). Notably, various authors proposed that Sub-Saharan Africa has a higher prevalence of epilepsy than other parts of the

world partly due to exposure to multiple parasites with epileptogenic potential, such as *Plasmodium falciparum*, *Onchocerca volvulus*, *Taenia solium*, *Toxocara canis*, and *T. gondii* (81-84). Persistent *T. gondii* infection can dampen the distribution of GABA synthesis enzyme glutamic acid decarboxylase 67 (GAD67) and induce microglia-neuron deleterious interactions resulting in the loss of perisomatic inhibitory synapses (85), which could contribute to pathogenic processes of neuropsychiatric diseases in general, and epilepsy in particular.

1.3 New insights into the neuroimmunology of *T. gondii* infection

1.3.1 Diet, menopause and the immune response

Environmental factors such as diet are linked to the immune response by the fact that changes in nutritional status impact immune cell metabolism and function (25, 26). It is now widely accepted that immune cell function determines the cellular metabolic state and that, conversely, alterations in cellular metabolism influence immune cell function (27, 28). Nonetheless, although the effects of whole organism nutritional or systemic metabolism status on immune cell function and metabolism are less well understood, various studies have shown that undernutrition, particularly in proteins, is associated with immunosuppression, which results to protection against several types of autoimmune disease but with increased susceptibility to infection (25). In addition, in an early study by Wing and colleagues (1983) aimed at determining the effect of starvation (acute nutritional deprivation) on macrophage function in mice, the capacity of peritoneal macrophages to kill *L. monocytogenes* was enhanced by starvation *in vitro*, and macrophage activity *in vivo* was increased by starvation as revealed by decreased multiplication in both spleens and livers of *Listeria monocytogenes* administered by intravenous injection. In contrast, still in this study, starved mice were not protected against *T. gondii* infection and macrophages from starved mice were unable to prevent tachyzoite multiplication *in vitro*, suggesting that macrophage function was enhanced against a bacterium but weakened against a protozoan opportunistic parasite, pointing out the complexity of immune function response to starvation (26).

On other hand, overnutrition is associated with low-grade, chronic inflammation that disrupts protective immunity, promotes autoreactivity, and increases the risk of metabolic and cardiovascular diseases; these effects of the nutritional status on immunity emerge from the effects of nutrition on circulating cytokines and immune cell populations, as observed in both human studies and mouse models (26). Notably, obesity causes a dysregulation throughout the immune system that affects the balance and levels of cytokines, adipokines, and innate and adaptive immune cells, which result in an alteration of the baseline activation state of immune cells and affect the ability of the host to combat pathogens and malignancy, and to respond

appropriately to vaccination, particularly in paediatric populations (27). In addition, T cells, which are critical members of the immune system that direct adaptive immune response, are influenced in their function by the systemic nutritional status on T cell metabolism and function. Numerous cytokines and hormones mediate the effects of both inadequate and overabundant nutrients on T cell metabolism and function through the expression and action of key regulatory signalling proteins, explaining why T cells are sensitive to malnutrition and obesity (26). Moreover, a meta-analysis articles reported that childhood obesity is associated with extensive changes in the serum levels of anti-inflammatory and inflammatory cytokines, proteins, but also in the number and behaviour of immune cells: (i) causing or exacerbating diseases such as atopic dermatitis (AD), obstructive sleep apnoea syndrome, asthma, and autoimmune diseases; and (ii) reducing the immune system responsiveness to vaccines and pathogens (28).

Similarly, menopause can also affect immune functions (29, 30). The menopausal transition affect many biological systems through complex mechanisms related, but not limited to, oestrogen deprivation; hence, the signs of menopause include: cardiovascular, weight, metabolic, and musculoskeletal changes, urogenital and skin atrophy, sexual dysfunction central nervous system-related disorders, and impaired immune system function (29). Some changes in the immune system during menopause and aging are comparable between genders, but women are far more affected by aging than men due to menopause-related hormonal decline, as oestrogens physiologically act as enhancers of the humoral immunity and androgens and progesterone as natural immune-suppressors (29). Besides aging, changes of the immune system have been attributed to oestrogen deprivation in postmenopausal women, which associate with increases in pro-inflammatory serum markers and in the response of cells to cytokines and with a decrease in CD4 T and B lymphocytes. The cytotoxic activity of NK cells and in the activity of IL-6 that seems to be associated with diseases that often occur in menopause such as atherosclerosis, diabetes, and cardiovascular diseases (30).

1.3.2 Innate immunity, sleep, motor, cognitive functions

The immune system is the main player in the prevention of cerebral toxoplasmosis in immunocompetent intermediate hosts such as humans or rodents. As part of the innate immune responses following *T. gondii* infection, astrocytes and microglia that act as sentinels, mediate alarmin crosstalk to start adaptive type 1 immunity in the CNS. Considering reports suggesting that Complement Component 3 (C3) can bind to *T. gondii* resulting in limited complement activation (for review see (86)), Briukhovetska and colleagues (2020) assessed the role of C5a/C5aR1 axis in the innate immune response in a mouse model of peritoneal *T. gondii* infection. C5aR1 activation drove early IFN- γ production and subsequent Inducible

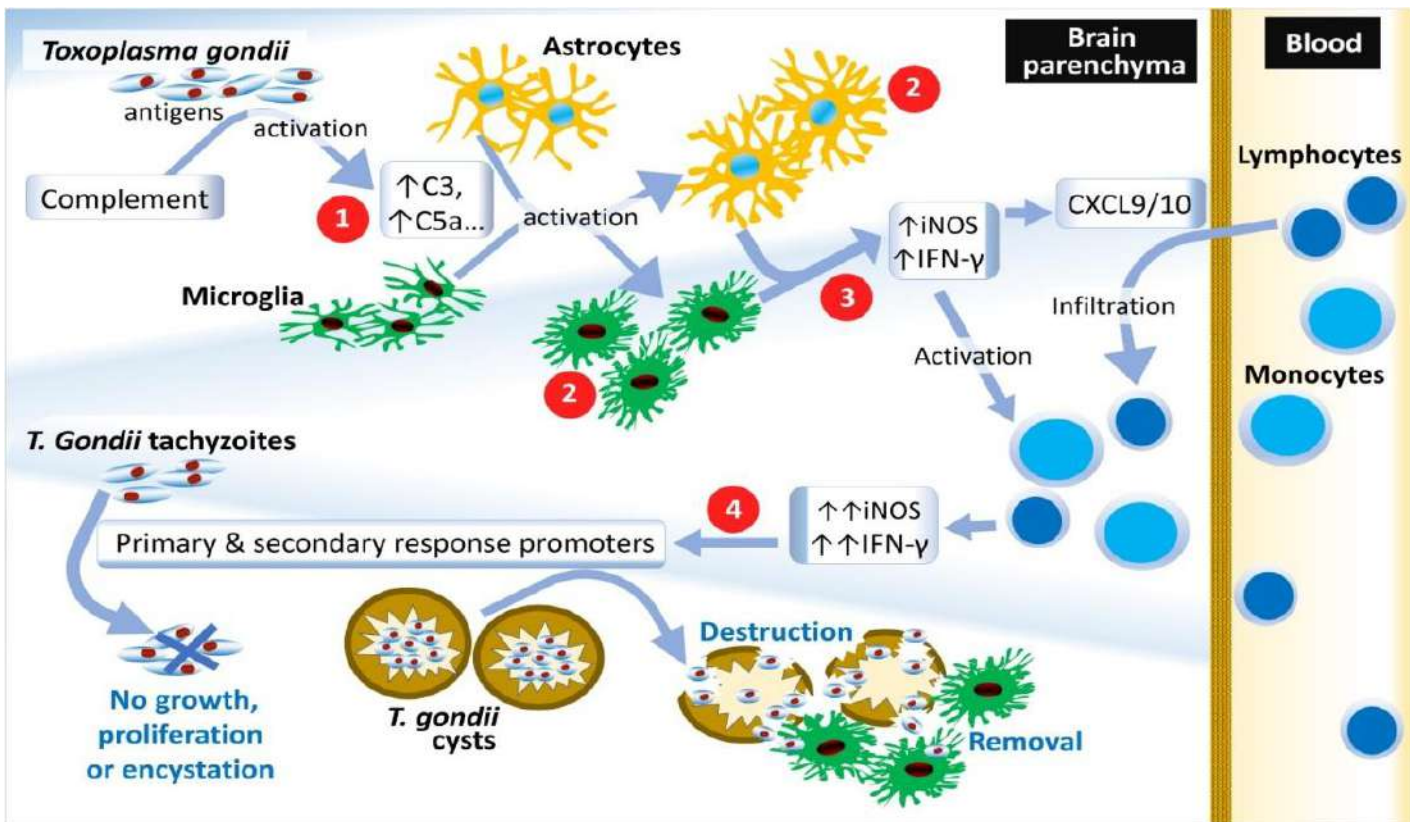
Nitric Oxide Synthase (iNOS) expression in the brain that resulted in the innate immune system activation critical to limit pathogen growth and to start parasite-specific adaptive immunity to control experimental *T. gondii* infection in susceptible immunocompetent hosts, both for systemic disease and cerebral toxoplasmosis management. Another study corroborated these findings and showed that *T. gondii* infection induces marked upregulations of C5a receptor and Complement Factor B (CFB) in the Mouse Brain through microglial activation (87). Such microglial activation, which contribute to *T. gondii* control context in the brain, requires the immunoproteasome subunits $\beta 1i/LMP2$, $\beta 2i/MECL-1$ and $\beta 5i/LMP7$ (88). Interestingly, an in vitro study reported that the Nrf2 pathway is required for intracellular replication of *T. gondii* in activated monocyte/macrophage-like RAW 264.7 murine cells (89). Comparable studies with *T. gondii*-infected microglial cell lines and other future studies on immune response hijacking by the parasite may reveal new therapeutic targets to prevent and treat cerebral toxoplasmosis.

Studies in *T. gondii* infected mice revealed a new brain-specific mechanism where astrocytes promote a protective immune response to *T. gondii* infection of the brain through local release of IL-33, whose signalling, in turn, triggers chemokine expression within brain tissue that is mandatory for the recruitment to the brain of blood-derived IFN- γ -expressing T cells and iNOS-expressing monocytes (90). Emerging reports suggest that *T. gondii* may mediate neurotransmitter dysfunction, a major driver of neuropsychiatric disorders, through immune signals' hijacking, genetic and epigenetic manipulations (for review see (91, 92)). For instance, In a recent study using infrared microspectroscopy to study host-parasite interaction at subcellular levels, RNA sequencing analysis of *T. gondii*-infected human brain microvascular endothelial cells (hBMECs) revealed significant changes in the expression of host cell genes in response to the infection (93). Likewise, a transcriptome analysis of mice lacking the cell adhesion glycoprotein and immune response key player CD44 under chronic infection with *T. gondii* revealed down-regulated expression of genes encoding for chemokines ligands and interferon (IFN)-inducible GTPase families, immunoglobulins, and major histocompatibility complex (MHC) class II antigens (94). Interestingly, a study assessing the impact of the host chromatin environment on *T. gondii* interference with IFN- γ -induced gene expression suggested epigenetic control of IFN- γ host responses by *T. gondii* during infection through a comprehensive blockade of histone modifications at parasite-inactivated promoters (95). Notably, IFN- γ -induced up-regulations of histone marks H4ac, H3K9ac and H3K4me3 and down-regulation of H3S10p at primary and secondary response promoters were abolished by infection with *T. gondii*, without alterations in total nuclear activities of histone acetyl transferases and histone deacetylases. Not surprisingly, a histone deacetylase (HDAC) Inhibitor was recently reported potent anti- toxoplasma activities in vitro and in vivo, including

the ability to control both acute and chronic *T. gondii* infections in mice (96). The emerging therapeutic targets against *T. gondii* infection are discussed further in section 4.2.2. Overall, the emerging reports strongly suggest that pathogen invasion starts early at the choroid plexus and would trigger the cerebral toxoplasmosis typical dysfunction of the blood-brain barrier (BBB) and neuroinflammation (97, 98), indicating a failure of the innate system to control the infection at this point. Notably, in this complex process, the persistence of *T. gondii* cysts would induce sustained neuroinflammation and BBB disruption, allowing leakage of circulating cytokines into the brain tissue, thereby further fuelling neuroinflammation (52).

1.3.3 Adaptive immunity

Figure 3 summarises the strategies used by *T. gondii* to hamper the anti-parasite immune response. The immune system employs T cells as effectors to control *T. gondii* cerebral infection through at least two distinct mechanisms based on parasite life cycle stages: (i) first, to prevent cerebral tachyzoite growth, proliferation, and transformation into cysts in the brain during the acute stage of infection, IFN- γ produced by brain-resident immune cells induces CXC Chemokine Ligand 9 (CXCL9) and CXCL10 expressions, which in turn promote CD4(+) and CD8(+) T cells' infiltration in the brain, where they will also be activated by IFN- γ produced by resident cells; and (ii) second, to remove *T. gondii* cysts from infected hosts' brains, the immune system promotes CD8(+) cytotoxic T cell penetration in the cysts for destruction, and an accumulation of microglia and macrophages for cyst elimination, through a perforin-dependent mechanism (16, 99). Signalling by IFN- γ and CD40, which triggers parasiticidal activity in *T. gondii*-infected macrophages, decreased cyst emergence in the mouse neuroblastoma cell line Neuro-2a, but had no impact on the infection (100), partly justifying the preferential harbouring of parasites by neurons during brain chronic infection. Moreover, *Toxoplasma* strain differences in susceptibility to IFN- γ , thus virulence, were reported and would partly emerge from the ability of *T. gondii* to secrete effector proteins that disturb host immunity. Early studies reported the ability of *T. gondii* to evade IFN- γ -mediated immunity through the secretion of the effector TgIST which strengthens its DNA binding activity by binding to STAT1 and recruiting the Mi-2/NuRD complex to STAT1-responsive promoters in the host cell (101, 102). On the same hand, *Toxoplasma*-secreted effector Dense Granule Proteins 15 (GRA15) limited parasite growth in IFN- γ -activated fibroblasts by inducing lysosomal degradation of the vacuole: (i) in human primary fibroblasts, it occurred through the recruitment of TRAF2 and TRAF6 ubiquitin ligases to the vacuole membrane, which enhanced the recruitment of ubiquitin receptors (p62/NDP52) and LC3B and GABARAP ubiquitin-like molecules; and (ii) in murine fibroblasts through TRAF6 recruitment and subsequent recruitment of immunity-related GTPases (103).



① *Tg* binding to C3 to stop complement response

② Induction of immune resident cells' pyroptosis

③ Interference with histones to stop IFN- γ /iNOS production

④ ↑H4ac/H3K9ac & ↓H3S10p histones to stop IFN- γ responses

Figure 3. Pathogenetic interference of *T. gondii* with the anti-parasite immune response

Source: Personal, present work

Similarly, in another study, host immune responses induced by *T. gondii* GRA15, and in a lesser extent GRA7 and GRA14, via the regulator of T-helper type 1 immunity Nuclear Factor-kappa B (NF κ B) limited parasite expansion (104). Also suggesting that *T. gondii* can modify the immune response mediated by NF- κ B signalling, a study using naïve TGD057 antigen-specific CD8 T cells (T57) isolated from transnuclear mice showed that naïve IFN- γ responses of CD8 T cells to vacuolar antigens is determined by *T. gondii* effectors and host machinery modulating the membranes of parasitophorous vacuoles through inflammasome-independent pathways (99). Notably, various *T. gondii* ROP5 isoforms and allele types suppressed IFN- γ responses of naïve T57 to parasite-infected bone marrow-derived macrophages in an antigen-dependent manner. T57 differentiation occurred independently of parasite virulence, but required macrophage expression of the pathogen sensors NLRP1 and NLRP3 and host immunity pathways downstream of the regulatory Immunity-Related GTPases (IRGs) such as Guanylate-Binding Proteins (GBPs), a key regulator of pyroptosis and apoptosis (105). However, some members of the conventional inflammasome cascade like IL-12, IL-18 or IL-1R would be only partially required, as suggested by decreased but not

abrogated T57 IFN- γ responses to parasite-infected ASC, caspase-1/11, and gasdermin D deficient cells (99).

Interestingly, data from an earlier study supported that the inhibition of the serine proteases DPP8 and DPP9 (DPP8/9), universal activators of functional NLRP1 alleles, may phenocopy the *T. gondii*-induced pyroptosis resulting to inflammatory host cell death (106), pointing out NLRP1-associated signalling molecules as potential pharmacological target in chronic *T. gondii* infection.

1.3.4 Neuronal involvement

The study of brain involvement in *T. gondii* infection provided new insights in neuroimmunology. For instance, a study characterizing neuronal death in murine chronic cerebral toxoplasmosis revealed that the Bax (pro-apoptosis) to Bcl-2 (anti-apoptosis) ratio, an indicator of apoptosis, was correlated with the mean parasite burden and levels of biomarkers of cell-mediated immunity, including Tumour Necrosis Factor (TNF) and iNOS (107). These authors also showed that although TNF/NF- κ B signalling keeps *T. gondii* under control, it deprives neurons of IGF-1R signalling, which is pivotal for synaptic plasticity and cognition (108), as observed in the pathogenesis of dementia (109, 110), providing another link between *T. gondii*-induced neuroinflammation and neuropsychiatric disorders. In addition, emerging data on the role of neurons in the context of neuroinflammation and infection challenge long-standing mainstream theories such as the concept that neurons would be often persistently infected because of the inability of immune cells such as CD8 $^{+}$ T cells to directly recognize them. In a study utilizing a *T. gondii*-Cre system allowing *in vivo* permanent tracking of neurons injected with parasite effector proteins, CD8(+) T cells clustered around these neurons (111), adding to the recent data suggesting that CD8(+) T cells may specifically recognize *T. gondii*-manipulated neurons. Differences between the observations of the previous studies and this study may emerge from the fact that most of the previous studies addressed *T. gondii*-host cell interactions *in vitro* and in non-neuronal cells.

Moreover, a recent study aimed at assessing the roles of oestradiol and progesterone in the relatively higher resistance of neurons to *T. gondii* infection, as compared to astrocytes, determined the effects of 17 β -oestradiol, progesterone, and the specific agonists and antagonists of their receptors on *T. gondii* infection in neuronal cultures (112). Notably, in this study, 17 β -oestradiol alone or in combination with tamoxifen reduced the number of infected neurons, while the progesterone and oestradiol combination decreased the number of intracellular parasites in infected neurons. Interestingly, it is well-established that these hormones mediate neuroprotective effects by reducing pro-inflammatory responses of

macrophages and astrocytes in the brain (113-115), and so doing, probably increase the susceptibility of these cells to be infected by *T. gondii* (116). Then, it appears that while progesterone and oestradiol contribute to neuron resistance to *T. gondii* infection, they may have the opposite effect on microglia and astrocyte, increasing their susceptibility to infection. As discussed later (section 4.2.3), such differences in resident cell response to *T. gondii* reflect high parasite adaptation to mammalian hosts, and may contribute to the long-term maintenance of the parasite with only mild/chronic affections in the immunocompetent host.

Interestingly, a study aimed at assessing how tissue architecture may affect neuron-*T. gondii* interactions in mice and humans proposed a method for *in situ* imaging of host cell-microbe interactions in complex tissue combining high-resolution imaging, new tissue clearing techniques, and three-dimensional reconstruction (117). As this technique allows overcoming *in vitro* culture limitations for mimicking whole organ architecture and the hurdles of *in vivo* imaging in complex tissue, future studies using it may provide new mechanistic insights into neuron-*T. gondii* interactions *in situ* and even into the neurobiology of resident cell-parasite interactions in general.

1.4 Advances in diagnosis, vaccine and drug antitoxoplasmosis development

1.4.1 Parasite detection and typing

Typically, central nervous system lymphoma-like lesions known as toxoplasmosis lesions are the main differential diagnosis of neurotoxoplasmosis by imaging during primary infection in immunocompetent patients, although in rare cases neurotoxoplasmosis can also present as meningoencephalitis (118). However, infection staging with this technique is challenging, therefore, parasite detection-based approaches were proposed to achieve this goal (119, 120), as well as parasite typing techniques to detect more virulent strains (121, 122).

1.4.2 Parasite detection for infection staging

Whole-cell tachyzoite lysate (TLA) currently used in standardized commercial tests for serodiagnosis of toxoplasmosis do not allow infection staging. More accurate recombinant tetravalent chimeric proteins containing fragments of AMA1, GRA1, ROP1, and SAG2 antigens were proposed as potential replacements for standardized commercial tests for toxoplasmosis serodiagnosis (119). These antigens mediated different antibodies at early and chronic phases of *T. gondii* infection, which were distinguishable in serum samples of infected mice and humans. Comparably, *T. gondii* bradyzoite and cyst envelope restricted protein BCLA/MAG2 displayed a sufficient antigenic and predictive power for use as biomarker for the serodetection of chronic infection and persistent parasites in mice (120). The diagnostic potential of *T. gondii* full-length AMA1 recombinant antigen was also reported, as it strongly

interacts with specific anti-*T. gondii* IgG (99.4%) and IgM (80.0%) antibodies (123). In another study, 607 peptides expressed uniquely during acute and chronic infection stages were characterized (124). On the same hand, proteomic analysis of urine of *T. gondii* infected mice, as an easily obtained blood filtration product, revealed 1802 proteins, of which 169 and 47 proteins differentially expressed during acute and chronic infections, respectively (125), that is, potential new diagnostic biomarkers for *T. gondii* infection and progression. Moreover, interestingly, Rehan and colleagues (2020) reported serum sialylated N-glycan as a novel biomarker correlating *T. gondii* infection and associated behaviours, particularly depression-like behaviour, in immunocompetent mice. In this study, changes in sialylated N-glycan expressions predicted the immune status of *T. gondii*-infected mice, and 1-methyl tryptophan, an inhibitor of the tryptophan catabolic enzyme indoleamine 2,3-dioxygenase, improved the disease and reduced depressive-like behaviour (126). This study adds to the evidence supporting *T. gondii* involvement in neuropsychiatric disease development.

1.4.3 Parasite typing

The *T. gondii* strain causing the infection is a key determinant of the disease outcome, as some atypical strains can even cause toxoplasmosis in both immunocompromised and susceptible immunocompetent individuals (121, 127). It is widely accepted that dominant strains in wildlife and patients are typically type 2 strains in Europe and types 1, 2, 3 and 12 strains in North America, while other strains would be predominant in other continents (40, 122, 128, 129). High-quality serological typing appears as a promising alternative for the identification of the *T. gondii* strain that infected a person than the currently used biopsy-based DNA methods which require equipment and reagents, high-quality samples, and trained personnel. Therefore, potential markers for *T. gondii* serological typing are being actively investigated. Notably, various novel proteins showed potential for *T. gondii* serotyping, including dense granule, rhoptry and surface proteins-derived peptides, such as: (i) a GRA7 peptide redesigned version which specifically distinguished type 3 from non-type 3 infections in rabbit, mouse, and human sera (121); and (ii) specific recombinant peptides from *T. gondii* dense granule GRA7, GRA6, GRA5, and GRA3 proteins which showed individual serum reactivities and allowed a serologic fingerprinting of the major strains causing toxoplasmosis in mice and humans (122). Furthermore, studies using nanotechnology also provided promising approaches for parasite serotyping. For instance, a simple colorimetric *T. gondii* serotyping method, based on AuNP gold nanoparticles conjugated with a synthetic polymorphic peptide derived from GRA6 antigen specific for *T. gondii* type 2, proved to be highly efficient to detect anti-GRA6 antibodies in both mice and human sera (130), indicating that a biosensor-based immunoassay using AuNPs could be used as a serotyping device.

1.4.4 Vaccine development

Efforts to overcome the challenges hampering the development of an effective vaccine against toxoplasmosis were recently reviewed (131-133). Thanks to significant progresses in genetic-engineering and related technologies in the last decade, new strategies for vaccine development have emerged, including vaccines based on live-attenuated vectors, epitope or multi epitope-based vaccines, recombinant protein vaccines, DNA vaccines, and prime-boost immunization strategies. Various potential candidates vaccine development emerged from studies in animals, including for example: (i) *T. gondii* surface antigen 1 (SAG1), the main surface antigen of the tachyzoite (132); (ii) rhoptry antigens, which are typically found in the phylum Apicomplexa (133); (iii) *T. gondii* Tyrosine Kinase-Like 1 gene (*tkl1*) (134), the Protein Phosphatase 2C (PP2C), secreted by *T. gondii* rhoptry organelles during host cell invasion (135); (iv) a cocktail expressing SAG1, rhoptry protein 2 (ROP2), and hepatitis B virus surface antigen (HBsAg) as genetic adjuvant (136); (v) recombinant GRA7 adjuvanted with recombinant profilin protein (rTgPF) (137); (vi) a hexavalent recombinant protein vaccine with Montanide ISA 50 V as adjuvant (138); (vii) Toll-like receptors 4 (TLR4) agonist 3-O-desacyl-4'-monophosphoryl lipid A and aluminium salts packed within natural extracts of β-glucan particles (139); (viii) flagellin in combination with TLR4 ligand-emulsion (GLA-SE) adjuvant (140); as well as (ix) *T. gondii* GR8 (141), GRA39 (142), histone deacetylase SIR2 (143), and various *T. gondii* live attenuated strains (144-146). Most of these vaccines provided a total protection against *T. gondii* infection in mice and, thus, warrant further studies considering the potential for human disease prevention.

1.4.5 New drug development

1.4.5.1 Emerging therapeutic targets

Considering the need for new drugs acting through mechanisms different from the standard pyrimethamine-based therapy, new therapeutic targets are needed. Many recent studies reported specific mechanisms supporting the success of *T. gondii* infection, cell invasion, and tissue cyst formation, thus, provided potential pharmacological targets. These reports are summarized in table I. Controversy exists on the actual importance of many of the signalling pathways and mechanisms for parasite dissemination, persistence, and drug resistance *in vitro* and in murine models, thus, on their true therapeutic potential for managing *T. gondii* infections in humans. For instance, type 2 Fatty Acid Synthesis (FAS2) pathway, i.e. apicoplast-based biosynthesis, was reported as crucial for parasite survival by early reports, leading to the long-held assumption that targeting parasite FAS2 pathway, holds a significant therapeutic potential against *T. gondii* infections (147). Recent studies challenged this assumption by reporting *T. gondii* ability to ingest host proteins to support its persistence (148),

and parasite acquisition of exogenous fatty acids, which renders FAS2 pathway dispensable (149).

Table I. Emerging therapeutic targets against *T. gondii* infection

Importance for <i>T. gondii</i> -infection in murine models and cells	
<i>Parasite factors favouring its dissemination and maintenance</i>	
Myb-like TF	Necessary for <i>T. gondii</i> differentiation (150)
MIC1/4	Inhibits inflammation, increases cell invasion (151, 152)
UbL-UbA	Important for synchronous cell division and virulence (153)
C-mannosylation	Promotes attachment to host cells and virulence (154)
GRA60	Modulates host cell autonomous immunity (155)
ROP17	Promotes autophagy-dependent survival (156)
Spindly	Controls levels of proteins in reserve for response to novel stresses (157)
MAG1	Secreted immunomodulator suppressing inflammasome activation (158)
GRA12	Support parasite virulence during acute and chronic infection (159)
FabZ	Essential for parasite growth and survival (160)
TgPiT	Key roles in phosphate import and parasite osmoregulation (161)
Antigen P18	Supports cell invasion and parasite virulence (162)
TgATG9	Pivotal for autophagy and long-term persistence in tissue cysts (163)
<i>HP1</i> gene	Critical for parasite defence against oxidative stress (164)
<i>Host systems hijacked by the parasite for a successful infection</i>	
MNK1/2-eIF4E	Reprogrammed to promote parasite survival (165)
miR-187	Downregulated to evade host immune surveillance (166)
CD209 lectins	Enhance host cells' invasion and dissemination (167)
C4b/factor H	Promote resistance to serum killing (168)
Hsp70	Prevent host cell death during intracellular multiplication (169)
mCherry	Cytosolic protein ingested to support parasite persistence (148)
CD36 receptor	Mediates parasite avirulence for long-term host-pathogen survival (170)

GRA: Dense Granule Proteins. **HP1:** Heterochromatin Protein 1. **Hsp:** heat shock protein. **MAG1:** Matrix Antigen 1. **MIC:** Microneme Proteins. **ROP:** Rhopty Protein. **TgPiT:** *T. gondii* ortholog of Inorganic Phosphate Transporter. **TF:** transcription factor. **UbL-UbA:** Ubiquitin-Like/Ubiquitin-Associated proteins.

These reports raise an alarm and call for more studies on a mechanism before assuming its therapeutic potential and moving into long and expensive pharmacological studies. In addition, intriguingly, a recent report addressing the Roles of the FAS2 pathway enzymes beta-hydroxyacyl-acyl carrier protein dehydratase (FabZ) and oxidoreductase short chain dehydrogenase/reductase family proteins ODSCI and ODSCII in the pathogenesis of *T. gondii*

infection reported that deletion of *FabZ*, but not *ODSCI* and *ODSCII*, decreased the brain cyst burden in mice. These findings suggest the complexity of FAS2 pathway role in the growth and virulence of *T. gondii*. Thus, as illustrated with this pathway, more studies aimed at characterizing potential therapeutic targets against *T. gondii* infection are warranted. Table I presents the emerging therapeutic targets against *T. gondii* infection.

1.4.5.2 Emerging therapeutics and potential of natural products

New anti-*T. gondii* drugs are highly needed: (*i*) to treat toxoplasmosis, considering that the opportunistic disease caused by *T. gondii* in immunocompromised and susceptible individuals may be severe, debilitating, and with poor prognosis; (*ii*) to clear the latent infection, given the aforementioned risk for developing neuropsychiatric disorders in asymptomatic immunocompetent individuals; and (*iii*) with regard to the limitations associated with first-line pyrimethamine and sulphadiazine combination therapy, such as limited efficacy, toxicity-related serious adverse events, and increasing resistance (171). Strategies to improve *T. gondii* sensitivity and decrease the toxicity of the pyrimethamine-based therapy have been proposed based on studies in infected mice, including the addition of the antifungal medication fluconazole to pyrimethamine and sulphadiazine combination (172) and the combination of pyrimethamine with endochin-like quinolone 334 (ELQ-334) and centrally acting alpha2A-adrenergic receptor agonist guanabenz (173). At least partly because the development of new drugs is an expensive and long process, various studies explored the anti-*T. gondii* potential of drugs approved by the FDA for other diseases and conditions, thus, repurposed well-characterized molecules, including notably the antimalarial agent lumefantrine (174) and HIV aspartyl protease inhibitor Aluvia (lopinavir/ritonavir) (175) (table II). A clinical trial assessing the safety and efficacy of co-trimoxazole (trimethoprim-sulfamethoxazole combination antibiotic) in HIV/AIDS patients with cerebral toxoplasmosis in Brazil reported good safety profile and efficacy (176), which is promising for these patients who are in dire need of new therapeutics.

Table II. Drugs approved for other diseases recently reported anti-*T. gondii* activities

Drug	Licensed use	Observations in <i>T. gondii</i>-infected mice
Aluvia (lopinavir/ritonavir)	Antiretroviral protease inhibitor	Impairment infectivity, reduction of brain cyst burden and inflammation (175, 177)
Auranofin	Rheumatoid arthritis	Pro-apoptotic effect on <i>T. gondii</i> tachyzoites and brain cyst burden reduction (178)
Imiquimod	Immunomodulator	Anti- <i>Toxoplasma</i> activity, reduction of brain cyst burden by boosting TLR-MyD88 signalling (179)
Koumiss	Probiotic	Inhibits <i>T. gondii</i> infection by increasing the abundance of bacteria with parasiticidal activity (180)
Lumefantrine	Antimalarial	<i>T. gondii</i> proliferation inhibition <i>in vitro</i> and parasite burden reduction <i>in vivo</i> (174)
Monensin	Antibiotic	Reduction of <i>T. gondii</i> growth and proliferation (181)
Nitazoxanide/spiramycin +metronidazole	Antibiotic, antiprotozoal	Parasite load decrease, survival time and mortality rate increase (182)
Spiramycin/propolis in chitosan/alginate Nps	Antibiotic, antiprotozoal	Good tissue penetration and BBB passage with marked parasite burden reduction in the brain (183)
Antibiotics + antibodies	Antibiotics	Virulence inhibition through blockade of inflammatory macrophage MIF* (184)
Rosuvastatin	Against abnormal lipids	Reduction of brain parasite burden and inflammation (185)
Tylvalosin	Antibiotic	Reduced brain histopathological score and improved survival rate in mice (186)
Valproic Acid	Antiepileptic	Inhibition of chronic <i>T. gondii</i> infection and brain inflammation (187)

MIF: Migration Inhibitory Factor. *Nps*: nanoparticles

Numerous potential therapeutic agents against *T. gondii* infection derived from natural products were also proposed (for review see (188)), including the antimalarial artemisinin derivatives artemether, artesunate, and dihydroartemisinin (189, 190) (table III), as well as molecules from other sources (table IV).

Table III. Natural products-derived compounds recently reported anti-*T. gondii* activities

Compound (origin)	Observations in <i>T. gondii</i> -infected mice
Artemisinin derivatives (from <i>Artemisia annua</i>)	Potent anti- <i>T. gondii</i> activity, generation of large numbers of lymphocytes and CD8(+) T cells benefiting the host, and low cytotoxicity <i>in vitro</i> and <i>in vivo</i> (189, 190)
Hederagenin (triterpenoid found in plant saponin and sapogenin)	Potent anti- <i>T. gondii</i> activity <i>in vitro</i> and <i>in vivo</i> with low cytotoxicity (191)
4-hydroxybenzaldehyde (isomer of an Orchidaceae product)	Restricts <i>T. gondii</i> intracellular growth through SIRT1-mediated autophagy <i>in vitro</i> (192)
Licarin-B (from seeds of <i>Myristica</i> spp. Trees)	Potent anti- <i>T. gondii</i> activity through parasite autophagy activation and mitochondrial damage (193)
Metacytofilin (from fungal <i>Metarhizium</i> species)	Inhibits DNA replication in <i>T. gondii</i> infected cells and enhance RNA degradation in the parasites (194)
Myrislignan (from <i>Myristica</i> spp. trees)	Anti- <i>T. gondii</i> activity with good bioavailability and safety profile (195)
Resveratrol (natural phenol isolated from berries and grapes)	Improvement of cerebral cortex homeostasis and neuroprotection in infected brains (196)
Tartrolon E (from a shipworm symbiotic bacterium)	Anti- <i>T. gondii</i> agent with broad spectrum anti-apicomplexan activity (197)
Toxin 2 mimetic peptides (from <i>Tityus serrulatus</i> venom)	Brain cerebral cyst decrease without hepatotoxicity and with immunomodulatory effects (198)
Urolithin-A (gut microflora product)	Improvement of cerebral toxoplasmosis and alteration of innate response towards predator odour (199)
XYP1 peptide (from <i>Lycosa coelestis</i> spider venom)	Potent anti- <i>Toxoplasma</i> activity with low cytotoxicity <i>in vitro</i> and <i>in vivo</i> (200)

In addition, various recent studies reported medicinal plants with anti-*T. gondii* activities. For instance, Saito and colleagues (2020) screened a library of traditional Chinese medicines for extracts and compounds reported to inhibit *T. gondii* growth. They found numerous medicinal plant extracts and compounds with reported good efficacy for *T. gondii* replication control in infected mice (201), thus, potential candidates for the development of new drugs against *T. gondii* infection. Similarly, an *in vitro* study assessing the potential anti-*Toxoplasma* and anti-*Plasmodium* activities of 43 crude extracts from Mongolian plants reported that *Amaranthus retroflexus* root extract had the more potent activity against *T. gondii*, while six other plants were more potent against the apicomplexan parasite and malaria agent *P. falciparum* (202). On the same hand, the ethanolic extract of leaves of *Annona muricate*

(soursop tree) (203) and the ethyl acetate extract of *Acorus calamus* (sweet flag) rhizome (204) showed anti-*T. gondii* activity in vitro and in vivo, while *Hypericum perforatum* (St John's-wort) extract and its product hyperforin inhibited *T. gondii* growth and infection-induced inflammatory responses of glial cells *in vitro* (205).

Table IV. Other compounds recently reported anti-*T. gondii* activities

Compound	Description	Specificity of anti- <i>T. gondii</i> activity in infected mice
Benzoxaborole AN13762	Antimalarial boron-containing compound	Parasiticidal targeting <i>T. gondii</i> CPSF3, catalytic subunit of <i>T. gondii</i> polyadenylation complex (206)
BKI-1748	Bumped kinase inhibitor	Decrease of cerebral parasite loads through targeting of CDPK1 (207)
Cysteine/serine protease inhibitors	Cysteine and serine protease inhibitors	Tachyzoite damage <i>in vitro</i> with decreased intracellular multiplication and cell invasion failure (208)
Endochin-like quinolone	Antibiotic and antimalarial	Potent inhibition of <i>T. gondii</i> proliferation and reduction of brain cysts (209)
<i>N,N'</i> -diarylureas	Anticancer and antimicrobial	Antiparasitic activity and submicromolar potency against <i>T. gondii</i> (210)
Nullscript	Inactive analog of HDAC inhibitor scriptaid	Inhibition of <i>T. gondii</i> growth and proliferation (211)
Optimized pyrazolopyrimidine	CDPK1 inhibitor	Parasite growth inhibition with good efficacy, selectivity, potency, and safety profile (212)
Triazine nitrile	Cathepsin L inhibitor	Parasiticidal agent crossing the blood-brain barrier in mice (213)

CDPK1: Ca^{2+} -dependent protein kinase 1. **HDAC:** histone deacetylase.

Altogether, these findings point out potential candidates for the development of new drugs against toxoplasmosis and malaria, two public health major challenges in need of new therapeutic avenues, and further support the importance of medicinal plants as readily sources of new compounds with therapeutic potential.

1.5 The medicinal plant *Garcinia kola* Heckel

G. kola Heckel is a perennial dicotyledonous plant growing to a size of about 12-14 m high and distributed out over forests of sub-Saharan Africa (214). *G. kola* flowers around December and January, and bears reddish yellowish- or orange-coloured fruits that are mature

between June and August (214). Mature fruits contain 2-4 seeds having a very sour tasting pulp giving them the vernacular name ‘bitter kola’ (7).

Table V. Taxonomy and classification of *G. kola*

KINGDOM	PLANTAE
CLADUS	<u>Angiosperms</u>
CLADUS	<u>Eudicots</u>
CLADUS	<u>Core Eudicots</u>
CLADUS	<u>Superrosids</u>
CLADUS	<u>Rosids</u>
CLADUS	<u>Eurosids I</u>
CLADUS	<u>Com</u>
ORDER	<u>Malpighiales</u>
FAMILY	Clusiaceae / Guttiferae
GENUS	<i>Garcinia</i>
SPECIES	<i>G. kola</i>

Source: https://commons.wikimedia.org/wiki/Category:Garcinia_kola?uselang=fr

G. kola is widely used traditionally to treat many diseases and for other purposes giving it a common name in most African countries as ‘wonder plant’ because every part of it has medicinal importance. Notably, the stem is been used as a chewing stick (traditional tooth brush which confers dental care due to its antibacterial activity.

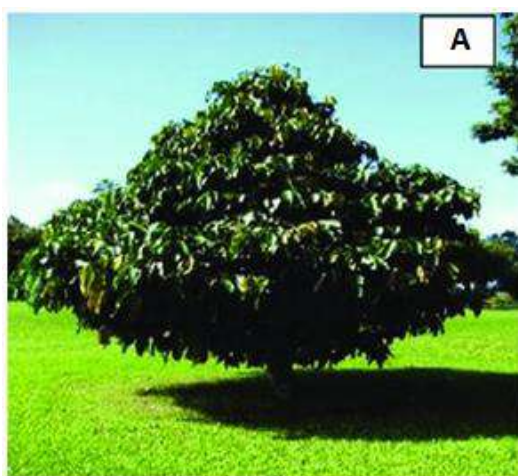


Figure 4. *Garcinia kola* tree (A) and its seeds (B).

The tree (A) and its seeds (B): Sources: (215) (A) and present work (B).

The raw stem bark is used as a purgative while the powdered stem bark is applied to malignant tumours, the latex/gum is used to treat/prevent gonorrhoea infection and is also

applied externally on fresh wounds to prevent bacterial contamination while the sap is used for treating skin diseases caused by parasites (215-217). Seeds are used to treat throat infections, cough, stomach upset and used as an aphrodisiac and fertility enhancing substance probably due to its vasodilator effects on the smooth muscles of the genitalia while the extracts of the various parts of the *Garcinia kola* plant has been used in traditional medicine for the treatment of various ailments such as urinary tract infections, liver disorders, hepatitis, diarrhoea, bronchitis, laryngitis, dysentery (217, 218).



Figure 5. Biochemical mechanisms of beneficial properties of *G. kola* biflavonoids

Source: (217)

1.6 Plant secondary metabolites

The vast and versatile pharmacological effects of medicinal plants are basically dependent on their phytochemical constituents. Generally, the phytochemical constituents of plants fall into two categories based on their role in basic metabolic processes, namely primary and secondary metabolites. Primary plant metabolites are involved in basic life functions. On the other hand, secondary plant metabolites are products of subsidiary pathways as the shikimic acid pathway. Medicinal effects of herbals are oriented towards the secondary plant metabolites. Secondary plant metabolites played an important role in alleviating several ailments in traditional medicine and folk uses. In modern medicine, they provided lead compounds for the production of medications for treating various diseases from migraine up to cancer. Secondary plant metabolites are classified according to their chemical structures into various classes (219). Plant secondary metabolites can be distinguished roughly into three classes of chemical compounds, namely alkaloids, phenolic compounds and terpenes. Each of these broad classes is comprised of many thousands of different individual compounds (220).

1.6.1 Alkaloids

Alkaloids are all secondary compounds and collection of miscellaneous elements and biomolecules, derived from amino acids or from transamination (221).

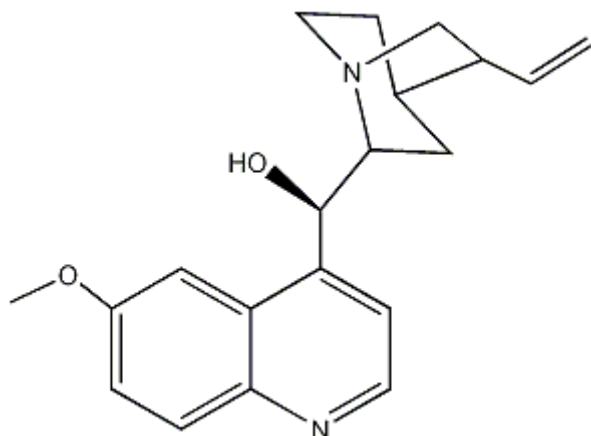


Figure 6. Structure of quinine

Source: (222)

Alkaloids contain nitrogen atom or atoms (amino or amido in some cases) in their structures. These nitrogen atoms are usually situated in some ring (cyclic) system. For example, indole alkaloids are those that contain nitrogen atom in the indole ring system. Generally based on structures, alkaloids can be divided into classes like indoles, quinolones, isoquinolones, pyrrolidines, pyridines, pyrrolizidines, tropanes, terpenoids and steroids. More than 3000 of alkaloids are known in over different 4000 plant species (223). Alkaloids are often divided into the following major groups:

- "True alkaloids", which contain nitrogen in the heterocycle and originate from amino acids. Their characteristic examples are atropine, nicotine and morphine;
- "Protoalkaloids", which contain nitrogen and also originate from amino acids but does not have heterocyclic ring. Examples include mescaline, adrenaline and ephedrine; and
- Pseudalkaloids – alkaloid-like compounds which do not originate from amino acids. This group includes, terpene-like and steroid-like alkaloids, as well as purine-like alkaloids such as caffeine, theobromine and theophylline.

Alkaloids showed anti-inflammatory, anticancer, analgesics, local anaesthetic, pain relief, neuropharmacological, antimicrobial, antifungal and many other activities. Alkaloids are useful as useful as diet ingredients, supplements and pharmaceuticals in medicine and in other applications in human life. Alkaloids are also important compounds in organic synthesis for searching new semisynthetic and synthetic compounds with possibly better biological activity than the parent compounds (223). Morphine is one of the most known alkaloids which had

been used and still is for medical purposes. This alkaloid is a powerful narcotic which is used for the relief of pain. Methyl ether derivative of morphine-----codeine----naturally occurring next to morphine in the opium puppy, possesses an excellent analgesic activity. Atropine for example is given as an injection to treat bradycardia (low heart rate). Alkaloids like Vincristine and vinblastine are used as chemotherapeutic agent in the treatment of many cancer types. Cocaine an alkaloid present in *Erythroxylum coca* is a potent local anaesthetic. Ergonovine, an alkaloid from the fungus *Claviceps purpurea* and the second alkaloid ephedrine isolated from Ephedra species both act as blood vessels constrictors. Also, ephedrine is used in bronchial asthma and to relieve discomfort of hay fever, sinusitis and common colds. Quinine is a powerful antimalarial agent and more often is replaced by synthetic drugs, which are more effective and less toxic. Another alkaloid from Cinchona species is quinidine which has medical application as treatment of irregular rhythms of the heartbeat or arrhythmias. Colchicine is another alkaloid present in plants of Liliaceae family known for ages to treat acute gout attacks (223).

1.6.2 Phenolic compounds

Phenolics are a type of secondary metabolite that can be found almost all over in plants. They are an aromatic molecule with a benzene ring (C6) and one or more hydroxyl groups that belong to a broad and diversified group. In general, phenolics are classified according to the number of carbon atoms in the molecule. Three different biosynthetic pathways produce phenolics:

- The shikimate/chorizmate or succinylbenzoate pathway, which produces phenylpropanoid derivatives(C6-C3)
- The acetate/malonate or polyketide pathway, which produces side chained elongated phenylpropanoids including the large group of flavonoids (C6-C3-C6) and some quinones and
- The acetate/mevalonate pathway, which produces the aromatic terpenoids, mostly monoterpenes, by dehydrogenation reactions (58).

Polyphenols are classified according to the number of phenol rings they contain and the structural elements that connect these rings as shown below. The major classes of polyphenols are phenolic acids, flavonoids, stilbenes and lignans.

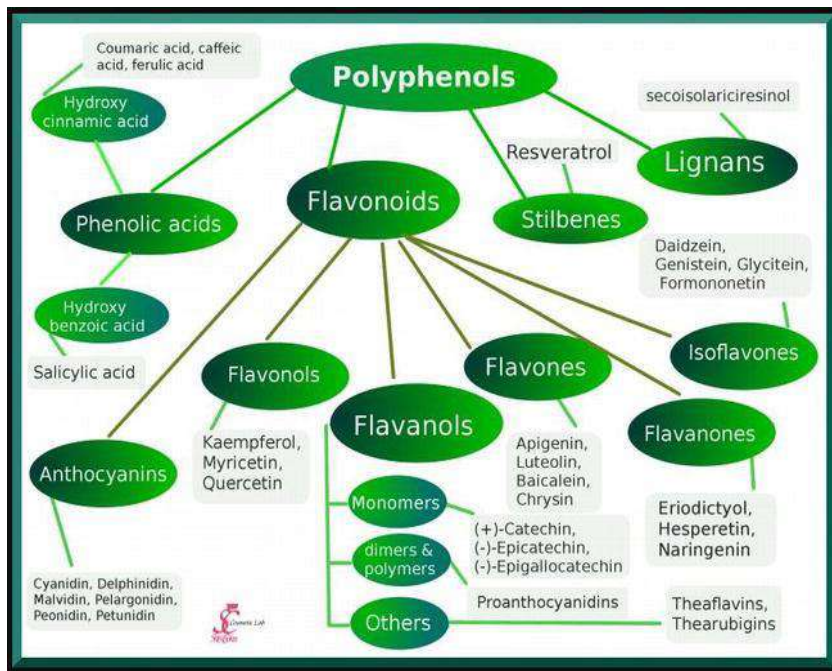


Figure 7. The different classes of polyphenols

Source: (224)

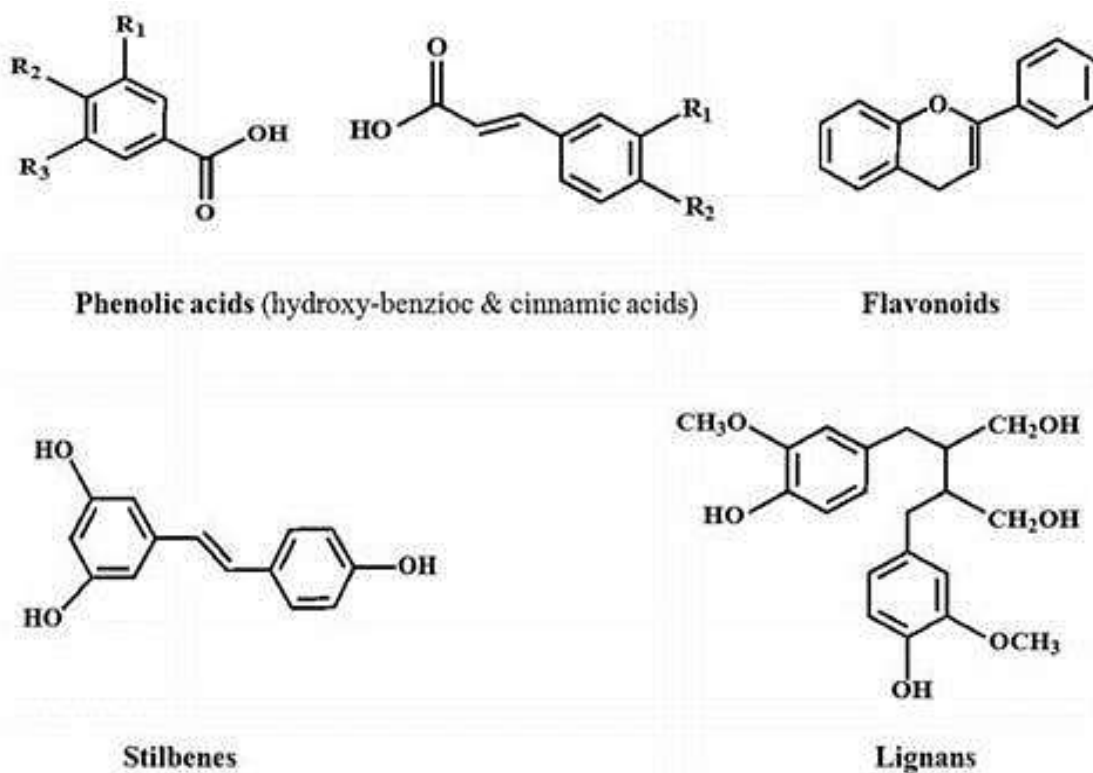


Figure 8. Structure of polyphenols

Source: (224)

Phenolic compounds have shown interesting bioactivities, such as antioxidant, antimicrobial, anti-inflammatory, and antiproliferative activities, among others, which has led

to great interest in their use by several industries (225). Polyphenolic compound quercetin protects the lipid peroxidation and oxidative stress, which in turn helps in antidiabetic activity. Resveratrol a stilbene polyphenol substantially proved for its anticancer potential via different in vitro and in vivo studies. Quercetin found in onion cause interruption in the formation of atherosclerotic plaques and inhibit the metalloproteinase I enzyme to reduce the mortality in patients with coronary heart diseases. Curcumin found in turmeric showed its neuroprotective potential via reduction in Alzheimer's disease pathogenesis (226). Flavonoids such as quercetin and phenolic acids such as ferulic acid have shown antifungal activity against some phytopathogens as *Alternaria alternata*, *Rhizoctonia solani*, *Fusarium oxysporum*, *Botrytis cinerea* and *Phytophthora infestans*. Naringin is a flavonoid compound that belongs to the subclass of flavones and is extensively distributed in citrus fruits such as bergamot and tomatoes. Naringin is a remarkable polyphenolic compound having wide organic effects on human wellbeing. This secondary metabolite incorporates a reduction in lipid peroxidation in lipid peroxidation biomarkers and protein carboxylation, advances glucose digestion, builds a cancer prevention agent, decreases levels of ROS and applies hostility to atherogenic and calming impacts (227).

Gallic acid is a part of “esters of gallotannins” having a strong antioxidant capacity and free radical scavenging potential. Likewise, gallic acid also possesses antibacterial, antiviral, anti-inflammatory, antitumor and apoptotic actions. Caffeic acid (CAA) is an important member of “hydroxycinnamic acid” with natural antioxidant and cardio-protective properties. Kaempferol is a yellow common natural “flavonoid” abundant in many plant-derived foods and traditional medicine. Its glycosides possess numerous pharmacological activities including antiradical capacity, antibacterial or antifungal activity, chemotherapeutics, neuroprotective, hypoglycaemic pain relieving and anti-allergic (227).

1.6.3 Terpenes

Terpenes, any member of a group of hydrocarbons that are often found in plants and animals and are believed to have evolved from isoprene, a hydrocarbon with five carbon atoms bonded to eight hydrogen atoms (C_5H_8). The name is frequently used to refer to the terpenoids, which are these hydrocarbons' oxygenated derivatives. Terpenes are a wide category of volatile unsaturated hydrocarbons present in plant essential oils, particularly in conifers and citrus trees. They are based on the formula C_5H_8 , which is a cyclic molecule. The terpene structure can contain one or more isoprene units. In the terpene structure, the unsaturation and functional groups can vary depending on the nature of the compound. Terpenes can be classified on the basis of isoprene units they contain.

- Monoterpene- These molecules contain two isoprene units.

- Sesquiterpenes- These molecules contain three isoprene units.
- Diterpenes- These molecules contain four isoprene units.
- Triterpenes- These molecules contain six isoprene units.

Terpene can be used for various purposes:

- Terpenes are used in aromatherapy.
- Terpene oil is used in cooking for adding flavours to the food.
- Terpene oil is used in vaping devices.
- Terpenes have a soothing property. Therefore, it is used in topical application.

Some terpenes are highly regarded for their therapeutic capabilities and have been used in ancient medicine for centuries. Other terpenes are newly researched but show promising results. A number of in vitro animal and clinical trials have shown that terpenes have a number of medicinal applications. Terpenes have been shown to be anti-inflammatory, antitumor, analgesic, antidepressant, anticancer, neuroprotective, anti-allergic, antibiotic, anti-mutagenic. Myrcene is the most common terpene found across cannabis strains, but also in fruity scent that can be found in mangoes, thyme, lemongrass and hops. In terms of benefits, myrcene is a known anti-inflammatory, analgesic, antibiotic and sedative compound. Pinene is the most commonly found terpene in plants including pine needles, rosemary, dill and basil. Pinene has shown to curb THC-induced short-term memory loss, increase concentration as well as open up the lung airways. Pinene has been used as an antiseptic and anti-inflammatory agent in many cultures throughout history. Limonene's scent is hard to miss. Aromas of lemons, oranges and other citrus varieties appear in cannabis strains that have the limonene terpene. Because of its pleasant citrus scent, limonene is used in multiple industrial cleaning products and fragrances. Limonene has been shown to have antibacterial, antifungal and anti-anxiety properties.

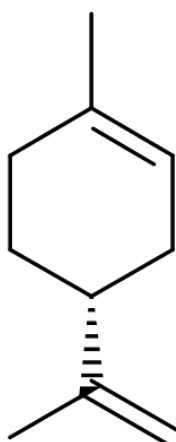


Figure 9. Structure of limonene

Source: (227)

1.7 Treatment of toxoplasmosis

Toxoplasma gondii is an obligate intracellular parasite. The anti-parasitic activity of molecules to be used for its treatment therefore must be able to penetrate cells and the cytoplasm where the parasite multiplies in the parasite vacuole surrounded by a thick membrane. The cyst wall is thick, it is an impermeable barrier for molecules. The slow metabolism of bradyzoites limits the effect of active drugs on parasite division, thus the compounds used generally have an anti-parasitic action which is exerted only on the tachyzoite form and not on cysts (228). Two families of drugs are used in the treatment of toxoplasmosis: macrolides and folic acid synthesis inhibitors, which are active on tachyzoites but have no effect on cysts (229).

1.7.1 Macrolides

They are parasitostatic and have good Intracellular penetration, they inhibit the growth of tachyzoites following prolonged incubation. Their effect is parasitostatic at high doses. Its tissue distribution is maximum in the placenta, liver, lungs and minimal in the brain and eye (230).

1.7.1.1 Spiramycin (Rovamycin®)

Spiramycin is the main macrolide used in the treatment of acquired toxoplasmosis during pregnancy. It has an inhibitory and non-lytic action, common to other macrolides (231). It does not present a teratogenic effect at normal doses and can be used during pregnancy without any risk.

1.7.1.2 Azithromycin (Zitromax®)

Has remarkable pharmacokinetic properties, it has a good action on the lung and liver but not in the brain (231).

1.7.1.3 Roxithromycin and Clarithromycin

Roxithromycin and Clarithromycin are characterized by minimal inhibitory concentrations levels, a long half-life, some meningeal diffusion and significantly higher serum, tissue and macrophage concentrations than spiramycin. Roxithromycin can reach inhibitory concentrations in the brain (232).

1.7.1.4 Clindamycin (Dalacine®)

It is a macrolide related to lincosamides, known for their good diffusion and good intracellular concentration. They are powerful inhibitors which can eliminate parasites in the blood (231). They are associated with pyrimethamine in the treatment of extra-neurological toxoplasmosis (233).

1.7.2 Folic acid synthesis inhibitors

1.7.2.1 Antifolics

They act by inhibiting the synthesis of folic acid by competition with dihydropteroate synthetase (DHPS), their diffusion is total in tissue, placental and in meninges.

1.7.2.2 Sulphonamides

Fast-acting sulfonamides are mainly represented by Sulfadiazine (Adiazine®), the most active on *T. gondii* and the most used despite the need for several daily dosing. Classes include: (i) the semi-delayed acting sulfonamides, including Cotrimoxazol (Bactrim®) which combine Trimethoprim and Sulfamethoxazole, allows spacing of daily doses; and (ii) the delay sulfonamides, which are essentially synergistic e.g. Sulfadoxine with pyrimethamine (Fansidar®) they have a long half-life (234).

1.7.3 Sulphones

They have in vitro activity against *T. gondii* and a synergistic effect with pyrimethamine. Dapsone (DISULONE®), is the only molecule marketed, its use is limited due to its hematological and neurological adverse effects (235).

1.7.4 Antifolinics

They act by inhibition of dihydrofolate reductase. Pyrimethamine is characterized by good tissue, placental and meningeal diffusion. It has a parasiticidal effect on tachyzoites of *Toxoplasma gondii* at very low concentrations and a synergy of action with sulfonamides and certain macrolides (235). To limit hematological side effects, Pyrimethamine must be administered with folic acid (232). Trimethoprim is less effective than pyrimethamine, is often associated with sulfamethoxazole (236, 237).

CHAPTER II: MATERIALS AND METHODS

2.1 Characteristics of the study

2.1.1 Type of study

This was a series of experimental studies

2.1.2 Place of study

- Bamenda (North west Region) for the harvesting and collection of *Garcinia kola* seeds
- Registration code 28837 was granted at the National Herbarium of Cameroon.
- Neuroscience, Biochemistry and Chemistry Laboratories of University of Yaoundé I, for conducting the experiments.

2.1.3 Study period

10th January 2020 - 10th October 2023

2.1.4 Animals

Eight-to-ten weeks rats ($156.7 \pm 4.1\text{g}$, N = 72) male (N = 48) and female (N = 24) Wistar rats were obtained in three waves (a fresh wave of the right size for each of the three *in vivo* experiment) from the Faculty of Science of the University of Yaoundé I (Yaoundé, Cameroon) and acclimatized to Neuroscience Laboratory conditions (Faculty of Medicine and Biomedical Sciences, University of Yaoundé I). Housed in groups of 3, animals had free access to water and food and were under a 12:12 light-dark cycle, at 25°C. All experimental procedures were approved by the institutional ethics committee (N° 0634/UYI/FMSB/VDRC/DAASR/CSD) and the animals were handled considering ethical rules relating to the protection of animals used for scientific purposes, particularly the European Commission Directive (2010/63/EU).

2.2 Experimental procedures

2.2.1 Objective 1 tasks

The first objective was to evaluate the cognitive disorders associated with chronic *T. gondii* infection in rats of the immune-competent and non-susceptible strain Wistar. Hence, the first series of studies was aimed at characterizing behavioural indicators of neurotoxoplasmosis occurring in the late stage of *T. gondii* infection in rats. Twelve animals were randomly divided in two groups (N = 6 per group, with 3 males and 3 females): (i) a non-infected control group injected with sterile saline (i.p.); and (ii) a group infected with *T. gondii* tachyzoites (TS-4/ATCC 40050) kindly provided by the Antimicrobial & Biocontrol Agents Unit of the University of Yaoundé I. Rats were injected (i.p.) once with 10 million *T. gondii* tachyzoites in suspension in 500 µL of sterile saline, considering pilot studies in our laboratory and previous reports (238, 239). The infection was confirmed when tachyzoites were observed in

blood smears from the tail vein 3 days after inoculation, both inside and outside leukocytes (238).

The animals were continuously monitored, video-recorded. Their body weight and body temperature (inner ear, infrared thermometry) were measured every three days. Two ethological tests namely the open field test (OFT), the elevated plus maze (EPM) paradigm as well as footprint analysis were performed sequentially at day post-infection (dpi) 88, that is 20 days after the infected animals displayed an inflection in body weight (see section 3.1). Two days after, all animals were sacrificed under deep anaesthesia when signs of terminal disease were observed in infected animals, to avoid prolonging animal suffering unnecessarily. Organs (brains, livers, kidneys, hearts, and lungs) and blood samples were collected. Blood smears were processed for Giemsa staining and counts of immune cells, *T. gondii* tachyzoites and cysts. In addition, brains were processed for Nissl (cresyl violet) staining and neuron counting using stereological techniques in anterior, posterior, and cerebellar areas pivotal for the motor and cognitive functions assessed in behavioural tests.

2.2.2 Objective 2 tasks

The second objective of this work was to assess the abilities of LPD, HFD, and ovariectomy to accelerate *T. gondii* infection course in Wistar rats. Thus, the tasks of the second series of studies where aimed at assessing whether undernutrition, overnutrition, or ovariectomy could accelerate the early stage of the infection into late stage neurotoxoplasmosis in live animals. Here, 30 animals were randomly divided in five groups ($N = 6$ / group, with 3 males and 3 females), of which a non-infected control group injected with sterile saline (i.p.) and fed with normal rat chow (15% protein, 3% fat, and 7% simple sugars [w/w]), and four groups infected with *T. gondii* tachyzoites: (i) a group fed with normal rat chow (infected control group); (ii) a group fed with low-protein diet (LPD, normal chow-like diet with 7% protein [w/w]) (240, 241); (iii) a group fed with a high-fat diet (HFD, 15% protein, 16% fat, and 33% simple sugars [w/w] prepared as described before (242)); and (iv) a group ovariectomised and allowed 14 days to recover from surgery before infection as described previously (243).

As in the previous series of experiment, after confirming the success of the infection, the animals were continuously monitored, video-recorded, their body weight and body temperature were measured every three days. Then, OFT test, EPM paradigm, and footprint analysis were performed sequentially at dpi 16 days post-infection (dpi) and 10 days after the occurrence of an inflection in the body weight curve of LPD-fed infected animals (see section 3.1). The day after (dpi 17), also to avoid unnecessary suffering, animals were sacrificed under deep anaesthesia and organs and blood samples were collected and stored. Brain sections were

randomly selected, processed for Nissl staining and neuron counting. Blood smears were stained using Giemsa and processed for the quantification of tachyzoites, cysts, and white blood cells.

2.2.3 Objective 3 tasks

The third and final objective of this work was to perform a phytochemical study of extracts of the medicinal plant *G. kola* (to ensure that they contained the same secondary metabolites as the extracts reported neuroprotective and antiparasitic properties) and to assess the therapeutic potential of *G. kola* extracts in *T. gondii*-infected rats fed LPD as brain functional alterations appeared the most severe in LPD-fed infected animals, as compared to HFD and ovariectomy in the previous series of *in vivo* studies (see section 3.2). Hence, the third series of studies started with the methanolic extraction of *G. kola* seeds followed by the phytochemical screening (qualitative and quantitative). Afterward, we assessed the therapeutic potential of fractions of the methanolic extract of *G. kola* against undernutrition-induced neurotoxoplasmosis in male rats.

More specifically, 30 male rats were randomly divided in five groups ($N = 6/\text{group}$), of which a non-infected control group injected with sterile saline (i.p.) and fed with normal rat chow and four groups infected with *T. gondii* tachyzoites and fed with LPD: an untreated group (infected control group) and three groups treated once daily with hexane, dichloromethane (DCM) and ethyl acetate fractions of *G. kola* methanolic extract at doses equivalent to the content of the neuroprotective and safe dose of crude extract (100 mg/kg) (31-33). Treatment with extracts started at 7 dpi, around the period where the first inflection in body weight was observed. The same procedures and approach as per the second series of studies were used then, including behavioural tests, body weight monitoring, and animal observation for the *in vivo* studies; brain staining with cresyl violet for neuron counting, and blood smear staining with Giemsa for the observation of tachyzoites, circulating cysts, and white blood cells. In addition, brains, livers and spleens were processed for hematoxylin and eosin (H&E) staining for histopathological analysis.

2.3 Plant material processing and phytochemical screening

2.3.1 Plant material processing

G. kola seeds were harvested during maturing period (August) in Bamenda, North West region of Cameroon. Seeds were authenticated in the National Herbarium of Cameroon by comparison to the botanic sample of R. Louzey number 11.981 registered under the code number 28837/HNC. A sample was stored for future reference. Then, seed coats were peeled off and seeds were cut into small pieces using a slide, for faster shade-drying at laboratory temperature.

Dried seeds were ground into powder using a grinding mill. The powder (2500 g) was mixed and extracted with methanol at 65°C (5 hours) using a Soxhlet extractor. A rotary evaporator was used for methanol evaporation and the methanolic extract obtained was processed for fractionation using hexane, DCM, and ethyl acetate solvents and a Soxhlet extractor as described by Iwu and colleagues (244). Briefly, to obtain the hexane fraction, the extractor was set at 65°C, 250ml of hexane was introduced into the system and the water supply was turned on. After 6 h of extraction, the supernatant (a yellow mixture of compounds) was separated and dried using a rotary evaporator (70°C). Hexane was also evaporated from the remainder of the methanolic extract, which was then mixed with DCM and extracted for 5 hours in a Soxhlet extractor set at 65°C to obtain the DCM fraction (supernatant of black texture after evaporation). After evaporation of DCM from the remainder of the methanolic extract, it was mixed with 100ml of distilled water and 150ml of EA in a decantation ball for 10 minutes and aqueous and organic (darker) phases were separated. In a second decantation, 150ml of EA were added to the aqueous phase and an organic phase was decanted (darker than the aqueous phase but less pronounced than in the first decantation). In a third decantation, 150ml of EA was added to the remaining aqueous phase and the organic phase was removed once again. The organic phase was clearer than the aqueous phase, which marked the end of the decantation process. Then, the EA fraction was obtained by: (i) mixing the organic phases obtained from the three decantation processes; (ii) using the drying agent anhydrous calcium chloride to remove any traces of water present in the organic phase mixture; and (iii) using a rotatory evaporator set at 70°C to remove the EA present in the mixture.

2.3.2 Qualitative phytochemical screening

We screened for the following secondary metabolites: alkaloids, phenols, flavonoids, terpenoids, tannins and saponins. We prepared a 2% solution of our extract in 10ml volume. We measured 0,2g of the extract and put in a conic tube. 5ml of ethanol was added to the extract. The mixture was homogenised using a magnetic agitator. The mixture was then topped up to 10ml using distilled water.

2.3.2.1 Test for polyphenols

Aim: To determine the presence of phenolic in the sample by Folin-Ciocalteu method, described by Singleton et al (1999)

Principle: Polyphenols in an alkaline medium reduce the phosphotungstic and phosphomolytic acids of the Folin-Ciocalteu's reagent into a mixture of blue tungsten and molybdenum oxides which absorb light at 765nm

Procedure: To 1ml of extract in a test tube, five drops of Iron III chloride (FeCl₃) were added, followed by 3 drops of Potassium cyanide. Observation of a greenish colour indicates the presence of polyphenols.

2.3.2.2 Test for terpenes

Aim: To determine the presence of terpenes in the sample

Principle: a brownish red interphase indicates the presence of Terpenes.

Procedure: To 1ml of extract in a test tube, 1 ml of glacial acetic acid was added followed by three to five drops of concentrated sulphuric acid at 10%. Observation of a brownish red interphase indicates the presence of Terpenes.

2.3.2.3 Test for alkaloids

Aim: To determine the presence of alkaloids in the sample

Principle: a yellowish white precipitate or creamy white precipitate indicates the presence of alkaloids.

Procedure: To 1ml of extract in a test tube, 3 to 5 drops of Valse Mayer's reagent (1.3g de HgCl₂ and 5g de KI for a volume of 100ml) were added. Observation of a yellowish white precipitate or creamy white precipitate indicates the presence of alkaloids.

2.3.2.4 Test for flavonoids

Aim: To estimate the amount of flavonoids, present in sample by aluminium. Method described by Zhishen et al. (1999) (4).

Principle: Aluminium chloride forms acid stable complexes with the C-4 keto group and either the C-3 or C-5 hydroxyl group of flavones and flavanols respectively.

Procedure: To 1ml of extract in a test tube, 1ml of sodium hydroxide (NaOH 2N) was added, followed by two to 3 drops of concentrated sulphuric acid. observation of an orange yellow coloration indicated the presence of Flavonoids.

2.3.2.5 Test for quinones

Aim: To estimate the amount of quinones, present in sample.

Principle: a red coloured complex is formed when sodium hydroxide reacts with quinones.

Procedure: To 1 ml of the extract in a test tube, was added few drops of Sodium hydroxide (NaOH) at 10%. The presence of a red coloration indicates the presence of Quinones.

2.3.2.6 Test for steroids

Aim: To estimate the number of steroids, present in sample.

Principle: a violet to blue or green colour complex is formed when Steroids reacts with acetic anhydride followed by concentrated sulphuric acid.

Procedure: To 1ml of the extract in a test tube was added 2ml of acetic anhydride followed by 2ml of concentrated sulphuric acid. The presence of a violet to blue or green colour indicates the presence of Steroids.

2.3.2.7 Test for coumarins

Aim: To estimate the number of coumarins, present in sample.

Principle: a green or blue to yellow colour upon addition of Nitric acid (HNO₃) indicates the presence of coumarins.

Procedure: To 1ml of extract in a test tube, 1ml of distilled water was added, followed by a few drops of 10% Iron III chloride (FeCl₃). The presence of a green or blue to yellow colour upon addition of Nitric acid (HNO₃) indicates the presence of coumarins.

2.3.2.8 Test for anthocyanins

Aim: To estimate the number of anthocyanins, present in sample.

Principle: the colour increases in acidic medium then turns to purplish blue in basic medium, indicating the presence of anthocyanins.

Procedure: 1 mL of the extract was placed in a test tube. To this was added 1 mL concentrated H₂SO₄ and then 1 mL of diluted Ammonia. In the presence of anthocyanins, the colour increases in acidic medium then turns to purplish blue in basic medium, indicating the presence of anthocyanins.

2.3.2.9 Test for mucilage

Aim: To estimate the number of mucilage, present in sample.

Principle: Obtaining a fluffy precipitate upon agitation indicates the presence of Mucilage.

Procedure: To 1ml of extract in a test tube, was added 3ml of absolute ethanol. Obtaining a fluffy precipitate upon agitation indicates the presence of Mucilage.

2.3.2.10 Test for saponins

Aim: To estimate the number of saponins, present in sample.

Principle: The presence of a stable foam after 15 min was considered as an indication for the presence of saponins

Procedure: Crude extract was mixed with 5 mL of distilled water in a test tube. The presence of a stable foam after 15 min was considered as an indication for the presence of saponins

2.3.2.11 Test for tannins

Aim: To estimate the number of tannins, present in sample.

Principle: a greenish brown or blue-black colour, it is positive for tannins.

Procedure: The test was carried out by taking 2 mL of each sample solvents, then heated in a water bath at 90 C for about 15 minutes. After heating, each of them added a few drops of FeCl₃. If each solution forms a greenish brown or blue-black colour, it is positive for tannins.

2.3.2.12 Test for catechic tannins

Aim: To estimate the number of catechic tannins, present in sample.

Principle: Observation of soluble red precipitate indicates the presence of catechic tannins.

2.3.2.13 Test for gallic tannins

Aim: To estimate the number of gallic tannins, present in sample.

Principle: presence of a dark blue precipitate indicates the presence of Gallic tannins.

Procedure: After filtration, the filtrate is saturated with pulverised sodium acetate followed by 1% FeCl₃. The presence of a dark blue precipitate indicates the presence of Gallic tannins.

2.3.3 Quantitative phytochemical screening

2.3.3.1 Total polyphenolic compounds

Aim: To determine the amount of total phenolic content present in the sample by Folin-Ciocalteu method, described by Singleton et al (1999) (3).

Principle: Polyphenols in an alkaline medium reduce the phosphotungstic and phosphomolytic acids of the Folin-Ciocalteu's reagent into a mixture of blue tungsten and molybdenum oxides which absorb light at 765nm.

Procedure: 1ml of each extract was added with 1ml of Folin-Ciocalteu reagent and 1ml of sodium carbonate into a glass test tube. The mixture was shaken and kept for 2 hours (120min). The absorbance was read at 760nm using a spectrometer. A calibration curve was produced in parallel under the same operating conditions were followed using gallic acid(1mg/ml) at different concentrations (0µg/ml to 1000µg/ml). The total polyphenols content is determined by extrapolation on a calibration curve. The polyphenol content is expressed in mg Equivalent of gallic acid/g of dry fraction (mg EAC/g MS), using the following formula

$$T = C \times V \times M$$

Where;

T= Content in Polyphenol compounds (mg EAC/g of dry extract)

C= Concentration of polyphenolic extract equivalent to gallic acid obtained from the calibration curve (mg/ml)

V= Volume of polyphenolic extract (ml)

M= Dry weight of polyphenolic extracts(g)

2.3.3.2 Total flavonoid content

Aim: To estimate the amount of flavonoids, present in sample by aluminum. Method described by Zhishen et al. (1999) (4). Aluminium chloride forms acid stable complexes with the C-4 keto group and either the C-3 or C-5 hydroxyl group of flavones and flavanols respectively.

Principle: these reagents forms an acid labile complexes with the orthodihydroxyls groups in the A- or B- rings of flavonoids resulting in pink colour formation, and it is measured at 510nm.

Procedure: In a glass test tube, 1ml of extracts, and 1ml of NaNO₂ 5% was added and mixed and the mixture was allowed for 5min. Next, 1ml of AlCl₃.6H₂O 10% were mixed. After 1 min, 1ml of NaOH was added. The solution was mixed well and the absorbance was measured against the reagent blank at 510 nm. The standard curve for total flavonoids was made using quercetin standard solution (0µg/ml to 1000µg/ml) under the same procedure as earlier described. The total flavonoids were expressed as milligrams equivalents of quercetin per g of dried fraction.

2.3.3.3 Total flavanol content

Aim: To estimate the amount of flavanol content present in sample by aluminium method described by Kumaran et al 2007 (5).

Principle: In ethanolic solution, flavanols are chelated by AlCl₃ (OD between 380- 400nm).

Procedure: In a glass test tube, a millilitre of extract, aluminium chloride and sodium acetate was added. The test tube was shake and kept for 2.5hours for incubation at a temperature of +20. The absorbance was read at 440nm. The flavanol content was determined by extrapolation from the calibration curve. The flavanols content was expressed in mg Equivalent of the quercetin.

2.3.3.4 Total Tannin content

Aim: Tannic acid stock solution (100ug/ml) was prepared fresh by dissolving 100mg of tannic acid in 1L distilled water.

Procedure: The 1,10-phenanthroline solution (0.015 mol/L) was prepared by dissolving 2.970g of 1,10-phenanthroline powder in 1L of distilled water. Iron (III) chloride hexahydrate solution (0.01 mol/L) was prepared by adding 1.350g Iron (III) chloride hexahydrate in distilled water and adding 1ml of hydrochloric acid (36%) and diluting with distilled water to 500ml. Ethylenediaminetetraacetic acid (EDTA) solution (0.05mol/L) was prepared by dissolving 1.850g of EDTA in 100ml distilled water. Aliquots of standard tannic acid were pipetted to 25ml flask so that the final concentrations were 0.5, 1.0, 2.0, 3.0 and 4.0 ug/ml. Each flask was added 2.5ml of Iron (III) chloride hexahydrate solution (0.01 mol/L) and the mixture was incubated in a water bath at 80°C for 20min. Mixture of 2.5ml of acetic buffer (pH 4.4), 5ml of 1,10-phenanthroline solution (0.015 mol/L) and 0.5ml. Ethylenediaminetetraacetic acid

(EDTA) solution (0.05mol/L) were added to each flask. When the solution was cooled, the volumetric flask was made up with distilled water to the mark. The absorbance of the solution was measured at a wavelength of 540nm relative to the blank. The measurements of the sample absorbance were used for the plotting of the calibration curve.

2.4 Ovariectomy

Female Wistar rats were bilaterally ovariectomized through the dorsal approach and using standard procedures, as previously described (243, 245). Briefly, animals were anaesthetized with Valium (10 mg/kg, i.p) and ketamine (50 mg/kg, i.p). The anaesthesia was confirmed by a reduction in respiratory rate and the lack of response following gentle pinching of footpad. Ventral incision was made through the skin on the right flank, and the ovary, oviduct, and top of the fallopian tubes were clamped and removed. Abdominal wall and Skin were sutured, and animals were returned to their cages. Comparable surgical procedure was performed in sham-operated rats, but ovaries were just palpated, not removed. Animals were administered with carprofen (Rimadyl®, 5 mg/kg s.c.) and amoxicillin (Clamoxyl®, 150mg /kg s.c.) for post-operative analgesia and antibiotic therapy, respectively, and monitored daily until confirmation of postsurgical recovery. They were infected 14 days after surgery, when endogenous hormonal decline was effective (243, 245).

2.5 Behavioural tests

2.5.1 Open field test (OFT)

The open field arena was a 50 cm high wooden box with 100 cm × 100 cm floor including a 40 cm × 40 cm central zone and a peripheral zone. In this test, a rat was placed facing the wall in a corner of the arena and the animal's activity was video recorded for 10 min. Vertical and horizontal activities were simultaneous video recorded using a computerized camera placed 130 cm above the arena with a 45° angle. The floor and walls of the arena were cleaned with 70% alcohol solution after each trial, to prevent bias due to olfactory cues.



Figure 10. Rat in the open field arena

Source: Personal, present work

The distance travelled in the arena, as well as the number of entries and time spent in the central zone and in corners were determined using motion tracking on image sequences in the Image Processing Toolbox® of MATLAB software (MathWorks, Natick, MA). The characteristics of episodes of stretch-attend posture (hindpaws stationary while the body is stretched forward for more than 3-sec), rearing (on hind paws and against wall), and grooming were scored from video recordings offline. Gait and head posture qualitative scores were also determined (0 to 9 based on the severity of alterations).

2.5.2 Elevated plus maze paradigm (EPM)

The EPM apparatus was raised 50 cm above ground level and consisted of two open arms (50 cm × 10 cm, no wall), two arms (50 cm × 10 cm) enclosed by wooden walls (40 cm high), and a common central platform (10 cm × 10 cm). Each rat was placed on the central platform facing an open arm and behaviour was recorded for 5-min. The performance on the EPM was recorded using a computerized video recording system including a camera placed 150 cm above the centre of the apparatus. After each trial, the floor and walls of the EPM were cleaned with a 70% ethanol solution. Video recordings were scored offline for the number of entries, time spent, and distance travelled in the arms, as well as episodes of head dipping above the open arm edge, grooming, and rearing. An entry occurred when all four limbs were within an arm.



Figure 11. Elevated plus maze

Source: Personal, present work

2.5.3 Footprint analysis (FPA)

The footprint analysis was performed for the assessment of motor abilities, in particular gait and balance (31, 246). Rats with inked paws were allowed to walk freely along an enclosed box (50 cm long, 10 cm wide, and 20 cm high walls) with a clean sheet of paper placed on the floor. For each animal, a valid trial over three consecutive trials was considered, in order to avoid abnormal patterns associated with the habituation phase (247). The footprint patterns and contacts were analysed, and the step width and length were determined using a computerized system.

2.6 Histopathological analyses

2.6.1 Blood sample processing

A thin blood smear was obtained by placing a drop of blood onto one end of a clean slide and by spreading it gently using the edge of a second slide. Then, blood smears were processed for May–Grünwald Giemsa, which makes it possible to observe the cytoplasm of monocytes, lymphocytes and the chromatin of the nuclei, as well as cells of mononuclear parasites such as *T. gondii* thanks to the May–Grünwald and the Giemsa, two neutral dyes which precipitate on the structures associated with cells (94). Standard procedures were used. Briefly, the blood smear previously mounted on a microscope slide was covered with 1ml of May–Grünwald in solution for 3 minutes; 1ml of buffer solution was carefully added and the mixture was left in contact for 1 minute. Excess dye was discarded by draining or rapid rinsing. The smear was covered with Giemsa R stain diluted 1/30 in a buffer (10 min); and the slide was quickly rinsed with

running water for 10 sec. Then, the stained smear was dehydrated and covered with a coverslip using the mounting medium DPX® (reference 4458, Sigma-Aldrich, Burlington, MA, USA). Observations of slides were made with a microscope with 40x (non-immersion) and 100x (immersion) objectives.

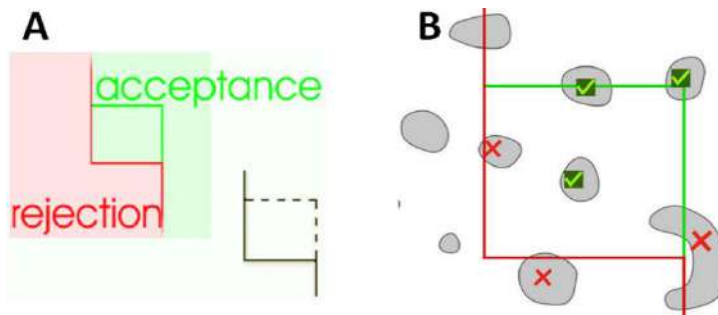


Figure 12. Method for cell counting in the blood

Source: www.stereology.info

A clear counting frame allowing objects' rigorous counting of cells was delimited (figure 12). Cells were counted using Cell Counter macro in the ImageJ software version 1.54g (National Institutes of Health, USA). To quantify the parasites against RBCs, the parasitized RBCs among 500-2,000 RBCs on the thin smear were counted and the results expressed as % parasitemia:

$$\% \text{ parasitemia} = (\text{parasitized RBCs}/\text{total RBCs}) \times 100$$

To quantify the circulating white blood cells (WBCs), the parasites were tallied against WBCs, until 500 parasites or 1,000 WBCs were counted, the results were expressed as parasites per microliter of blood, using the WBC count, or otherwise assuming 8,000 WBCs per microliter blood.

$$\text{Parasites/microliter blood} = (\text{parasites}/\text{WBCs}) \times \text{WBC count per microliter} <\text{or } 8,000>$$

The number of cysts present was also counted and expressed as cysts per microliter.

2.6.2 Tissue processing

Brains were cut in two halves following the cerebral hemispheres (sagittal plan). One half (either left or right, but the same for all animals) was processed for histopathological studies, while the other half was conserved for future studies. The half destined to histopathological studies were fixed for 2-h in Karnovsky's fixative (50% glutaraldehyde and formaldehyde in 0.2M PBS), then cut entirely in the transversal plane (thickness 5 μm). A series of sections were stained with hematoxylin and eosin (H&E) using standard protocols, and processed for microscopic examination to assess histopathological changes. Analyses were performed with a computerized light microscope (20x and 40x objectives).

2.6.2.1 Fixing and trimming

After sacrifice of the rats, the organs (brain, kidney, liver, and spleen) were removed and immersed in a fixative liquid (formaldehyde 10%, 10x the volume of the organ) for 8 hours (95). Then trimming, which consist of reducing the tissue into smaller regions for the study, was carried out.

Alcohol Dehydration: After fixation, the organs, were washed with phosphate buffer saline (pH=7.4) to remove formaldehyde. The organs were placed in cassettes on which was written the unique identifying number previously assigned to the animals from which the organs were collected. The brains were then dehydrated by immersion in ethanol baths (diluted with distilled water) of increasing concentration (50%, 70%, 96%, 100% and 100%)

Clarification: Before being cast in a mould containing paraffin melted by heating, we made our organs stay in xylene which is an alcohol-loving benzene hydrocarbon and not very polar can mix with both alcohol and paraffin. This state allows the realization of cuts thin and regular which requires dehydrated tissue because paraffin is hydrophobic (95).

Impregnation: Organs stayed in molten paraffin baths at 55-60°C in order to allow the occupation of liquid spaces by paraffin

Inclusion: We introduced the organ into moulds, while orienting the organ and filling the mould of molten paraffin, then we placed them on a cold surface and obtained paraffin blocks containing the organs ready for microtome sectioning.

Sections and tissue recovery: The paraffin blocks were cut in the transversal plane with a microtome and the obtained 4 μ m thick sections were collected in a water bath on microscope slides coated with a substance allowing greater adhesion of biological tissues by the manufacturer (silane).

2.6.2.2 H&E (Haematoxylin and eosin) staining

Hematoxylin and eosin (H&E) staining was performed on the sections previously mounted on slides to accentuate contrasts and better recognize plasma membranes (dark purple), nuclei (grey or dark pink) and cytoplasm (pink clear) cells. To do this, the sections were deparaffinized with xylene (1 minute immersion), rehydrated with decreasing concentrations of ethanol (diluted with water distilled: 100%, 96%, 70%, 50%, distilled water) to allow the action of the dyes which are in aqueous solution (95). After 10 minutes in haematoxylin, the slides were washed abundantly with running water then placed for a few moments in phosphate buffer until development by sections of dark blue colour. The slides were rinsed with distilled water then with warm water for three minutes. The sections were placed for 5 minutes in eosin, washed briefly in running water and next in 95% alcohol and in absolute alcohol, then put

briefly in xylene and the slide were placed in an incubator for one hour and mounted between slides and coverslip using DPX. The slides were observed at 20x, 40x and 100x objectives.

2.6.2.3 Nissl staining and stereological counts on brain sections

Three sections throughout the brain anterior zone including the anterior cingulate cortex, the brain posterior zone including the posterior parietal cortex, and the cerebellar zone including the dentate nucleus were selected using systematic random sampling, i.e. starting from a random point, then progressing with a fixed periodic interval (8 μ m in this study).

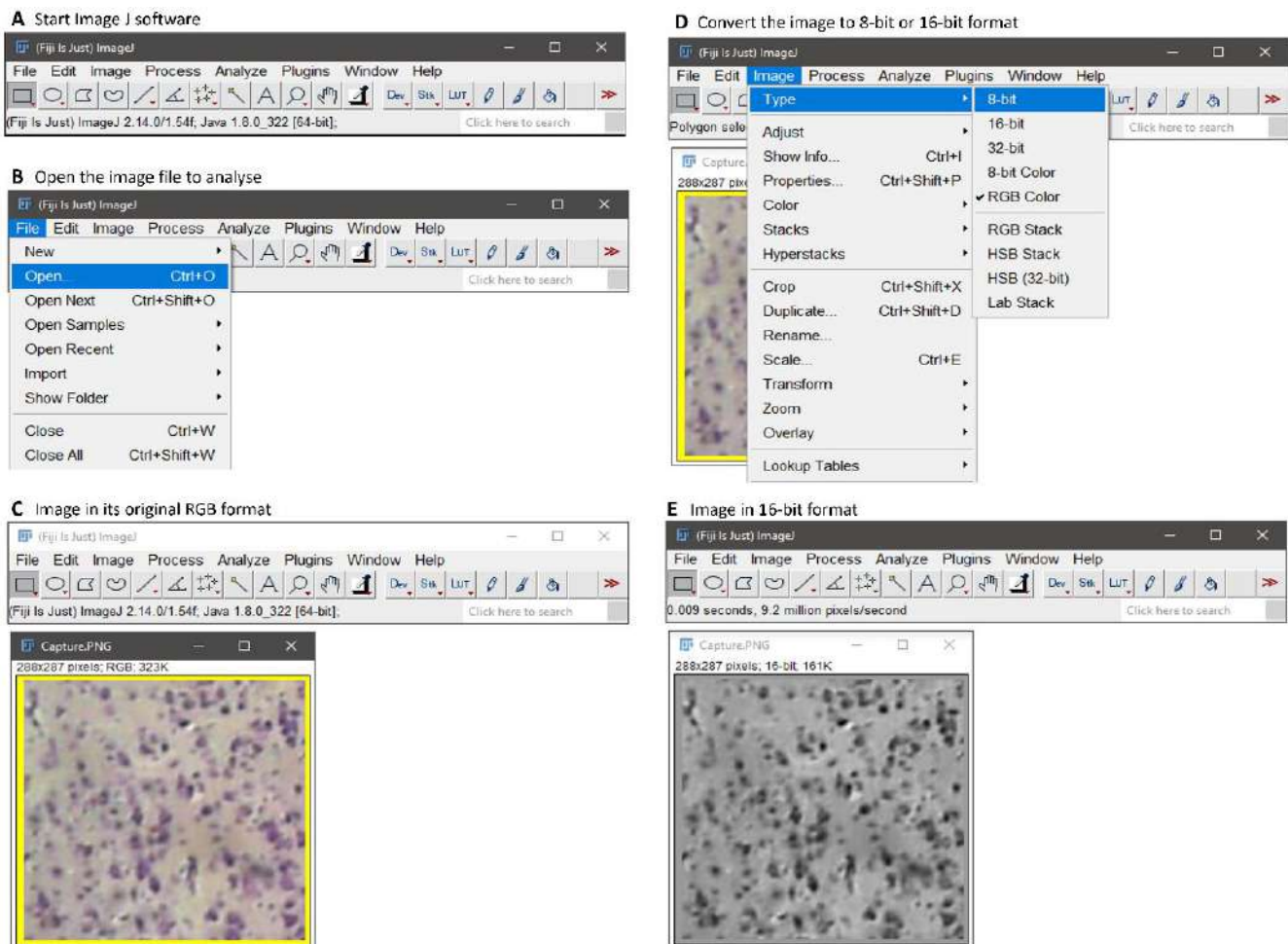


Figure 13. RGB image to obtain a 16-bit image

The selected sections were processed for cresyl violet (Nissl) staining using standard procedures. Briefly, after deparaffinizing with xylene (2x for 10 minutes), sections were hydrated by immersion in ethanol baths diluted with distilled water of decreasing concentration (100%, 100%, 96%, 70%, and 50%, 5 minutes for each step), stained by immersion in cresyl violet solution for 5 minutes (for 100 ml: 0.02g of cresyl violet acetate and 0.25 ml of glacial acetic acid in distilled water), rinsed in three changes of distilled water, dehydrated by immersion in ethanol baths of increasing concentration (50%, 70%, 96%, 100% and 100%), cleared in three changes of xylene, and mounted with DPX.

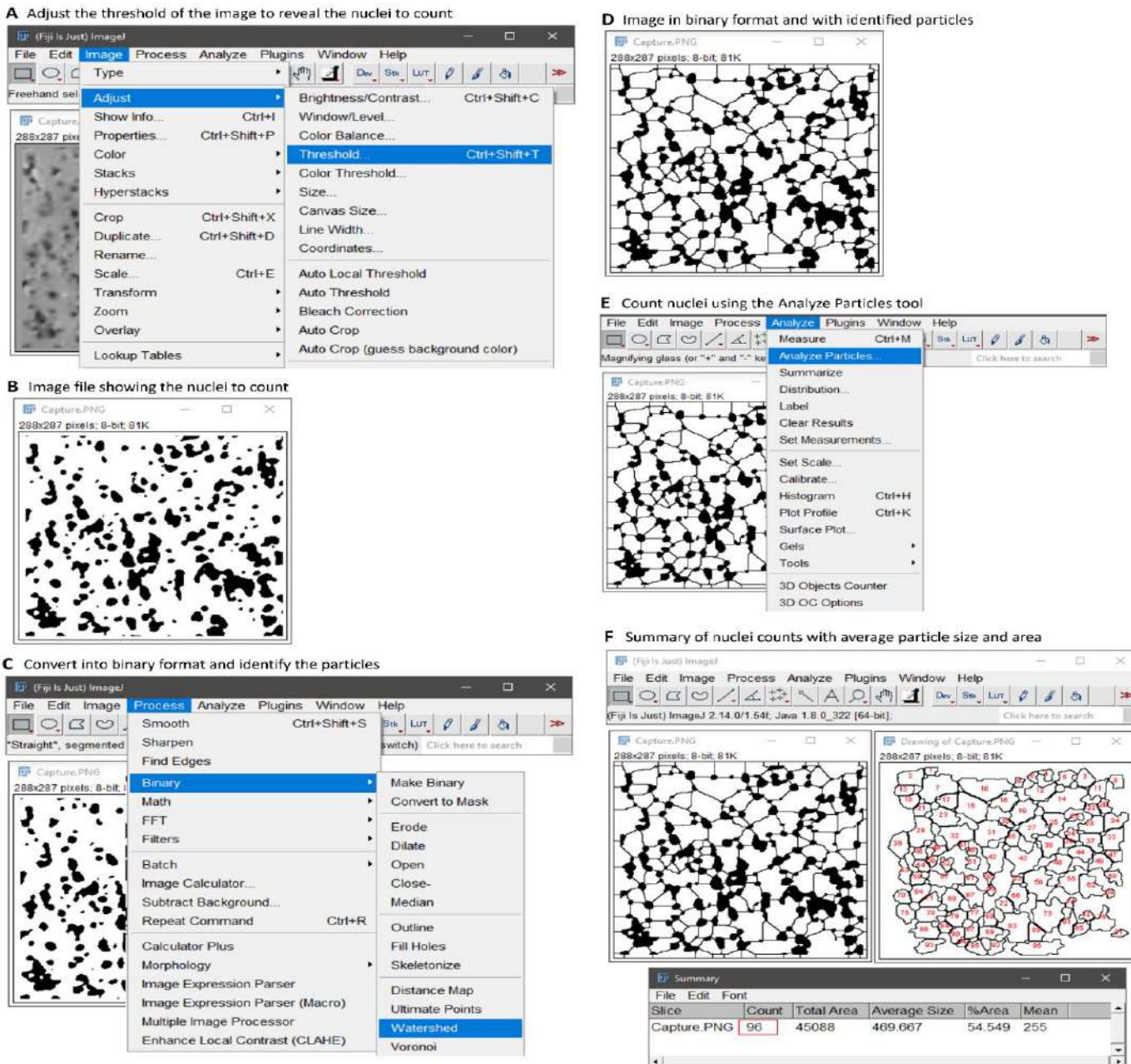


Figure 14. Binary image for automatic counts

Then neuron nuclei were counted: (i) in the anterior cingulate cortex and in the medial septal nucleus for brain anterior zone sections; (ii) in the posterior parietal cortex and around the fornix (perifornical area) in the lateral hypothalamic area for the brain posterior zone; and (iii) in the cerebellar molecular layer and dentate nucleus for the cerebellar zone. Neuron nuclei counts were performed on micrographs (taken at 40x objective) of the areas of interest using semi-automatic counting with ImageJ software. More specifically, neuron nuclei were counted automatically using Nucleus Counting macro of Image J as shown in figures 13 and 14. We did manual observation to check the particles counted to ensure that they all are neuron nuclei and that nuclei crossing the lower and left borders were discarded (figure 12). In addition to

neuron nuclei counts, ImageJ software automatically determined the average size of the nuclei counted and the percent of total area occupied by these nuclei.

2.7 Data analysis

Statistical significance of inter-group differences in body weight, body temperature, and cognitive and motor indicators revealed by footprint analysis, the EPM, and the OFT were assessed using one-way ANOVA, followed by Least Square Difference (LSD) test for inter-couple comparisons (OriginPro 8 software, OriginLab Co, Northampton, MA). Differences with $P < 0.05$ were considered significant. Data are presented as mean \pm SEM.

CHAPTER III: RESULTS

3.1 Cognitive disorders associated with chronic *T. gondii* infection in rats

3.1.1 Body weight, temperature, and blood glucose

Figure 15 shows the changes in body weight (figures 15A, B), body temperature (figure 15C), and blood glucose level (figure 15D) at 90 dpi.

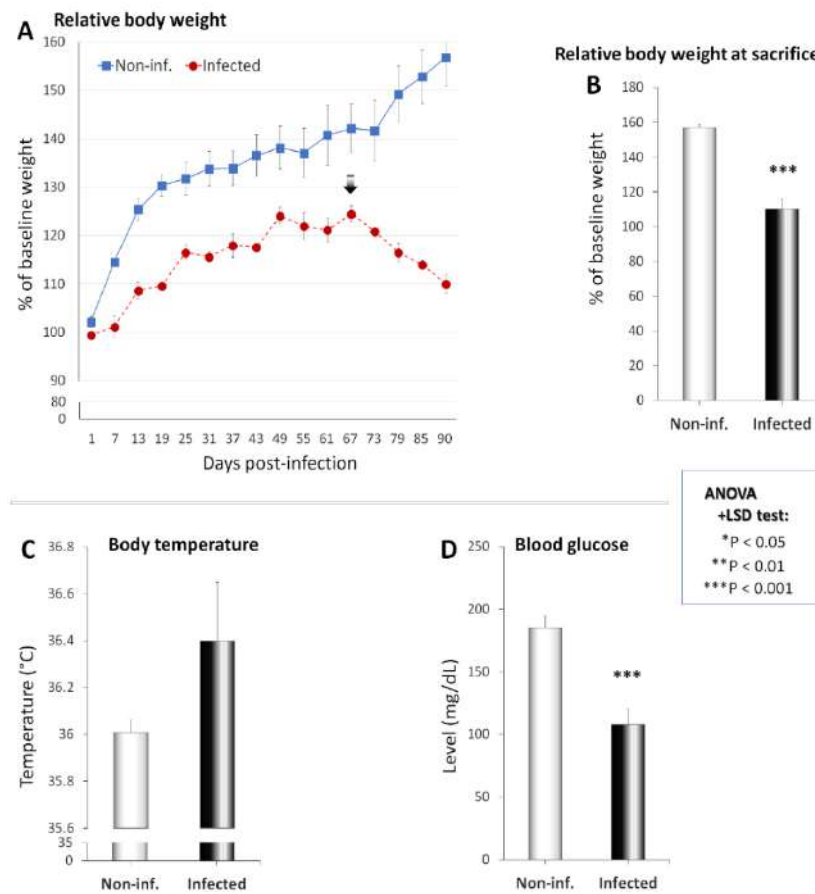


Figure 15. Body weight, temperature and blood glucose at 90 dpi

Note the curve inflection (arrow) at day 67 post-infection in infected animals (A).

The growth curve of non-infected rats was positive and was made of 3 linear epochs: a first one between day 1 and day 19 (curve equation: $y = 9.56x + 94.25$, $R^2 = 0.97$), a second slower between dpi 25 and 61 ($y = 1.34x + 130.68$, $R^2 = 0.91$), and a last one faster than the latter and slower than the first between dpi 67 and 90 ($y = 4.04x + 136.52$, $R^2 = 0.93$) (figure 15A). All along, the relative body weight was statistically significant compared to the baseline week values (table VI).

Instead, whereas the growth curve of infected rats also showed 3 linear epochs parallel to non-infected animals, some differences were observed (figure 15A). Although in a lesser extent, the fastest increase was also observed between day 1 and day 19 ($y = 3.81x + 95.23$, $R^2 = 0.90$), followed by an epoch of slower growth between dpi 25 and 61 ($y = 1.17x + 114.63$, $R^2 = 0.65$). However, an inflection point was observed around dpi 67, from which the body

weight started to decrease linearly ($y = -3.58x + 127.97$, $R^2 = 0.99$). The relative body weight that was significantly higher was restored to baseline values from 73 dpi (as indicated by lack of statistical difference) (table VI). Infected rats displayed lower increases in body weight than non-infected rats all along the study, particularly marked from 73 dpi where the decrease in body weight started (table VI).

Table VI. Body weight changes in infected rats over 90 days

Dpi	Compared to baseline		Infected vs. Non-infected
	Non-infected	Infected	
1	0.020*	0.334	0.018*
7	0.002**	0.048*	8.6E-4***
13	4.7E-4***	0.036*	4.6E-4***
19	0.001**	0.019*	0.007**
25	4.7E-4***	0.028*	0.006**
31	0.006**	0.017*	0.011*
37	0.001**	0.027*	0.010*
43	0.002**	0.012*	0.031*
49	0.004**	0.022*	0.040*
55	0.004**	0.043*	0.032*
61	0.001**	0.014*	0.020*
67	2.2E-4***	0.046*	0.030*
73	0.002**	0.068	0.003**
79	2.4E-4***	0.096	0.002**
85	0.001**	0.210	8.7E-4***
90	0.020*	0.334	0.018*

Dpi: day post-infection. ANOVA+LSD test: *P<0.05; **P<0.01; ***P<0.001.

The average relative body weight at sacrifice was significantly lower in infected rats compared to the non-infected ($P = 8.7E-4$) (figure 15B). An increase in body temperature was observed in infected rats, but with a high interindividual variability preventing statistical significance (figure 15C). On the other hand, the blood glucose level was significantly lower in the infected rats ($P = 0.006$ vs. non-infected rats) (table VII) (figure 15D).

3.1.2 Long-term infection effects on gait

The effects of long-term infection with *T. gondii* on gait quality indicators of rats are shown in figure 16. Unlike the non-infected, the *T. gondii*-infected animals seemed to use their anterior footpads more and their heels less, particularly at the front limbs (figures 16A, B). Compared to non-infected rats, the *T. gondii*-infected animals also had significant reductions in stride length ($P = 0.001$) (figure 16C) and step length ($P = 0.035$) (figure 16D), but only a slight and non-significant decrease in step width (table VII) (figure 16E).

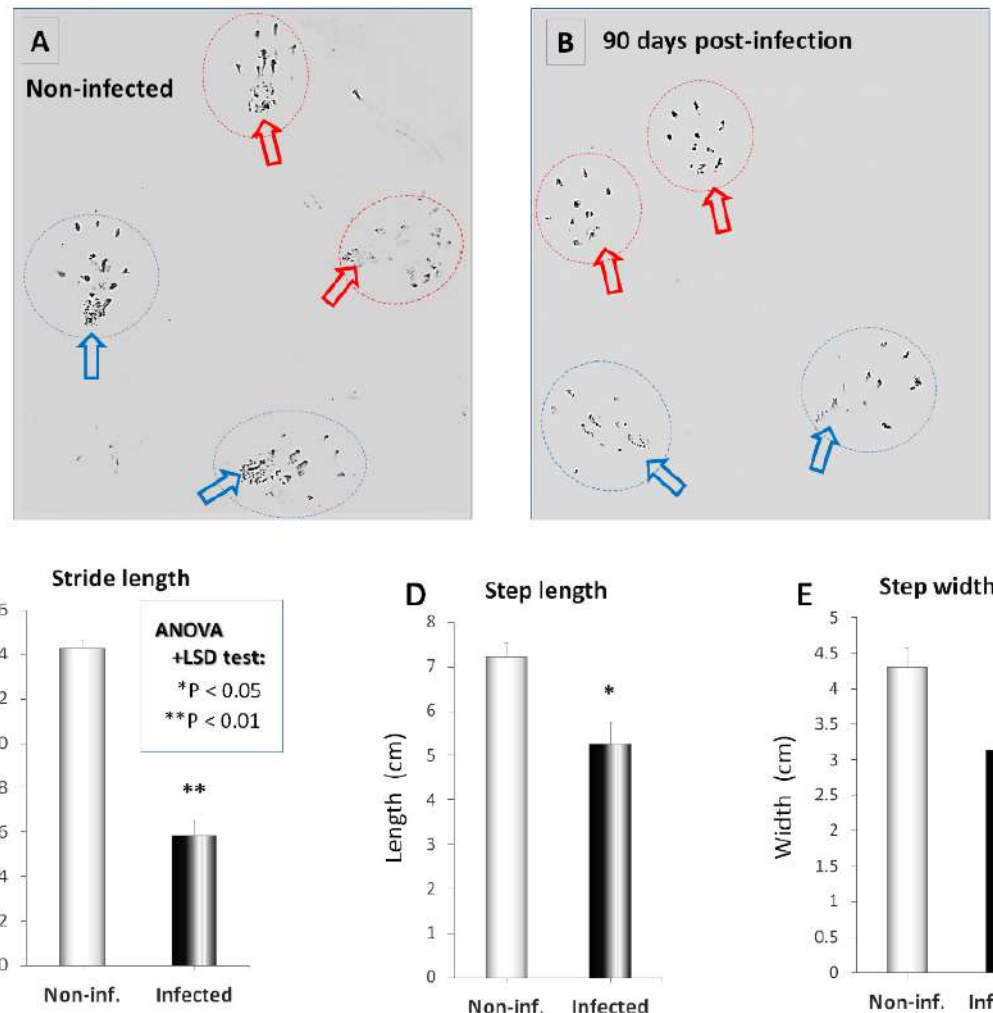


Figure 16. Gait quality indicators in the terminal stage

A, B. Footprints of representative non-infected (**A**) and *T. gondii*-infected (**B**) animals. Red (respectively blue) arrows indicate the front limbs (respectively the hindlimbs).

C-E. Average stride length (**C**), step length (**D**) and step width (**E**) of non-infected control animals and *T. gondii*-infected animals in the terminal stage of infection.

3.1.3 Long-term infection effects on organ weight

Figure 17 shows the effects of long-term infection with *T. gondii* on the relative organ weight of rats. Increases were observed in the brain, heart, and kidney relative weights of infected animals compared to the non-infected counterparts, however with a high interindividual variability preventing statistical significance (table VII) (figures 17A, B and F, respectively). Similarly, non-significant changes were observed in the relative weight of the lungs (figure 17C) and liver (figure 17D) (table VII). A significant decrease was observed in the relative weight of the spleen of infected animals ($P = 0.001$ vs. non-infected) (figure 17E).

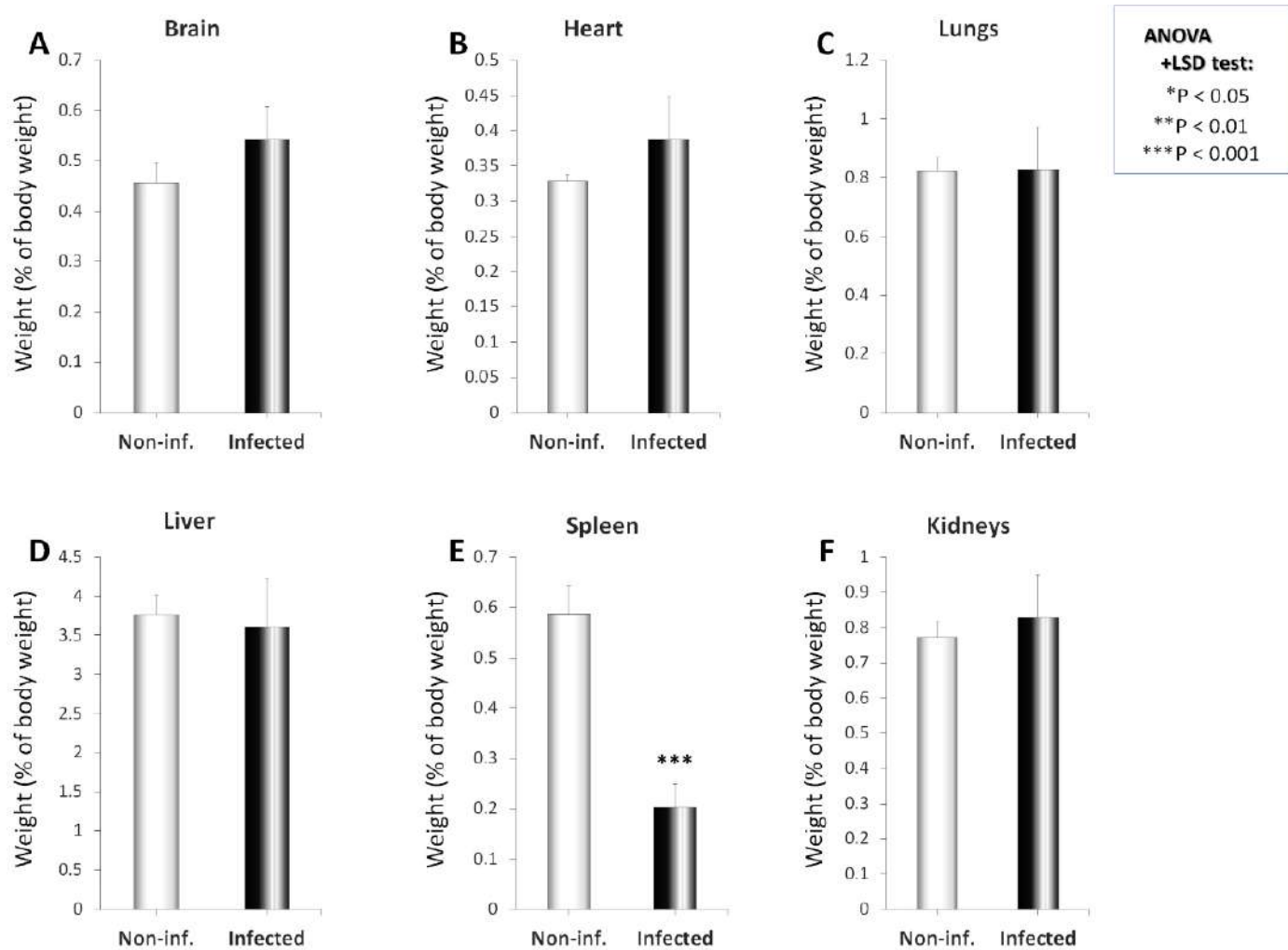


Figure 17. Organ weight relative to body weight in the terminal stage

Table VII. Physiological parameter and gait quality indicators changes

Infected	Infected	Infected	Infected
Body weight	Body temperature	Blood glucose	Stride length
Non-inf. 8.7E-4***	Non-inf. 0.258	Non-inf. 0.006**	Non-inf. 0.001**
Step length	Step width	Brain weight	Heart weight
Non-inf. 0.035*	Non-inf. 0.200	Non-inf. 0.336	Non-inf. 0.436
Lung weight	Liver weight	Spleen weight	Kidney weight
Non-inf. 0.974	Non-inf. 0.831	Non-inf. 7.7E-4***	Non-inf. 0.691

ANOVA+LSD test: *P<0.05; **P<0.01; ***P<0.001.

3.1.4 Long-term infection effects on OFT cognitive and motor indicators

3.1.4.1 Locomotion

Figure 18 shows the effects of long-term infection with *T. gondii* on locomotion and grooming-related parameters. Compared to non-infected, infected rats displayed significant decreases (table VIII) in the number of episodes of locomotion (figure 18A), in the distance covered

(figure 18B), and in the total time spent walking (figure 18C) in the arena. Non-statistically significant decreases were observed in the scores of head posture (figure 18H) and gait (figure 18I) of the infected animals compared to the non-infected (table VIII).

Table VIII. OFT motor function indicators of infected rats in the terminal stage

Infected Locomotion episode, n	Infected Distance covered	Infected Locomotion time
Non-inf. 3.0E-5***	Non-inf. 0.010*	Non-inf. 1.1E-4***
Grooming latency	Grooming episodes, n	Grooming time
Non-inf. 0.012*	Non-inf. 0.130	Non-inf. 0.096
Paw licking episodes, n	Head posture score	Gait score
Non-inf. 0.003**	Non-inf. 0.075	Non-inf. 0.075

ANOVA+LSD test: *P<0.05; **P<0.01; ***P<0.001.

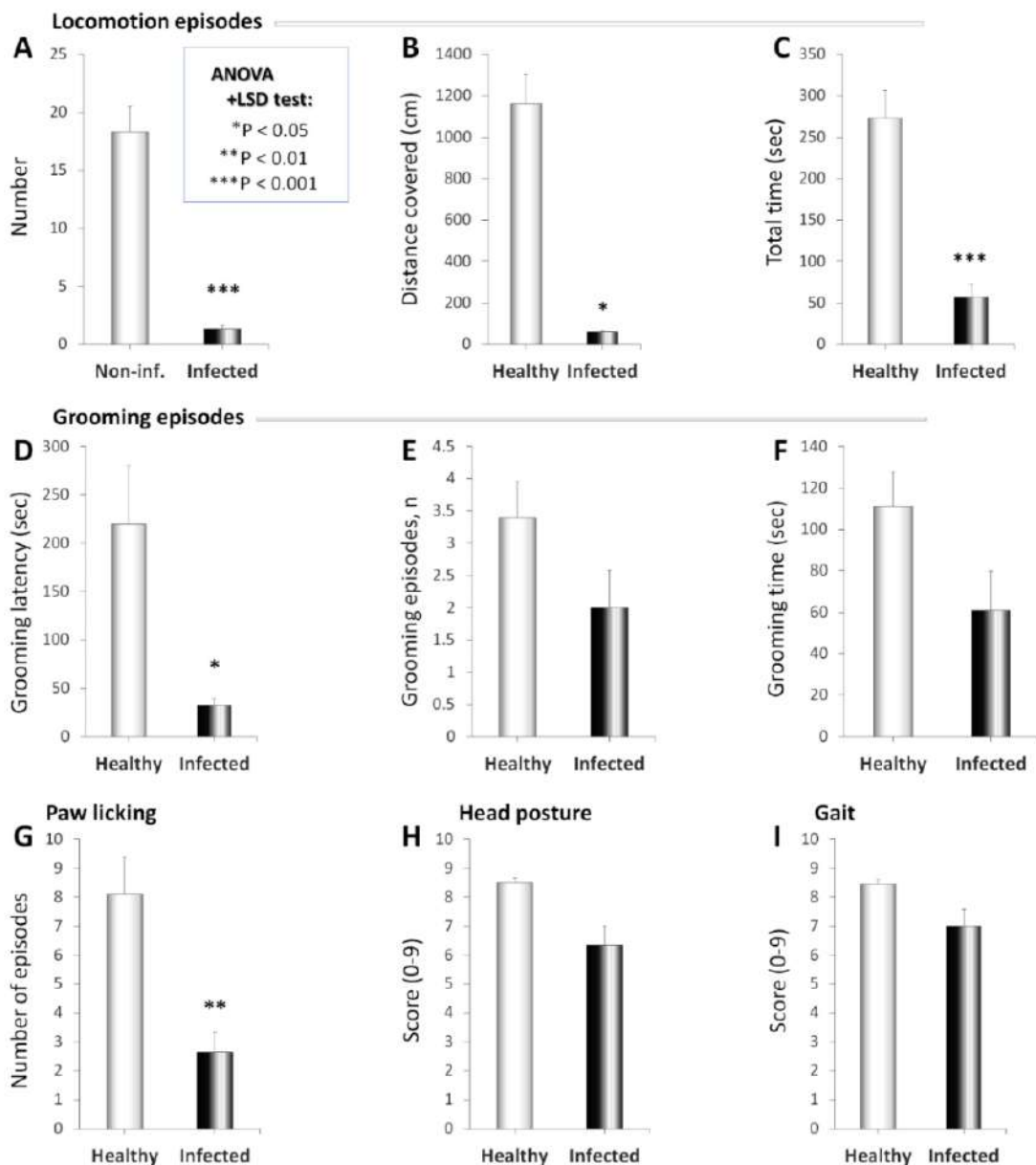


Figure 18. Locomotion and grooming-related parameters in the terminal stage

Besides, compared to the non-infected, the infected rats displayed significant decreases (table VIII) in grooming latency (figure 18D) and paw licking (figure 18G), as well as non-statistically significant decreases in grooming episode number (figure 18E) and time (figure 18F).

3.1.4.2 Rearing episodes

The rearing activities and arena angle time of long-term infected rats are shown in figure 19. The number of entries in the arena angles of infected rats was reduced significantly compared to the non-infected rats (table IX, figure 19A). Also compared to the non-infected group, the infected group spent a significantly higher time in the arena angles (table IX, figure 19B).

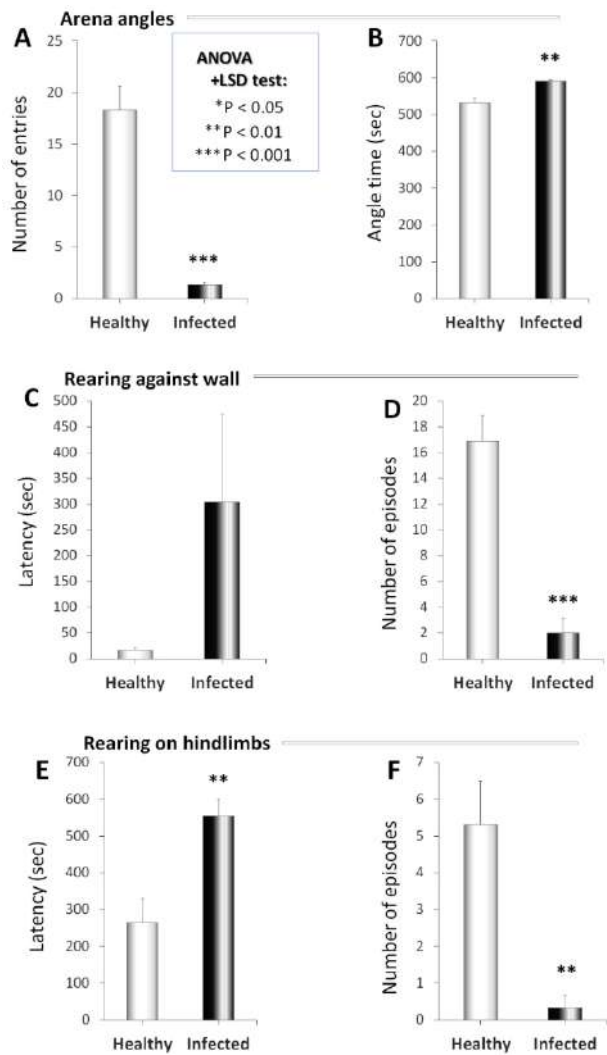


Figure 19. Rearing activities and arena angle time in the terminal stage

While an increase with high interindividual variability was observed in the latency to the first episode of rearing against wall (figure 19C), the infected rats showed a significant decrease in the number of episodes of rearing against walls ($P < 0.001$ compared to the non-infected rats) (table IX) (figure 19D). In addition, the latency to the first episode of rearing on hindlimbs was significantly increased (figure 19E) and the number of episodes of rearing on hindlimbs markedly decreased (figure 19F) in the infected rats compared to the non-infected rats (table IX).

Table IX. Rearing and arena angle entries in the terminal stage

Infected	Infected	Infected
Angle entries	Angle time	Rearing against wall latency
Non-inf. 4.1E-5***	Non-inf. 0.001**	Non-inf. 0.235
Rearing against walls, n	Rearing on hindlimb latency	Rearing on hindlimb, n
Non-inf. 5.6E-5***	Non-inf. 0.005**	Non-inf. 0.002**

ANOVA+LSD test: *P<0.05; **P<0.01; ***P<0.001.

3.1.4.3 Arena centre and close to wall activities

Figure 20 shows the effects of long-term infection with *T. gondii* on the arena centre and close to wall activities of rats. A significant increase ($P < 0.001$) in the latency to enter the arena centre (figure 20A), a significant ($P < 0.01$) reduction in the distance covered in the arena centre (figure 20B), as well as significant decreases ($P < 0.001$) in the number of entries in the arena centre (figure 20C) and in the time spent in the arena centre (figure 20D) were observed in the infected rats compared to the non-infected (table X).

Table X. Centre activities and stretched-attend posture in the terminal stage

Infected	Infected	Infected
Arena centre latency	Arena centre distance	Arena centre entries
Non-inf. 9.0E-6***	Non-inf. 0.001**	Non-inf. 2.0E-4***
Arena centre time	Distance covered close to walls	Close to wall area entries
Non-inf. 3.8E-4***	Non-inf. 2.9E-5***	Non-inf. 0.001**
Close to wall time	Stretched-attend posture latency	Stretched-attend posture time
Non-inf. 3.3E-9***	Non-inf. 0.002**	Non-inf. 1.1E-5***

ANOVA+LSD test: *P<0.05; **P<0.01; ***P<0.001.

The infected rats showed a significant decrease ($P < 0.01$ compared to non-infected rats, table X) in the latency to the first episode of stretched-attend posture in the arena (figure 20E) and a significant increase ($P < 0.001$) in the stretched-attend posture total time (figure 20F). In addition, infected rats displayed significant reductions ($P < 0.01$ compared to non-infected rats, table X) in the distance covered (figure 20G), in the number of entries (figure 20H), and in the total time spent (figure 20I) in the area close to the walls.

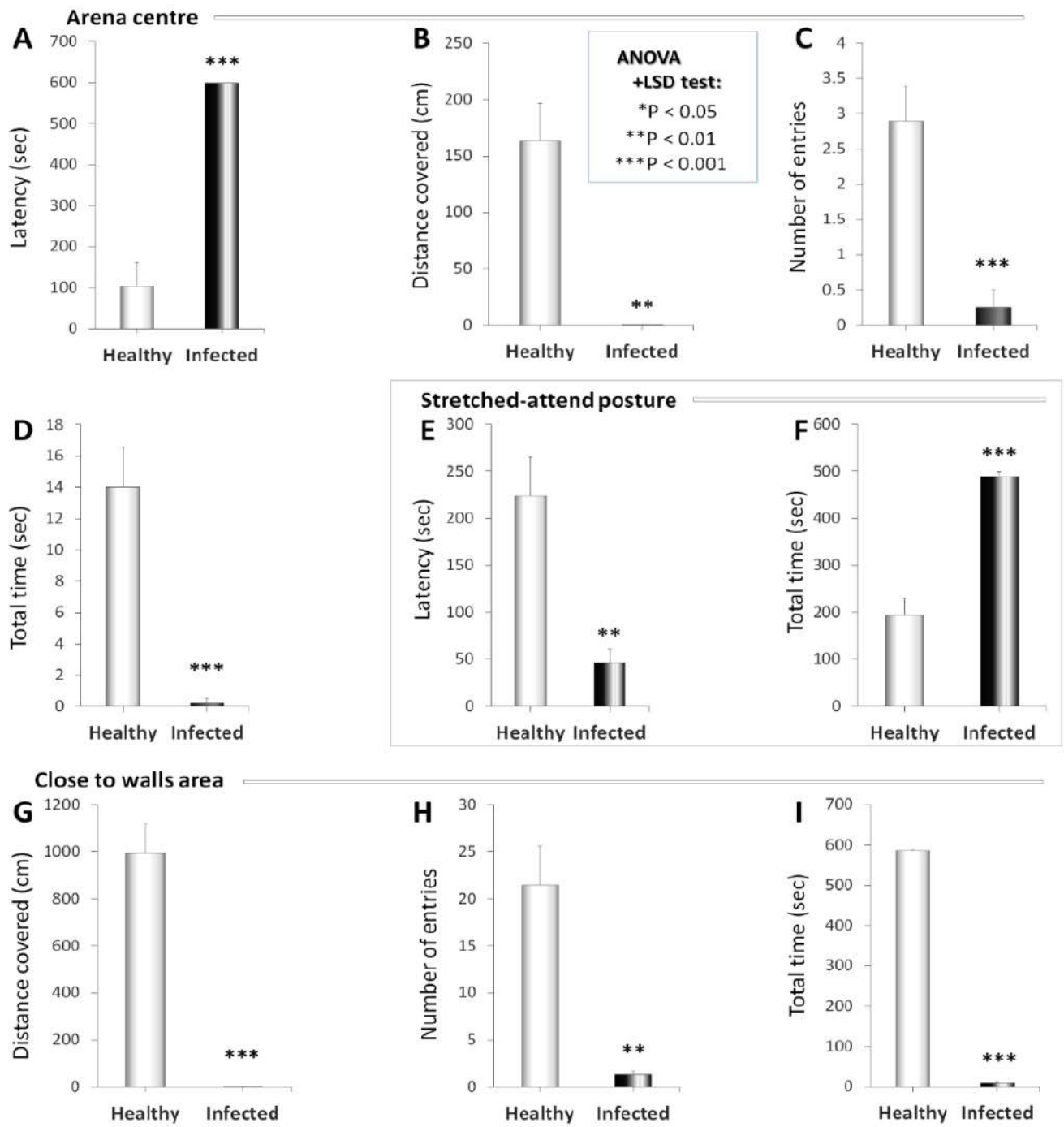


Figure 20. Arena centre and close to wall activities in the terminal stage

3.1.5 Long-term infection effects on EPM cognitive and motor indicators

3.1.5.1 Motor function indicators

Figure 21 shows the effects of long-term infection with *T. gondii* on EPM motor indicators. Compared to non-infected, infected rats displayed significant decreases (table XI) in the distance covered in the maze (figure 21A), both in the first (figure 21B), and last (figure 21C) minutes. Decreases in the time spent active were observed overall (figure 21D) and in the first minute (figure 21E), but only in a lesser extent in the last minute (figure 21F) where the difference was not statistically significant (table XI). Similarly, the speed in the maze was

significantly decreased (figure 21G), particularly in the first minute (figure 21H) but not in the last minute where a high interindividual variability was observed (figure 21I) (table XI).

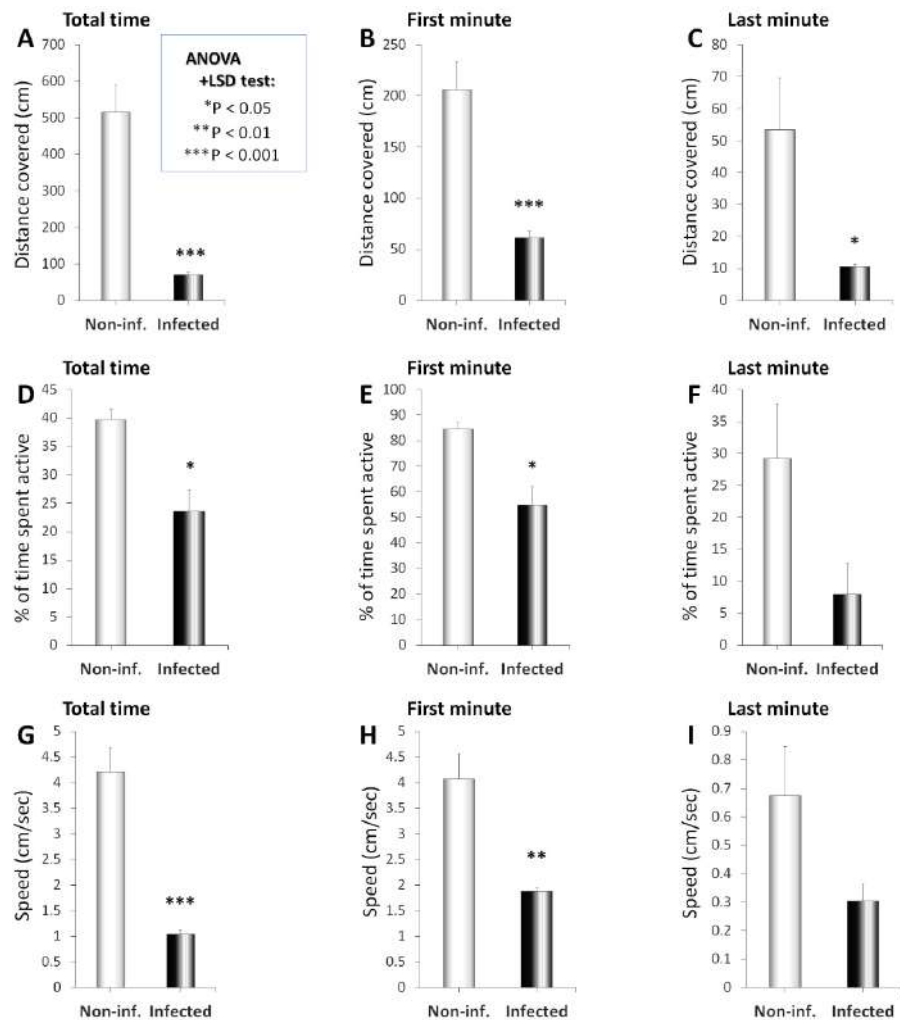


Figure 21. EPM motor indicators in the terminal stage

Table XI. EPM motor function indicators of infected rats in the terminal stage

Infected	Infected	Infected
Total distance covered	Total activity time	Total average speed
Non-inf. 1.9E-4***	Non-inf. 0.032*	Non-inf. 8.4E-5***
1st min distance	1st min activity time	1st min speed
Non-inf. 3.9E-4***	Non-inf. 0.039*	Non-inf. 0.002**
4th min distance	4th min activity time	4th min speed
Non-inf. 0.027*	Non-inf. 0.056	Non-inf. 0.069

ANOVA+LSD test: *P<0.05; **P<0.01; ***P<0.001.

3.1.5.2 Arm latency and time

Figure 22 shows the effects of long-term infection with *T. gondii* on EPM arm latency and time.

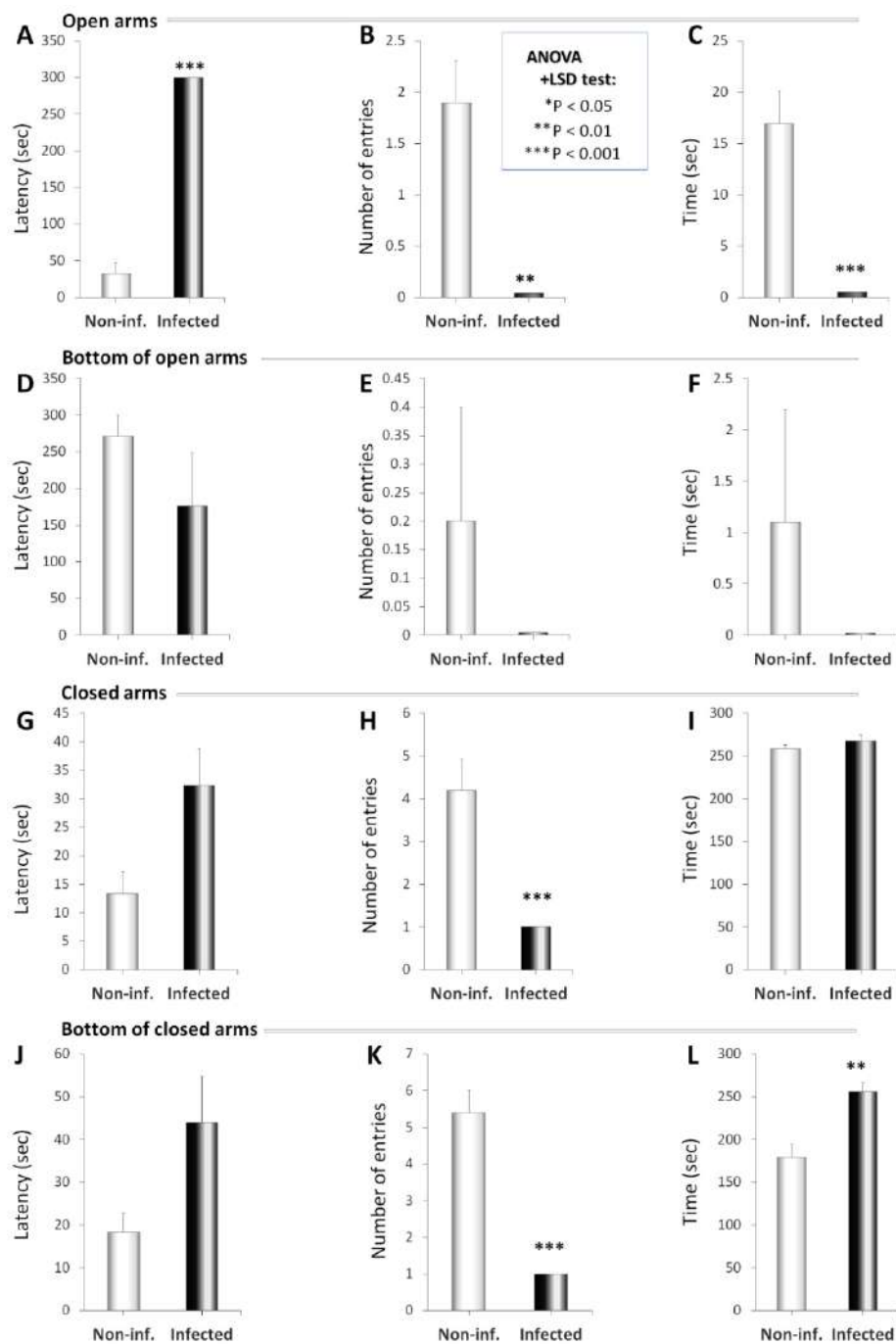


Figure 22. EPM arm latency and time in the terminal stage

The infected rats had a significantly higher latency time to the first exploration of the open arms ($P < 0.001$ compared to the non-infected rats, table XII) (figure 22A), significantly lower number of entries (figure 22B) and time spent (figure 22C) in the open arms. No significant change was observed in the latency to explore the bottom of the open arms, but compared to the non-infected (figure 22D), the infected rats displayed a very low number of entries in the bottom of the open arms (figures 22E, F). Increases were observed in the latency to enter the closed arms (figure 22G) and their bottom (15J), but with a high interindividual variability (table XII).

Table XII. Arm entry time and latency of infected rats in the terminal stage

Infected	Infected	Infected
Open arm latency	Open arm entries	Open arm time
Non-inf. 1.2E-8***	Non-inf. 0.001**	Non-inf. 0.001**
Open arm bottom latency	Open arm bottom entries	Open arm bottom time
Non-inf. 0.319	Non-inf. 0.343	Non-inf. 0.343
Closed arm latency	Closed arm entries	Closed arm time
Non-inf. 0.073	Non-inf. 0.002**	Non-inf. 0.305
Bottom of CA latency	Bottom of CA entries	Bottom of CA time
Non-inf. 0.130	Non-inf. 6.9E-5***	Non-inf. 0.002**

ANOVA+LSD test: *P<0.05; **P<0.01; ***P<0.001. CA. Closed arms.

The number of entries in the closed arms (figure 22H) and in their bottom (figure 22K) were significantly decreased in the infected rats compared to the non-infected (table XII). While no marked change was observed in the time spent in the closed arms (figure 22I), a statistically significant increase was observed in the time spent in the bottom of the closed arms (figure 22L) (table XII).

3.1.5.3 Head dipping and rearing episodes

Figure 23 shows the effects of long-term infection with *T. gondii* on head dipping and rearing episodes in the EPM maze. The infected rats showed a higher but non-statistically significant latency to the first head dipping episode compared to the non-infected rats (table XIII) (figure 23A). Instead, they had significantly lower episode numbers (figure 23B) and time spent in head dipping posture (figure 23C).

Also compared to the non-infected rats, the infected rats showed a non-statistically significant increase in the latency to the first episode of rearing against wall (figure 23D), and a significant decrease (P < 0.001 compared to the non-infected rats) in rearing against wall episode number (figure 23E) (table XIII). In addition, the infected rats had a significantly higher latency to the first rearing on hindlimbs (P < 0.05 compared to the non-infected rats, table XIII) (figure 23F) and a markedly small number of episodes of rearing on hindlimbs (figure 23G).

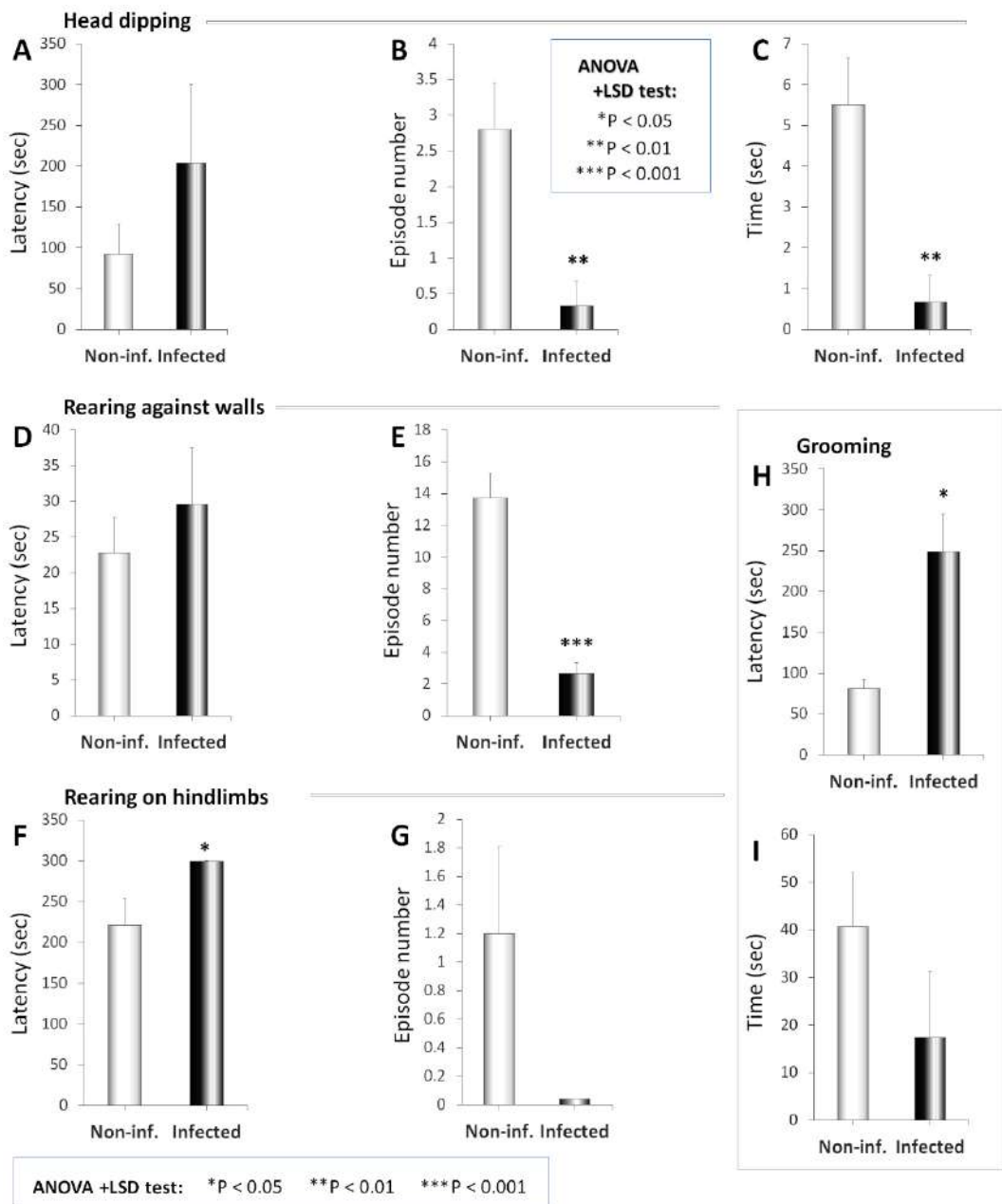


Figure 23. Head dipping and rearing in the maze in the terminal stage

Furthermore, the latency to the first grooming episode in the maze was increased in the infected rats ($P < 0.05$ compared to the non-infected, table XIII) (figure 23H), and a decrease with high interindividual variability was observed in the total time they spent grooming (figure 23I).

3.1.5.4 Central platform and stretched-attend posture

Figure 24 shows the effects of long-term infection with *T. gondii* on EPM maze central platform entries and stretched-attend posture (SAP) episodes. The infected rats, compared to the non-infected, had a significantly lower number of entries in the central platform of the maze

($P < 0.001$, table XIII) (figure 24A) and a slight and non-statistically significant increase in the time spent in the central platform (figure 24B).

Table XIII. Head dipping and thigmotaxis indicators in the terminal stage

	Infected	Infected
Head dipping latency		
Non-inf	0.369	
Head dipping time		
Non-inf	0.004**	
Rearing against walls, n		
Non-inf	4.6E-5***	
Rearing on hindlimbs, n		
Non-inf	0.081	
Central platform time		
Non-inf	0.375	
SAP at CA entrance, n		
Non-inf	0.009**	
Grooming latency		
Non-inf.	0.030*	
		0.251

ANOVA+LSD test: * $P < 0.05$; ** $P < 0.01$; *** $P < 0.001$. CA: Closed arms. SAP: Stretched-attend posture.

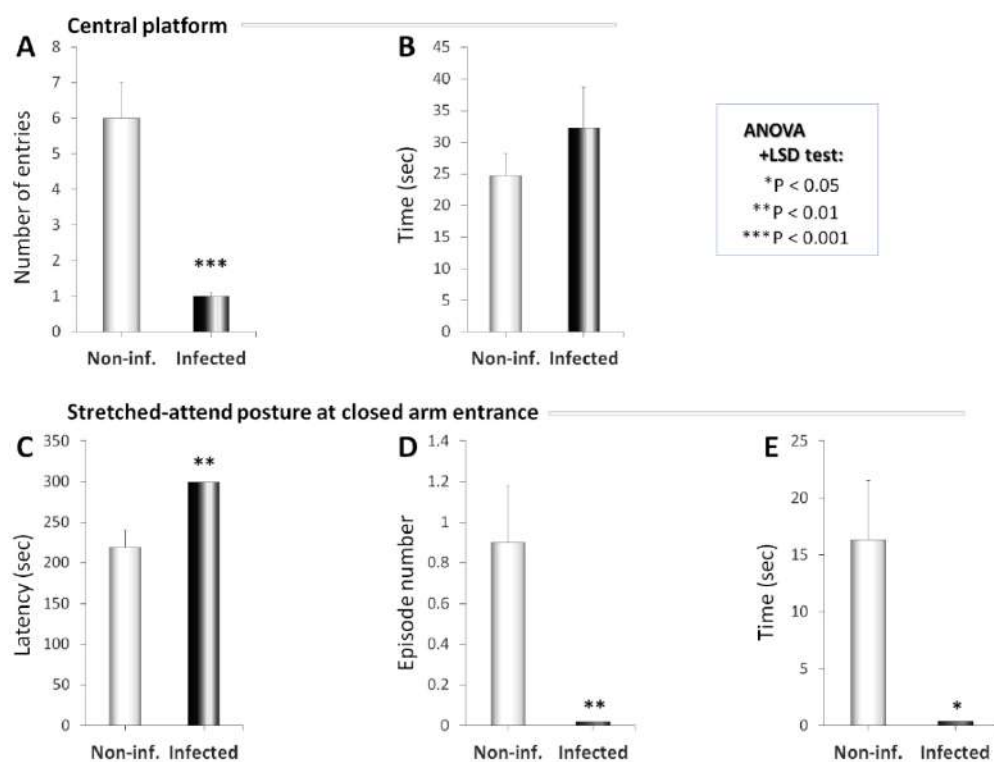


Figure 24. Central platform entries and attend posture in the maze in the terminal stage

On the other hand, also compared to the non-infected, the infected rats showed a significant increase in the latency to the first episode of stretched-attend posture at closed arm

entrance (figure 24C) (table XIII) and very few episodes of stretched-attend posture at closed arm entrance (figure 24D, E).

3.2 Diet, ovariectomy and *T. gondii* infection course in rats

3.2.1 Physiological parameters and gait

3.2.1.1 Body weight changes

Figure 25 presents the progression of the relative body weight (figure 25A), the relative body weight at sacrifice (figure 25B), as well as the body temperature (figure 25C), the blood glucose level (figure 25D), and the number of faecal boli emitted during the open-field test (figure 25E).

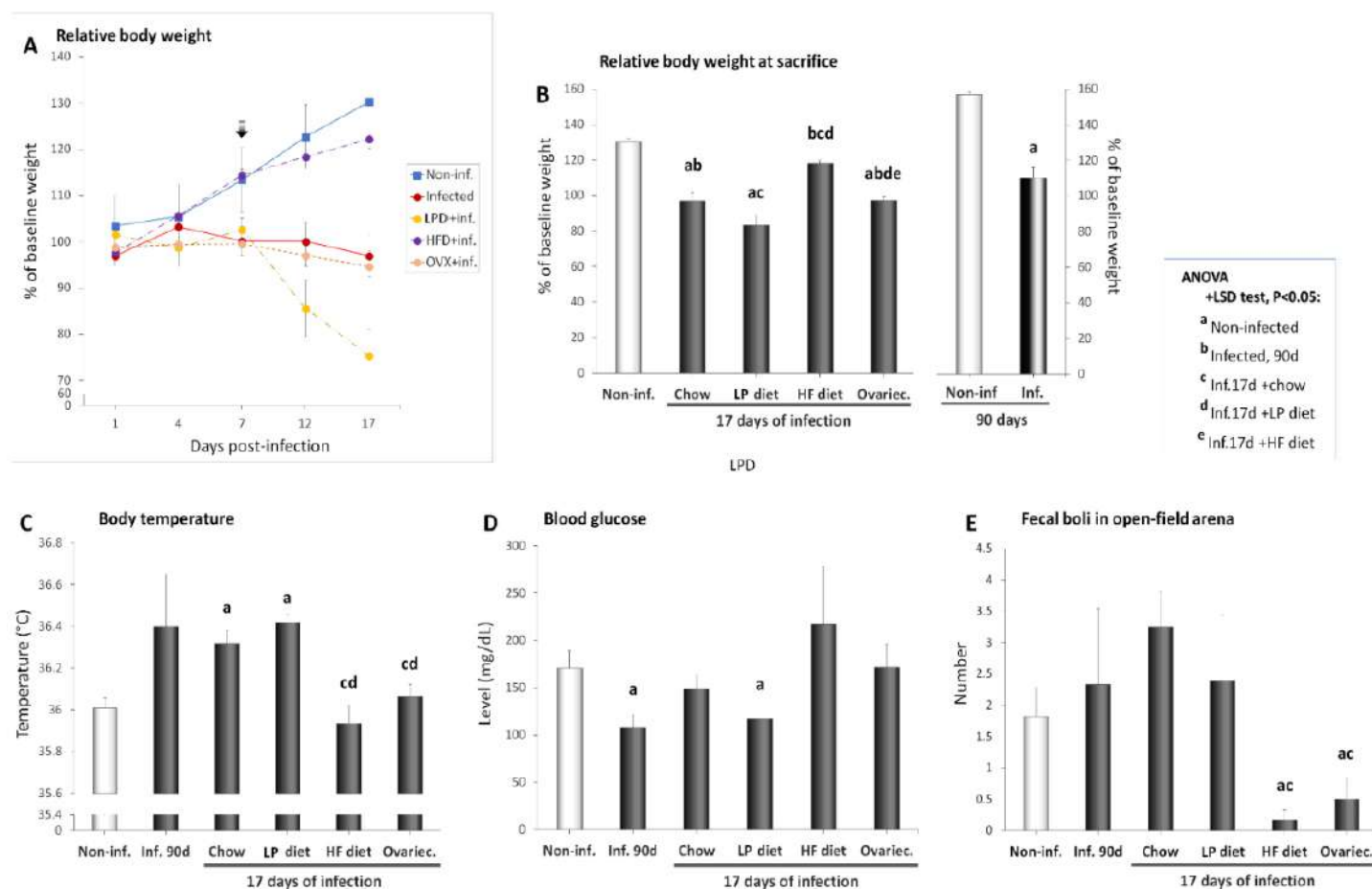


Figure 25. Body weight, temperature and blood glucose 17 days post-infection

Note the curve inflection (arrow) at day 7 post-infection in infected rats fed low-protein diet (A).

The non-infected animal group displayed a linear increase in relative body weight along the study ($y = 7.09x + 93.75$, $R^2 = 0.97$), as the infected group fed HFD, although the relative body weight of the latter grew slower ($y = 6.17x + 93.11$, $R^2 = 0.96$) (figure 25A). From 4 dpi, the relative body weights of these animals were statistically significant compared to baseline

values (table XIV). Instead, the infected groups displayed only slight increases in relative body weight in the first days after infection, with linear decreases from day 4 for the infected group control ($y = -1.90x + 104.82$, $R^2 = 0.91$) and for the infected ovariectomized rats ($y = -1.68x + 101.85$, $R^2 = 0.88$) (figure 25A). The relative body weights of these animals remained comparable to the baseline values, as indicated by the lack of a statistically significant differences (table XIV). However, the infected group fed LPD showed a polynomial progression ($y = -2.55x^2 + 8.74x + 94.57$, $R^2 = 0.92$) with an inflection point at 7 dpi from which a linear decrease 7-fold faster than the infected control started ($y = -13.63x + 115.07$, $R^2 = 0.98$) (figure 25A). Compared to baseline values, significant decreases in relative body weight were observed in the infected animals fed LPD (table XIV)

Table XIV. Body weight changes in infected rats over 17 days

	Days post-infection				
	1	4	7	12	17
Intra-group vs. day 1					
Non-infected	0.084	3.5E-5***	9.6E-7***	3.6E-8***	
Infected, 17d	0.846	0.409	0.550	0.239	
LPD+Inf.17d	0.011*	0.721	0.018*	0.001**	
HFD +inf.17d	0.297	1.6E-4***	2.0E-4***	1.7E-4***	
OVX +inf.17d	0.726	0.392	0.086	0.074	
Compared to non-infected group					
Infected, 17d	0.020*	0.846	0.409	0.550	0.239
LPD+Inf.17d	0.279	0.011*	0.721	0.018*	0.001**
HFD +inf.17d	0.079	0.297	1.6E-4***	2.0E-4***	1.7E-4***
OVX +inf.17d	0.217	0.726	0.392	0.086	0.074
Compared to Infected (17d) group					
LPD+Inf.17d	0.092	0.471	0.093	0.098	0.003**
HFD +inf.17d	0.812	0.004**	1.2E-6***	4.6E-7***	3.2E-7***
OVX +inf.17d	0.582	0.639	0.448	0.575	0.972
Compared to infected animals fed low-protein diet					
HFD +inf.17d	0.911	0.060	0.001**	4.7E-4***	6.7E-4***
OVX +Inf.17d	0.721	0.599	0.518	0.670	0.962
Compared to infected animals fed high-fat diet					
OVX +inf.17d	0.495	0.610	0.492	0.299	0.755

OVX: ovariectomy. ANOVA+LSD test: *P<0.05; **P<0.01; ***P<0.001.

Except for animals fed HFD, the average relative body weight of all the infected animals sacrificed at 17 dpi were significantly lower compared to non-infected animals ($P < 0.001$, table XV). Relative body weights were 35.09%, 57.14%, and 34.81% lower than non-infected group values, respectively for the infected control, the animals fed LPD, and the ovariectomized (figure 25B). The average relative body weight of the group sacrificed at the terminal stage of the infection (90 days) was 42.42% lower compared to non-infected group

(figure 25B, $P = 0.016$). Instead, the average relative body weight of animals fed HFD was only 10.65% lower than non-infected group values (figure 25B), and was significantly higher than values of other infected animals (table XV).

Table XV. Physiological parameter changes in infected rats at 17 dpi

		17 days post-infection				
		Inf. 90d	+Chow	+LPD	+HFD	+OVX
Relative body weight at sacrifice						
Non-inf.	0.016*	6.0E-6***	4.7E-6***	0.294	4.4E-8***	
Inf. 90d		0.048*	0.211	0.012*	0.048*	
Chow			0.030*	2.1E-4***	0.283	
LPD				1.2E-5***	0.003**	
HFD					0.001**	
Body temperature						
Non-inf.	0.258	0.001**	1.1E-5***	0.456	0.447	
Inf. 90d		0.776	0.944	0.197	0.315	
Chow			0.188	0.004**	0.010*	
LPD				0.001**	6.5E-4***	
HFD					0.221	
Blood glucose level						
Non-inf.	0.018*	0.365	0.020*	0.498	0.985	
Inf. 90d		0.070	0.567	0.139	0.104	
Chow			0.088	0.323	0.471	
LPD				0.167	0.145	
HFD					0.514	
Faecal boli number in open-field arena						
Non-inf.	0.719	0.064	0.625	0.005**	0.037*	
Inf. 90d		0.540	0.968	0.211	0.263	
Chow			0.494	1.7E-4***	7.5E-4***	
LPD					0.142	
HFD					0.408	

OVX: ovariectomy. ANOVA+LSD test: * $P < 0.05$; ** $P < 0.01$; *** $P < 0.001$.

3.2.1.2 Body temperature, blood glucose levels and faecal boli

A high interindividual difference was observed in the average body temperature at sacrifice of the group of rats infected after 90 days of infection, while two groups of infected animals sacrificed at 17 dpi, namely animals fed HFD and ovariectomized animals, displayed body temperatures comparable to non-infected animals (figure 25C, table XV). On the other hand, infected control group and animals fed LPD presented with significant increases in body temperature at sacrifice compared to the non-infected group and to other infected groups sacrificed at 17 dpi (figure 25C, table XV). In addition, the blood glucose levels at sacrifice of

rats sacrificed at 17 dpi were comparable with non-infected group levels (figure 25D, table XV), except for animals fed LPD that displayed significant decreases ($P = 0.020$ compared to non-infected group). Significant decreases were also observed in animals sacrificed around 90 dpi ($P = 0.018$ compared to non-infected group) (figure 25D). Instead, while most infected animal groups showed increases with high interindividual differences in the faecal boli emitted in the open-field test performed the day before sacrifice, hence increases without statistically significant differences (table XV), infected animals fed HFD and ovariectomized animals displayed significant decreases in the faecal body number (figure 25D, table XV).

3.2.1.3 Gait quality indicator changes

Figure 26 shows gait quality indicator changes. As shown for representative cases (figures 26A-F) the analysis of footprints revealed that unlike non-infected animals (figure 26A), all the infected animals presented with a tendency to use their anterior footpads more and their heels less during locomotion (figures 26B-F). This alteration was particularly marked in infected animals sacrificed after 90 days (figure 26B) and in animals fed LPD (figure 26D).

Significant decreases were observed in the average lengths of strides (figure 26G) and steps (figure 26H) of all infected groups compared to the non-infected control group ($P < 0.001$, table XVI). However, the decrease in stride length of the infected control was significantly less marked than the other infected groups ($P < 0.01$, table XVI). The decrease in step length was comparable between all infected groups, except for animals fed LPD that displayed statistically lower lengths compared to animals fed HFD and ovariectomized animals (figure 26H, table XVI). Instead, the widths of the steps were significantly lower compared to the non-infected control group for infected control groups sacrificed at 17 dpi and 90 dpi and for animals fed LPD, but not for animals fed HFD and ovariectomized animals that displayed high interindividual variabilities (figure 26I, table XVI).

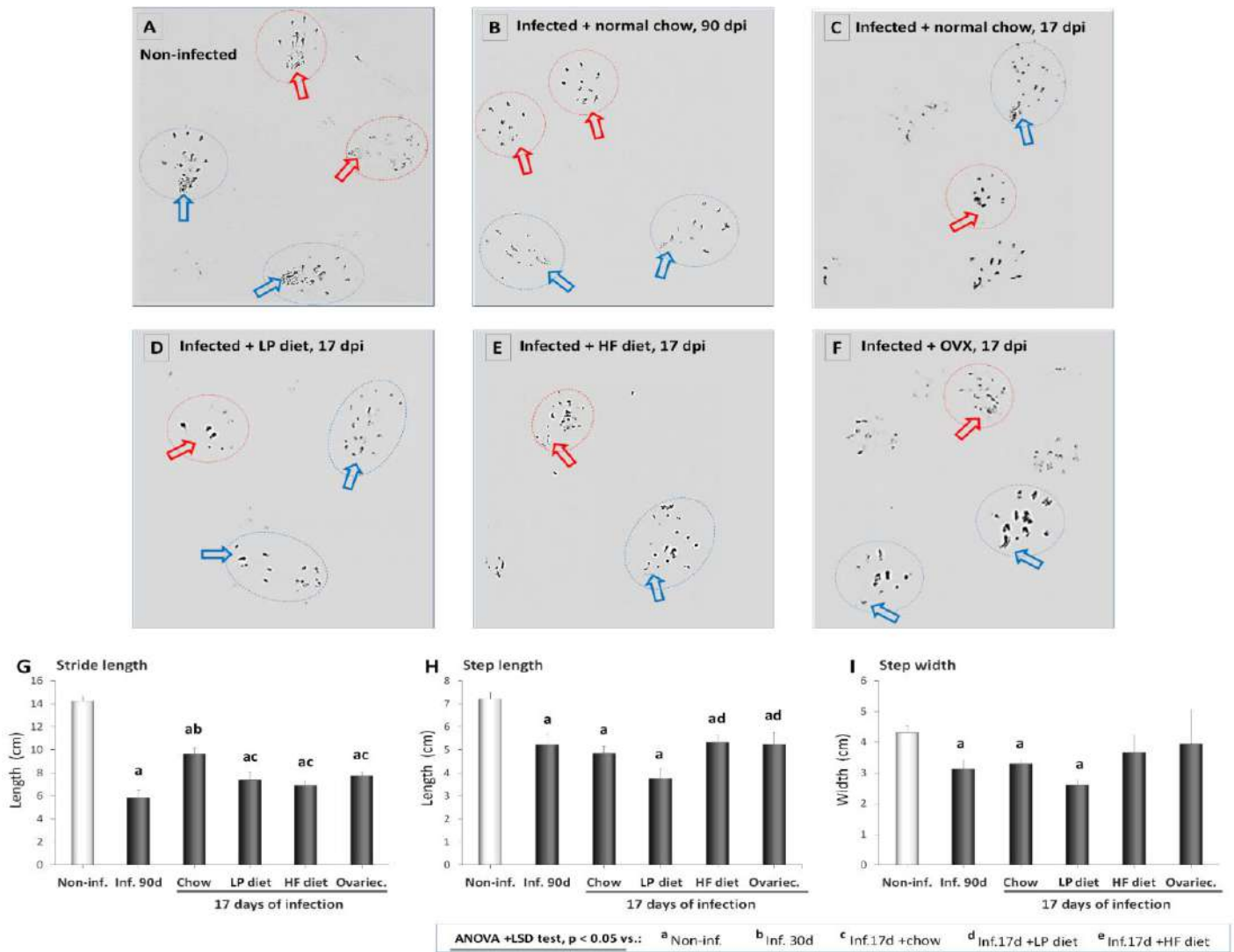


Figure 26. Gait quality indicator changes

A-F. Footprints of representative non-infected (**A**) and *T. gondii*-infected animals fed normal chow for 90 days (**B**) or 17 days (**C**), fed low-protein (PP) diet (**D**), high-fat (HF) diet (**E**), or ovariectomized (**F**). Note that, unlike the non-infected (**A**), the infected use their anterior footpads more and their heels less (**B-F**), particularly those fed PP diet (**D**).

G-I. Average stride length (**G**), step length (**H**) and step width (**I**) of non-infected control animals and *T. gondii*-infected animals (17 days) exposed to various physiological and environmental factors.

Table XVI. Gait quality indicator changes

		17 days post-infection				
		Inf. 90d	+Chow	+LPD	+HFD	+OVX
Stride length						
Non-inf.	0.001**	8.8E-7***	4.5E-5***	7.4E-8***	2.1E-8***	
Inf. 90d		0.006**	0.147	0.255	0.077	
Chow			0.022*	0.001**	0.011*	
LPD				0.546	0.658	
HFD					0.192	
Step length						
Non-inf.	0.026*	9.7E-6***	8.7E-5***	4.7E-4***	0.008**	
Inf. 90d		0.538	0.068	0.874	0.978	
Chow			0.059	0.285	0.513	
LPD				0.015*	0.046*	
HFD					0.901	
Step width						
Non-inf.	0.029*	0.002**	4.6E-5***	0.320	0.492	
Inf. 90d		0.637	0.212	0.436	0.180	
Chow			0.011*	0.563	0.226	
LPD				0.122	0.031*	
HFD					0.702	

OVX: ovariectomy. **ANOVA+LSD test:** *P<0.05; **P<0.01; ***P<0.001.

3.2.1.4 Organ weight

The changes observed in the organ weights relative to body weights of rats ovariectomized or exposed to different diets are presented in figure 27.

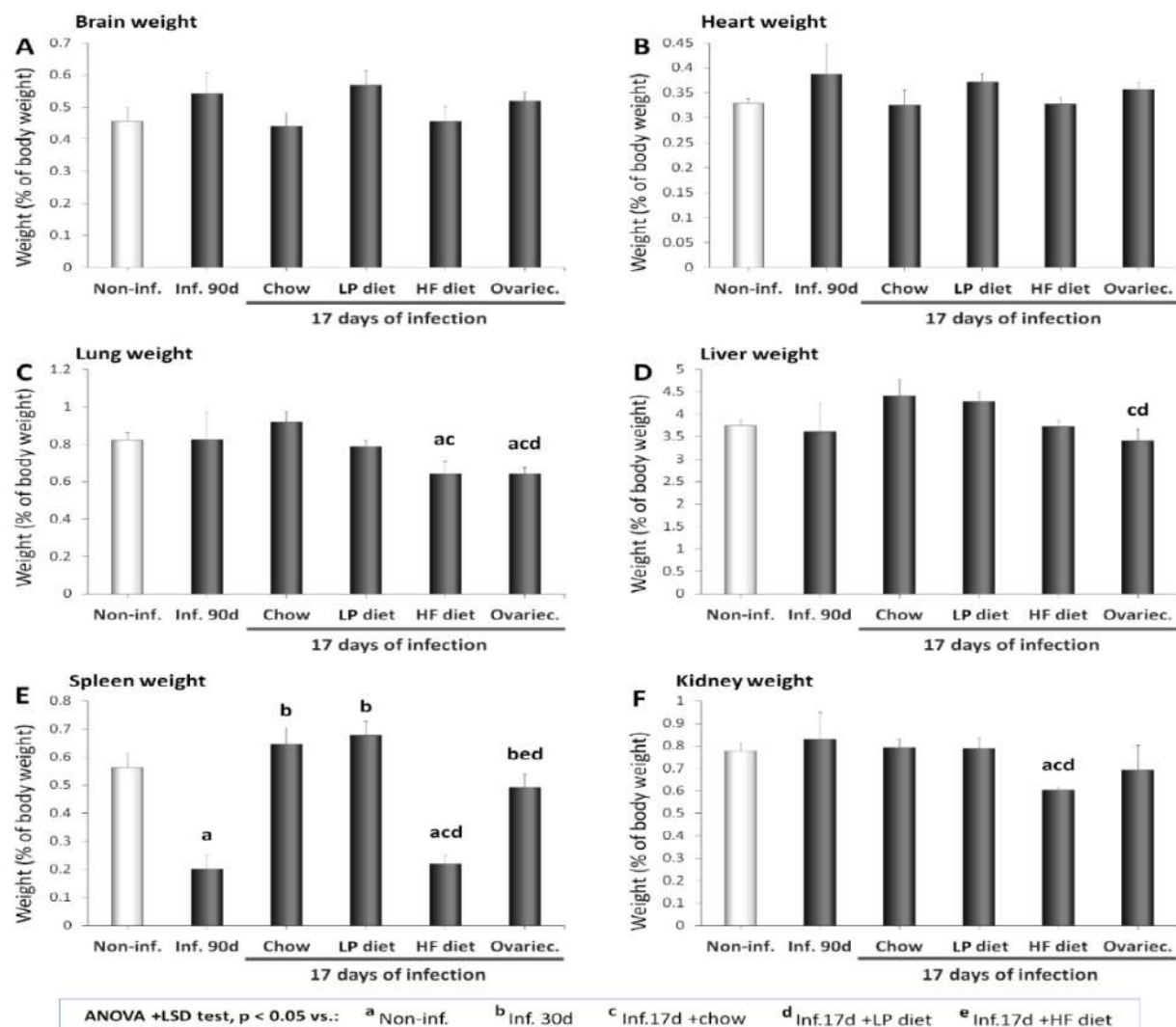


Figure 27. Organ weight relative to body weight at day 17 post-infection

Compared to non-infected animals, non-statistically significant increases in relative brain weights (figure 27A) and heart weights (figure 27B) were observed in infected animals sacrificed around 90 dpi, fed LPD, and ovariectomized, with non-infected-like weights in the other groups (figures 27A, B; table XVII). Relative lung weights were significantly lower in rats fed HFD or ovariectomized (figure 27C, table XVII). Non-statistically significant increases in relative liver weight were observed in the infected control group and in animals fed LPD (figure 27D).

Intriguingly, infected animals sacrificed around 90 dpi and animals fed HFD showed significant decreases in relative spleen weight compared to non-infected animals and to the other infected groups ($P < 0.01$, figure 27D, table XVII). Also compared to non-infected animals and to the infected control groups, animals fed HFD displayed a decrease in kidney weight (figure 27F, table XVII).

Table XVII. Inter-group differences in organ weight at 17 dpi

	Inf. 90d	17 days post-infection			
		+Chow	+LPD	+HFD	+OVX
Brain					
Non-inf.	0.336	0.799	0.103	0.991	0.229
Inf. 90d		0.267	0.753	0.343	0.778
Chow			0.069	0.822	0.143
LPD				0.119	0.383
HFD					0.271
Heart					
Non-inf.	0.436	0.927	0.056	0.917	0.160
Inf. 90d		0.429	0.834	0.425	0.665
Chow			0.198	0.972	0.385
LPD				0.062	0.478
HFD					0.184
Lungs					
Non-inf.	0.974	0.172	0.499	0.046*	0.005**
Inf. 90d		0.601	0.809	0.330	0.322
Chow			0.053	0.008**	6.3E-4***
LPD				0.087	0.012*
HFD					0.982
Liver					
Non-inf.	0.851	0.093	0.058	0.933	0.298
Inf. 90d		0.330	0.386	0.870	0.787
Chow			0.766	0.084	0.034*
LPD				0.053	0.027*
HFD					0.318
Spleen					
Non-inf.	0.001**	0.300	0.127	2.3E-5***	0.303
Inf. 90d		1.9E-4***	1.8E-4***	0.749	0.005**
Chow			0.691	9.5E-6***	0.059
LPD				2.9E-4***	0.019*
HFD					0.001**
Kidneys					
Non-inf.	0.718	0.733	0.836	8.2E-4***	0.173
Inf. 90d		0.809	0.788	0.205	0.382
Chow			0.939	1.5E-4***	0.098
LPD				0.016*	0.172
HFD					0.105

OVX: ovariectomy. **ANOVA+LSD test:** *P<0.05; **P<0.01; ***P<0.001.

3.2.2 OFT changes

3.2.2.1 Locomotion episodes

Figures 28A-C and table XVIII present the impact of ovariectomy, LPD, and HFD on the effects of *T. gondii* infection on the locomotion episode number (figure 28A), length (figure 28B), and on the distance covered (figure 28C) in the OFT arena.

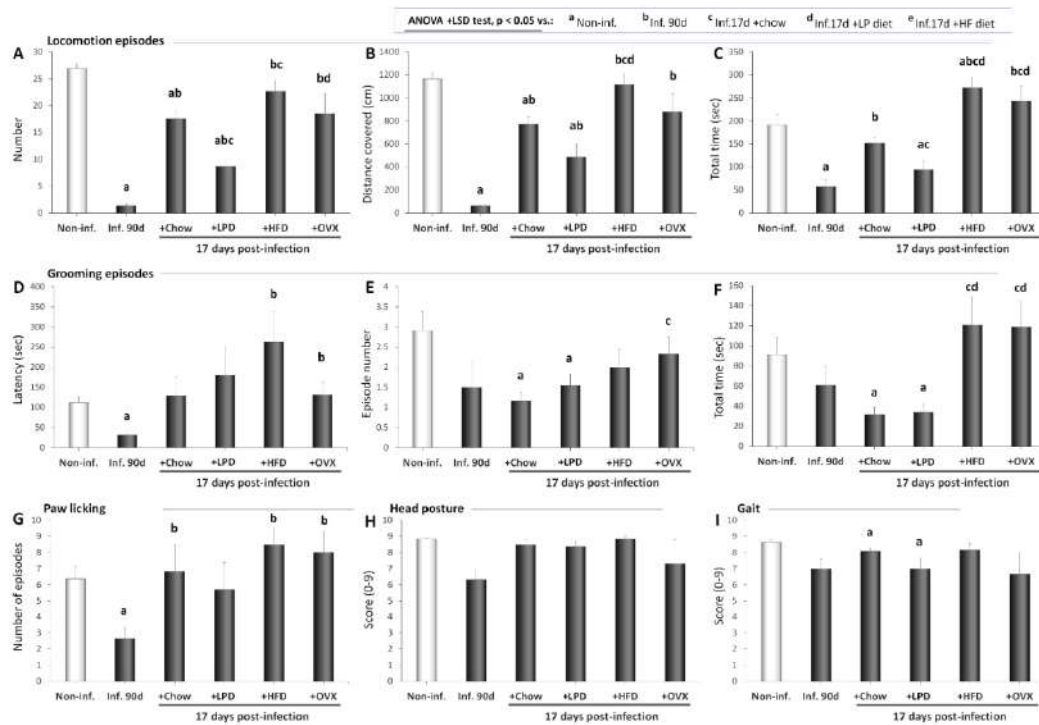


Figure 28. Locomotion and grooming-related parameters at 17 days post-infection

The infected rats sacrificed around 90 dpi, the disease control rats and the infected rats fed LPD showed significantly lower locomotion episode numbers compared to the non-infected group ($p < 0.001$, figure 28A, table XVIII). However, the disease control rats sacrificed at 17 dpi had a higher number of episodes than the infected rats fed LPD, which in turn had a higher number of episodes than the infected rats sacrificed around 90 dpi. No significant change was observed in ovariectomized and in animals fed HFD compared to the non-infected, as high interindividual variabilities were observed; however, the values of the firsts were significantly higher than the groups of infected rats where marked decreases were observed (figure 28A, table XVIII). Similar results were observed with the distance covered (figure 28B) and locomotion total time (figure 28C), although in addition, the infected rats fed HFD showed a statistically significant increase in the latter OFT motor function indicator compared also to the non-infected group ($P < 0.05$) (table XVIII).

Table XVIII. OFT motor function indicators of infected rats at 17 dpi

	Inf. 90d	Infected, 17 days			
		+Chow	+LPD	+HFD	+OVX
Locomotion episode number					
Non-inf.	1.4E-11***	2.0E-5***	1.6E-8***	0.105	0.074
Inf. 90d		6.5E-8***	0.001**	1.2E-4***	0.006**
Chow			2.5E-4***	0.070	0.825
LPD				2.8E-4***	0.047*
HFD					0.358
Distance covered					
Non-inf.	1.8E-9***	2.0E-4***	1.6E-4***	0.665	0.133
Inf. 90d		3.8E-7***	0.005**	9.2E-5***	0.003**
Chow			0.051	0.013*	0.556
LPD				0.001**	0.072
HFD					0.227
Locomotion time					
Non-inf.	4.9E-4***	0.144	0.004**	0.026*	0.210
Inf. 90d		0.004**	0.160	1.0E-4**	0.001**
Chow			0.020*	0.002**	0.035*
LPD				8.3E-5***	0.004**
HFD					0.501
Grooming latency					
Non-inf.	3.6E-4***	0.717	0.360	0.107	0.570
Inf. 90d		0.063	0.064	0.029*	0.023*
Chow			0.557	0.174	0.969
LPD				0.444	0.540
HFD					0.161
Grooming episode number					
Non-inf.	0.125	0.005**	0.025*	0.186	0.380
Inf. 90d		0.651	0.951	0.549	0.325
Chow			0.292	0.133	0.040*
LPD				0.412	0.153
HFD					0.600
Grooming time					
Non-inf.	0.281	0.006**	0.008**	0.385	0.391
Inf. 90d		0.258	0.289	0.116	0.113
Chow			0.818	0.023*	0.019
LPD				0.025*	0.021*
HFD					0.962
Paw licking episode number					
Non-inf.	0.006**	0.800	0.725	0.114	0.330
Inf. 90d		0.037*	0.123	0.002**	0.011*
Chow			0.637	0.402	0.598
LPD				0.175	0.311
HFD					0.776
Head posture score					
Non-inf.	0.061	0.300	0.252	1.000	0.357
Inf. 90d		0.064	0.067	0.057	0.558
Chow			0.825	0.332	0.471
LPD				0.274	0.510
HFD					0.358
Gait score					
Non-inf.	0.096	0.036*	0.034*	0.313	0.208
Inf. 90d		0.193	1.000	0.172	0.828
Chow			0.139	0.857	0.347
LPD				0.150	0.831
HFD					0.331

ANOVA+LSD test: *P<0.05; **P<0.01; ***P<0.001.

3.2.2.2 Grooming episodes

Figures 28D-G and table XVIII present the impact of ovariectomy, LPD, and HFD on the effects of *T. gondii* infection on the grooming latency (figure 28D), episode number (figure 28E) and time (figure 28F), and the number of episodes of paw licking or short grooming (figure 28G). No statistically significant change was observed in the grooming latency, except for rats sacrificed around 90 dpi that displayed a markedly shorter latency compared to the non-infected group ($P < 0.001$), and to the infected ovariectomized and to the HFD-fed rats ($P < 0.05$) (figure 28D, table XVIII). Marked decreases in grooming episode number were observed in all infected groups, with significant differences compared to non-infected group for the infected control group sacrificed at 17 dpi and for animals fed LPD (figure 28E, table XVIII). The infected control group sacrificed at 17 dpi and animals fed LPD also displayed significant decreases in grooming time compared to non-infected group ($P < 0.01$), but also to the infected ovariectomized and to the HFD-fed rats ($P < 0.05$) (figure 28F, table XVIII). The number of paws' licking episodes was higher in all groups sacrificed at 17 dpi, though with a high interindividual variability, except for LPD-fed animals whose licking episode number was slightly lower instead (figure 28G). The licking episode number was significantly lower in infected animals sacrificed around 90 dpi compared to non-infected animals ($P < 0.01$) and to groups sacrificed at 17 dpi (figure 28G, table XVIII).

3.2.2.3 Head posture and gait scores

Figures 28H, I and table XVIII present the impact of ovariectomy, LPD, and HFD on the effects of *T. gondii* infection on the scores of head posture (figure 28H) and gait (figure 28I). No statistically significant change was observed in head posture score, although marked decreases were observed in infected animals sacrificed around 90 dpi and in ovariectomized animals (figure 28H, table XVIII). Decreases in gait score were observed in all infected groups, with statistically significant differences compared to non-infected group for disease control animals sacrificed at 17 dpi and animals fed LPD (figure 28I, table XVIII).

3.2.2.4 Arena angle entries

Figures 29A, B and table XIX present the impact of ovariectomy, LPD, and HFD on the effects of *T. gondii* infection on the number of entries (figure 29A) and time spent (figure 29B) in the angles of the OFT arena. Compared to non-infected animals, significantly less entries in the arena angles were observed in infected animals sacrificed around 90 dpi, in disease control sacrifice at 17 dpi, and in animals fed LPD, whereas a higher number of entries was observed in animals fed HFD and no change was observed in ovariectomized animals (figure 29A, table XIX). The number of entries in arena angles in other infected groups were still significantly higher than the number of entries in animals sacrificed around 90 dpi (figure 29A, table XIX).

In addition, the number of entries in arena angles in LPD-fed group was markedly lower than infected groups fed normal chow or HFD (figure 29A, table XIX). The time spent in the angles of the arena was significantly higher in all infected groups compared to non-infected animals, except for animals sacrificed around 17 dpi (figure 29B, table XIX). The time spent in the angles by animals sacrificed around 90 dpi was significantly higher than values of all the other infected groups (figure 29B, table XIX). Compared to infected control animals sacrificed around 17 dpi, all other groups sacrificed that day had significantly higher angle times (figure 29B, table XIX).

3.2.2.5 Rearing episodes

Figures 29C-E and table XIX present the impact of ovariectomy, LPD, and HFD on the effects of *T. gondii* infection on rearing against wall and rearing on hindlimbs' episode latency (figures 29C and 22E respectively) and number (figure 29D and 22F respectively). While a non-statistically significant decrease (respectively, increase) in the latency to the first episode of rearing against wall was observed in animals sacrificed around 90 dpi (respectively, HFD-fed and ovariectomized animals) compared to non-infected animals, statistically significant increases were observed in infected animals sacrificed at 17 dpi and in animals fed LPD (figure 29C, table XIX). Instead, compared to non-infected animals, all infected animals displayed marked decreases in the number of episodes of rearing against wall, which were statistically significant except for animals fed HFD (figure 29D, table XIX). However, the numbers of episodes of rearing against wall of all groups sacrificed at 17 dpi were still significantly higher than values of animals sacrificed around 90 dpi, although animals fed LPD had the lowest values of all groups sacrificed at 17 dpi (figure 29D, table XIX).

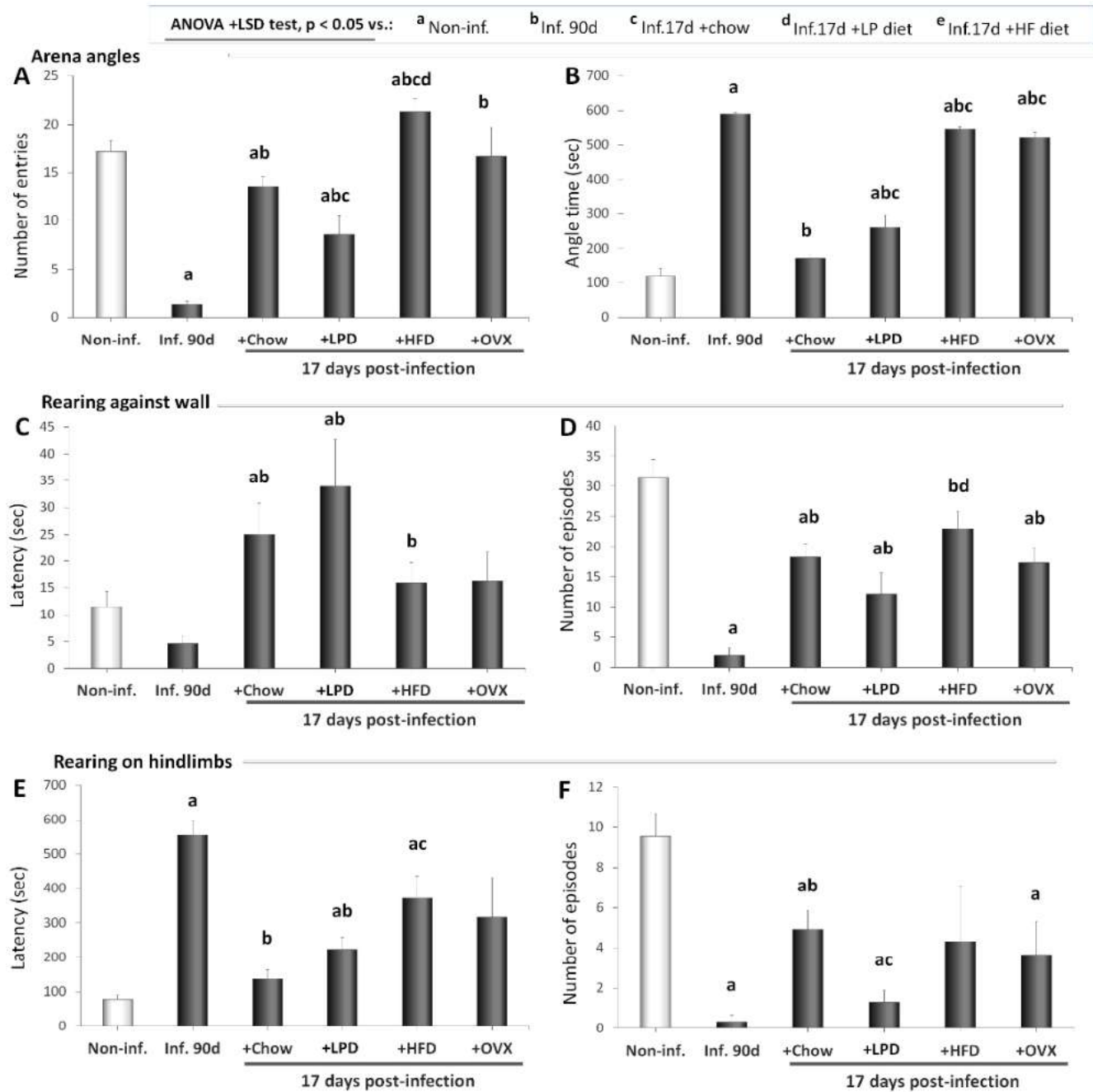


Figure 29. Rearing activities and arena angle time at 17 days post-infection

Table XIX. Rearing and arena angle entries at 17 dpi

		Infected, 17 days				
		Inf. 90d	+Chow	+LPD	+HFD	+OVX
Angle entries						
Non-inf.	3.0E-8***	0.030*	0.002**	0.034*	0.880	
Inf. 90d		5.7E-8***	0.004**	1.0E-5***	0.004**	
Chow			0.039*	0.001**	0.379	
LPD				8.7E-5***	0.054	
HFD					0.208	
Angle time						
Non-inf.	1.4E-9***	0.059	0.003**	9.3E-10***	4.8E-10***	
Inf. 90d		1.1E-14***	4.1E-6***	0.001**	0.007**	
Chow			0.028*	2.0E-15***	1.9E-8***	
LPD				1.0E-5***	1.3E-5***	
HFD					0.204	
Rearing against wall latency						
Non-inf.	0.052	0.048*	0.032*	0.360	0.451	
Inf. 90d		0.004**	0.008**	0.028*	0.082	
Chow			0.404	0.199	0.280	
LPD				0.082	0.107	
HFD					0.960	
Rearing against wall episode number						
Non-inf.	8.4E-7***	0.002**	4.5E-4***	0.054	0.002**	
Inf. 90d		2.4E-5***	0.018*	3.2E-4***	0.001**	
Chow			0.160	0.208	0.783	
LPD				0.028*	0.240	
HFD					0.152	
Rearing on hindlimb latency						
Non-inf.	0.006**	0.055	0.003**	0.006**	0.096	
Inf. 90d		0.002**	0.002**	0.052	0.102	
Chow			0.066	0.013*	0.186	
LPD				0.078	0.470	
HFD					0.690	
Rearing on hindlimb episode number						
Non-inf.	8.2E-6***	0.006**	1.4E-5***	0.127	0.015*	
Inf. 90d		0.001**	0.186	0.209	0.100	
Chow			0.005**	0.848	0.528	
LPD				0.329	0.223	
HFD					0.841	

ANOVA+LSD test: *P<0.05; **P<0.01; ***P<0.001.

Infected animals sacrificed around 90 dpi and animals fed LPD or HFD displayed marked and statistically significant increases in the latency to the first episode of rearing on hindlimbs compared to non-infected animals, but not ovariectomized animals that presented with a high interindividual variability and disease control animals sacrificed at 17 dpi that had slight increases (figure 29E, table XIX).

The rearing on hindlimbs' latency was higher in animals sacrificed around 90 dpi compared to the groups sacrificed at 17 dpi, with statistically significant differences compared to disease control animals sacrificed at 17 dpi and animals fed LPD (figure 29E, table XIX). In addition, animals fed HFD displayed marked and statistically significant increases compared to disease control animals sacrificed at 17 dpi (figure 29E, table XIX). Moreover, all infected animals showed markedly lower numbers of episodes of rearing on hindlimbs compared to non-infected animals, with the lowest numbers observed in groups of animals sacrificed around 90 dpi or fed LPD (figure 29F, table XIX).

3.2.2.6 Arena centre entries

Figures 30A-D and table XX present the impact of ovariectomy, LPD, and HFD on the effects of *T. gondii* infection on the latency to first entry (figure 30A), distance covered (figure 30B), number of entries (figure 30C), and time spent (figure 30D) in the central area of the OFT arena. The latency to the first entry to the arena centre was markedly higher in all infected groups compared to non-infected groups, with the lowest increase in disease control animals sacrificed at 17 dpi, the higher increase in infected animals sacrificed at 90 dpi, and a high interindividual variability in ovariectomized animals (figure 30A, table XX). Similarly, all infected groups displayed marked decreases compared to non-infected groups in the distance covered (figure 30B), the number of entries (figure 30C), and time spent (figure 30D) in the arena centre. The most significant decreases were observed in infected animals sacrificed at 90 dpi and in animals fed LPD ($P < 0.001$), while the less marked decreased were observed in disease control animals sacrificed at 17 dpi ($P < 0.01$), with high interindividual variabilities in ovariectomized and HFP-fed groups (figures 30B-D, table XX).

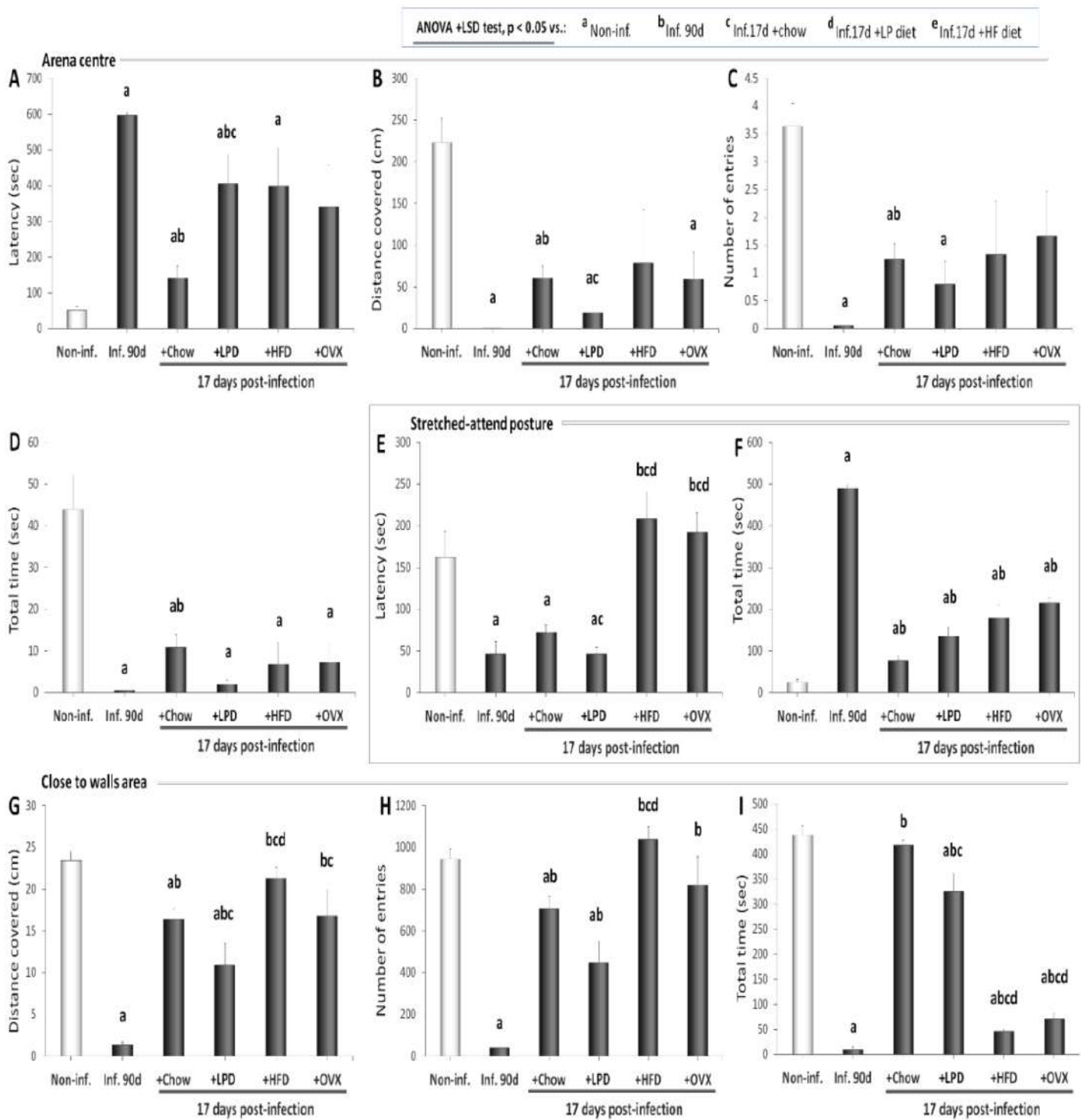


Figure 30. Arena centre and close to wall activities at 17 days post-infection

Table XX. Centre activities and stretched-attend posture at 17 dpi

		Infected, 17 days			
	Inf. 90d	+Chow	+LPD	+HFD	+OVX
Arena centre latency					
Non-inf.	1.3E-14***	0.021*	0.002**	0.021*	0.055
Inf. 90d		2.2E-8***	0.040*	0.118	0.080
Chow			0.010*	0.058	0.152
LPD				0.966	0.663
HFD					0.720
Arena centre distance					
Non-inf.	2.0E-5***	2.0E-4***	2.6E-5***	0.078	0.002**
Inf. 90d		0.001**	0.080	0.274	0.113
Chow			0.027*	0.799	0.976
LPD				0.398	0.258
HFD					0.802
Arena centre entries					
Non-inf.	4.8E-6***	1.4E-4***	1.1E-4	0.063	0.062
Inf. 90d		0.001**	0.087	0.221	0.093
Chow			0.382	0.936	0.641
LPD				0.624	0.367
HFD					0.795
Arena centre time					
Non-inf.	2.4E-4***	0.002**	3.4E-4***	0.002**	0.001**
Inf. 90d		0.004**	0.071	0.254	0.155
Chow			0.015	0.530	0.526
LPD				0.408	0.283
HFD					0.944
Distance covered close to walls					
Non-inf.	1.0E-9***	0.005**	0.001**	0.244	0.418
Inf. 90d		9.3E-8***	0.002**	6.7E-6***	0.002**
Chow			0.039*	0.002**	0.478
LPD				1.8E-4***	0.052
HFD					0.183
Close to wall area entries					
Non-inf.	3.0E-10***	2.6E-4***	0.001**	0.234	0.089
Inf. 90d		3.3E-8***	0.005**	1.0E-5***	0.004**
Chow			0.079	0.016	0.904
LPD				0.004**	0.172
HFD					0.226
Close to wall time					
Non-inf.	1.7E-10***	0.322	0.015**	2.6E-10***	4.6E-11***
Inf. 90d		7.4E-15***	1.8E-5***	3.7E-4***	0.004**
Chow			0.034*	1.4E-15***	3.3E-10***
LPD				4.3E-5***	5.1E-5***
HFD					0.118
Stretched-attend posture latency					
Non-inf.	0.006**	0.017*	0.004**	0.317	0.451
Inf. 90d		0.217	0.984	0.003**	0.001**
Chow			0.037*	0.007**	0.002**
LPD				0.003**	0.001**
HFD					0.691
Stretched-attend posture time					
Non-inf.	3.4E-9***	0.003**	0.001**	0.004**	1.4E-7***
Inf. 90d		2.0E-11***	3.0E-8***	1.1E-4***	3.5E-7***
Chow			0.045*	0.021*	1.3E-6***
LPD				0.291	0.010*
HFD					0.329

ANOVA+LSD test: *P<0.05; **P<0.01; ***P<0.001.

3.2.2.7 Stretched-attend posture episodes

Figures 30E, F and table XX present the impact of ovariectomy, LPD, and HFD on the effects of *T. gondii* infection on SAP latency (figure 30E) and time (figure 30F) in the OFT arena. Compared to the non-infected group, significant decreases were observed in the SAP latency of infected control animals sacrificed at 17 dpi or around 90 dpi and in those fed LPD, while a slight increase was observed in animals fed HFD or ovariectomized (figure 30E, table XX). Differences between animals fed HFD or ovariectomized were statistically significant compared to the other groups of infected animals (figure 30E, table XX). All infected groups showed marked increases in SAP total time compared to the non-infected group (figure 30F, table XX). However, the highest increase was observed in infected animals sacrificed around 90 dpi, with significant differences compared to the other groups of infected animals (figure 30F, table XX).

3.2.2.8 Close to wall activities

Figures 30G-I and table XX present the impact of ovariectomy, LPD, and HFD on the effects of *T. gondii* infection on the distance covered (figure 30G), number of entries (figure 30H), and time spent (figure 30I) in the area close to the walls of the OFT arena. Significant decreases (table XX) were observed in animals sacrificed around 90 dpi, fed LPD, and in a lesser extent, in the disease control animals sacrificed at 17 dpi in both the distance covered (figure 30G) and the entries (figure 30H) in the area close to the arena walls. Only slight changes were observed in HFD-fed and ovariectomized groups, whose values were significantly higher than values of groups sacrificed around 90 dpi, and in a lesser extent, infected control animals sacrificed at 17 dpi and those fed LPD (figures 30G, H and table XX).

Instead, significant decreases in time spent in the area close to the walls of the arena were observed for animals sacrificed around 90 dpi, fed LPD, HFD, or ovariectomized, but not disease control animals sacrificed at 17 dpi (figure 30I, table XX). Compared to the latter, all other infected groups sacrificed at 17 dpi showed significantly decreased close to wall time (figure 30I, table XX).

3.2.3 EPM changes

3.2.3.1 Distance covered and speed

Figure 31 and table XXI present the impact of ovariectomy, LPD, and HFD on the effects of *T. gondii* infection on the distance covered (figures 31A-C), the percent of time spent active (figures 31D-F), and the speed (figures 31G-I) in the centre of the OFT arena. Compared to the non-infected group, to infected control animals sacrificed at 17 dpi, and to HFD-fed group, animals sacrificed around 90 dpi and in a lesser extent the group fed LPD displayed markedly

lower decreases in the total distance covered in the EPM maze (figure 31A, table XXI). The same trend was observed in the distance covered in the EPM maze during the first minute of the test (figure 31B, table XXI). Instead, overall all infected animals showed decreases in the distance covered in the EPM maze during the last minute of the test, with the most marked and only statistically significant decrease in the infected group sacrificed around 90 dpi (figure 31C, table XXI).

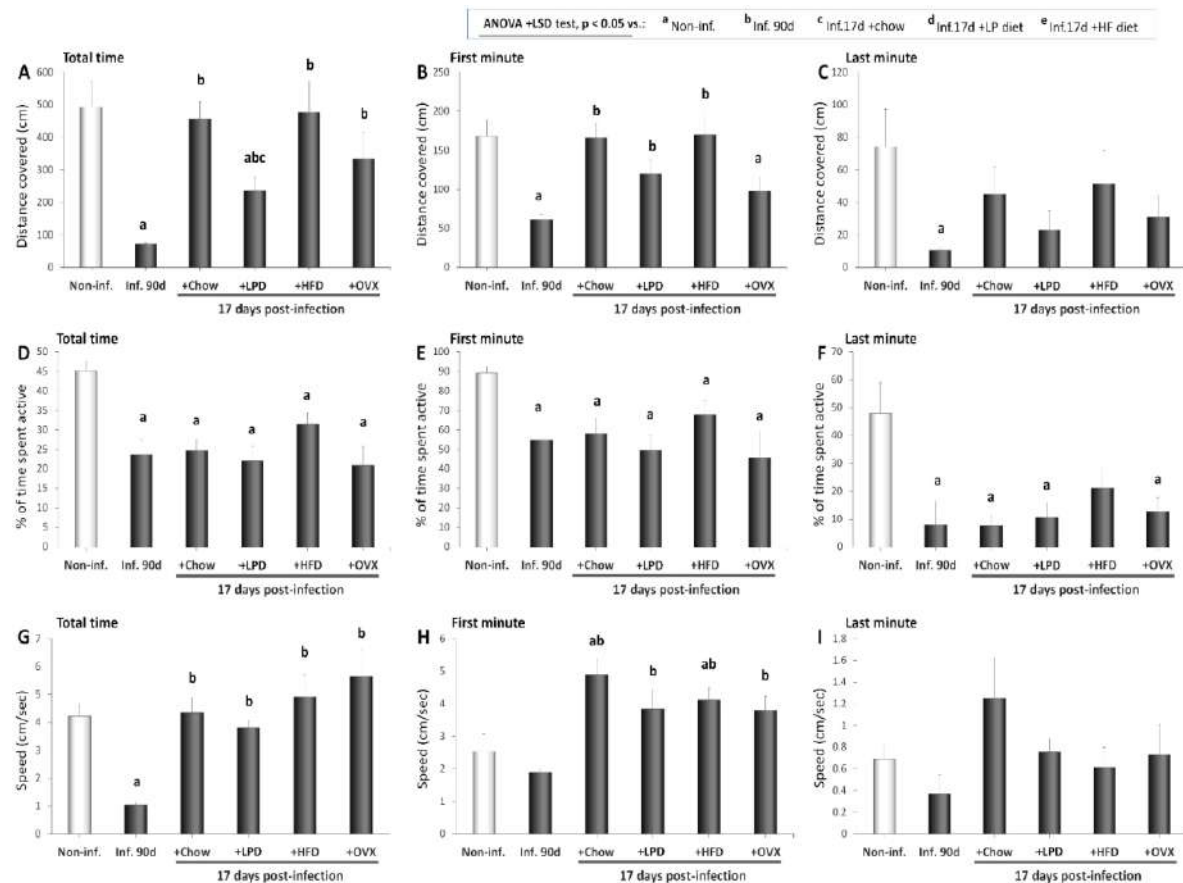


Figure 31. EPM motor indicators at 17 days post-infection

Except for HFD-fed rats that were less affected, all infected animals presented with comparable changes in the total time spent active (figure 31D), the time spent active in the first minute (figure 31E), and the time spent active in the last minute (figure 31F) of the test, notably, significant decreases of about 49%, 38%, and 80%, respectively, compared to the non-infected group (table XXI).

Table XXI. Motor function indicators of infected rats at 17 dpi

	Inf. 90d	Infected, 17 days			
		+Chow	+LPD	+HFD	+OVX
Total distance covered					
Non-inf.	2.60E-4***	0.706	0.010*	0.893	0.176
Inf. 90d		2.70E-5***	0.004**	0.007**	0.022*
Chow			0.005**	0.863	0.232
LPD				0.052	0.310
HFD					0.276
1st min distance					
Non-inf.	3.20E-4***	0.942	0.093	0.965	0.021*
Inf. 90d		1.70E-4***	0.012*	0.014*	0.112
Chow			0.091	0.919	0.019*
LPD				0.187	0.404
HFD					0.07
4th min distance					
Non-inf.	0.021*	0.325	0.069	0.472	0.125
Inf. 90d		0.075	0.310	0.100	0.163
Chow			0.309	0.811	0.526
LPD				0.259	0.649
HFD					0.417
Total activity time					
Non-inf.	0.012*	2.00E-5***	7.10E-5	0.004**	0.003**
Inf. 90d		0.816	0.781	0.179	0.684
Chow			0.562	0.128	0.516
LPD				0.070	0.861
HFD					0.108
1st min activity time					
Non-inf.	0.025*	0.003**	3.10E-4***	0.031*	0.021*
Inf. 90d		0.778	0.638	0.255	0.569
Chow			0.461	0.382	0.453
LPD				0.105	0.806
HFD					0.184
4th min activity time					
Non-inf.	0.009**	0.007**	0.011*	0.058	0.016*
Inf. 90d		0.947	0.724	0.145	0.520
Chow			0.639	0.100	0.423
LPD				0.227	0.770
HFD					0.330
Total average speed					
Non-inf.	1.6E-4***	0.840	0.450	0.436	0.221
Inf. 90d		1.1E-4***	7.7E-8***	0.004**	0.005**
Chow			0.378	0.551	0.280
LPD				0.210	0.120
HFD					0.578
1st min average speed					
Non-inf.	0.277	0.006**	0.124	0.034*	0.088
Inf. 90d		1.3E-4***	0.009**	0.002**	0.006**
Chow			0.197	0.243	0.124
LPD				0.700	0.968
HFD					0.601
4th min average speed					
Non-inf.	0.261	0.207	0.713	0.739	0.896
Inf. 90d		0.081	0.204	0.387	0.312
Chow			0.256	0.171	0.290
LPD				0.537	0.939
HFD					0.734

ANOVA+LSD test: *P<0.05; **P<0.01; ***P<0.001.

The average speed in the maze was comparable between the non-infected animals and almost all the infected groups, with the exception of the infected group sacrificed around 90 dpi whose speed was significantly lower than all other groups (figure 31G, table XXI). Non-

infected animals and the infected animals sacrificed around 90 dpi had comparable speeds the first minute spent in the maze, which were significantly lower than values in the infected groups sacrificed at 17 dpi (figure 31H, table XXI). No statistically significant difference between non-infected and infected groups was observed in the animal speed in the arena the last minute (figure 31I, table XXI).

3.2.3.2 Arm entries

Figure 32 and table XXII present the impact of ovariectomy, LPD, and HFD on the effects of *T. gondii* infection on the open arm latency (figure 32A), number of entries (figure 32B), time (figure 32C), on the open arm bottom latency (figure 32D), entries (figure 32E), time (figure 32F), on the closed arm latency (figure 32G), entries (figure 32H), time (figure 32I), and on the closed arm bottom latency (figure 32J), entries (figure 32K), and time (figure 32L). All infected animals showed increases in open arm latency compared to non-infected animals, with significant differences for infected animals sacrificed around 90 dpi, disease control animals sacrificed at 17 dpi and animals fed LPD (figure 32A, table XXII). The most marked increases were observed in infected animals sacrificed around 90 dpi, which were significantly higher than disease control animals sacrificed at 17 dpi and animals fed LPD (figure 32A, table XXII). HFD-fed and ovariectomized groups displayed high interindividual differences (figure 32A, table XXII).

In addition, all infected animals showed decreases in open arm entries and time compared to non-infected animals, with the most marked decreases in infected animals sacrificed around 90 dpi (figures 32B, C and table XXII). As for the latency, whereas HFD-fed and ovariectomized groups presented with high interindividual differences, and significant differences were observed in disease control animals sacrificed at 17 dpi and animals fed LPD compared to animals sacrificed around 90 dpi (figure 32B, table XXII). No statistically significant difference (table XXII) was observed compared to non-infected animals or between infected groups in open arm bottom latency (figure 32D), entries (figure 32E), time (figure 32F).

Increases were observed in infected animals sacrificed around 90 dpi, in LPD-fed and in ovariectomized compared to non-infected group, although with high interindividual variability (figure 32G, table XXII). The number of entries to closed arms of animals sacrificed around 90 dpi or fed LPD were significantly decreased compared to non-infected group and to disease control animals sacrificed at 17 dpi (figure 32H, table XXII).

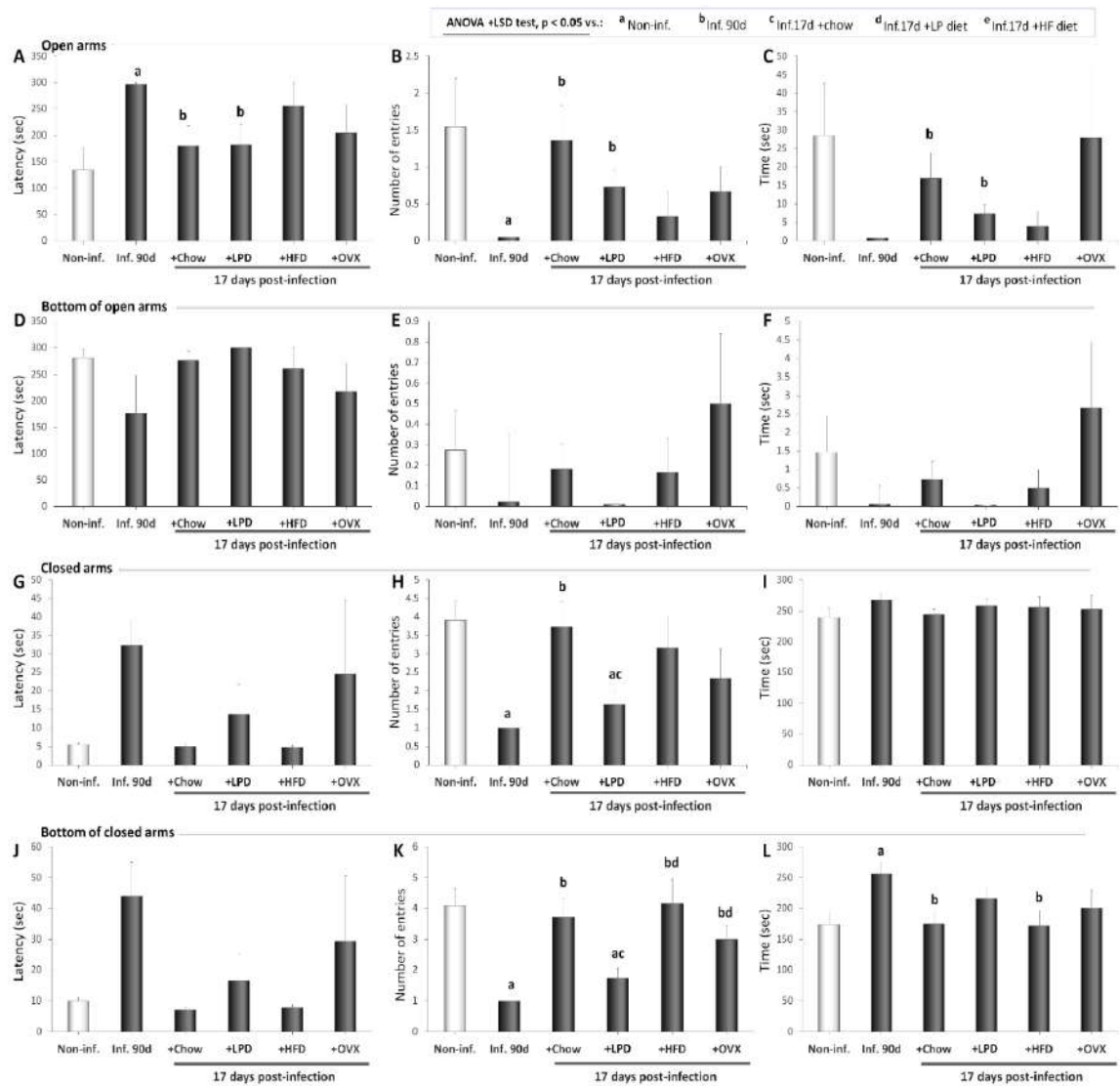


Figure 32. EPM arm latency and time at 17 days post-infection

Instead, no statistically significant change was observed in closed arm time (figure 32I, table XXII) and closed arm bottom latency (figure 32J, table XXII). Closed arm bottom number of entries (respectively, time) was significantly decreased (respectively, increased) in animals sacrificed around 90 dpi, and in a lesser extent, animals fed LPD, compared to non-infected group (figures 32K, L and table XXII).

Table XXII. Arm entry time and latency of infected rats at 17 dpi

	Inf. 90d	Infected, 17 days			
		+Chow	+LPD	+HFD	+OVX
Open arm latency					
Non-inf.	0.003**	0.418	0.411	0.070	0.324
Inf. 90d		0.011*	0.016*	0.398	0.146
Chow			0.972	0.226	0.722
LPD				0.247	0.748
HFD					0.486
Open arm entries					
Non-inf.	0.039*	0.824	0.260	0.120	0.250
Inf. 90d		0.016*	0.012*	0.363	0.102
Chow			0.248	0.095	0.247
LPD				0.358	0.885
HFD					0.496
Open arm time					
Non-inf.	0.073	0.474	0.173	0.125	0.985
Inf. 90d		0.037*	0.014*	0.363	0.196
Chow			0.226	0.133	0.595
LPD				0.493	0.323
HFD					0.262
Open arm bottom latency					
Non-inf.	0.282	0.845	0.265	0.641	0.293
Inf. 90d		0.298	0.231	0.377	0.671
Chow			0.194	0.717	0.326
LPD				0.363	0.181
HFD					0.527
Open arm bottom entries					
Non-inf.	0.884	0.698	0.192	0.685	0.579
Inf. 90d		0.703	0.423	0.685	0.739
Chow			0.167	0.943	0.413
LPD				0.363	0.203
HFD					0.409
Open arm bottom time					
Non-inf.	0.260	0.521	0.171	0.402	0.565
Inf. 90d		0.413	0.391	0.668	0.231
Chow			0.181	0.754	0.332
LPD				0.363	0.191
HFD					0.283
Closed arm latency					
Non-inf.	0.052	0.664	0.344	0.384	0.388
Inf. 90d		0.050	0.108	0.050	0.724
Chow			0.319	0.750	0.377
LPD				0.301	0.633
HFD					0.370
Closed arm entries					
Non-inf.	2.7E-4***	0.837	0.003**	0.486	0.134
Inf. 90d		0.003**	0.132	0.056	0.158
Chow			0.018*	0.624	0.212
LPD				0.153	0.459
HFD					0.498
Closed arm time					
Non-inf.	0.091	0.772	0.292	0.474	0.644
Inf. 90d		0.050	0.434	0.552	0.549
Chow			0.297	0.559	0.751
LPD				0.921	0.828
HFD					0.903
Bottom of closed arm latency					
Non-inf.	0.089	0.066	0.456	0.193	0.403
Inf. 90d		0.077	0.110	0.080	0.558
Chow			0.291	0.600	0.342
LPD				0.329	0.599
HFD					0.357
Bottom of closed arm entries					
Non-inf.	2.1E-4***	0.660	0.002**	0.939	0.144
Inf. 90d		0.001**	0.054	0.010*	0.007**
Chow			0.011*	0.668	0.349
LPD				0.026*	0.044*
HFD					0.236
Bottom of closed arm time					
Non-inf.	0.002**	0.956	0.137	0.941	0.450
Inf. 90d		0.003**	0.096	0.020*	0.118
Chow			0.148	0.905	0.473
LPD				0.198	0.675
HFD					0.464

ANOVA+LSD test: *P<0.05; **P<0.01; ***P<0.001.

3.2.3.3 Head dipping episodes

Figures 33A-C and table XXIII present the impact of ovariectomy, LPD, and HFD on the effects of *T. gondii* infection on the head dipping episode latency (figure 33A), number (figure 33B) and time (figure 33C). No statistically significant difference was observed compared to non-infected animals or between infected groups in head dipping latency (figure 33A, table XXIII). Except for the ovariectomized group, all infected groups displayed significant decreases compared to non-infected animals and to disease control animals sacrificed at 17 dpi (figures 33B, C, and table XXIII).

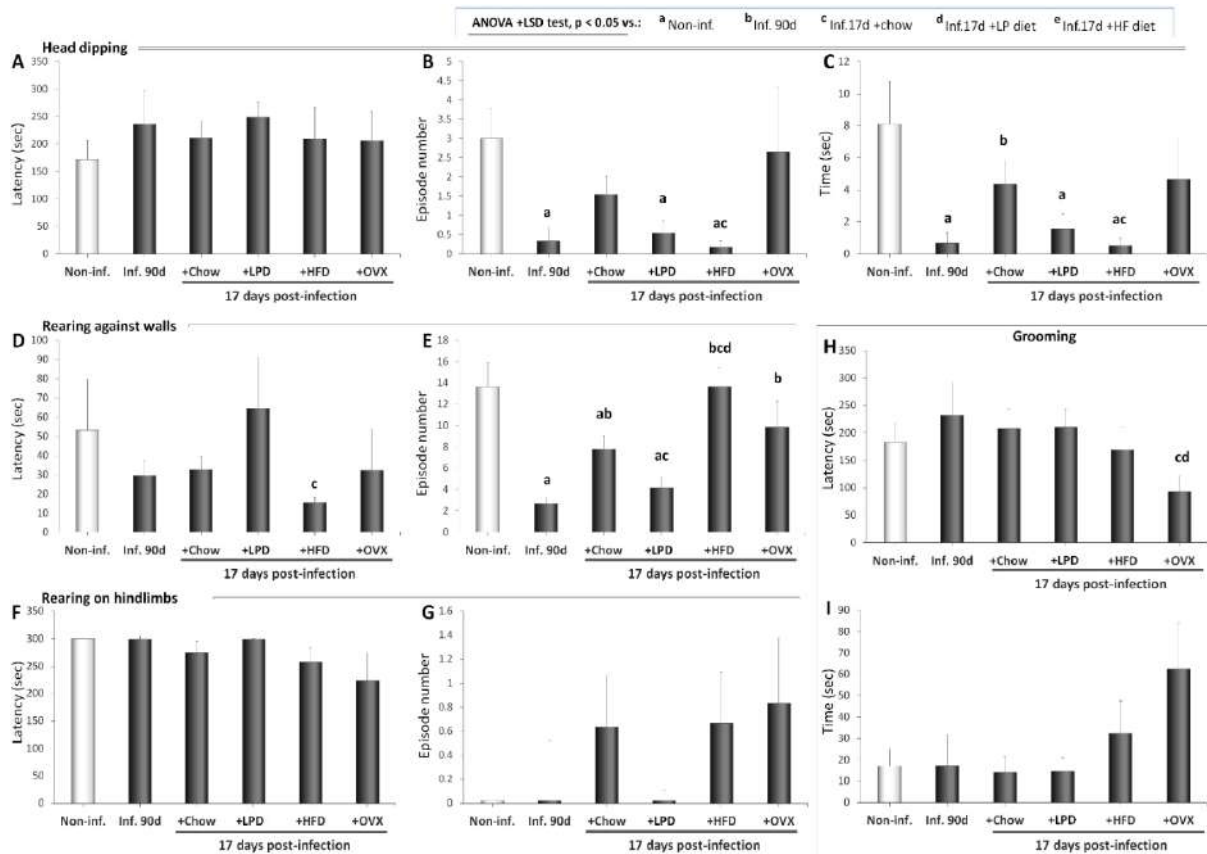


Figure 33. Head dipping and rearing in the maze at 17 days post-infection

Table XXIII. Head dipping and thigmotaxis indicators after 17 days of infection

	Inf. 90d	Infected, 17 days			
		+Chow	+LPD	+HFD	+OVX
Head dipping latency					
Non-inf.	0.430	0.411	0.100	0.594	0.595
Inf. 90d		0.747	0.864	0.766	0.733
Chow			0.378	0.976	0.938
LPD				0.556	0.494
HFD					0.972
Head dipping entries					
Non-inf.	0.010	0.140	0.014*	0.006**	0.862
Inf. 90d		0.063	0.658	0.685	0.224
Chow			0.096	0.018*	0.542
LPD				0.302	0.263
HFD					0.195
Head dipping time					
Non-inf.	0.021*	0.244	0.039*	0.018*	0.371
Inf. 90d		0.046*	0.466	0.851	0.183
Chow			0.135	0.033*	0.921
LPD				0.345	0.292
HFD					0.166
Rearing against walls latency					
Non-inf.	0.409	0.464	0.767	0.184	0.547
Inf. 90d		0.792	0.235	0.202	0.917
Chow			0.270	0.040*	0.987
LPD				0.097	0.362
HFD					0.478
Number of episodes of rearing against walls					
Non-inf.	0.001***	0.036*	0.002***	0.992	0.273
Inf. 90d		0.004**	0.244	0.001**	0.033*
Chow			0.037*	0.022*	0.489
LPD				0.001**	0.074
HFD					0.238
Rearing on hindlimb latency					
Non-inf.	0.423	0.251	0.341	0.175	0.187
Inf. 90d		0.263	0.547	0.181	0.191
Chow			0.254	0.618	0.376
LPD				0.177	0.188
HFD					0.569
Number of rearing on hindlimbs					
Non-inf.	0.391	0.172	0.341	0.175	0.185
Inf. 90d		0.453	0.583	0.421	0.362
Chow			0.243	0.961	0.782
LPD				0.235	0.232
HFD					0.814
Grooming latency					
Non-inf.	0.518	0.629	0.566	0.815	0.074
Inf. 90d		0.741	0.765	0.435	0.126
Chow			0.951	0.501	0.027*
LPD				0.448	0.018*
HFD					0.167
Grooming time					
Non-inf.	0.993	0.778	0.802	0.404	0.093
Inf. 90d		0.853	0.872	0.496	0.122
Chow			0.962	0.315	0.076
LPD				0.321	0.078
HFD					0.281

ANOVA+LSD test: *P<0.05; **P<0.01; ***P<0.001.

3.2.3.4 Rearing and grooming episodes

Figures 33D-I and table XXIII present the impact of ovariectomy, LPD, and HFD on the effects of *T. gondii* infection on the rearing against wall latency (figure 33D) and number (figure 33E), on the rearing on hindlimbs latency (figure 33F) and number (figure 33G), and on the grooming episode latency (figure 33H) and time (figure 33I). No statistically significant difference was observed in rearing against wall latency between infected groups and non-infected animals, while LPD-fed latency was significantly higher than HFD-fed latency (figure 33D, table XXIII). The numbers of rearing against wall episodes were lower in infected animals sacrificed around 90 dpi or fed LPD compared to infected controls sacrificed at 17 dpi, HFD-fed, and ovariectomized animals (figure 33E, table XXIII). Despite slight decreases in rearing on hindlimb latency (figure 33F) and increases in episode number (figure 33G), no statistically significant difference was observed between infected and non-infected groups (table XXIII). Moreover, the latency (figure 33H) and time (figure 33I) of grooming episodes were comparable between infected and non-infected groups (table XXIII).

3.2.3.5 Central platform activities

Figure 34 and table XXIV present the impact of ovariectomy, LPD, and HFD on the effects of *T. gondii* infection on the central platform entries (figure 34A) and time (figure 34B), and on SAP episode latency (figure 34C), number (figure 34D), and time (figure 34E). Compared to non-infected animals and to disease control group sacrificed at 17 dpi, the number of entries to the central platform was decreased in infected animals sacrificed at 90 dpi or fed LPD (figure 34A, table XXIV). No statistically significant difference was observed between infected and non-infected groups in central platform time (figure 34B, table XXIV).

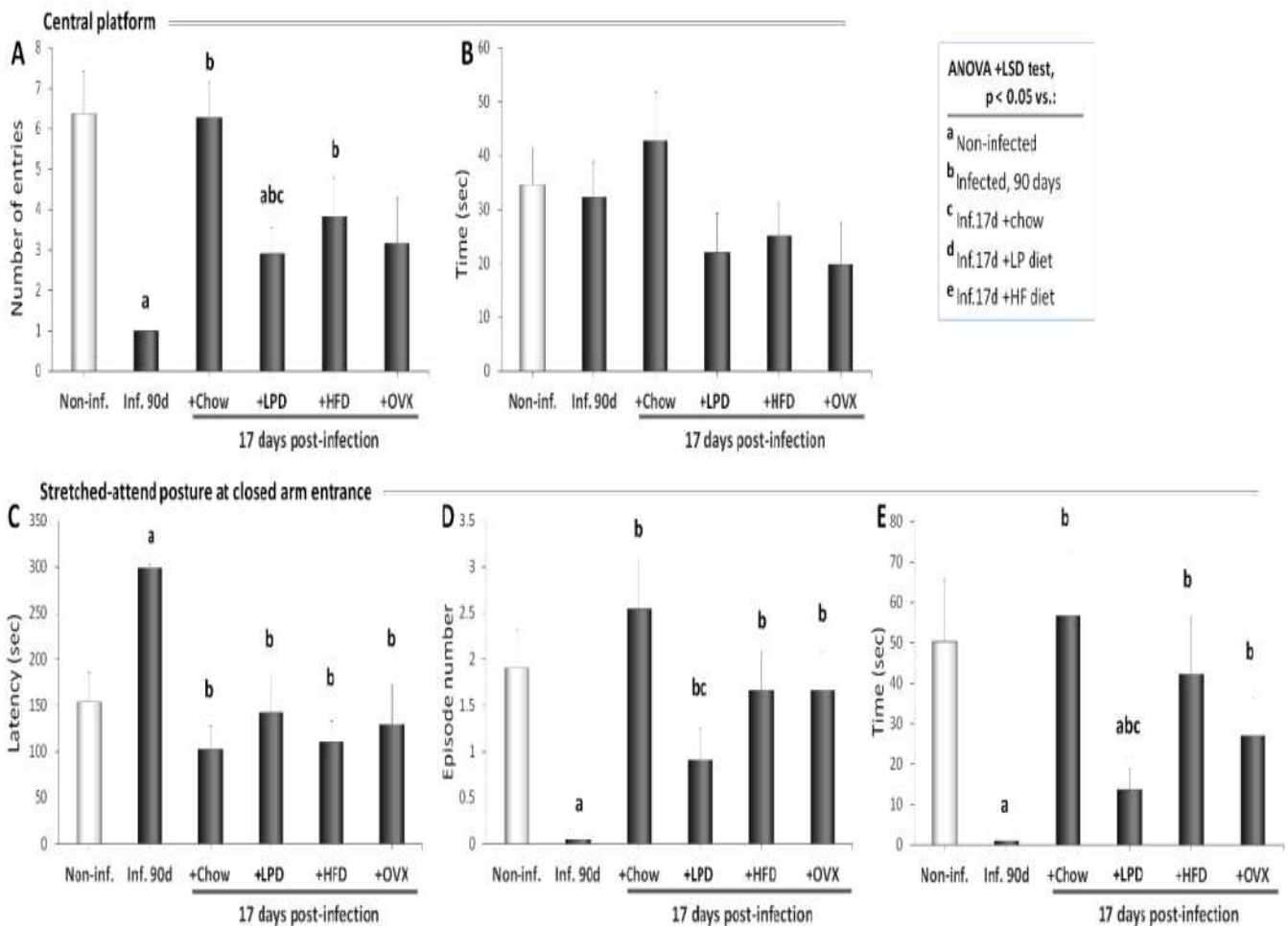


Figure 34. Centre entries and attend posture in the maze at 17 days post-infection

The SAP latency was significantly increased in infected animals sacrificed at 90 dpi compared to the non-infected group and to all the infected groups sacrificed at 17 dpi (figure 34C, table XXIV). Instead, SAP episode number (figure 34D) and time (figure 34E) were significantly decreased in infected animals sacrificed at 90 dpi and LPD-fed animals compared to the non-infected group and to the other infected groups (table XXIV).

Table XXIV. Activities around maze central platform at 17 dpi of infection

		Infected, 17 days				
		Inf. 90d	+Chow	+LPD	+HFD	+OVX
Central platform entries						
Non-inf.	4.50E-4***	0.948	0.012*	0.094	0.060	
Inf. 90d		1.30E-4***	0.012*	0.030*	0.115	
Chow			0.006**	0.081	0.054	
LPD				0.435	0.848	
HFD					0.662	
Central platform time						
Non-inf.	0.822	0.473	0.225	0.325	0.178	
Inf. 90d		0.366	0.321	0.455	0.256	
Chow			0.087	0.124	0.071	
LPD				0.743	0.841	
HFD					0.598	
Latency to stretched-attend posture at closed arm entrance						
Non-inf.	0.001***	0.230	0.828	0.294	0.668	
Inf. 90d		1.60E-5***	0.002***	3.70E-4***	0.012*	
Chow			0.401	0.805	0.607	
LPD				0.492	0.829	
HFD					0.715	
Number of stretched-attend posture episodes at closed arm entrance						
Non-inf.	0.001**	0.355	0.078	0.688	0.688	
Inf. 90d		0.001**	0.024*	0.011*	0.011*	
Chow			0.019*	0.214	0.214	
LPD				0.190	0.190	
HFD					1.000	
Time of stretched-attend posture at closed arm entrance						
Non-inf.	0.008**	0.770	0.042*	0.706	0.215	
Inf. 90d		0.004**	0.023*	0.031*	0.036*	
Chow			0.021*	0.502	0.123	
LPD				0.104	0.254	
HFD					0.393	

ANOVA+LSD test: *P<0.05; **P<0.01; ***P<0.001.

3.2.4 Sex differences in OFT and EPM cognitive indicators

3.2.4.1 OFT – locomotion, grooming and gait

Figure 35 and table XXV present the impact of LPD and sex on the effects of *T. gondii* infection on the locomotion episode number (figure 35A), distance covered (figure 35B), locomotion time (figure 35C); grooming episode latency (figure 35D), number (figure 35E), and time (figure 35F); as well as paw licking episode number (figure 35G), and scores of head posture (figure 35H), and gait (figure 35I). Compared to females and to non-infected males, infected males fed LPD showed significantly lower locomotion episode numbers, distance covered, and locomotion time (figures 35A-C, table XXV). Significant differences were also observed

between non-infected males and LPD-fed infected males in grooming latency (figure 35D, table XXV). Inter-sex differences (table XXV) were observed in non-infected animals' locomotion episode number (figure 35A) and in LPD-fed infected animals' grooming episode number (figure 35E), head posture score (figure 35H), and gait score (figure 35I).

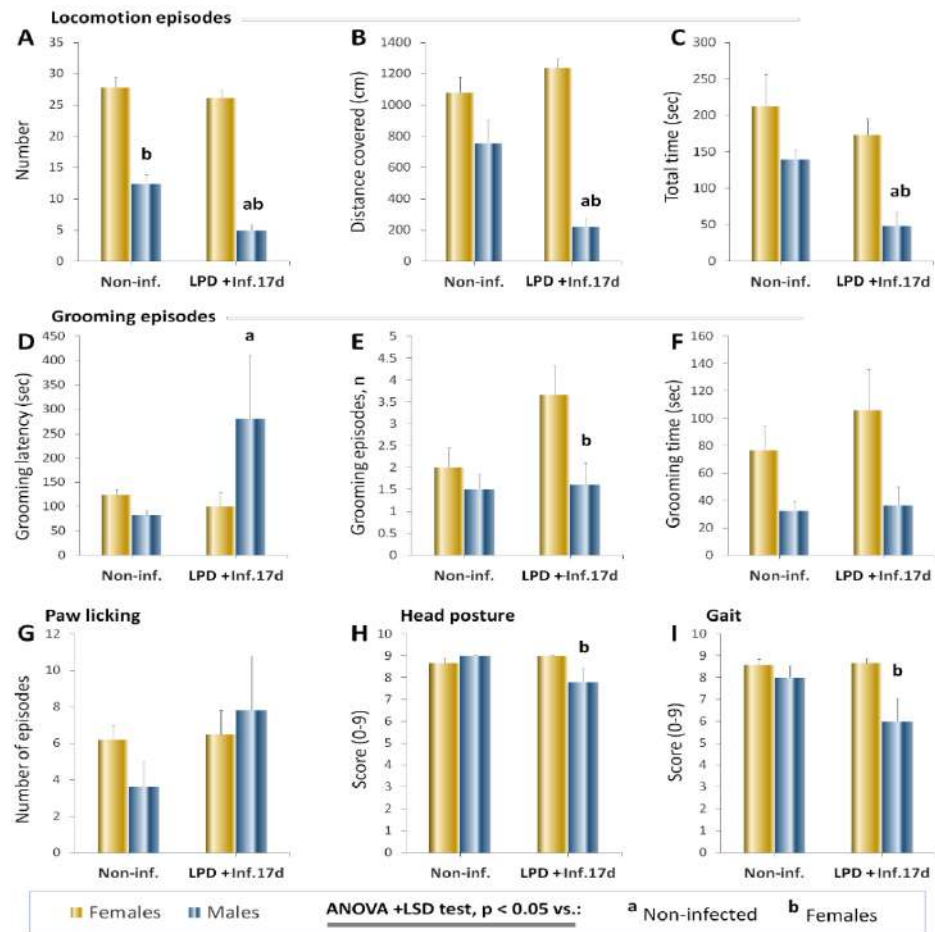


Figure 35. Locomotion and grooming-related parameters of rats fed LPD

Table XXV. Sex comparisons in OFT indicators of rats fed LPD

Locomotion episode number		Distance covered	
Vs. Non-inf.	Vs. females	Vs. Non-inf.	Vs. females
Inf. F 0.425	Non-inf. 1.1E-4***	Inf. F 0.166	Non-inf. 0.105
Inf. M 0.002**	Infected 1.3E-7***	Inf. M 0.011*	Infected 3.5E-7***
Locomotion time		Grooming latency	
Vs. Non-inf.	Vs. females	Vs. Non-inf.	Vs. females
Inf. F 0.404	Non-inf. 0.139	Inf. F 0.440	Non-inf. 0.014*
Inf. M 0.005**	Infected 0.002**	Inf. M 0.169	Infected 0.175
Grooming episode number		Grooming time	
Vs. Non-inf.	Vs. females	Vs. Non-inf.	Vs. females
Inf. F 0.079	Non-inf. 0.389	Inf. F 0.421	Non-inf. 0.061
Inf. M 0.870	Infected 0.041*	Inf. M 0.816	Infected 0.081
Paw licking episode number		Head posture score	
Vs. Non-inf.	Vs. females	Vs. Non-inf.	Vs. females
Inf. F 0.852	Non-inf. 0.132	Inf. F 0.145	Non-inf. 0.186
Inf. M 0.233	Infected 0.677	Inf. M 0.074	Infected 0.049*
Gait score		Arena centre latency	
Vs. Non-inf.	Vs. females	Vs. Non-inf.	Vs. females
Inf. F 0.840	Non-inf. 0.347	Inf. F 0.939	Non-inf. 0.071
Inf. M 0.129	Infected 0.023*	Inf. M 0.229	Infected 0.001**
Arena centre distance		Arena centre entries	
Vs. Non-inf.	Vs. females	Vs. Non-inf.	Vs. females
Inf. F 0.711	Non-inf. 0.001**	Inf. F 0.359	Non-inf. 0.064
Inf. M 0.192	Infected 0.003**	Inf. M 0.160	Infected 0.001**
Arena centre time		Distance covered close to walls	
Vs. Non-inf.	Vs. females	Vs. Non-inf.	Vs. females
Inf. F 0.320	Non-inf. 0.018*	Inf. F 0.179	Non-inf. 0.238
Inf. M 0.335	Infected 0.006**	Inf. M 0.006**	Infected 7.1E-7***
Close to wall area entries		Close to wall time	
Vs. Non-inf.	Vs. females	Vs. Non-inf.	Vs. females
Inf. F 0.353	Non-inf. 0.088	Inf. F 0.926	Non-inf. 0.261
Inf. M 0.009**	Infected 8.3E-7***	Inf. M 0.680	Infected 0.008**
Stretched-attend posture latency		Stretched-attend posture time	
Vs. Non-inf.	Vs. females	Vs. Non-inf.	Vs. females
Inf. F 0.217	Non-inf. 0.019*	Inf. F 0.203	Non-inf. 0.017*
Inf. M 0.022*	Infected 0.050	Inf. M 3.8E-4***	Infected 9.6E-6***
Angle entries		Angle time	
Vs. Non-inf.	Vs. females	Vs. Non-inf.	Vs. females
Inf. F 0.668	Non-inf. 0.221	Inf. F 0.628	Non-inf. 0.198
Inf. M 0.011*	Infected 3.0E-4***	Inf. M 0.477	Infected 0.003**
Rearing against wall latency		Rearing against wall episode number	
Vs. Non-inf.	Vs. females	Vs. Non-inf.	Vs. females
Inf. F 0.421	Non-inf. 0.855	Inf. F 0.720	Non-inf. 0.126
Inf. M 0.005**	Infected 0.001**	Inf. M 0.019*	Infected 2.9E-5***
Rearing on hindlimb latency		Rearing on hindlimb episode number	
Vs. Non-inf.	Vs. females	Vs. Non-inf.	Vs. females
Inf. F 0.567	Non-inf. 0.317	Inf. F 0.393	Non-inf. 0.002**
Inf. M 0.019*	Infected 7.4E-7***	Inf. M 0.018	Infected 0.001**

3.2.4.2 OFT – centre and close to wall activities

Figure 36 and table XXV present the impact of LPD and sex on the effects of *T. gondii* infection on the arena central area latency (figure 36A), distance covered (figure 36B), entries (figure 36C) and total time (figure 36D); SAP episode latency (figure 36E) and time (figure 36F); as well as the distance covered (figure 36G), the number of entries (figure 36H), and the total time spent (figure 36I) in the area close to the OFT arena walls. Compared to females and to non-infected males, infected males fed LPD showed significantly higher SAP time (figure 36F, and table XXV) and lower close to wall area distance and entries (figures 36G, H, and table XXV).

In addition, a significantly lower SAP latency was observed in LPD-fed infected males compared to non-infected males (figure 36E, table XXV). Inter-sex differences (table XXV) were observed in non-infected animals' arena distance (figure 36B) and time (figure 36B), in SAP latency (figure 36E) and time (figure 36F); as well as in LPD-fed infected animals' arena distance (figure 36B) and time (figure 36B), and in close to wall time (figure 36I).

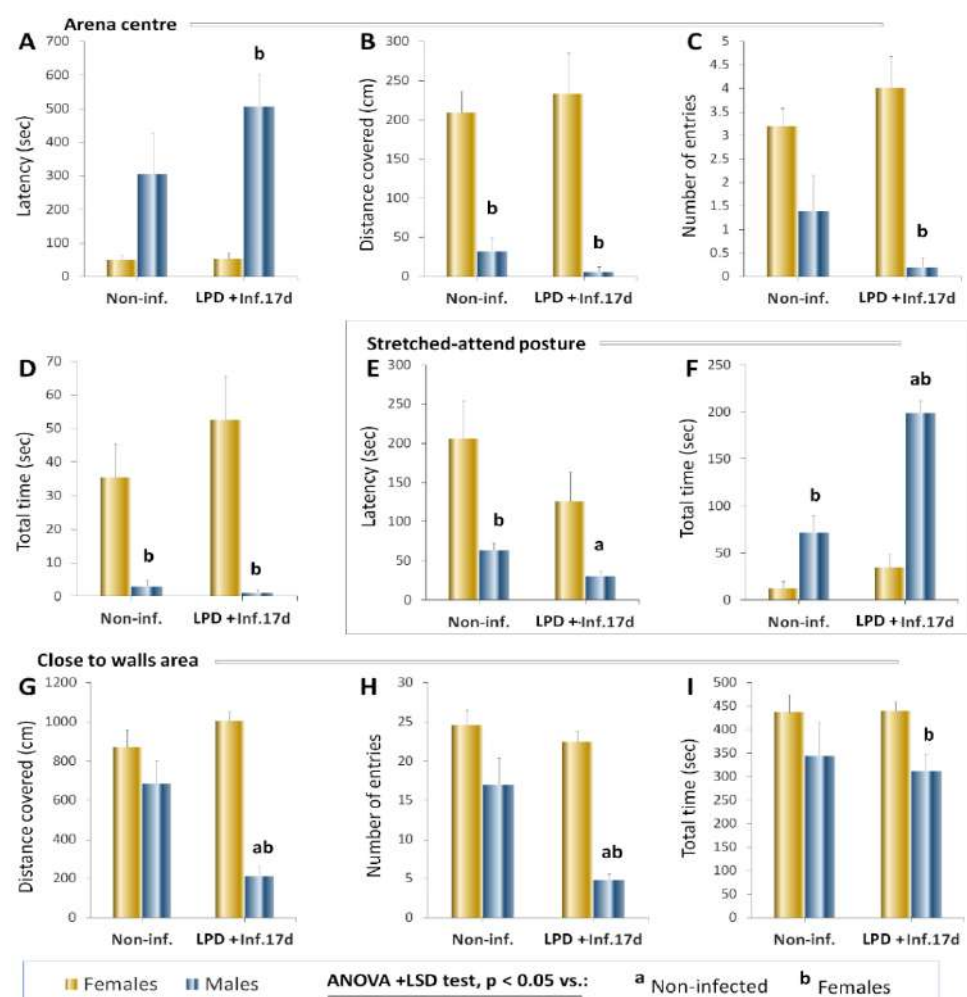


Figure 36. Arena centre and close to wall activities of rats fed LPD

3.2.4.3 OFT – angle entries and rearing episodes

Figure 37 and table XXV present the impact of LPD and sex on the effects of *T. gondii* infection on the arena angles' entries (figure 37A) and time (figure 37B), on the rearing against wall latency (figure 37C) and episode number (figure 37D), and on the rearing on hindlimbs' latency (figure 37E) and episode number (figure 37F). Compared to females and to non-infected males, infected males fed LPD showed significantly lower arena angle entries (figure 37A, table XXV) and higher rearing against wall and rearing on hindlimbs' latencies (figures 37C, E, and table XXV). In addition, significant inter-sex differences (table XXV) were observed, notably a decrease in rearing on hindlimbs' episodes (figure 37F) in non-infected animals, as well as angle time increase (figure 37B) and rearing on hindlimbs' decrease (figure 37F) in LPD-fed infected animals.

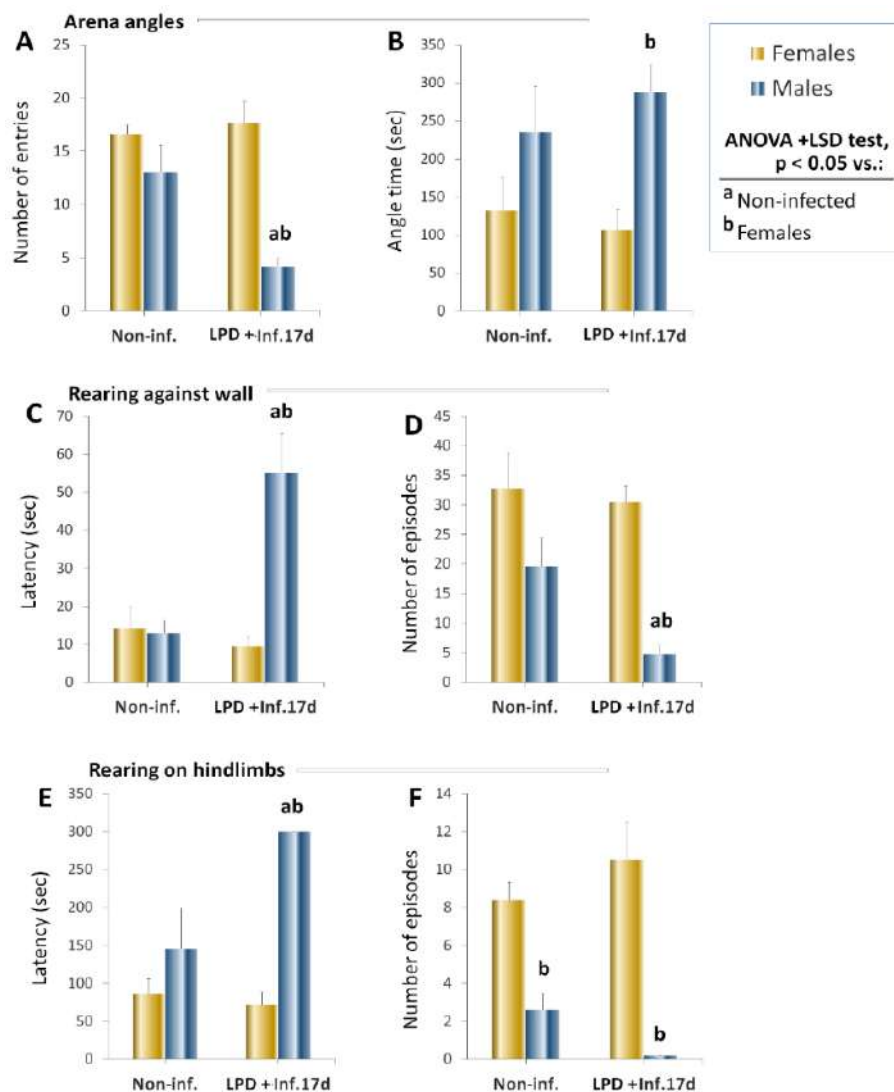


Figure 37. Rearing activities and arena angle time of rats fed LPD

3.2.4.4 EPM motor indicators

Figure 38 and table XXVI present the impact of LPD and sex on the effects of *T. gondii* infection on the distance covered in the EPM maze (figures 38A-C), on the percent of time spent active (figures 38D-F), and on the animal speed in the maze (figures 38G-I). Compared to females and to non-infected males, infected males fed LPD showed significantly lower values of total and first minute distances (figures 38A, B, and table XXVI) and percent of time spent active (figures 3.2.4.1.1total test time and first minute percent of time spent active (figures 38D, E), and an increase in first minute speed (figure 38H); and (ii) in LPD-fed infected animals, namely a decrease in last minute percent of time spent active (figure 38F), and an increase in first minute speed (figure 38H). Notably, unlike for the first minute, no statistically significant difference was observed in locomotor activity indicators in the last minute of the test between the non-infected and the LPD-fed infected animals (figures 38C, F, I, and table XXVI).

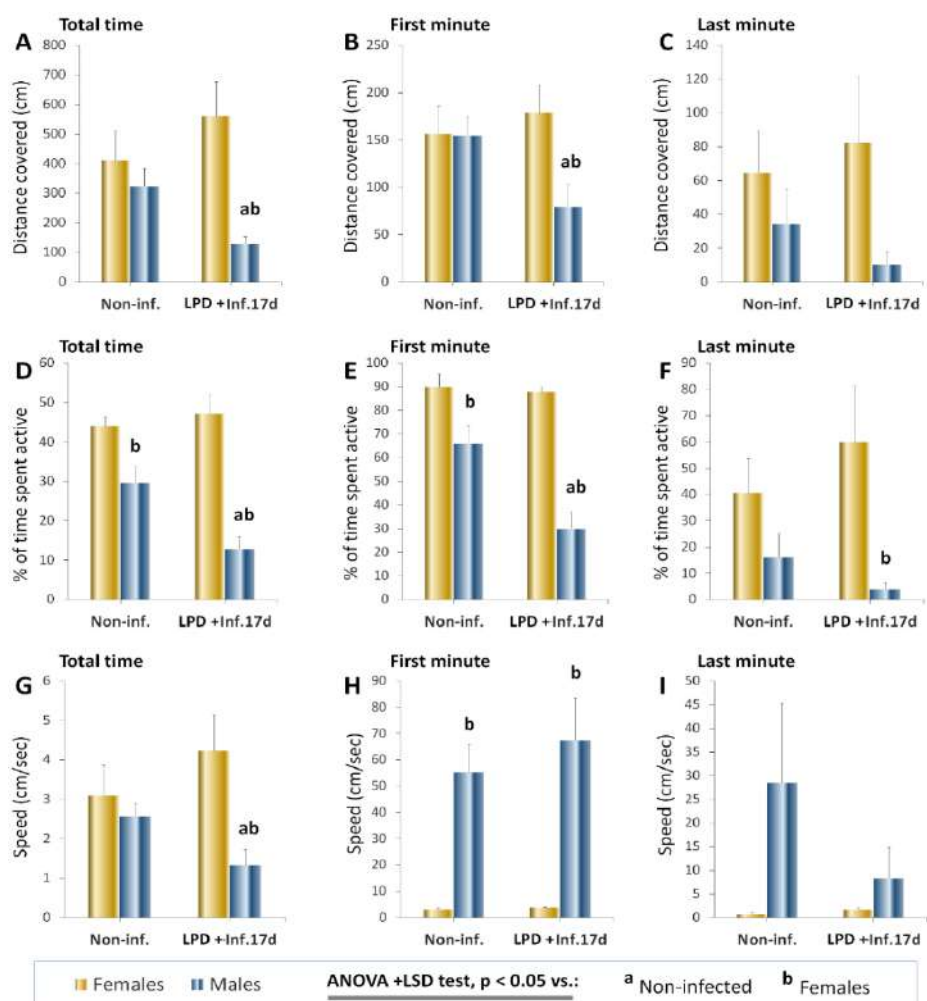


Figure 38. EPM motor indicators of rats fed LPD

Table XXVI. Sex comparisons of EPM cognitive indicators of rats fed LPD

Total distance covered		1st min distance	
Vs. Non-inf.	Vs. females	Vs. Non-inf.	Vs. females
Inf. F 0.356	Non-inf. 0.445	Inf. F 0.614	Non-inf. 0.950
Inf. M 0.020*	Infected 0.009**	Inf. M 0.036*	Infected 0.031*
4th min distance		Total activity time	
Vs. Non-inf.	Vs. females	Vs. Non-inf.	Vs. females
Inf. F 0.720	Non-inf. 0.363	Inf. F 0.537	Non-inf. 0.020*
Inf. M 0.328	Infected 0.134	Inf. M 0.014*	Infected 0.001**
1st min activity time		4th min activity time	
Vs. Non-inf.	Vs. females	Vs. Non-inf.	Vs. females
Inf. F 0.782	Non-inf. 0.033*	Inf. F 0.434	Non-inf. 0.143
Inf. M 0.007**	Infected 0.001**	Inf. M 0.269	Infected 0.012*
Total average speed		1st min average speed	
Vs. Non-inf.	Vs. females	Vs. Non-inf.	Vs. females
Inf. F 0.383	Non-inf. 0.521	Inf. F 0.348	Non-inf. 0.002**
Inf. M 0.036*	Infected 0.013*	Inf. M 0.540	Infected 0.027*
4th min average speed		Head dipping latency	
Vs. Non-inf.	Vs. females	Vs. Non-inf.	Vs. females
Inf. F 0.096	Non-inf. 0.170	Inf. F 0.715	Non-inf. 0.172
Inf. M 0.328	Infected 0.463	Inf. M 0.903	Infected 0.368
Head dipping entries		Head dipping time	
Vs. Non-inf.	Vs. females	Vs. Non-inf.	Vs. females
Inf. F 0.835	Non-inf. 0.039*	Inf. F 0.637	Non-inf. 0.113
Inf. M 0.338	Infected 0.120	Inf. M 0.390	Infected 0.140
Rearing against walls latency		Episodes of rearing against walls, n	
Vs. Non-inf.	Vs. females	Vs. Non-inf.	Vs. females
Inf. F 0.470	Non-inf. 0.344	Inf. F 0.581	Non-inf. 0.119
Inf. M 0.098	Infected 0.160	Inf. M 0.005**	Infected 0.004**
Rearing on hindlimb latency		Number of rearing on hindlimbs	
Vs. Non-inf.	Vs. females	Vs. Non-inf.	Vs. females
Inf. F 0.389	Non-inf. 0.389	Inf. F 0.900	Non-inf. 0.900
Inf. M 0.753	Infected 0.900	Inf. M 0.339	Infected 0.339
Grooming latency		Grooming time	
Vs. Non-inf.	Vs. females	Vs. Non-inf.	Vs. females
Inf. F 0.321	Non-inf. 0.961	Inf. F 0.419	Non-inf. 0.384
Inf. M 0.611	Infected 0.611	Inf. M 0.249	Infected 0.304

3.2.4.5 EPM – head dipping and rearing episodes

Figure 39 and table XXVI present the impact of LPD and sex on the effects of *T. gondii* infection on the head dipping episodes' latency (figure 39A), number (figure 39B), and time (figure 39C), on the rearing against wall episode latency (figure 39D) and number (figure 39E), on the rearing on hindlimbs' episode latency (figure 39F) and number (figure 39G), and on the grooming latency (figure 39H) and time (figure 39I) in the EPM maze. Compared to females and to non-infected males, infected males fed LPD showed a significantly lower rearing against

wall episode number (figure 39E, table XXVI). In addition, compared to females, LPD-fed infected male group showed a significantly lower number of episodes of head dipping (figure 39B, table XXVI).

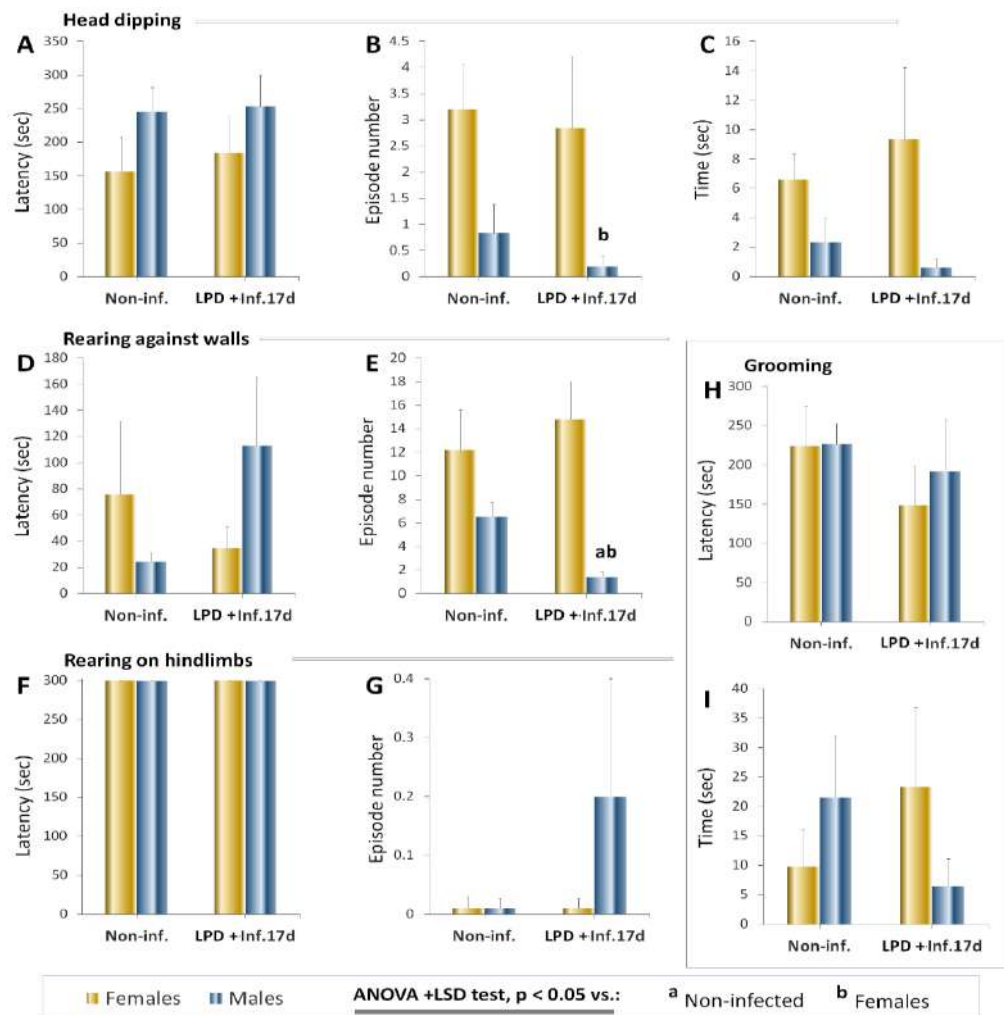


Figure 39. Head dipping and rearing in the maze of rats fed LPD

3.2.4.6 EPM – arm entries

Figure 40 and table XXVII present the impact of LPD and sex on the effects of *T. gondii* infection on the open arm latency (figure 40A), number of entries (figure 40B), time (figure 40C), on the open arm bottom latency (figure 40D), entries (figure 40E), time (figure 40F), on the closed arm latency (figure 40G), entries (figure 40H), time (figure 40I), and on the closed arm bottom latency (figure 40J), entries (figure 40K), and time (figure 40L). No statistically significant difference was observed between female and male groups and their non-infected counterparts (table XXVII). Instead, closed arm and closed bottom entries were lesser in males compared to females (figures 40H, K and table XXVII).

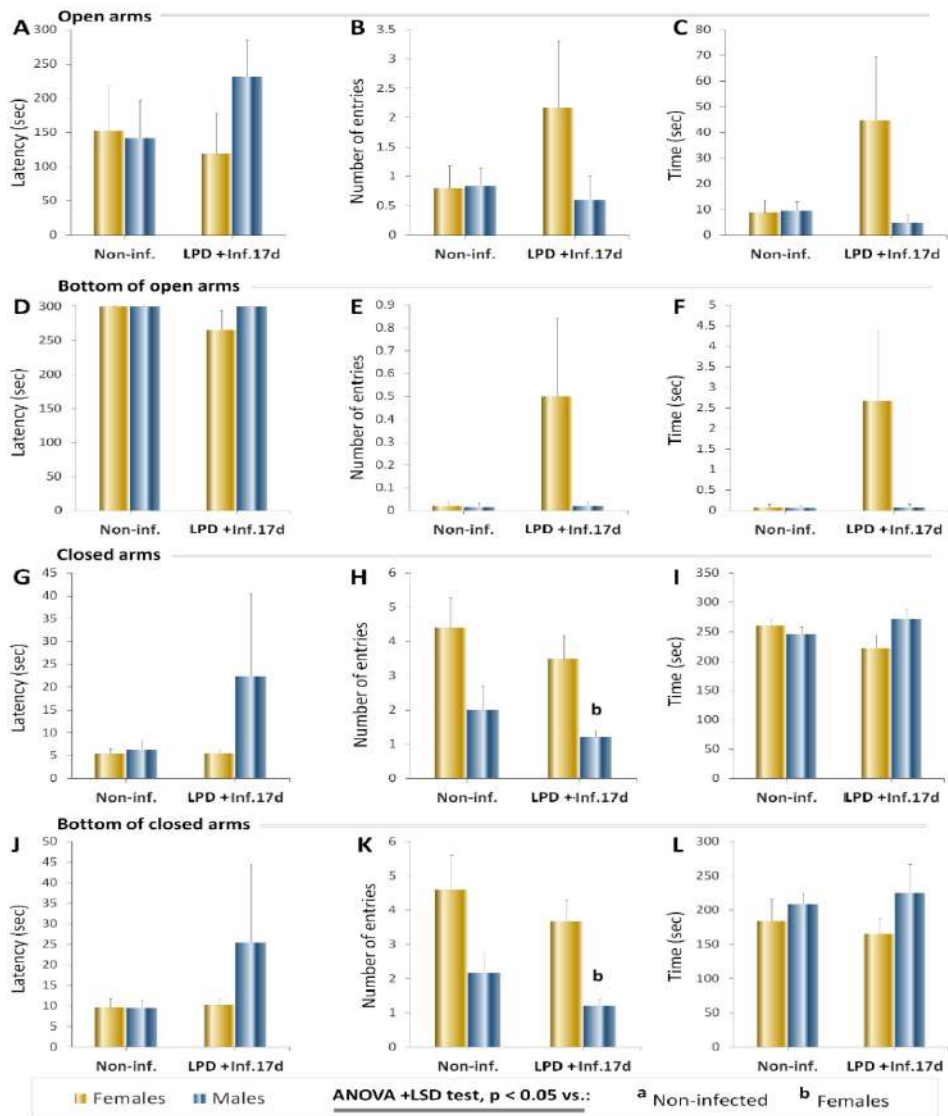


Figure 40. EPM arm latency and time of rats fed LPD

Table XXVII. Sex comparisons of EPM arm visits by rats fed LPD

Open arm latency		Open arm entries											
Vs. Non-inf.	Vs. females	Vs. Non-inf.	Vs. females										
Inf. F	0.704	Non-inf.	0.898										
Inf. M	0.283	Infected	0.199										
Open arm time		Open arm bottom latency											
Vs. Non-inf.	Vs. females	Vs. Non-inf.	Vs. females										
Inf. F	0.224	Non-inf.	0.908										
Inf. M	0.371	Infected	0.178										
Open arm bottom entries		Open arm bottom time											
Vs. Non-inf.	Vs. females	Vs. Non-inf.	Vs. females										
Inf. F	0.236	Non-inf.	0.900										
Inf. M	0.900	Infected	0.236										
Closed arm latency		Closed arm entries											
Vs. Non-inf.	Vs. females	Vs. Non-inf.	Vs. females										
Inf. F	0.941	Non-inf.	0.704										
Inf. M	0.357	Infected	0.330										
Closed arm time		Closed arm bottom latency											
Vs. Non-inf.	Vs. females	Vs. Non-inf.	Vs. females										
Inf. F	0.176	Non-inf.	0.403										
Inf. M	0.241	Infected	0.120										
Bottom of closed arm entries		Bottom of closed arm time											
Vs. Non-inf.	Vs. females	Vs. Non-inf.	Vs. females										
Inf. F	0.424	Non-inf.	0.049										
Inf. M	0.157	Infected	0.007**										
Central platform entries		Central platform time											
Vs. Non-inf.	Vs. females	Vs. Non-inf.	Vs. females										
Inf. F	0.648	Non-inf.	0.337										
Inf. M	0.017*	Infected	0.013*										
Latency to SAP at closed arm entrance		SAP at closed arm entrance, n											
Vs. Non-inf.	Vs. females	Vs. Non-inf.	Vs. females										
Inf. F	0.329	Non-inf.	0.806										
Inf. M	0.864	Infected	0.659										
Time of SAP at closed arm entrance		Vs. Non-inf.	Vs. females	Vs. Non-inf.	Vs. females	Inf. F	0.267	Non-inf.	0.075	Inf. M	0.579	Infected	0.218
Vs. Non-inf.	Vs. females	Vs. Non-inf.	Vs. females										
Inf. F	0.267	Non-inf.	0.075										
Inf. M	0.579	Infected	0.218										

3.2.4.7 EPM – central platform activities

Figure 41 and table XXVII present the impact of LPD and sex on the effects of *T. gondii* infection on the central platform entries (figure 41A) and time (figure 41B), and on SAP episode latency (figure 41C), number (figure 41D), and time (figure 41E). No statistically significant difference was observed between infected and non-infected groups and between sexes (table XXVII).

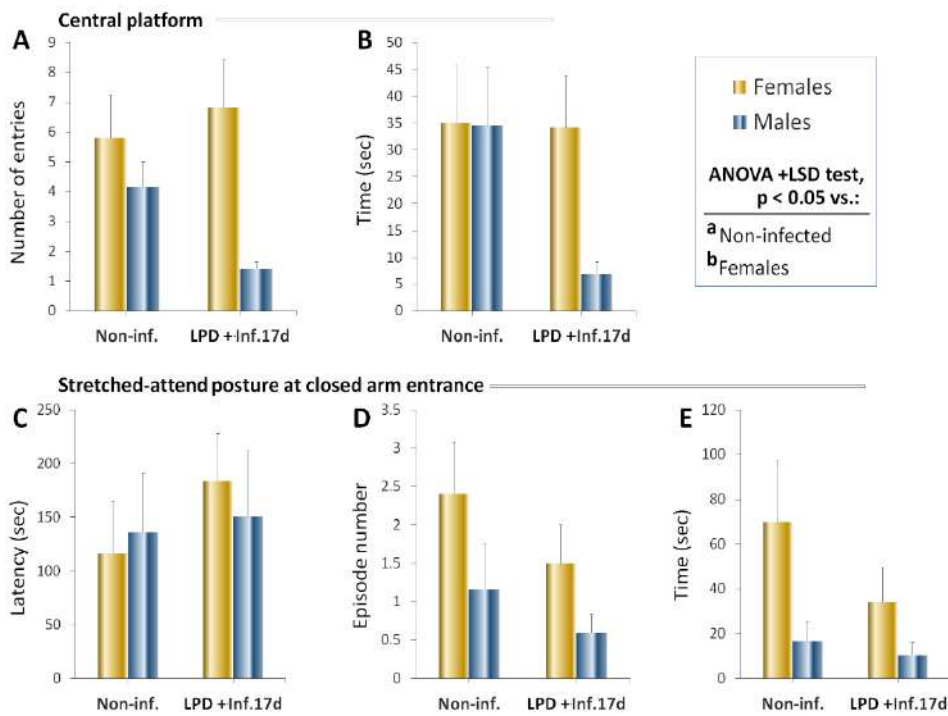


Figure 41. Centre entries and attend posture in the maze of rats fed LPD

3.2.5 Parasite and immune cell count in the blood

Figure 42 shows blood smears of representative animals. While non-infected animals presented with normal blood smears (figure 42A), all infected groups displayed increases in white blood cell (WBC) density (figures 42B-F), particularly marked in terminal-stage infected animals (figure 42B), HFD-fed animals (figure 42D), and ovariectomised infected animals (figure 42E). In addition, the infected rats fed chow (figure 42C), and to a lesser extent HFD- (figure 42D) and LPD-fed (figure 42F) animals, had a large number of circulating *T. gondii* cysts in their blood.

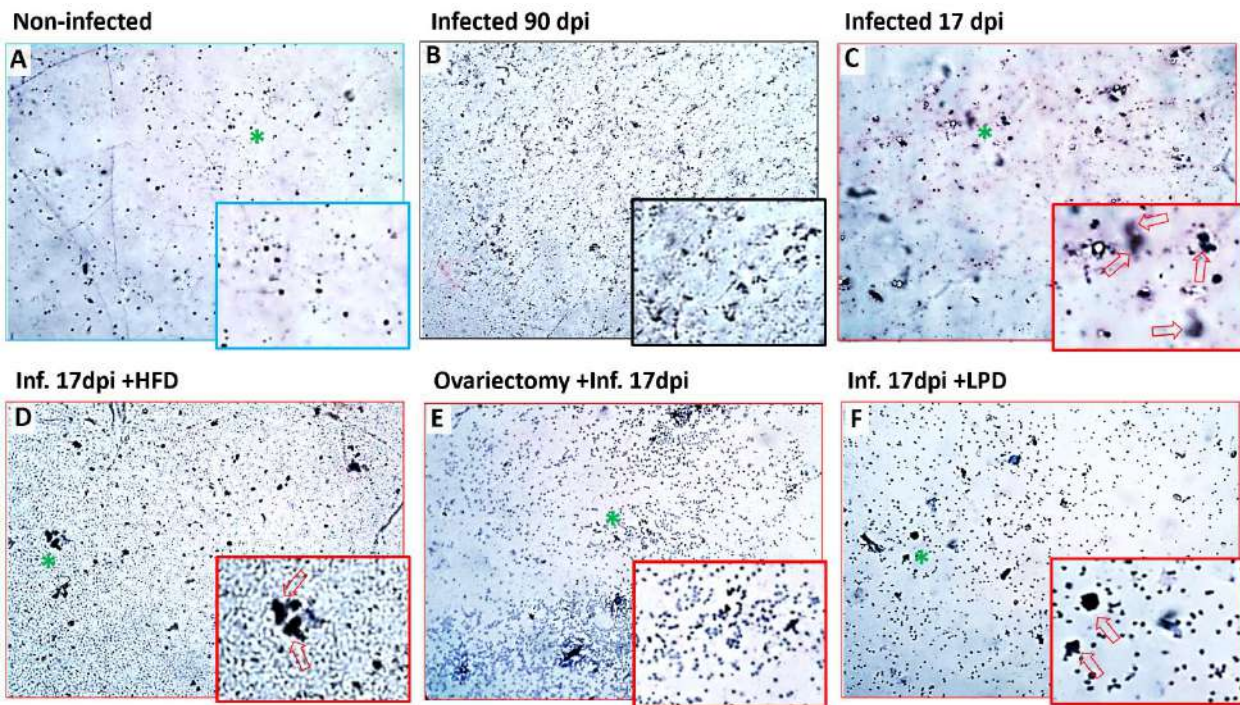


Figure 42. Blood smears of representative animals

*Green asterisks: areas magnified in the insets. Red arrows: *T. gondii* cysts. Note the high number of cysts in the early stage of infection (C) but not in the terminal stage (B).*

Figure 43 shows parasite and white blood cell counts, while table XXVIII presents the results of inter-group comparisons for statistical significance. Cysts and tachyzoites were not present in non-infected animals (figures 43A, B). Terminal-stage infected animals had the lowest cyst count (figure 43A) and the highest tachyzoite count (figure 43B).

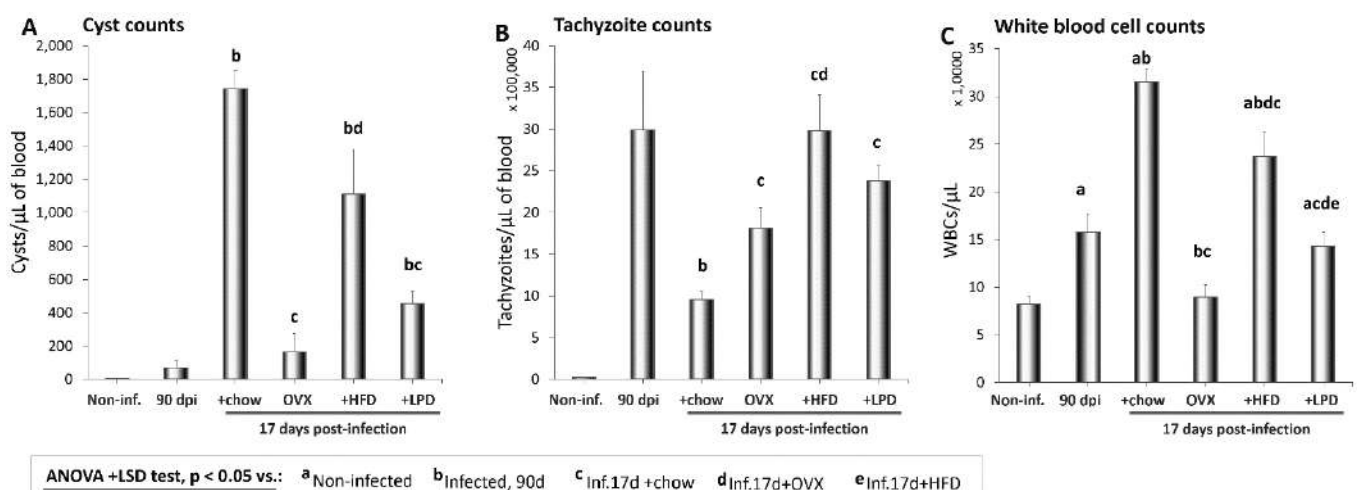


Figure 43. Blood parasite and immune cell counts

*Blood counts of *T. gondii* cysts (A) and tachyzoites (B), and white blood cells (C). Note the higher number of white blood cells in the infected groups compared to the non-infected (C).*

Untreated early-stage chow-fed rats (early-stage infection control group) had the highest cyst count (figure 43A) and the lowest tachyzoite count of all untreated animals (figure 43B). Instead, compared to the early-stage infection control group, LPD-fed and ovariectomised infected groups, but not the HFD-fed infected group (respectively, HFD-fed, LPD-fed, and ovariectomised infected groups) presented with significantly decreased cyst counts (respectively, increased tachyzoite count) (figures 43A, B and table XXVIII). Moreover, except for the ovariectomized infected rats, all infected animals showed significantly higher WBC counts (table XXVIII), with the highest counts in untreated early-stage infected rats fed chow, followed by HFD-fed (figure 43C). These groups had markedly higher WBC counts than all the other infected groups (table XXVIII).

Table XXVIII. Blood cell count comparisons

		Infected 17 days				
		Inf .90 days	+chow	+OVX	+HFD	+PPD
Cyst counts						
Non-inf.	0.184	2.1E-8***	0.191	0.002**	1.3E-4***	
Inf.90d		5.9E-8***	0.452	0.003**	0.001**	
+chow			1.4E-6***	0.054	7.0E-6***	
+OVX				0.009**	0.070	
+HFD					0.059	
Tachyzoite counts						
Non-inf.	0.002**	3.1E-6***	3.0E-5***	4.7E-5***	2.5E-7***	
Inf.90d		0.016*	0.144	0.986	0.460	
+chow			0.009**	0.001**	5.6E-5***	
+OVX				0.042*	0.112	
+HFD					0.270	
WBC counts						
Non-inf.	0.003**	8.2E-8***	0.646	1.4E-4***	0.004**	
Inf.90d		9.2E-5***	0.012*	0.028*	0.539	
+chow			8.2E-7***	0.029*	1.3E-5***	
+OVX				3.7E-4***	0.019*	
+HFD					0.008**	

3.2.6 Brain neuronal density

3.2.6.1 Brain anterior areas: cingulate cortex and medial septal nucleus

All the infected groups without treatment showed neuronal losses and decreased neuronal densities in the anterior cingulate cortex, more in terminal-stage infected rats and in early-stage infected rats fed LPD than others (figures 44B-F).

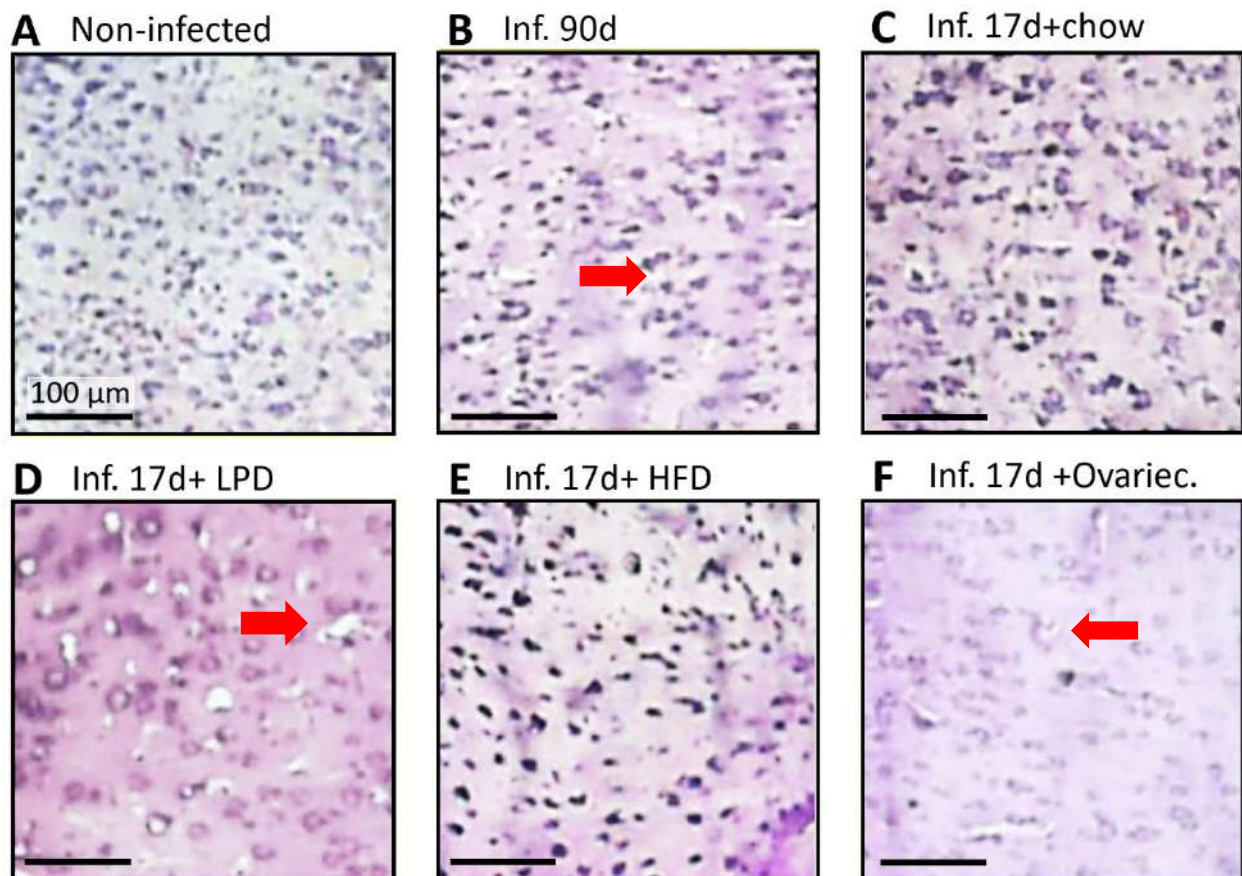


Figure 44. Micrographs of anterior cingulate cortices of representative animals

Red arrow: Neuronal loss in infected 90 days, LPD-fed and ovariectomized (**B,D,F**).

The infected groups without treatment showed a decreased neuronal density in the medial septal nucleus particularly marked in terminal-stage infected rats and in early-stage infected rats than others (figures 45B-F).

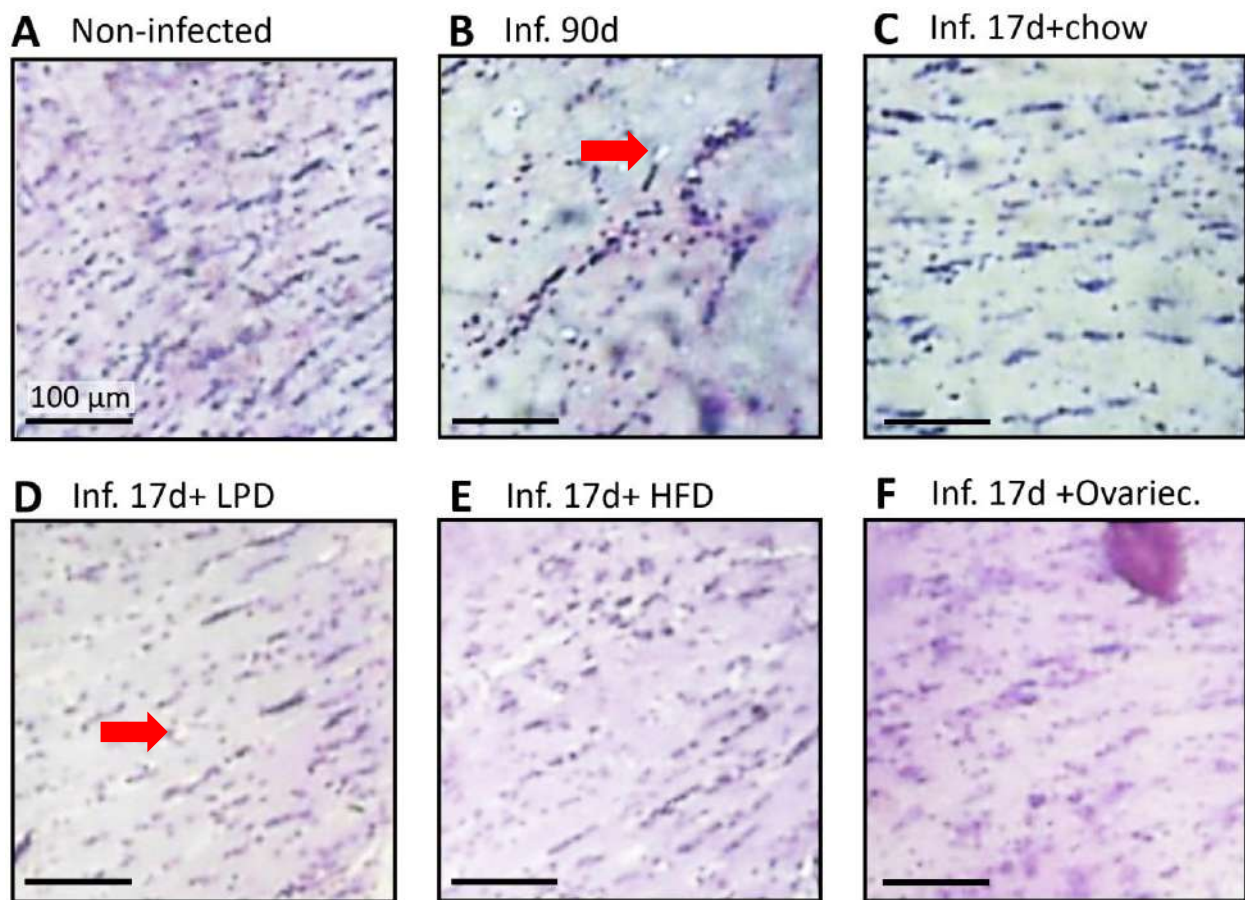
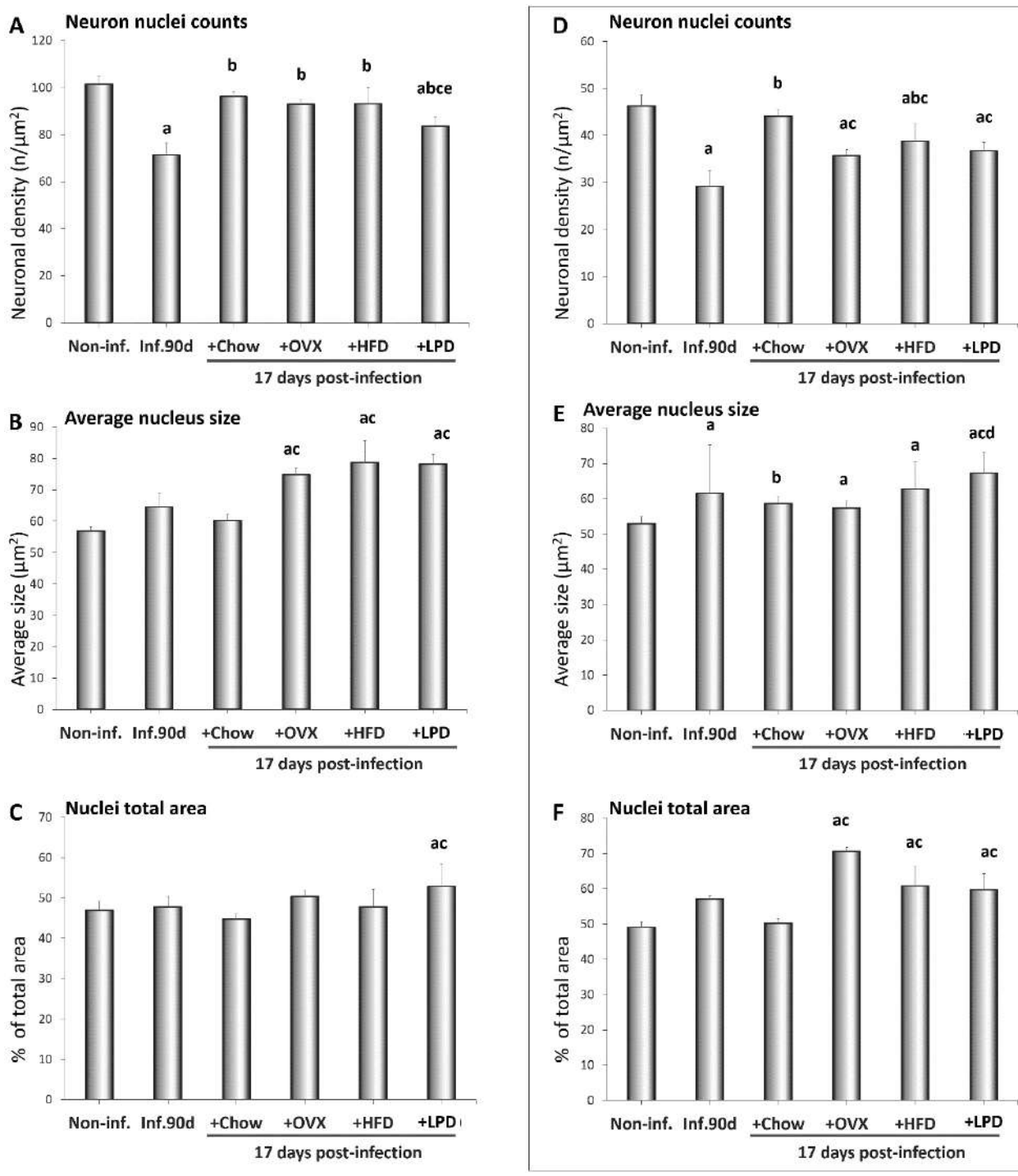


Figure 45. Micrographs of medial septal nuclei of representative animals

Red arrow: Neuronal losses in the late stage and LPD-fed infected animals (B, D).

Compared to the non-infected rats, the terminal-stage infected rats had a significantly lower neuronal density in the anterior area of the cingulate cortex (Figure 46A, table XXIX). Compared to the 17 days infected rats fed normal chow, the 17 days infected rats fed LPD had a significantly lower neuronal density in the anterior area of the cingulate cortex and in the anterior area of the medial septal nucleus (figures 46A, D and table XXIX).



ANOVA +LSD test, $p < 0.05$ vs.: a Non-infected b Infected, 90d c Inf.17d +chow d Inf.17d+OVX e Inf.17d+HFD

Figure 46. Average counts in brain anterior areas

Counts in the anterior cingulate cortex (A-C) and in the medial septal nucleus (D-F).

Increases in the average nucleus size (Figure 46B, E) and in nuclei total area (figures 46C, F) were observed in the cingulate cortices and in the medial septal nuclei of LPD-fed, HFD-fed and ovariectomized groups compared to non-infected and early-stage infected chow-fed groups (table XXIX).

Table XXIX. cell count comparisons in brain anterior areas

		Infected 17d			
	Inf.90d	+Chow	+OVX	+HFD	+LPD
Counts in the anterior cingulate cortex					
Non-inf.	1.9E-5***	0.131	0.189	0.115	3.0E-5***
Inf.90d		3.6E-6***	0.030*	0.003**	0.029*
+Chow			0.521	0.446	1.4E-4***
+OVX				0.975	0.119
+HFD					0.040*
Average size of neuron nuclei in the anterior cingulate cortex					
Non-inf.	0.084	0.228	0.001**	8.2E-9***	1.2E-6***
Inf.90d		0.570	0.489	0.057*	0.219
+Chow			0.009**	4.2E-5***	2.3E-5***
+OVX				0.631	0.635
+HFD					0.951
% area of neuron nuclei in the anterior cingulate cortex					
Non-inf.	0.907	0.377	0.435	0.881	0.036*
Inf.90d		0.555	0.773	0.998	0.326
+Chow			0.112	0.465	4.5E-4***
+OVX				0.710	0.522
+HFD					0.257
Counts in the medial septal nucleus					
Non-inf.	0.001**	0.375	0.031*	0.020*	0.002**
Inf.90d		1.3E-4***	0.230	0.016*	0.082
+Chow			0.024*	0.030*	0.002**
+OVX				0.423	0.813
+HFD					0.464
Average size of neuron nuclei in the medial septal nucleus					
Non-inf.	9.2E-7***	0.077***	7.0E-9***	1.4E-5***	3.9E-6***
Inf.90d		9.6E-5***	0.372	0.971	0.115
+Chow			6.1E-9***	5.2E-6***	7.5E-5***
+OVX				0.338	0.001**
+HFD					0.053
% area of neuron nuclei in the medial septal nucleus					
Non-inf.	0.075	0.554	2.4E-5***	0.010*	0.001**
Inf.90d		0.125	0.148	0.733	0.731
+Chow			3.3E-6***	0.004**	0.001**
+OVX				0.244	0.070
+HFD					0.818

3.2.6.2 Brain posterior areas: parietal cortex and lateral hypothalamus

Compared to the non-infected rats (figure 47A), terminal-stage infected showed the most marked decrease in neuronal density among all the groups in the posterior parietal cortex (figures 47B-F). LPD-fed infected rats also showed a marked decrease in neuronal density in the posterior parietal cortex, but in addition, animals of this group presented with enlarged

neuron nuclei (figure 47D). To a lesser extent, enlarged nuclei were also observed in the 17 days infected rats fed normal chow (figure 47C), LPD-fed infected rats untreated (figure 47D), as well as HFD-fed (figure 47E) and ovariectomised infected rats (figure 47F).

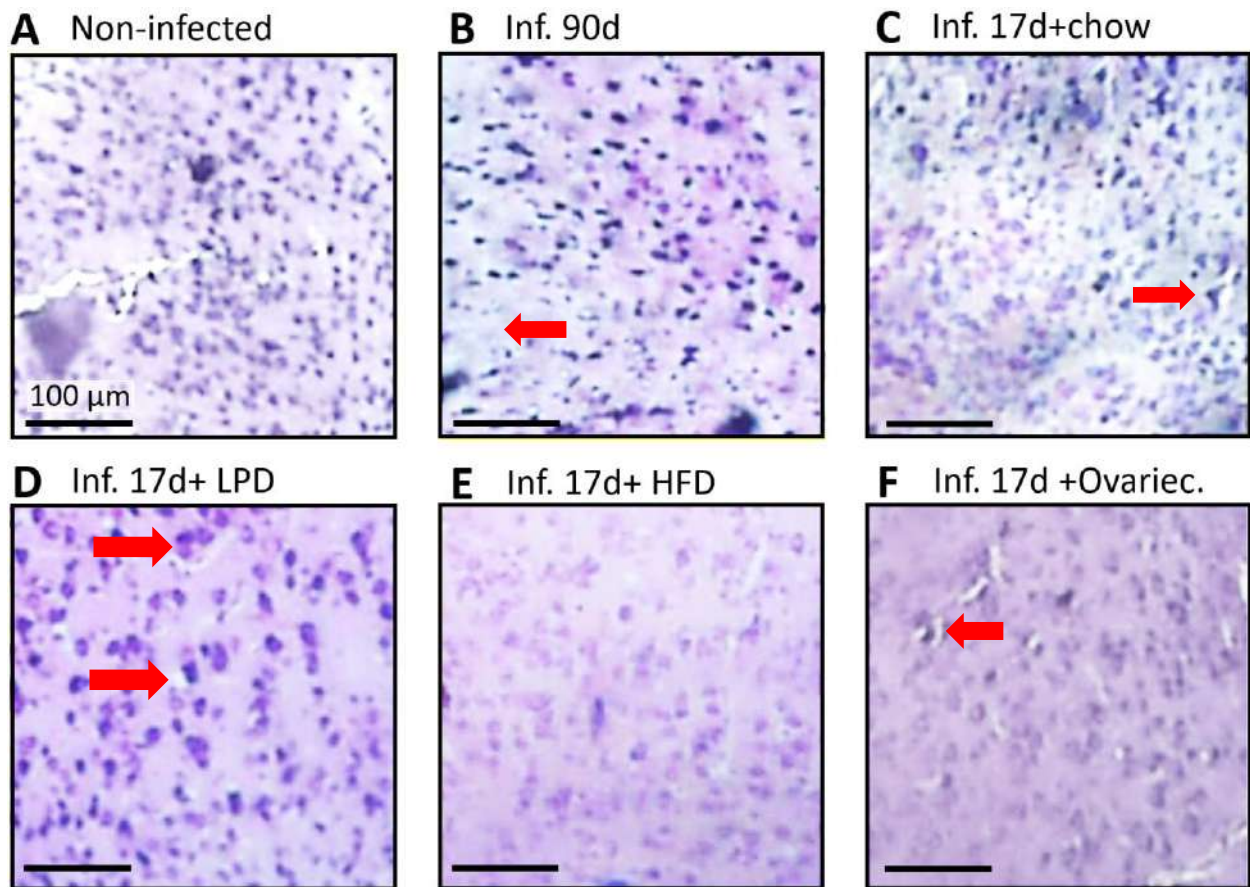


Figure 47. Micrographs of posterior parietal cortices of representative animals

Red arrows: Neuron nuclei enlargement and loss in the infected groups.

Compared to the non-infected rats (figure 48A), LPD-fed infected rats displayed very enlarged neuron nuclei and a massive loss of neurons (figure 48D) in the lateral hypothalamic area. To a lesser extent, enlarged nuclei were also observed in the 17 days infected rats fed normal chow (figure 58C), LPD-fed infected rats untreated (figure 48D), as well as HFD-fed (figure 48E) and ovariectomised (figure 48F) infected rats. Instead, terminal-stage infected showed a marked decrease in neuronal density (figure 48B).

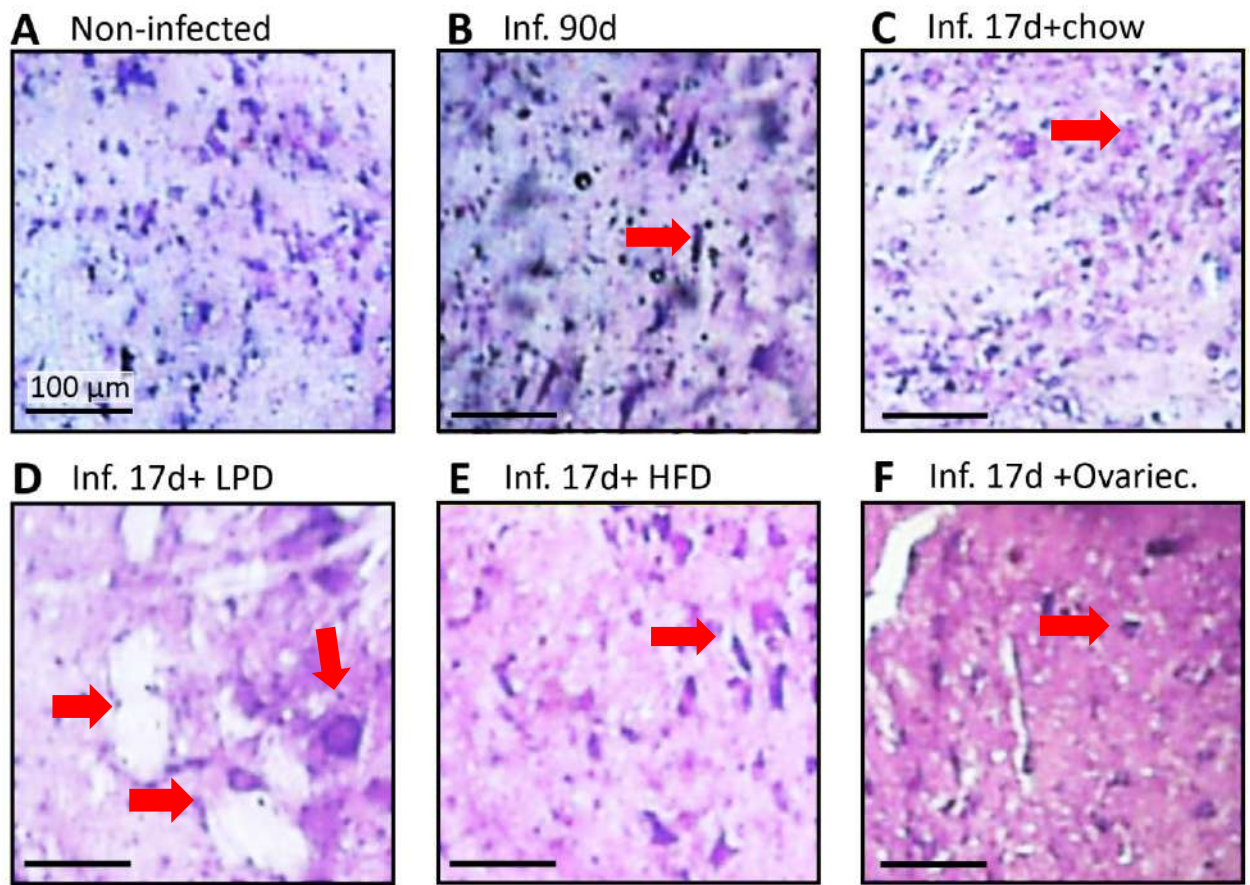
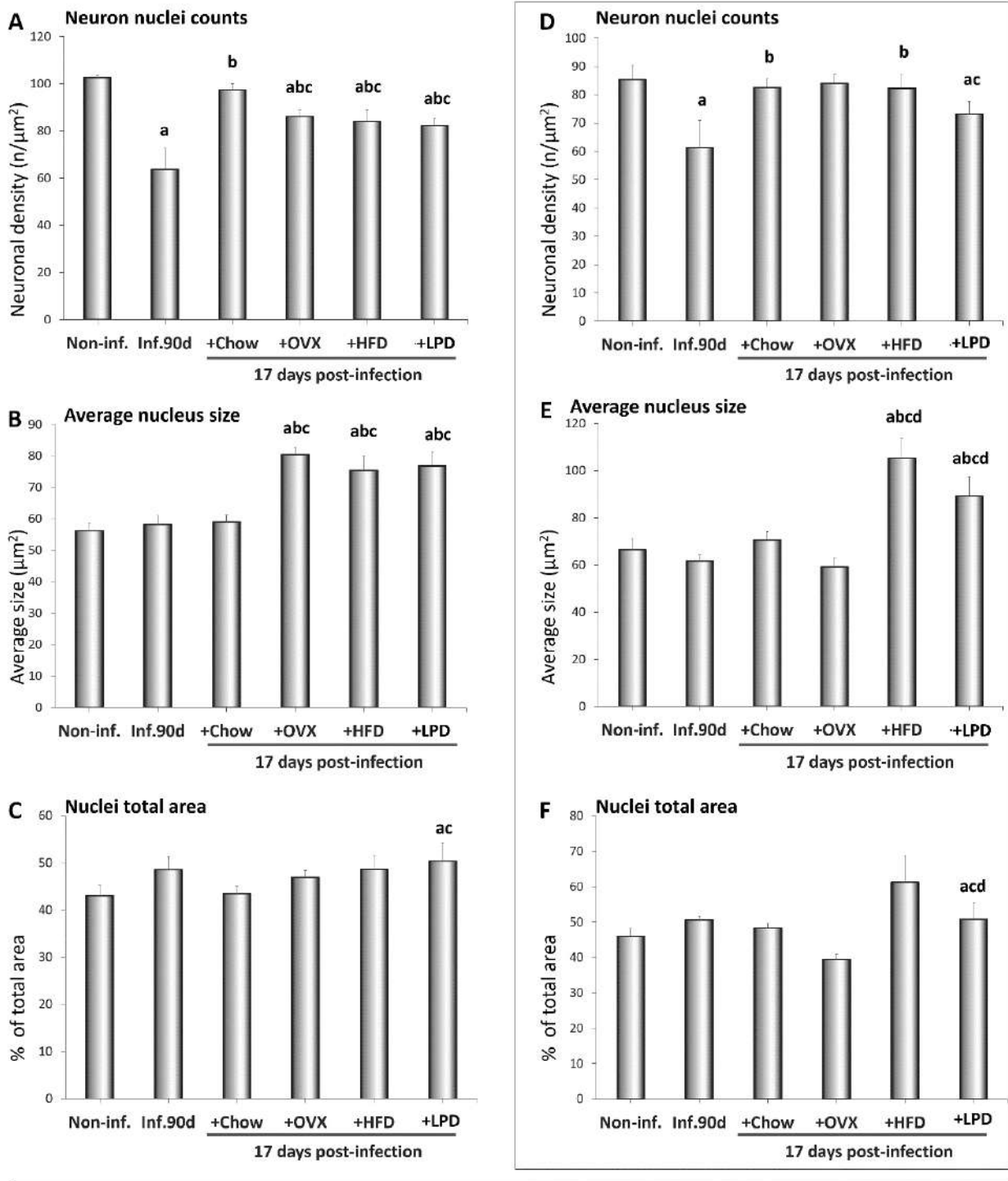


Figure 48. Micrographs of lateral hypothalamic area of representative animals
Red arrows: Neuron nuclei enlargement and massive neuron loss in the infected groups.

Compared to the non-infected rats, the terminal-stage infected rats had a statistically significant decrease in their neuronal density in the posterior parietal cortex (figure 49A) and in the lateral hypothalamic area (figure 49D) (table XXX). Less marked decreases in neuronal densities were also observed in the early-stage infected groups, with the most marked decrease in LPD-fed group (figures 49A, D and table XXX).



ANOVA +LSD test, $p < 0.05$ vs.: **a** Non-infected **b** Infected, 90d **c** Inf.17d +chow **d** Inf.17d+OVX **e** Inf.17d+HFD

Figure 49. Average counts in brain posterior areas

Counts in the posterior parietal cortex (A-C) and lateral hypothalamic (perifornical) area (D-F).

Compared to non-infected, terminal-stage infected, and early-stage infected chow-fed groups, LPD-fed, HFD-fed and ovariectomized groups (respectively, LPD-fed group only) displayed significantly increased average nuclei size (respectively, in nuclei total area) in both the

posterior parietal cortex (figures 49A-C) and the lateral hypothalamic area (figures 49D-F) (table XXX).

Table XXX. Cell count comparisons in the brain posterior areas

		Infected 17d			
	Inf.90d	+Chow	+OVX	+HFD	+LPD
Counts in the posterior parietal cortex					
Non-inf.	1.8E-8***	0.079	5.6E-5***	2.2E-8***	4.0E-6***
Inf.90d		1.3E-5***	0.030*	0.016*	0.031*
+Chow			0.033*	0.003**	0.001**
+OVX				0.722	0.554
+HFD					0.732
Average size of neuron nuclei in the posterior parietal cortex					
Non-inf.	0.673	0.416	9.6E-6***	1.4E-4***	0.001**
Inf.90d		0.862	0.002**	0.010*	0.046*
+Chow			3.6E-5***	0.001**	0.001**
+OVX				0.448	0.665
+HFD					0.855
% area of neuron nuclei in the posterior parietal cortex					
Non-inf.	0.192	0.871	0.324	0.175	0.028*
Inf.90d		0.122	0.700	0.988	0.689
+Chow			0.274	0.138	0.017*
+OVX				0.730	0.406
+HFD					0.688
Counts in the perifornical zone of the lateral hypothalamic area					
Non-inf.	0.027*	0.616	0.881	0.684	0.028*
Inf.90d		0.013*	0.066	0.047*	0.097
+Chow			0.843	0.957	0.034*
+OVX				0.797	0.061
+HFD					0.074
Average size of neuron nuclei in the perifornical zone of the lateral hypothalamic area					
Non-inf.	0.591	0.488	0.466	2.2E-4***	0.020*
Inf.90d		0.248	0.785	0.001**	0.063
+Chow			0.189	1.0E-4***	0.026*
+OVX				0.003**	0.054
+HFD					0.217
% area of neuron nuclei in the perifornical zone of the lateral hypothalamic area					
Non-inf.	0.289	0.376	0.286	0.003**	0.253
Inf.90d		0.489	0.177	0.079	0.964
+Chow			0.064	0.001**	0.457
+OVX				0.020*	0.136
+HFD					0.087

3.2.6.3 Cerebellar areas: molecular layer and dentate nucleus

Compared to the non-infected rats (figure 50A), terminal-stage infected showed the most marked decrease in neuronal density among all the groups in the molecular layer of the cerebellar cortex (figures 50B-F). LPD-fed and HFD-fed infected rats also showed a marked decrease in neuronal density (figures 50D, E).

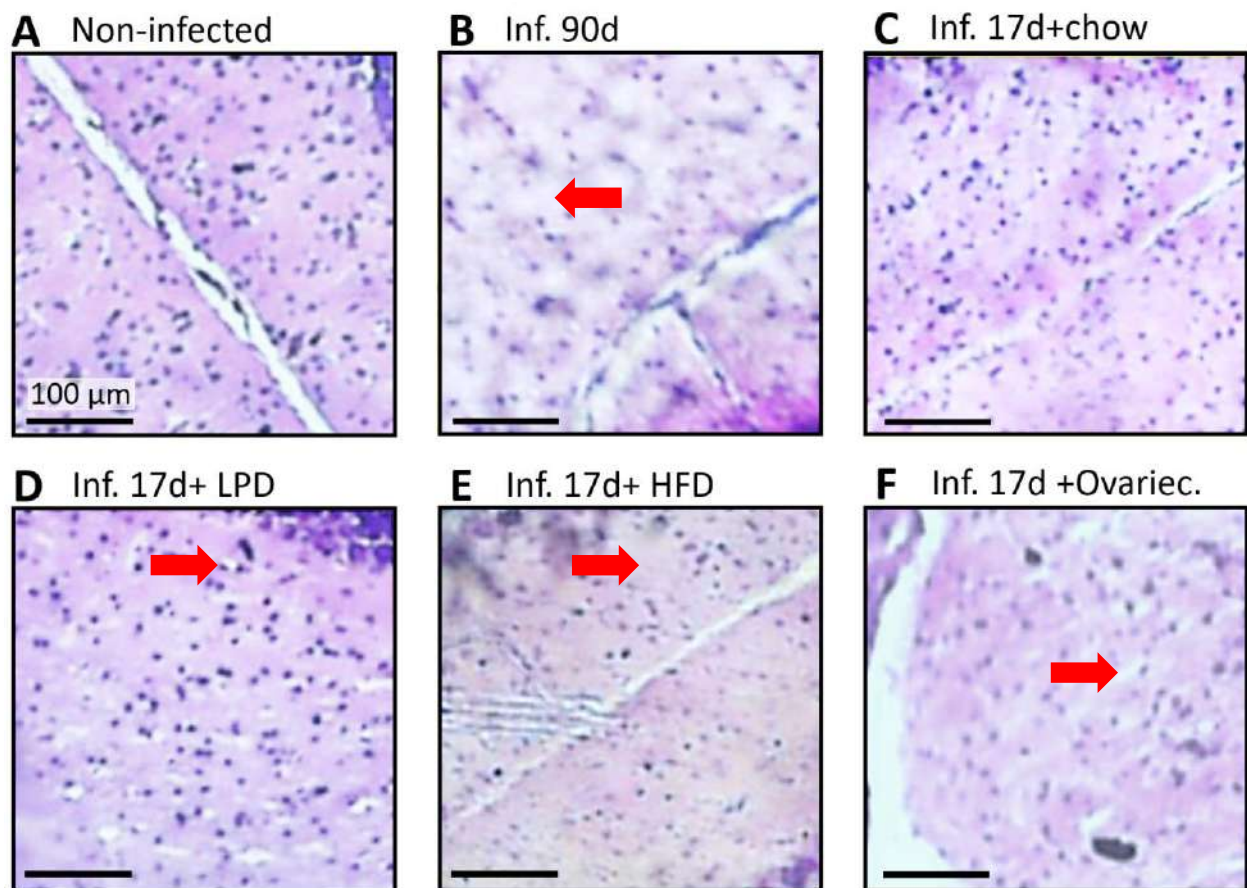


Figure 50. Molecular layer of cerebellar cortices of representative animals

Red arrow: Neuronal loss induced by the infection.

Compared to the non-infected rats (figure 51A), terminal-stage infected rats presented with a marked decrease in large neuron nuclei density (figure 51B), while marked losses in neuronal nuclei were observed in LPD-fed infected rats (figure 51D). Damaged nuclei were observed in the 17 days infected rats fed normal chow (figure 51C), HFD-fed (figure 51E) and ovariectomised (figure 51F) infected rats.

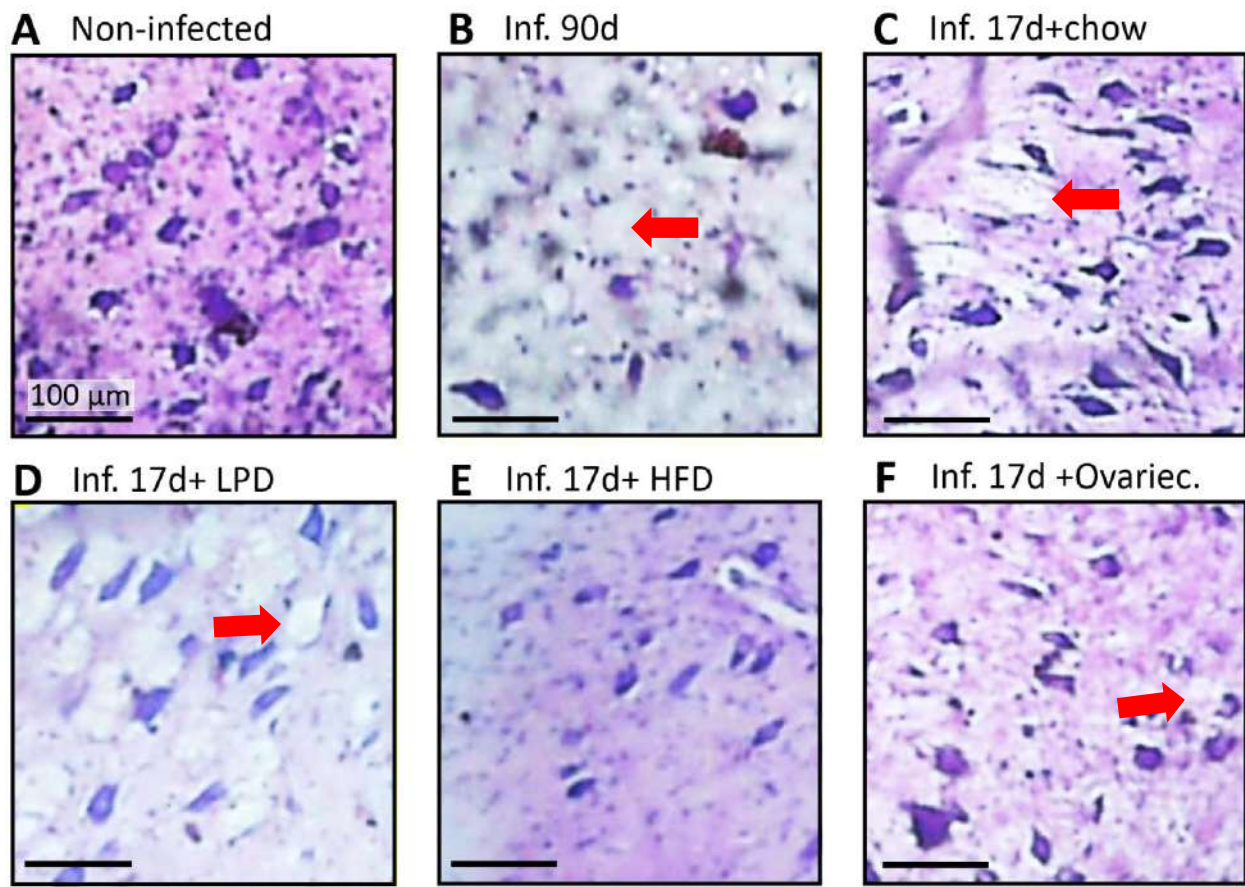


Figure 51. Micrographs of cerebellar dentate nuclei of representative animals

Red arrow: Large neuron loss in infected groups (B,C,D,F).

Significant decreases in neuronal density were observed in all infected groups, except for chow-fed rats sacrificed at early stage (respectively, chow-fed rats sacrificed at early stage and ovariectomized infected rats) compared to the non-infected rats in the cerebellar molecular layer (figure 52A) (respectively, in the dentate nucleus, including large neurons, figure 52D) (table XXXI).

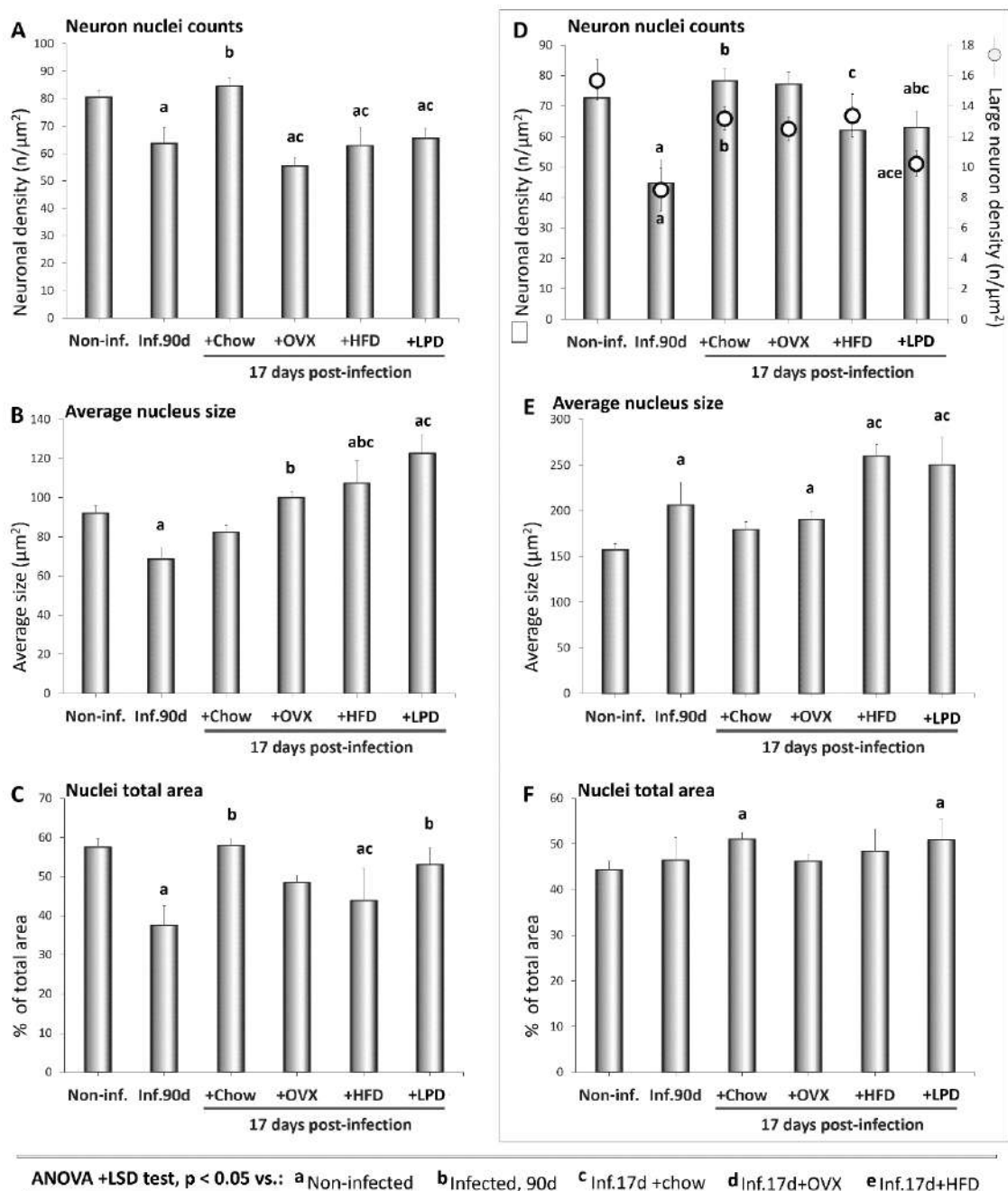


Figure 52. Average counts in cerebellar areas

Counts in the cerebellar molecular layer (A-C) and dentate nucleus (D-F).

Compared to non-infected, terminal-stage infected, and early-stage infected chow-fed groups, LPD-fed, HFD-fed and, to a lesser extent, ovariectomized groups displayed significantly increased average nuclei size in both the cerebellar molecular layer (figure 52B) and the dentate nucleus (figure 52E) (table XXXI). Decreases in the nuclei total area (respectively, increases) were observed in the cerebellar molecular layer (respectively, in the dentate nucleus) of HFD-fed rats (respectively, chow-fed and LPD-fed rats) (figures 52C, F and table XXXI).

Table XXXI. Cell count comparisons in the cerebellar areas

	Infected 17d				
	Inf.90d	+Chow	+OVX	+HFD	+LPD
Counts in the molecular layer of the cerebellar cortex					
Non-inf.	0.006**	0.305	2.0E-4***	1.5E-4***	0.007**
Inf.90d		0.008**	0.379	0.897	0.863
+Chow			4.9E-4***	1.3E-4***	0.001**
+OVX				0.316	0.354
+HFD					0.706
Average size of neuron nuclei in the molecular layer of the cerebellar cortex					
Non-inf.	0.015*	0.074	0.440	0.091	0.037*
Inf.90d		0.094	0.034*	0.022*	0.077
+Chow			0.062	0.004**	0.004**
+OVX				0.659	0.453
+HFD					0.448
% area of neuron nuclei in the molecular layer of the cerebellar cortex					
Non-inf.	4.6E-4***	0.870	0.160	0.005**	0.325
Inf.90d		3.0E-5***	0.258	0.384	0.040*
+Chow			0.083	0.001**	0.225
+OVX				0.598	0.594
+HFD					0.132
Counts of all neuronal nuclei in the cerebellar dentate nucleus					
Non-inf.	2.1E-4***	0.272	0.490	0.066	0.046*
Inf.90d		0.001**	0.013*	0.090	0.039*
+Chow			0.899	0.027*	0.012*
+OVX				0.137	0.097
+HFD					0.913
Counts of large neurons in the cerebellar dentate nucleus					
Non-inf.	0.007**	0.095	0.238	0.212	0.002**
Inf.90d		0.009**	0.069	0.001**	0.316
+Chow			0.706	0.887	0.017*
+OVX				0.505	0.203
+HFD					0.013*
Average size of neuron nuclei in the cerebellar dentate nucleus					
Non-inf.	0.011*	0.066	0.028*	2.4E-4***	4.5E-4***
Inf.90d		0.227	0.596	0.278	0.350
+Chow			0.563	0.002**	0.004**
+OVX				0.148	0.196
+HFD					0.813
% area of neuron nuclei in the cerebellar dentate nucleus					
Non-inf.	0.633	0.006**	0.673	0.345	0.046*
Inf.90d		0.232	0.970	0.795	0.417
+Chow			0.203	0.481	0.949
+OVX				0.766	0.386
+HFD					0.621

3.3 Phytochemical screening and therapeutic potential of *G. kola* in infected rats

3.3.1 Plant extraction and phytochemical screening

The extraction yields were 14.8% for the hexane fraction, 13% for the DCM fraction and 15.5% for the ethyl acetate fraction. The results of the qualitative and quantitative screening of *G. kola* extracts are presented in tables XXXII and XXXIII respectively.

Table XXXII. Qualitative analysis of total phenolic content

Tests	<i>G. kola</i> extract fractions		
	Hexane	Ethyl Acetate	DCM
Alkaloids	+	+	+
Anthocyanins	-	-	-
Catechic tannins	-	+	-
Coumarins	+	-	+
Flavonoids	+	-	+
Gallic tannins	-	-	-
Mucilage	-	-	-
Phenolic groups	+	+	+
Quinones	-	+	+
Saponins	+	-	+
Steroids	-	-	-
Terpenoids	+	+	+

(+) Presence, (-) absence

The estimation of concentrations of some secondary metabolites revealed high levels of phenolic compounds and flavonoids in all extracts (table XXXIII).

Table XXXIII. Results of quantitative phytochemistry

Metabolites	Hexane	Ethyl Acetate	DCM
Flavanols (mg Eqg of dry extract)	74.74± 0.30	51.96± 0.42	58.57± 0.49
Flavonoids (mg Eqg ^{##} of dry extract)	257.5± 5	215.83±1.67	141.38± 10.18
Phenolic compounds (mg EGAg [#] of dry extract)	176.76± 9.41	920.88±3.52	232.64 ± 4.70
Tannins (mg ETag ^{##} of dry extract)	18.58±0.23	23.76±2.4	15.03±0.45

Values are mean ± standard error of the mean (SEM), n=3. [#]mg EGAg: milligrams of gallic acid equivalents (GAE) per gram. ^{##}mg Eqg: milligram per equivalent per gram. ^{##}mg ETag: milligrams of tannic acid per gram.

3.3.2 Body weight, temperature and blood glucose level

Figure 56A shows the body weights relative to baseline values of infected rats fed LPD and treated with *G. kola* extracts, while figure 56B shows the weights of these animals at sacrifice.

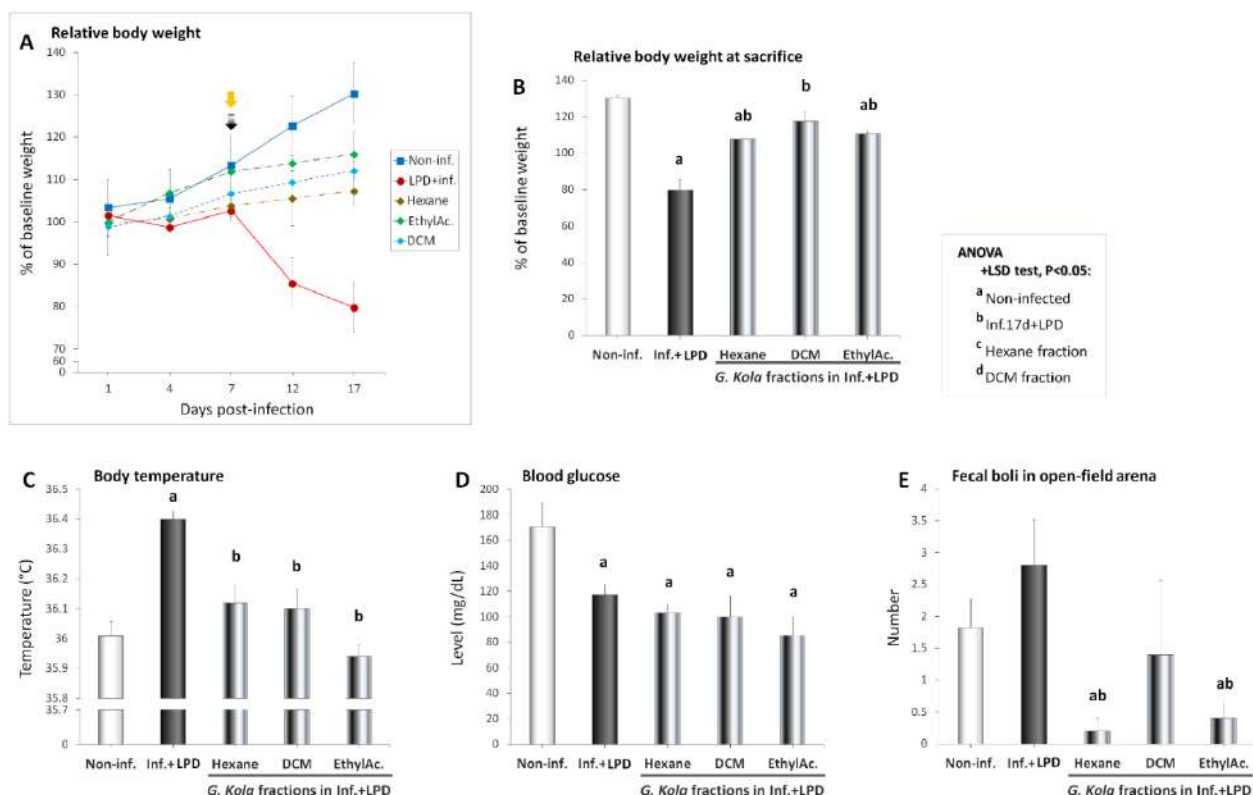


Figure 53. Body weight, temperature and blood glucose after treatment

The following observations are done in the different treatment groups: the non-infected rat group had an increase in body weight throughout the experimentation. The gain in weight was statistically significant compared to dpi 1 values (figure 56A, table XXXIV). Unlike LPD-fed rats that displayed a decrease in body weight from 7 dpi, the infected groups treated with *G. kola* extracts showed increases in body weight throughout the experimentation, with the most marked effects with ethyl acetate fraction (figure 56A, table XXXIV). Treatment with all *G. kola* extracts

resulted in increases in the body weight at sacrifice (figure 56B). However, only treatment with DCM fraction restored the body weight to values comparable to non-infected animals (figure 56B, table XXXIV).

Table XXXIV. Body weight changes in infected rats after treatment

	Days post-infection				
	1	4	7	12	17
Compared to day 1 values					
Non-infected	0.084	3.5E-5***	9.6E-7***	3.6E-8***	
LPD +Inf.17d	0.011*	0.721	0.018*	5.8E-4***	
Hexane fraction +Inf	0.417	0.876	0.539	0.346	
DCM fraction +Inf	0.543	0.145	0.094	0.066	
Ethyl acetate fraction +Inf	0.282	0.118	0.037*	0.021*	
Compared to non-infected					
LPD +Inf.17d	0.279	0.011*	0.721	0.018*	0.001**
Hexane fraction +Inf	0.366	0.417	0.876	0.539	0.346
DCM fraction +Inf	0.680	0.543	0.145	0.094	0.066
Ethyl acetate fraction +Inf	0.070	0.282	0.118	0.037*	0.021*
Compared to infected, 17d					
Hexane fraction +Inf	0.643	0.808	0.490	0.300	0.203
DCM fraction +Inf	0.853	0.398	0.105	0.072	0.053
Ethyl acetate fraction +Inf	0.232	0.939	0.028*	0.005**	0.003**
Compared to Hexane fraction-treated					
DCM fraction +Inf	0.982	0.405	0.154	0.119	0.095
Vs. LPD+Inf.17d	0.701	0.533	0.064	0.033*	0.022*
Compared to DCM fraction-treated					
Ethyl acetate fraction +Inf	0.903	0.872	0.469	0.313	0.205

ANOVA+LSD test: *P<0.05; **P<0.01; ***P<0.001.

Table XXXV. Physiological parameter changes after treatment

	LPD+Inf.17d	LPD +Inf. 17d + <i>G. kola</i> fractions		
		Hexane	Dichloromethane	Ethyl acetate
Relative body weight at sacrifice				
Non-inf.	4.7E-6***	2.8E-7***	0.088	4.5E-6***
LPD+Inf.17d		8.4E-4***	7.3E-4***	3.7E-4***
Hex. fraction			0.164	0.204
DCM fraction				0.319
Body temperature				
Non-inf.	2.7E-6***	0.173	0.281	0.287
LPD+Inf.17d		0.005**	0.006**	1.8E-5***
Hex. fraction			0.822	0.038
DCM fraction				0.071
Blood glucose level				
Non-inf.	0.020*	0.005**	0.017*	0.003**
LPD+Inf.17d		0.188	0.391	0.104
Hex. fraction			0.875	0.318
DCM fraction				0.521
Faecal boli number in open-field arena				
Non-inf.	0.265	0.007**	0.752	0.017*
LPD+Inf.17d		0.005**	0.339	0.009**
Hex. fraction			0.365	0.545
DCM fraction				0.445

ANOVA+LSD test: *P<0.05; **P<0.01; ***P<0.001.

Instead, treatment with all *G. kola* extracts prevented the increase in body temperature observed at sacrifice in untreated LPD-fed infected rats (figure 56C) and maintained the body temperature to values comparable to non-infected animals (figure 56C, table XXXV). Treatment with *G. kola* extracts did not improve the low level of blood glucose observed in untreated LPD-fed infected rats (figure 56D, table XXXV). Interestingly, the increase with high interindividual variability observed in the number of faecal boli in untreated LPD-fed infected rats was prevented by treatment with the extracts, with non-infected-like values in DCM fraction-treated group and significant decreases in groups treated with hexane and ethyl acetate fractions (figure 56E, table XXXV).

3.3.3 Gait quality indicators

Compared to the non-infected rats, the infected rats fed LPD had significantly lower stride lengths (figure 57F), step lengths (figure 57G), and step widths (figure 57H, table XXXVI). Unlike the treatment with the hexane fraction that did not improve the stride length, treatments with DCM and ethyl acetate fractions resulted in significantly higher stride length values compared to untreated infected rats fed LPD, although these values were still lower than non-infected group values (figure 57F, table XXXVI). Comparable changes were observed after treatment with *G. kola* extracts in step length (figure 43G) and step width (figure 43H), except

that these parameters were improved to non-infected-like values (figures 43F-H, table XXXVI).

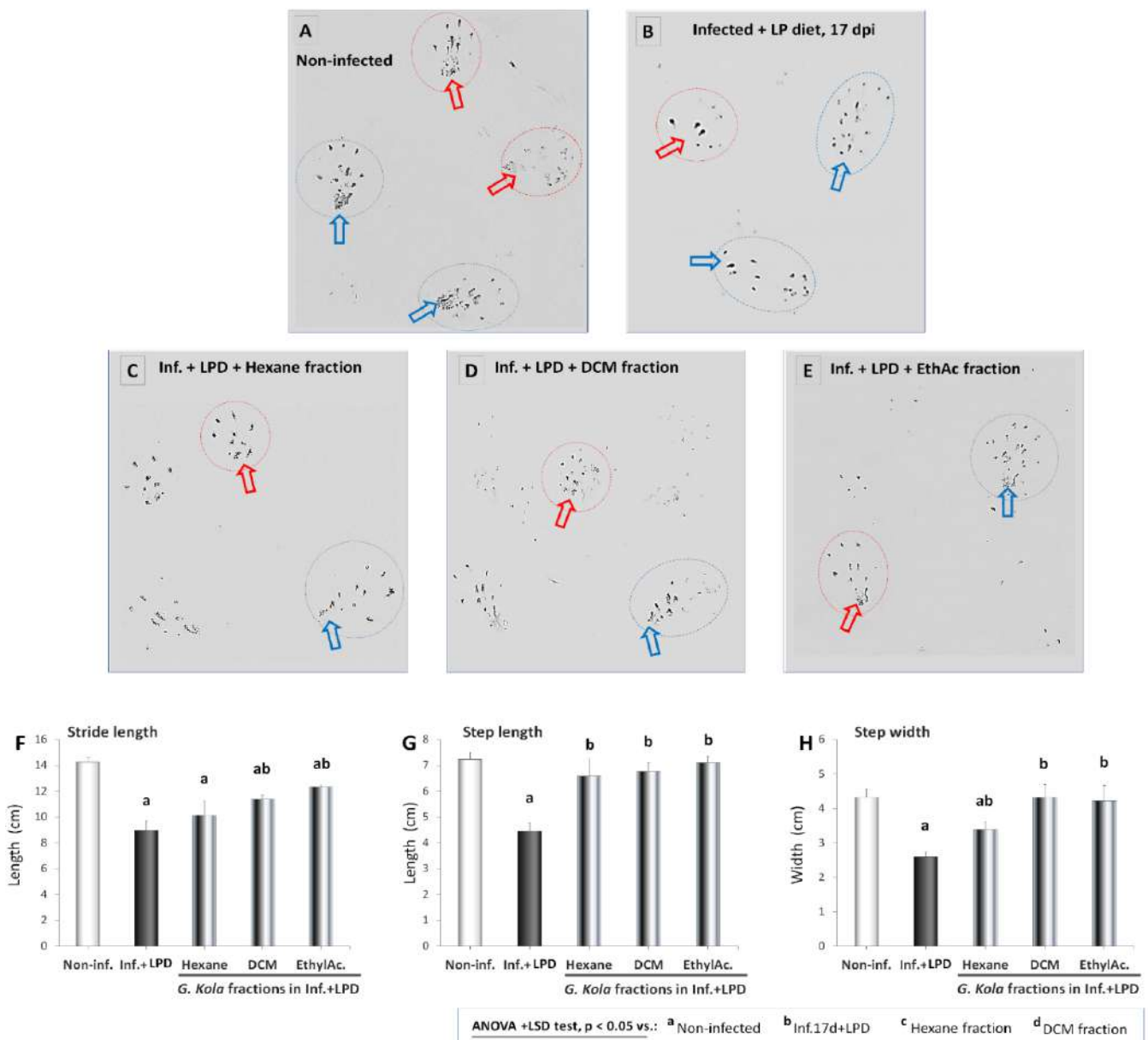


Figure 54. Gait quality indicators after treatment

A, E. Footprints of representative non-infected (**A**) and animals infected with *T. gondii* for 17 days fed low-protein (PP) diet and untreated (**B**) or treated with *Garcinia kola* hexane (**C**), dichloromethane (DCM) (**D**), and ethyl acetate (EthAc) fractions (**E**). Note that unlike the untreated (**B, C**) and as the non-infected (**A**) treated animals tend to use both heels and footpads (**C-E**).

F-H. Average stride length (**F**), step length (**G**) and step width (**H**) of *T. gondii*-infected animals (17 days) fed low-protein diet.

Table XXXVI. Gait quality indicator differences after treatment

	LPD+Inf.17d	LPD +Inf. 17d + <i>G. kola</i> fractions		
		Hexane	Dichloromethane	Ethyl acetate
Stride length				
Non-inf.	1.0E-5***	0.016*	7.2E-5***	2.2E-4***
LPD+Inf.17d		0.385	0.009**	8.3E-4***
Hex. fraction			0.342	0.114
DCM fraction				0.044*
Step length				
Non-inf.	3.1E-6***	0.404	0.313	0.728
LPD+Inf.17d		0.028*	2.8E-4***	1.9E-5***
Hex. fraction			0.791	0.496
DCM fraction				0.455
Step width				
Non-inf.	8.4E-6***	0.011*	0.992	0.872
LPD+Inf.17d		0.012*	0.007**	0.017*
Hex. fraction			0.072	0.137
DCM fraction				0.883

ANOVA+LSD test: *P<0.05; **P<0.01; ***P<0.001.

3.3.4 Organ weight

Figure 58 presents the weights of brain (figure 58A), heart (figure 58B), lung (figure 58C), liver (figure 58D), spleen (figure 58E), and kidneys (figure 58F) relative to body weight.

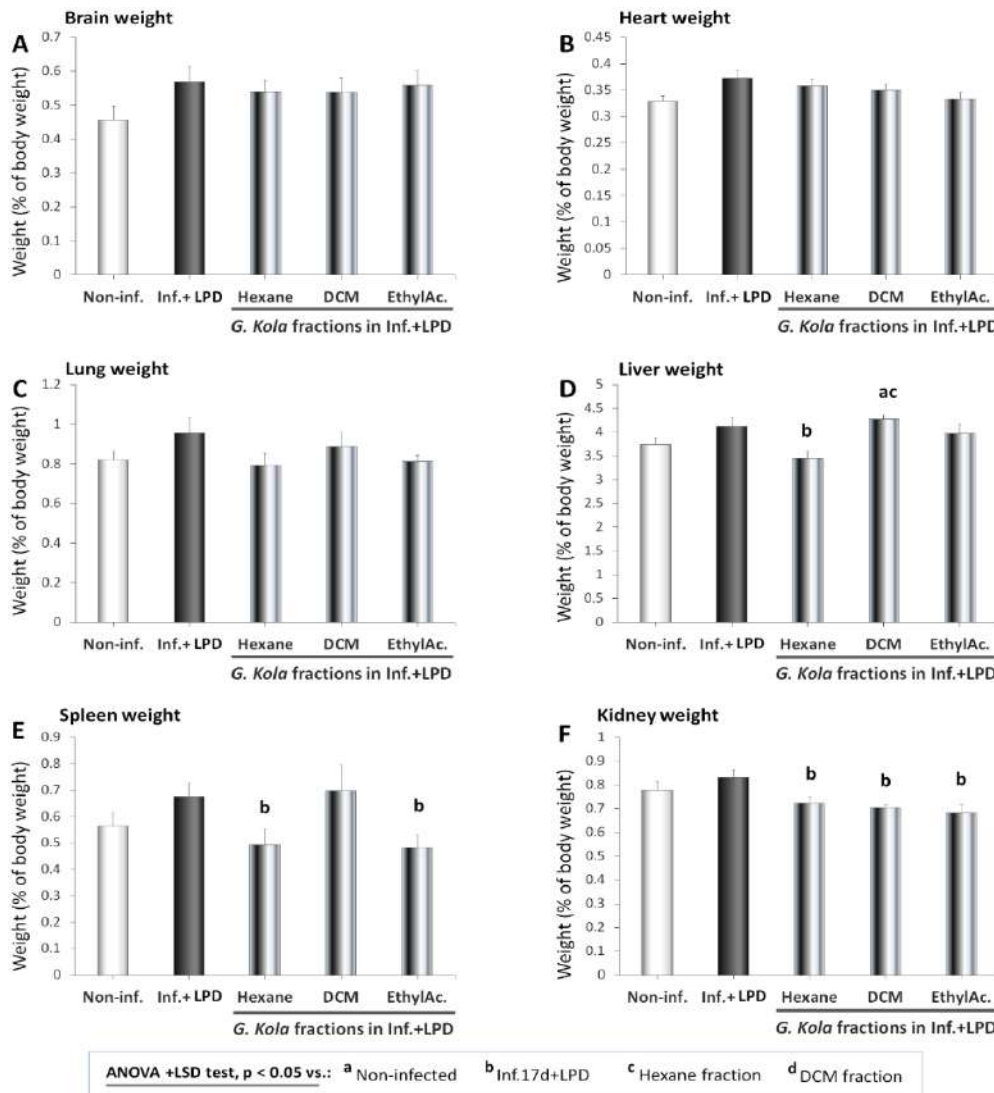


Figure 55. Organ weight relative to body weight after treatment

No statistically significant difference was observed in the weights of brain (figure 58A), heart (figure 58B), and lung (figure 58C) (table XXXVII). An increase in liver weight was observed in animals treated with hexane fraction (respectively, DCM fraction) compared to untreated animals fed LPD (respectively, both untreated animals fed LPD and non-infected animals) (figure 58D, table XXXVII). Significant decreases in spleen (figure 58E) and kidney (figure 58F) weights were observed in animals treated with hexane fraction, ethyl acetate fraction, and to a lesser extent, DCM fraction, compared to untreated animals fed LPD (table XXXVII).

Table XXXVII. Inter-group differences in organ weight after treatment

	LPD+Inf.17d	LPD +Inf. 17d + <i>G. kola</i> fractions		
		Hexane	Dichloromethane	Ethyl acetate
Brain				
Non-inf.	0.103	0.163	0.190	0.128
LPD+Inf.17d		0.613	0.629	0.873
Hex. fraction			0.995	0.739
DCM fraction				0.749
Heart				
Non-inf.	0.056	0.110	0.193	0.769
LPD+Inf.17d		0.509	0.280	0.087
Hex. fraction			0.640	0.195
DCM fraction				0.343
Lungs				
Non-inf.	0.152	0.687	0.475	0.842
LPD+Inf.17d		0.125	0.535	0.112
Hex. fraction			0.356	0.771
DCM fraction				0.394
Liver				
Non-inf.	0.100	0.187	0.008**	0.400
LPD+Inf.17d		0.011*	0.463	0.569
Hex. fraction			0.003**	0.082
DCM fraction				0.237
Spleen				
Non-inf.	0.127	0.372	0.275	0.267
LPD+Inf.17d		0.040*	0.863	0.020*
Hex. fraction			0.122	0.893
DCM fraction				0.101
Kidneys				
Non-inf.	0.272	0.274	0.084	0.081
LPD+Inf.17d		0.025*	0.002**	0.008**
Hex. fraction			0.545	0.371
DCM fraction				0.568

ANOVA+LSD test: *P<0.05; **P<0.01; ***P<0.001.

3.3.5 OFT

3.3.5.1 Locomotion and grooming

Compared to the non-infected rats, the infected rats fed LPD had a significantly lower locomotion episodes number ($P < 0.001$) (figure 59A). Compared to the non-infected rats, the infected rats fed LPD and treated with the hexane fraction had a significantly lower locomotion episodes number ($P = 0.009$) (figure 59A). Compared to the infected rats fed LPD, the infected rats fed LPD and treated with the DCM fraction of the *G. kola* extract had a significantly higher locomotion episodes number ($P = 0.036$) (figure 59A). Compared to the infected rats fed LPD,

the infected rats fed LPD and treated with the ethyl acetate fraction of the *G. kola* extract had a significantly higher locomotion episodes number ($P = 0.038$) (figure 59A).

Compared to the non-infected rats, the infected rats fed LPD had a significantly lower distance covered ($P < 0.001$) (figure 59B). Compared to the non-infected rats, the infected rats fed LPD and treated with the hexane fraction had a significantly lower distance covered ($P = 0.031$) (figure 59B). Compared to the infected rats fed LPD, the infected rats fed LPD and treated with the DCM fraction of the *G. kola* extract had a significantly higher distance covered ($P = 0.023$) (figure 59B). Compared to the infected rats fed LPD, the infected rats fed LPD and treated with the ethyl acetate fraction of the *G. kola* extract had a significantly higher distance covered ($P = 0.025$) (figure 59B).

Compared to the non-infected rats, the infected rats fed LPD had a significantly lower locomotion time ($P = 0.002$) (figure 59C). Compared to the infected rats fed LPD, the infected rats fed LPD and treated with the hexane fraction had a significantly higher locomotion time ($P = 0.018$) (figure 59C). Compared to the infected rats fed LPD, the infected rats fed LPD and treated with the DCM fraction of the *G. kola* extract had a significantly higher locomotion time ($P = 0.033$) (figure 59C).

Compared to the infected rats fed LPD, the infected rats fed LPD and treated with the ethyl acetate fraction of the *G. kola* extract had a significantly higher locomotion time ($P = 0.031$) (figure 59D). Compared to the non-infected rats, the infected rats fed LPD had a significantly lower grooming episode number ($P = 0.035$) (figure 59D).

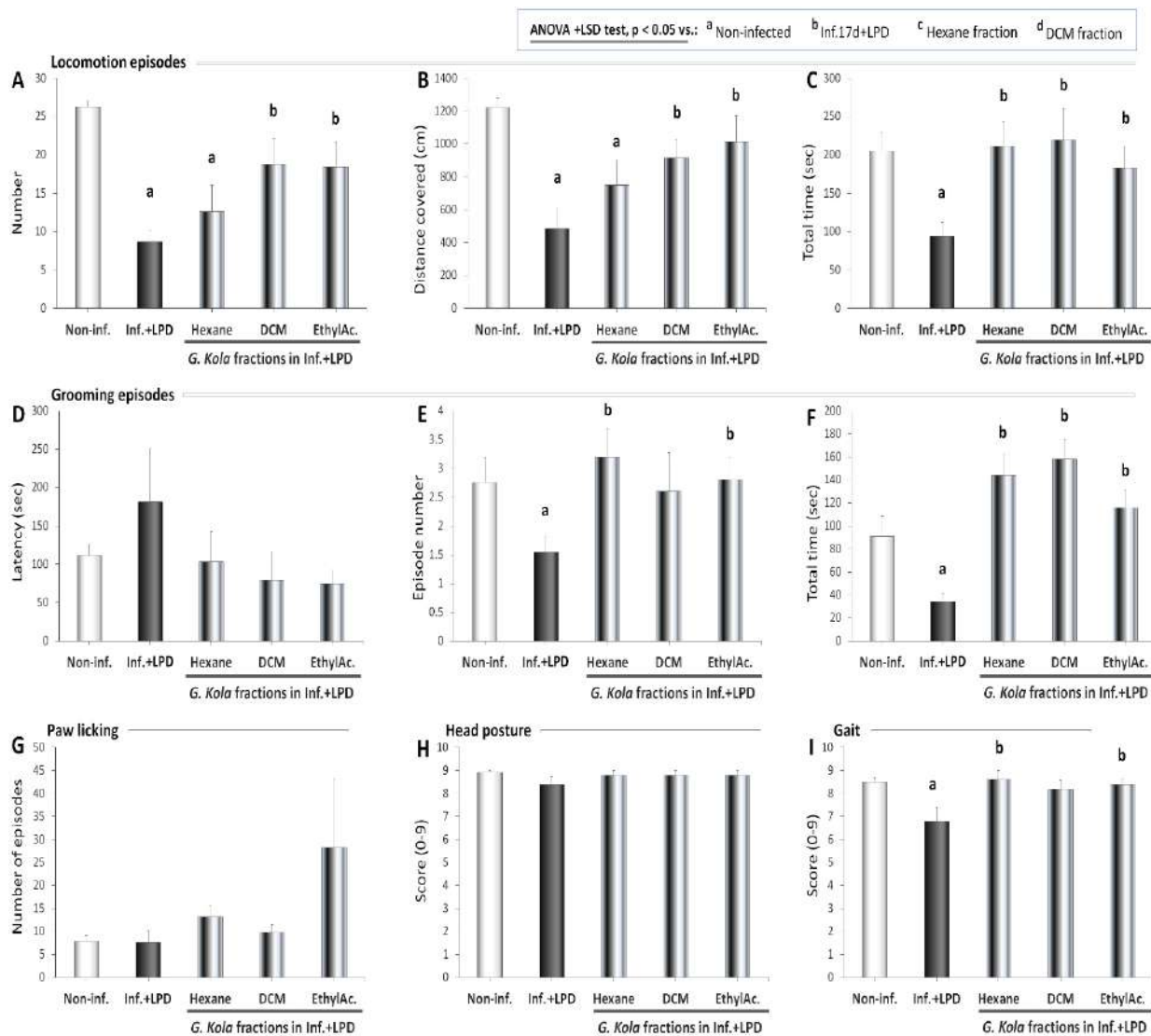


Figure 56. Locomotion and grooming-related parameters after treatment

Compared to the infected rats fed LPD, the infected rats fed LPD and treated with the hexane fraction had a significantly higher grooming episode number ($P = 0.023$) (figure 59E). Compared to the infected rats fed LPD, the infected rats fed LPD and treated with the ethyl acetate fraction of the *G. kola* extract had a significantly higher grooming episode number ($P = 0.026$) (figure 59E).

Table XXXVIII. OFT motor function indicators of infected rats after treatment

	LPD+Inf.17d	LPD +Inf. 17d + G. kola fractions	Hexane	Dichloromethane	Ethyl acetate
Locomotion episode number					
Non-inf.	4.6E-8***		0.009**	0.091	0.075
LPD+Inf.17d			0.321	0.036*	0.038*
Hex. fraction				0.233	0.258
DCM fraction					0.934
Distance covered					
Non-inf.	7.4E-5***		0.031*	0.051	0.267
LPD+Inf.17d			0.200	0.023*	0.025*
Hex. fraction				0.410	0.256
DCM fraction					0.617
Locomotion time					
Non-inf.	0.002**		0.870	0.758	0.579
LPD+Inf.17d			0.018*	0.033*	0.031*
Hex. fraction				0.877	0.533
DCM fraction					0.486
Grooming latency					
Non-inf.	0.360		0.846	0.438	0.144
LPD+Inf.17d			0.352	0.221	0.174
Hex. fraction				0.656	0.527
DCM fraction					0.921
Grooming episode number					
Non-inf.	0.035*		0.511	0.858	0.933
LPD+Inf.17d			0.023*	0.206	0.026*
Hex. fraction				0.496	0.536
DCM fraction					0.805
Grooming time					
Non-inf.	0.008***		0.057	0.015*	0.312
LPD+Inf.17d			0.002**	0.001**	0.004**
Hex. fraction				0.581	0.274
DCM fraction					0.101
Paw licking episode number					
Non-inf.	0.911		0.092	0.393	0.249
LPD+Inf.17d			0.129	0.476	0.244
Hex. fraction				0.277	0.377
DCM fraction					0.289
Head posture score					
Non-inf.	0.170		0.612	0.612	0.612
LPD+Inf.17d			0.329	0.329	0.329
Hex. fraction				1.000	1.000
DCM fraction					1.000
Gait score					
Non-inf.	0.023*		0.830	0.502	0.756
LPD+Inf.17d			0.028*	0.073	0.033*
Hex. fraction				0.486	0.683
DCM fraction					0.668

ANOVA+LSD test: *P<0.05; **P<0.01; ***P<0.001.

Compared to the non-infected rats, the infected rats fed LPD had a significantly lower grooming time ($P = 0.008$) (Figure 59F). Compared to the infected rats fed LPD, the infected rats fed LPD and treated with the hexane fraction had a significantly higher grooming time (P

$= 0.002$) (figure 59F). Compared to the infected rats fed LPD, the infected rats fed LPD and treated with the DCM fraction of the *G. kola* extract had a significantly higher grooming time ($P = 0.001$) (figure 59F). Compared to the infected rats fed LPD, the infected rats fed LPD and treated with the ethyl acetate fraction of the *G. kola* extract had a significantly higher grooming time ($P = 0.004$) (figure 59F).

No significant change was observed in paw licking episode number (figure 59G) and in head posture score (figure 59H). Instead, compared to the non-infected rats, the infected rats fed LPD had a significantly lower gait score ($p=0.023$) (figure 59I).

3.3.5.2 Rearing and arena angle activities

Compared to the non-infected rats, the infected rats fed LPD had a significantly lower angle entry ($P = 0.001$) (figure 60A). Compared to the non-infected rats, the infected rats fed LPD had a significantly higher angle time ($P = 0.001$) (figure 60B). Compared to the non-infected rats, the infected rats fed LPD and treated with the hexane fraction had a significantly higher angle time ($P = 0.011$) (figure 60B). Compared to the non-infected rats, the infected rats fed LPD and treated with the DCM fraction of the *G. kola* extract had a significantly higher angle time ($P = 0.002$) (figure 60B). Compared to the infected rats fed LPD and untreated, the infected rats fed LPD and treated with the DCM fraction of the *G. kola* extract had a significantly higher angle time ($P = 0.015$) (figure 60B). Compared to the non-infected rats, the infected rats fed LPD and treated with the ethyl acetate fraction of the *G. kola* extract had a significantly higher angle time ($P = 0.036$) (figure 60B).

Compared to the non-infected rats, the infected rats fed LPD had a significantly higher rearing against wall latency ($P = 0.031$) (figure 60C). Compared to the infected rats fed LPD and untreated, the infected rats fed LPD treated with the hexane fraction had a significantly lower rearing against wall latency ($P = 0.031$) (figure 60C). Compared to the infected rats fed LPD and untreated, the infected rats fed LPD treated with the ethyl acetate fraction of the *G. kola* extract had a significantly lower rearing against wall latency ($P = 0.013$) (figure 60C).

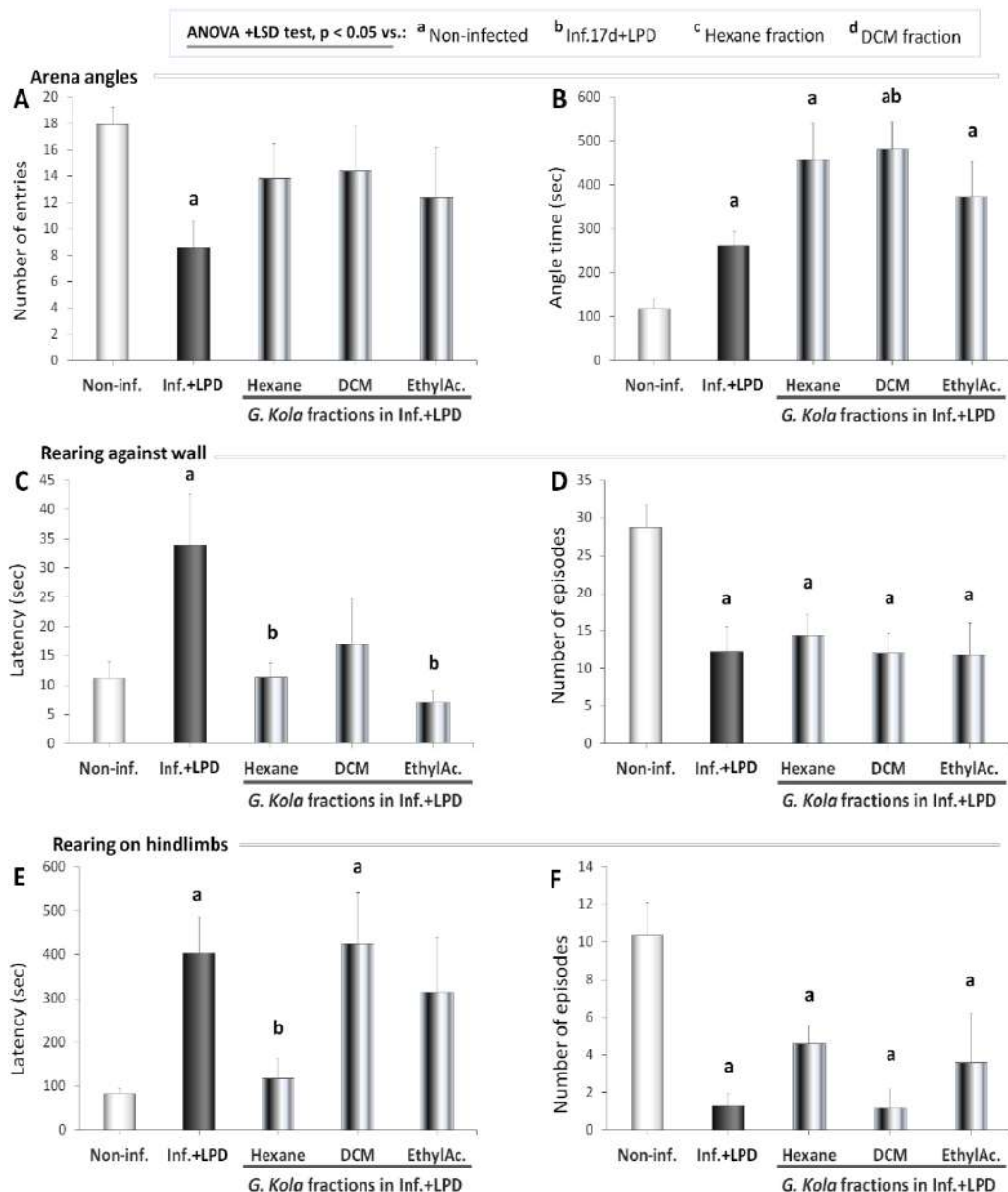


Figure 57. Rearing activities and arena angle time at 17 days post-infection

Compared to the non-infected rats, the infected rats fed LPD had a significantly lower rearing against wall episodes number ($P = 0.002$) (figure 60D). Compared to the non-infected rats, the infected rats fed LPD treated with the hexane fraction had a significantly lower rearing against wall episodes number ($P < 0.001$) (figure 60D). Compared to the non-infected rats, the infected rats fed LPD treated with the DCM fraction of the *G. kola* extract had a significantly lower rearing against wall episodes number ($P = 0.001$) (figure 60D). Compared to the non-infected rats, the infected rats fed LPD treated with the ethyl acetate fraction of the *G. kola* extract had a significantly lower rearing against wall episodes number ($P = 0.003$) (figure 60D).

Table XXXIX. Rearing and arena angle entries after treatment

	LPD+Inf.17d	LPD +Inf. 17d + <i>G. kola</i> fractions		
		Hexane	Dichloromethane	Ethyl acetate
Angle entries				
Non-inf.	0.001**	0.214	0.380	0.227
LPD+Inf.17d		0.150	0.185	0.404
Hex. fraction			0.893	0.770
DCM fraction				0.705
Angle time				
Non-inf.	0.003**	0.011*	0.002**	0.036*
LPD+Inf.17d		0.069	0.015*	0.270
Hex. fraction			0.814	0.480
DCM fraction				0.317
Rearing against wall latency				
Non-inf.	0.031*	0.968	0.510	0.237
LPD+Inf.17d		0.031*	0.168	0.013*
Hex. fraction			0.515	0.191
DCM fraction				0.266
Rearing against wall episode number				
Non-inf.	0.002**	4.2E-6***	0.001**	0.003**
LPD+Inf.17d		0.157	0.637	0.662
Hex. fraction			0.319	0.434
DCM fraction				0.974
Rearing on hindlimb latency				
Non-inf.	0.004**	0.492	0.041*	0.138
LPD+Inf.17d		0.010*	0.883	0.567
Hex. fraction			0.055	0.200
DCM fraction				0.533
Rearing on hindlimb episode number				
Non-inf.	2.8E-4***	0.001**	2.4E-4***	0.026*
LPD+Inf.17d		0.535	0.773	0.494
Hex. fraction			0.429	0.664
DCM fraction				0.434

ANOVA+LSD test: *P<0.05; **P<0.01; ***P<0.001.

Compared to the non-infected rats, the infected rats fed LPD had a significantly higher rearing on hindlimb latency ($P = 0.004$) (figure 60E). Compared to the infected rats fed LPD and untreated, the infected rats fed LPD treated with the hexane fraction had a significantly lower rearing on hindlimbs latency ($P = 0.010$) (figure 60E). Compared to the non-infected rats, the infected rats fed LPD treated with the DCM fraction of the *G. kola* extract had a significantly higher rearing on hindlimbs latency ($P = 0.041$) (figure 60E).

Compared to the non-infected rats, the infected rats fed LPD had a significantly lower rearing on hindlimb episode number ($P < 0.001$) (figure 60F). Compared to the non-infected

rats, the infected rats fed LPD treated with the hexane fraction had a significantly lower rearing on hindlimbs episodes number ($P = 0.001$) (figure 60F). Compared to the non-infected rats, the infected rats fed LPD treated with the DCM fraction of the *G. kola* extract had a significantly higher rearing on hindlimbs episodes number ($P < 0.001$) (figure 60F). Compared to the non-infected rats, the infected rats fed LPD treated with the ethyl acetate fraction of the *G. kola* extract had a significantly lower rearing on hindlimbs episodes number ($P = 0.026$) (figure 60F).

3.3.5.3 Arena centre and close to wall activities

Compared to the non-infected rats, the infected rats fed LPD had a significantly higher arena centre latency ($P = 0.002$) (figure 61A). Compared to the non-infected rats, the infected rats fed LPD treated with the hexane fraction had a significantly higher arena centre latency ($P = 0.021$) (figure 61A). Compared to the untreated infected rats fed LPD, the infected rats fed LPD treated with the hexane fraction had a significantly lower arena centre latency ($P = 0.037$) (figure 61A). Compared to the untreated infected rats fed LPD, the infected rats fed LPD treated with the ethyl acetate fraction of the *G. kola* extract had a significantly lower arena centre latency ($P = 0.009$) (figure 61A).

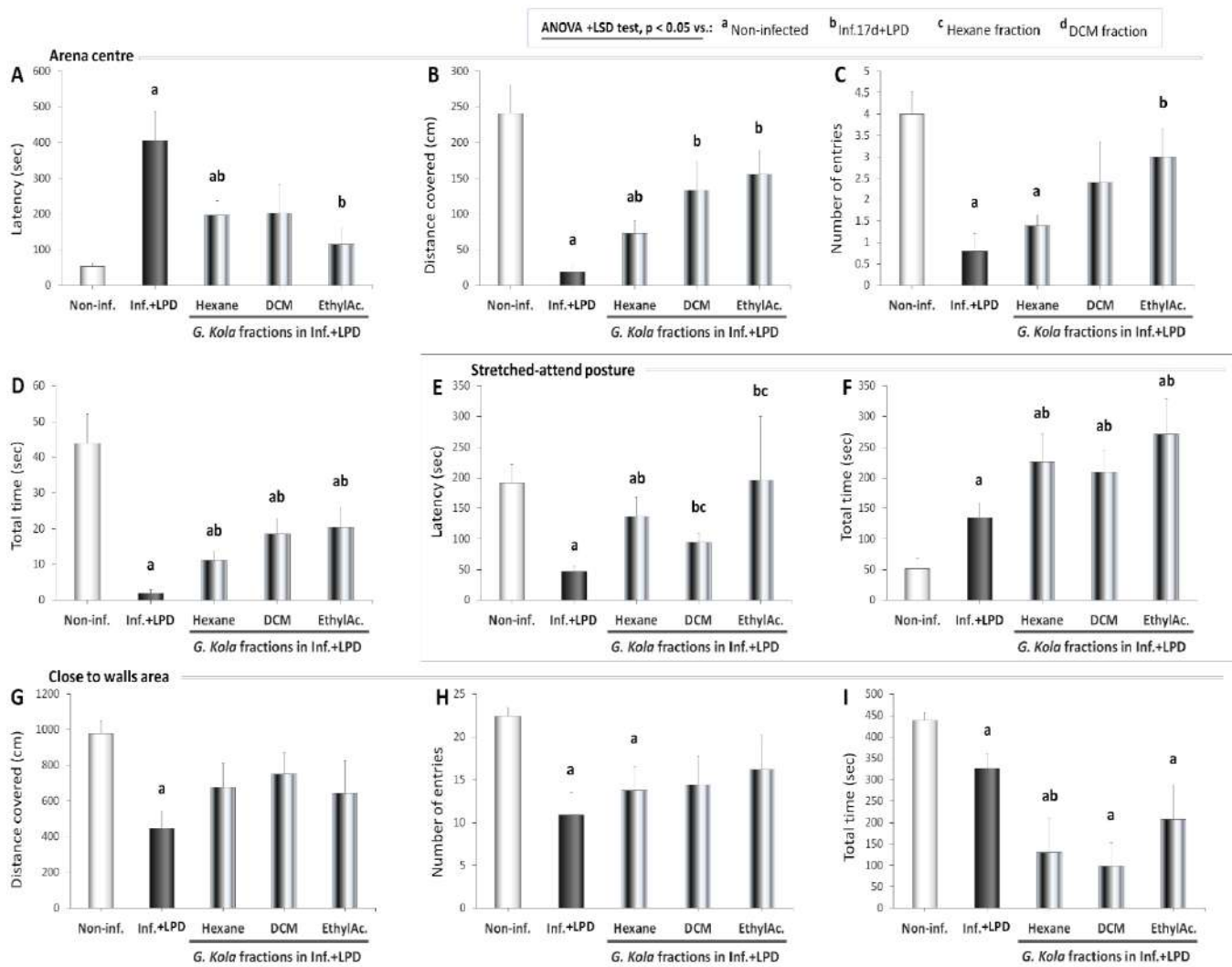


Figure 58. Arena centre and close to wall activities after treatment

Compared to the non-infected rats, the infected rats fed LPD had a significantly lower arena centre distance ($P < 0.001$) (figure 61B). Compared to the non-infected rats, the infected rats fed LPD treated with the hexane fraction had a significantly lower arena centre distance ($P = 0.001$) (figure 61B). Compared to the untreated infected rats fed LPD, the infected rats fed LPD treated with the hexane fraction had a significantly higher arena centre distance ($P = 0.032$) (figure 61B). Compared to the untreated infected rats fed LPD, the infected rats fed LPD treated with the DCM fraction of the *G. kola* extract had a significantly higher arena centre distance ($P = 0.041$) (figure 61B). Compared to the untreated infected rats fed LPD, the infected rats fed LPD treated with the ethyl acetate fraction of the *G. kola* extract had a significantly higher arena centre distance ($P = 0.012$) (figure 61B).

Table XL. Centre activities and stretched-attend posture after treatment

	LPD+Inf.17d	LPD +Inf. 17d + G. kola fractions		
		Hexane	Dichloromethane	Ethyl acetate
Arena centre latency				
Non-inf.	0.002**	0.021*	0.133	0.264
LPD+Inf.17d		0.037*	0.099	0.009**
Hex. fraction			0.948	0.234
DCM fraction				0.384
Arena centre distance				
Non-inf.	1.2E-4***	0.001**	0.077	0.121
LPD+Inf.17d		0.032*	0.041*	0.012*
Hex. fraction			0.213	0.068
DCM fraction				0.669
Arena centre entries				
Non-inf.	1.2E-4***	4.6E-4***	0.178	0.252
LPD+Inf.17d		0.236	0.169	0.021*
Hex. fraction			0.349	0.063
DCM fraction				0.609
Arena centre time				
Non-inf.	3.4E-4***	0.002**	0.016*	0.033*
LPD+Inf.17d		0.014*	0.017*	0.030*
Hex. fraction			0.184	0.189
DCM fraction				0.807
Distance covered close to walls				
Non-inf.	3.9E-4***	0.094	0.143	0.145
LPD+Inf.17d		0.213	0.083	0.379
Hex. fraction			0.695	0.892
DCM fraction				0.643
Close to wall area entries				
Non-inf.	0.002**	0.027*	0.077	0.204
LPD+Inf.17d		0.454	0.438	0.308
Hex. fraction			0.893	0.637
DCM fraction				0.744
Close to wall time				
Non-inf.	0.015*	0.016*	0.002**	0.044*
LPD+Inf.17d		0.069	0.010*	0.230
Hex. fraction			0.753	0.517
DCM fraction				0.303
Stretched-attend posture latency				
Non-inf.	0.017*	0.004**	0.317	0.451
LPD+Inf.17d		0.037*	0.007**	0.002**
Hex. fraction			0.003**	0.001**
DCM fraction				0.691
Stretched-attend posture time				
Non-inf.	0.003**	0.001**	0.004**	1.4E-7***
LPD+Inf.17d		0.045*	0.021*	1.3E-6***
Hex. fraction			0.291	0.010*
DCM fraction				0.329

ANOVA+LSD test: *P<0.05; **P<0.01; ***P<0.001.

Compared to the non-infected rats, the infected rats fed LPD had a significantly lower arena centre entries ($P < 0.001$) (figure 61C). Compared to the non-infected rats, the infected

rats fed LPD treated with the hexane fraction had a significantly lower arena centre entries ($P < 0.001$) (figure 61C). Compared to the untreated infected rats fed LPD, the infected rats fed LPD treated with the ethyl acetate fraction of the *G. kola* extract had a significantly higher arena centre entry ($P = 0.021$) (figure 61C).

Compared to the non-infected rats, the infected rats fed LPD had a significantly lower arena centre time ($P < 0.001$) (figure 61D). Compared to the non-infected rats, the infected rats fed LPD treated with the hexane fraction had a significantly lower arena centre time ($P = 0.002$) (figure 61D). Compared to the untreated infected rats fed LPD, the infected rats fed LPD treated with the hexane fraction had a significantly higher arena centre time ($P = 0.014$) (figure 61D). Compared to the non-infected rats, the infected rats fed LPD treated with the DCM fraction of the *G. kola* extract had a significantly higher arena centre time ($P = 0.016$) (figure 61D). Compared to the untreated infected rats fed LPD, the infected rats fed LPD treated with the DCM fraction of the *G. kola* extract had a significantly higher arena centre time ($P = 0.017$) (figure 61D). Compared to the non-infected rats, the infected rats fed LPD treated with the ethyl acetate fraction of the *G. kola* extract had a significantly lower arena centre time ($P = 0.033$) (figure 61D). Compared to the untreated infected rats fed LPD, the infected rats fed LPD treated with the ethyl acetate fraction of the *G. kola* extract had a significantly higher arena centre time ($P = 0.030$) (figure 61D).

Compared to the non-infected rats, the infected rats fed LPD had a significantly lower stretch attend posture latency ($P = 0.017$) (figure 61E). Compared to the non-infected rats, the infected rats fed LPD treated with the hexane fraction had a significantly lower stretch attend posture latency ($P = 0.004$) (figure 61E). Compared to the untreated infected rats fed LPD, the infected rats fed LPD treated with the hexane fraction had a significantly higher stretch attend posture latency ($P = 0.037$) (figure 61E). Compared to the untreated infected rats fed LPD, the infected rats fed LPD treated with the DCM fraction of the *G. kola* extract did not have a significantly higher stretch attend posture latency ($P = 0.317$) (figure 61E). Compared to the infected rats fed LPD and treated with the hexane fraction, the infected rats fed LPD treated with the DCM fraction of the *G. kola* extract had a significantly lower stretch attend posture latency ($P = 0.003$) (figure 61E). Compared to the untreated infected rats fed LPD, the infected rats fed LPD treated with the ethyl acetate fraction of the *G. kola* extract had a significantly higher stretch attend posture latency ($P = 0.002$) (figure 61E). Compared to the infected rats fed LPD and treated with the hexane fraction, the infected rats fed LPD treated with the ethyl acetate fraction of the *G. kola* extract had a significantly higher stretch attend posture latency ($P = 0.001$) (figure 61E).

Compared to the non-infected rats, the infected rats fed LPD had a significantly higher stretch attend posture time ($P = 0.003$) (figure 61F). Compared to the non-infected rats, the infected rats fed LPD treated with the hexane fraction had a significantly higher stretch attend posture time ($P = 0.045$) (figure 61F). Compared to the untreated infected rats fed LPD, the infected rats fed LPD treated with the hexane fraction had a significantly higher stretch attend posture time ($P = 0.045$) (figure 61F). Compared to the non-infected rats, the infected rats fed LPD treated with the DCM fraction of the *G. kola* extract had a significantly higher stretch attend posture time ($P = 0.004$) (figure 61F). Compared to the untreated infected rats fed LPD, the infected rats fed LPD treated with the DCM fraction of the *G. kola* extract had a significantly higher stretch attend posture time ($P = 0.021$) (figure 61F). Compared to the non-infected rats, the infected rats fed LPD treated with the ethyl acetate fraction of the *G. kola* extract had a significantly higher stretch attend posture time ($P < 0.001$) (figure 61F). Compared to the untreated infected rats fed LPD, the infected rats fed LPD treated with the ethyl acetate fraction of the *G. kola* extract had a significantly higher stretch attend posture time ($P < 0.001$) (figure 61F).

Compared to the non-infected rats, the infected rats fed LPD had a significantly lower distance covered close to walls ($P < 0.001$) (figure 61G). Compared to the non-infected rats, the infected rats fed LPD had a significantly lower close to wall area entries ($P = 0.002$) (figure 61H). Compared to the non-infected rats, the infected rats fed LPD treated with the hexane fraction had a significantly lower close to wall area entries ($P = 0.027$) (figure 61H).

Compared to the non-infected rats, the infected rats fed LPD had a significantly lower close to wall time ($P = 0.015$) (figure 61I). Compared to the non-infected rats, the infected rats fed LPD treated with the hexane fraction had a significantly lower close to wall time ($P = 0.016$) (figure 61I). Compared to the untreated infected rats fed LPD, the infected rats fed LPD treated with the hexane fraction had a significantly lower close to wall time ($P = 0.010$) (figure 61I). Compared to the non-infected rats, the infected rats fed LPD treated with the DCM fraction of the *G. kola* extract had a significantly lower close to wall time ($P = 0.002$) (figure 61I). Compared to the non-infected rats, the infected rats fed LPD treated with the ethyl acetate fraction of the *G. kola* extract had a significantly lower close to wall time ($P = 0.044$) (figure 61I).

3.3.6 EPM

3.3.6.1 EPM motor indicators

Compared to the non-infected rats, the infected rats fed LPD had a significantly lower total distance covered ($P < 0.001$) (figure 62A). Compared to the non-infected rats, the infected rats fed LPD treated with the hexane fraction had a significantly lower total distance covered ($P < 0.001$) (figure 62A). Compared to the non-infected rats, the infected rats fed LPD treated with the DCM fraction of the *G. kola* extract had a significantly lower total distance covered ($P = 0.009$) (figure 62A). Compared to the non-infected rats, the infected rats fed LPD treated with the ethyl acetate fraction of the *G. kola* extract had a significantly lower total distance covered ($P = 0.048$) (figure 62A).

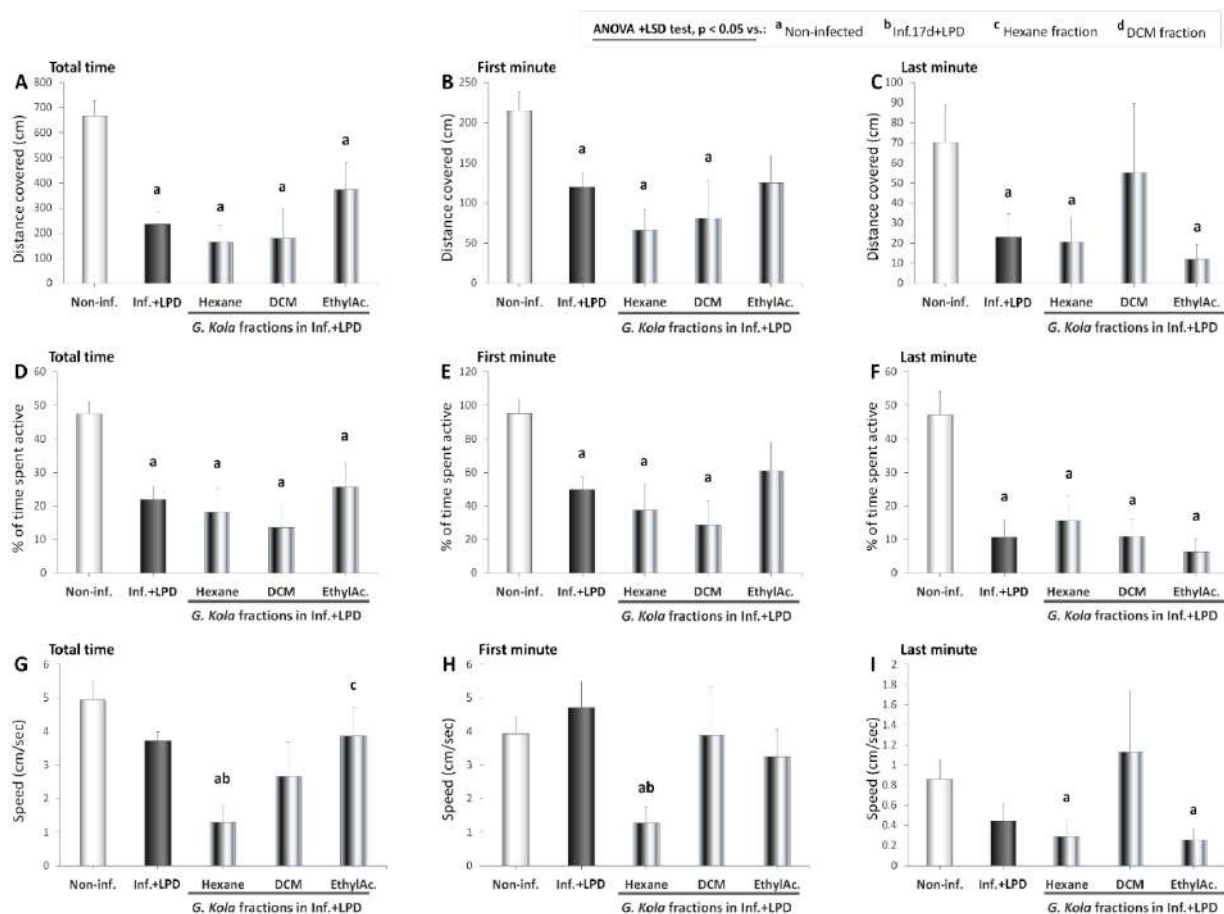


Figure 59. EPM motor indicators after treatment

Compared to the non-infected rats, the infected rats fed LPD had a significantly lower first minute distance covered ($P = 0.004$) (figure 62B). Compared to the non-infected rats, the infected rats fed LPD treated with the hexane fraction had a significantly lower first minute distance covered ($P < 0.001$) (figure 62B). Compared to the non-infected rats, the infected rats fed LPD treated with the DCM fraction of the *G. kola* extract had a significantly lower first minute distance covered ($P = 0.041$) (figure 62B).

Compared to the non-infected rats, the infected rats fed LPD had a significantly lower 4th minute distance covered ($P = 0.048$) (figure 62C). Compared to the non-infected rats, the infected rats fed LPD treated with the hexane fraction had a significantly lower 4th minute distance covered ($P = 0.043$). (figure 62C). Compared to the non-infected rats, the infected rats fed LPD treated with the ethyl acetate fraction of the *G. kola* extract had a significantly lower 4th minute distance covered ($P = 0.013$) (figure 62C).

Table XLI Motor function indicators of infected rats after treatment

	LPD+Inf.17d	LPD +Inf. 17d + G. kola fractions		
		Hexane	Dichloromethane	Ethyl acetate
Total distance covered				
Non-inf.	2.2E-5***	1.5E-5***	0.009**	0.048*
LPD+Inf.17d		0.381	0.680	0.284
Hex. fraction			0.907	0.138
DCM fraction				0.262
1st min distance				
Non-inf.	0.004**	3.1E-4***	0.041*	0.051
LPD+Inf.17d		0.108	0.468	0.899
Hex. fraction			0.789	0.191
DCM fraction				0.464
4th min distance				
Non-inf.	0.048*	0.043*	0.712	0.013*
LPD+Inf.17d		0.888	0.423	0.437
Hex. fraction			0.393	0.568
DCM fraction				0.285
Total activity time				
Non-inf.	1.0E-4***	0.002**	0.004**	0.028*
LPD+Inf.17d		0.643	0.323	0.667
Hex. fraction			0.652	0.476
DCM fraction				0.260
1st min activity time				
Non-inf.	5.4E-4***	0.005**	0.006**	0.113
LPD+Inf.17d		0.500	0.246	0.572
Hex. fraction			0.676	0.339
DCM fraction				0.188
4th min activity time				
Non-inf.	5.3E-4***	0.007**	9.9E-4***	1.3E-4***
LPD+Inf.17d		0.601	0.958	0.524
Hex. fraction			0.630	0.303
DCM fraction				0.494
Total average speed				
Non-inf.	0.082	9.3E-5***	0.097	0.323
LPD+Inf.17d		3.9E-4***	0.366	0.882
Hex. fraction			0.273	0.028*
DCM fraction				0.391
1st min average speed				
Non-inf.	0.422	0.001**	0.974	0.493
LPD+Inf.17d		0.002**	0.635	0.225
Hex. fraction			0.147	0.069
DCM fraction				0.715
4th min average speed				
Non-inf.	0.121	0.043	0.682	0.016*
LPD+Inf.17d		0.545	0.325	0.379
Hex. fraction			0.241	0.876
DCM fraction				0.221

ANOVA+LSD test: *P<0.05; **P<0.01; ***P<0.001.

Compared to the non-infected rats, the infected rats fed LPD had a significantly lower total activity time ($P < 0.001$) (figure 62D). Compared to the non-infected rats, the infected rats

fed LPD treated with the hexane fraction had a significantly lower total activity time ($P = 0.002$) (figure 62D). Compared to the non-infected rats, the infected rats fed LPD treated with the DCM fraction of the *G. kola* extract had a significantly lower total activity time ($P = 0.004$) (figure 62D). Compared to the non-infected rats, the infected rats fed LPD treated with the ethyl acetate fraction of the *G. kola* extract had a significantly lower total activity time ($P = 0.028$) (figure 62D).

Compared to the non-infected rats, the infected rats fed LPD had a significantly lower 1st minute activity time ($P < 0.001$) (figure 62E). Compared to the non-infected rats, the infected rats fed LPD treated with the hexane fraction had a significantly lower 1st minute activity time ($P = 0.005$) (figure 62E). Compared to the non-infected rats, the infected rats fed LPD treated with the DCM fraction of the *G. kola* extract had a significantly lower 1st minute activity time ($P = 0.006$) (figure 62E).

Compared to the non-infected rats, the infected rats fed LPD had a significantly lower 4th minute activity time ($P < 0.001$) (figure 62F). Compared to the non-infected rats, the infected rats fed LPD treated with the hexane fraction had a significantly lower 4th minute activity time ($P = 0.007$) (figure 62F). Compared to the non-infected rats, the infected rats fed LPD treated with the DCM fraction of the *G. kola* extract had a significantly lower 4th minute activity time ($P < 0.001$) (figure 62F). Compared to the non-infected rats, the infected rats fed LPD treated with the ethyl acetate fraction of the *G. kola* extract had a significantly lower 4th minute activity time ($P < 0.001$). (figure 62F).

Compared to the non-infected rats, the infected rats fed LPD treated with the hexane fraction had a significantly lower total average speed ($P < 0.001$) (figure 62G). Compared to the untreated infected rats fed LPD, the infected rats fed LPD treated with the hexane fraction had a significantly lower total average speed ($P < 0.001$) (figure 62G).

Compared to the non-infected rats, the infected rats fed LPD treated with the hexane fraction had a significantly lower 1st minute average speed ($P = 0.001$) (figure 62H). Compared to the untreated infected rats fed LPD, the infected rats fed LPD treated with the hexane fraction had a significantly 1st minute average speed ($P = 0.002$) (figure 62H). Compared to the non-infected rats, the infected rats fed LPD treated with the hexane fraction had a significantly lower 4th minute average speed ($P = 0.043$) (figure 62I). Compared to the non-infected rats, the infected rats fed LPD treated with the ethyl acetate fraction of the *G. kola* extract had a significantly lower 4th minute average speed ($P = 0.016$) (figure 62I).

3.3.6.2 Arm latency and time

Compared to the non-infected rats, the untreated infected rats fed LPD had a significantly higher open arm latency ($P = 0.019$) (figure 63A). Compared to the untreated infected rats fed LPD, the infected rats fed LPD treated with the hexane fraction had a significantly lower open arm latency ($P = 0.023$) (figure 63A). Compared to the untreated infected rats fed LPD, the infected rats fed LPD treated with the ethyl acetate fraction of the *G. kola* extract had a significantly lower open arm latency ($P = 0.011$). (figure 63A). Compared to the non-infected rats, the untreated infected rats fed LPD had a significantly lower open arm entry ($P = 0.003$) (figure 63B). Compared to the non-infected rats, the infected rats fed LPD treated with the hexane fraction had a significantly lower open arm entries ($P = 0.006$) (figure 63B). Compared to the non-infected rats, the untreated infected rats fed LPD had a significantly higher open arm time ($P = 0.029$) (figure 63C).

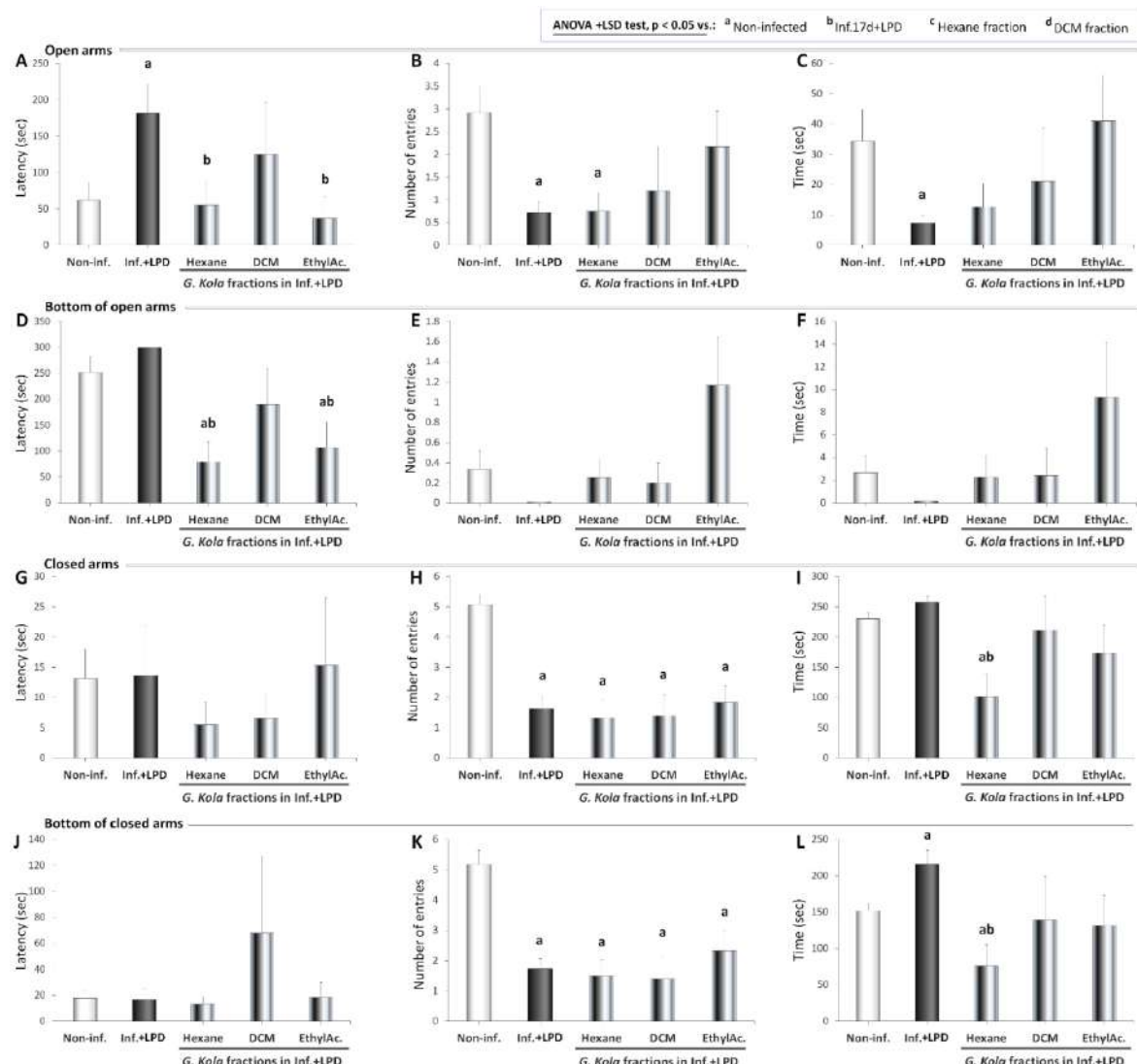


Figure 60. EPM arm latency and time after treatment

Compared to the non-infected rats, the infected rats fed LPD treated with the hexane fraction had a significantly lower of open arm bottom latency ($P = 0.002$) (figure 63D). Compared to the untreated infected rats fed LPD, the infected rats fed LPD treated with the hexane fraction had a significantly lower of open arm bottom latency ($P < 0.001$) (figure 63D). Compared to the non-infected rats, the infected rats fed LPD treated with the ethyl acetate fraction of the *G. kola* extract had a significantly lower of open arm bottom entries ($P = 0.031$) (figure 63E). Compared to the untreated infected rats fed LPD, the infected rats fed LPD treated with the ethyl acetate fraction of the *G. kola* extract had a significantly lower of open arm bottom time ($P = 0.010$) (figure 63F).

Table XLII. Arm entry time and latency of infected rats after treatment

	LPD+Inf.17d	LPD +Inf. 17d + G. kola fractions		
		Hexane	Dichloromethane	Ethyl acetate
Open arm latency				
Non-inf.	0.019*	0.875	0.440	0.541
LPD+Inf.17d		0.023*	0.509	0.011*
Hex. fraction			0.409	0.695
DCM fraction				0.304
Open arm entries				
Non-inf.	0.003**	0.006**	0.171	0.460
LPD+Inf.17d		0.962	0.658	0.133
Hex. fraction			0.685	0.152
DCM fraction				0.462
Open arm time				
Non-inf.	0.029*	0.112	0.539	0.726
LPD+Inf.17d		0.515	0.487	0.077
Hex. fraction			0.681	0.135
DCM fraction				0.415
Open arm bottom latency				
Non-inf.	0.143	0.002**	0.445	0.031*
LPD+Inf.17d		1.3E-4***	0.180	0.010*
Hex. fraction			0.199	0.655
DCM fraction				0.348
Open arm bottom entries				
Non-inf.	0.104	0.752	0.637	0.151
LPD+Inf.17d		0.191	0.374	0.058
Hex. fraction			0.856	0.119
DCM fraction				0.106
Open arm bottom time				
Non-inf.	0.105	0.863	0.928	0.234
LPD+Inf.17d		0.248	0.374	0.110
Hex. fraction			0.962	0.214
DCM fraction				0.237
Closed arm latency				
Non-inf.	0.955	0.230	0.310	0.858
LPD+Inf.17d		0.381	0.449	0.904
Hex. fraction			0.837	0.431
DCM fraction				0.483
Closed arm entries				
Non-inf.	1.1E-6***	4.5E-5***	0.003**	7.0E-4***
LPD+Inf.17d		0.679	0.771	0.774
Hex. fraction			0.943	0.549
DCM fraction				0.631
Closed arm time				
Non-inf.	0.071	0.006**	0.763	0.286
LPD+Inf.17d		0.001**	0.459	0.132
Hex. fraction			0.143	0.256
DCM fraction				0.614
Bottom of closed arm latency				
Non-inf.	0.913	0.552	0.436	0.980
LPD+Inf.17d		0.734	0.429	0.923
Hex. fraction			0.398	0.708
DCM fraction				0.443
Bottom of closed arm entries				
Non-inf.	1.3E-5***	5.3E-5***	0.003**	0.006**
LPD+Inf.17d		0.726	0.704	0.441
Hex. fraction			0.916	0.353
DCM fraction				0.377
Bottom of closed arm time				
Non-inf.	0.011*	0.027*	0.846	0.649
LPD+Inf.17d		0.001**	0.280	0.108
Hex. fraction			0.378	0.303
DCM fraction				0.915

ANOVA+LSD test: *P<0.05; **P<0.01; ***P<0.001.

No significant change was observed in the latency to the closed arm entry (figure 63G). Compared to the non-infected rats, the untreated infected rats fed LPD had a significantly lower closed arm entry ($P < 0.001$) (figure 63H). Compared to the non-infected rats, the infected rats fed LPD treated with the hexane fraction had a significantly lower closed arm entry ($P < 0.001$) (figure 63H). Compared to the non-infected rats, the infected rats fed LPD treated with the DCM fraction of the *G. kola* extract had a significantly lower closed arm entry ($P = 0.003$) (figure 63H). Compared to the non-infected rats, the infected rats fed LPD treated with the ethyl acetate fraction of the *G. kola* extract had a significantly lower closed arm entry ($P < 0.001$) (figure 63H).

Compared to the non-infected rats, the infected rats fed LPD treated with the hexane fraction had a significantly lower closed arm time ($P = 0.006$) (figure 63I). No significant change was observed in the bottom of closed arm latency (figure 63J). Compared to the non-infected rats, the untreated infected rats fed LPD had a significantly lower bottom of closed arm entries ($P < 0.001$), but also the infected rats fed LPD treated with the hexane fraction ($P = 0.001$), the DCM fraction ($P = 0.003$), and the ethyl acetate fraction ($P = 0.006$) (figure 63K). Compared to the non-infected rats, the untreated infected rats fed LPD had a significantly higher bottom of closed arm time ($P = 0.011$) (figure 63L). Compared to the non-infected rats, the infected rats fed LPD treated with the hexane fraction had a significantly lower bottom of closed arm time ($P = 0.027$) (figure 63L). Compared to the untreated infected rats fed LPD, the infected rats fed LPD treated with the hexane fraction had a significantly lower bottom of closed arm time ($P = 0.001$) (figure 63L).

3.3.6.3 Head dipping and rearing

Compared to the non-infected rats, the untreated infected rats fed LPD had a significantly higher head dipping latency ($P < 0.001$) (figure 64A). Compared to the untreated infected rats fed LPD, the infected rats fed LPD treated with the hexane fraction had a significantly lower head dipping latency ($P < 0.001$) (figure 64A). Compared to the untreated infected rats fed LPD, the infected rats fed LPD treated with the ethyl acetate fraction of the *G. kola* extract had a significantly lower head dipping latency ($P < 0.001$) (figure 64A).

Compared to the non-infected rats, the untreated infected rats fed LPD had a significantly lower head dipping episode ($P < 0.001$) (figure 64B). Compared to the non-infected rats, the infected rats fed LPD treated with the hexane fraction had a significantly lower head dipping episode ($P = 0.003$) (figure 64B). Compared to the untreated infected rats fed LPD, the infected rats fed LPD treated with the ethyl acetate fraction of the *G. kola* extract had a significantly higher head dipping episode ($P = 0.015$) (figure 64B). Compared to the infected rats fed LPD treated with the hexane fraction, the infected rats fed LPD treated with

the ethyl acetate fraction of the *G. kola* extract had a significantly higher head dipping episode ($P = 0.030$) (figure 64B).

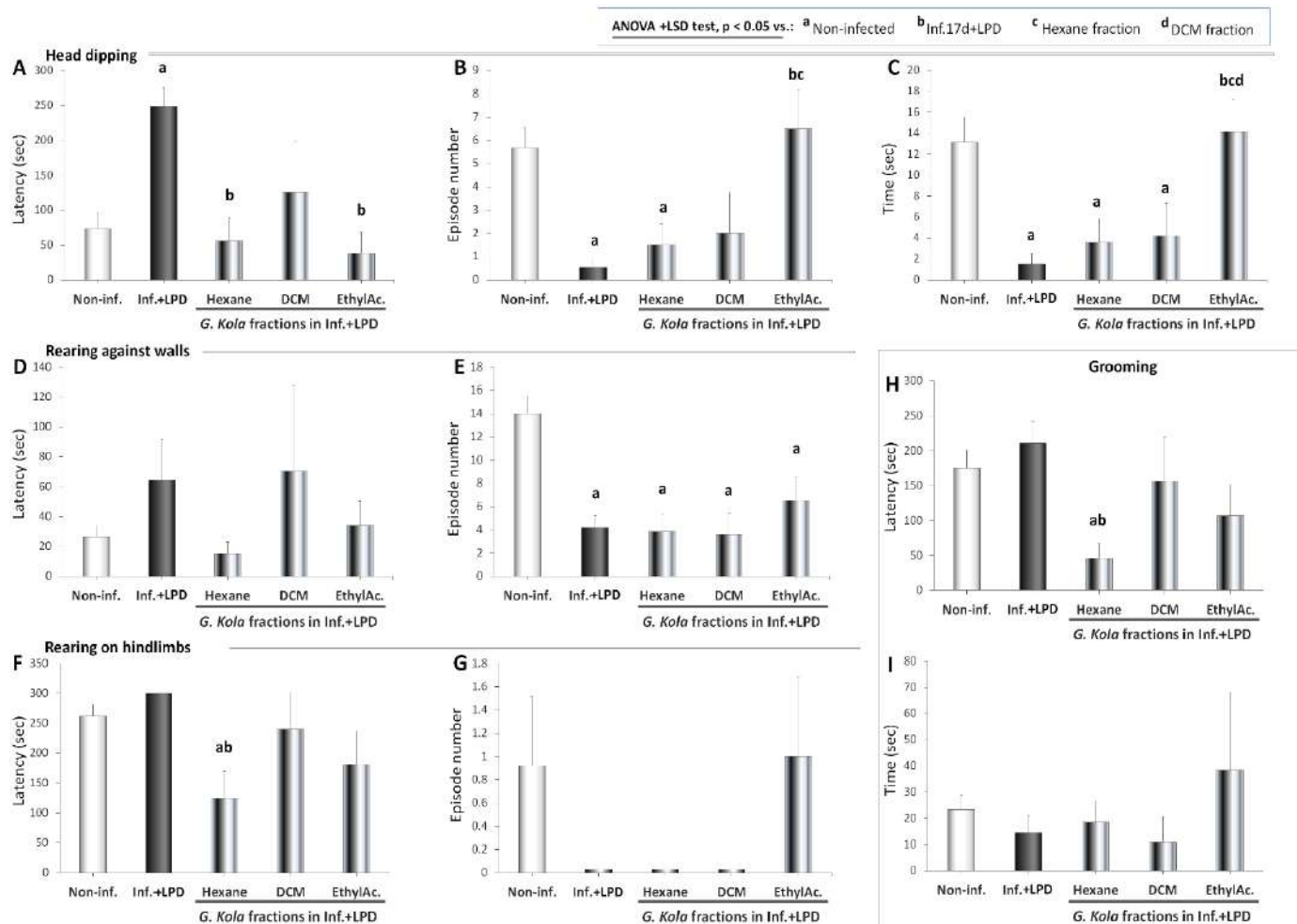


Figure 61. Head dipping and rearing in the maze after treatment

Compared to the non-infected rats, the untreated infected rats fed LPD had a significantly lower head dipping time ($P < 0.001$) (figure 64C). Compared to the non-infected rats, the infected rats fed LPD treated with the hexane fraction had a significantly lower head dipping time ($P = 0.008$) (figure 64C). Compared to the non-infected rats, the infected rats fed LPD treated with the DCM fraction of the *G. kola* extract had a significantly lower head dipping time ($P = 0.048$) (figure 64C). Compared to the untreated infected rats fed LPD, the infected rats fed LPD treated with the ethyl acetate fraction of the *G. kola* extract had a significantly higher head dipping time ($P = 0.007$) (figure 64C). Compared to the infected rats fed LPD treated with the hexane fraction, the infected rats fed LPD treated with the ethyl acetate fraction of the *G. kola* extract had a significantly higher head dipping time ($P = 0.018$) (figure 64C). Compared to the infected rats fed LPD treated with the DCM fraction of the *G. kola* extract,

the infected rats fed LPD treated with the ethyl acetate fraction of the *G. kola* extract had a significantly higher head dipping time ($P = 0.048$) (figure 64C).

Table XLIII. Head dipping and thigmotaxis indicators after treatment

	LPD+Inf.17d	LPD +Inf. 17d + G. kola fractions		
		Hexane	Dichloromethane	Ethyl acetate
Head dipping latency				
Non-inf.	8.9E-5***	0.660	0.513	0.373
LPD+Inf.17d		2.1E-4***	0.166	2.1E-4***
Hex. fraction			0.403	0.705
DCM fraction				0.302
Head dipping entries				
Non-inf.	1.1E-4***	0.003**	0.111	0.672
LPD+Inf.17d		0.334	0.459	0.015*
Hex. fraction			0.809	0.030*
DCM fraction				0.097
Head dipping time				
Non-inf.	4.5E-4***	0.008**	0.048*	0.800
LPD+Inf.17d		0.416	0.452	0.007**
Hex. fraction			0.876	0.018*
DCM fraction				0.048*
Rearing against walls latency				
Non-inf.	0.196	0.302	0.491	0.690
LPD+Inf.17d		0.103	0.929	0.347
Hex. fraction			0.396	0.339
DCM fraction				0.572
Number of episodes of rearing against walls				
Non-inf.	2.7E-5***	9.3E-5***	0.001**	0.014*
LPD+Inf.17d		0.853	0.791	0.343
Hex. fraction			0.924	0.321
DCM fraction				0.319
Rearing on hindlimb latency				
Non-inf.	0.085	0.014*	0.748	0.217
LPD+Inf.17d		0.002**	0.374	0.083
Hex. fraction			0.160	0.444
DCM fraction				0.489
Number of rearing on hindlimbs				
Non-inf.	0.152	0.193	0.275	0.928
LPD+Inf.17d		0.339	0.374	0.203
Hex. fraction			0.612	0.239
DCM fraction				0.305
Grooming latency				
Non-inf.	0.396	8.3E-4***	0.799	0.216
LPD+Inf.17d		4.4E-4***	0.474	0.085
Hex. fraction			0.156	0.258
DCM fraction				0.531
Grooming time				
Non-inf.	0.319	0.633	0.315	0.638
LPD+Inf.17d		0.708	0.763	0.468
Hex. fraction			0.567	0.544
DCM fraction				0.416

ANOVA+LSD test: * $P < 0.05$; ** $P < 0.01$; *** $P < 0.001$.

No significant change was observed in the rearing against wall latency (figure 64D).

Compared to the non-infected rats, the untreated infected rats fed LPD had a significantly lower number of episodes of rearing against walls ($P < 0.001$) (figure 64E). Compared to the non-infected rats, the infected rats fed LPD treated with the hexane fraction had a significantly

lower number of episodes of rearing against walls ($P < 0.001$) (figure 64E). Compared to the non-infected rats, the infected rats fed LPD treated with the DCM fraction of the *G. kola* extract had a significantly lower number of episodes of rearing against walls ($P = 0.001$) (figure 64E). Compared to the non-infected rats, the infected rats fed LPD treated with the ethyl acetate fraction of the *G. kola* extract had a significantly lower number of episodes of rearing against walls ($P = 0.014$) (figure 64E).

Compared to the non-infected rats, the infected rats fed LPD treated with the hexane fraction had a significantly lower rearing on hindlimbs latency ($P = 0.014$). (Figure 64F). Compared to the untreated infected rats fed LPD, the infected rats fed LPD treated with the hexane fraction had a significantly lower rearing on hindlimbs latency ($P = 0.002$) (figure 64F). No significant change was observed in the number of episodes of rearing on hindlimbs (figure 64G). Compared to the non-infected rats, the infected rats fed LPD treated with the hexane fraction had a significantly lower grooming latency ($P < 0.001$) (figure 64H). Compared to the untreated infected rats fed LPD, the infected rats fed LPD treated with the hexane fraction had a significantly lower grooming latency ($P < 0.001$) (figure 64H). No significant change was observed in the grooming time (figure 64I).

3.3.6.4 Centre entries and attend posture

Compared to the non-infected rats, the untreated infected rats fed LPD had significantly lower central platform entries ($P < 0.001$) (figure 65A). Compared to the non-infected rats, the infected rats fed LPD treated with the hexane fraction had a significantly lower central platform entry ($P < 0.001$) (figure 65A). Compared to the non-infected rats, the infected rats fed LPD treated with the DCM fraction of the *G. kola* extract had a significantly lower central platform entry ($P = 0.025$) (figure 65A). Compared to the non-infected rats, the infected rats fed LPD treated with the ethyl acetate fraction of the *G. kola* extract had a significantly lower central platform entries ($P = 0.030$) (figure 65A). Compared to the untreated infected rats fed LPD, the infected rats fed LPD treated with the ethyl acetate fraction of the *G. kola* extract had a significantly higher central platform entry ($P = 0.003$) (figure 65A). Compared to the infected rats fed LPD treated with the hexane fraction, the infected rats fed LPD treated with the ethyl acetate fraction of the *G. kola* extract had a significantly higher central platform entry ($P = 0.004$) (figure 65A).

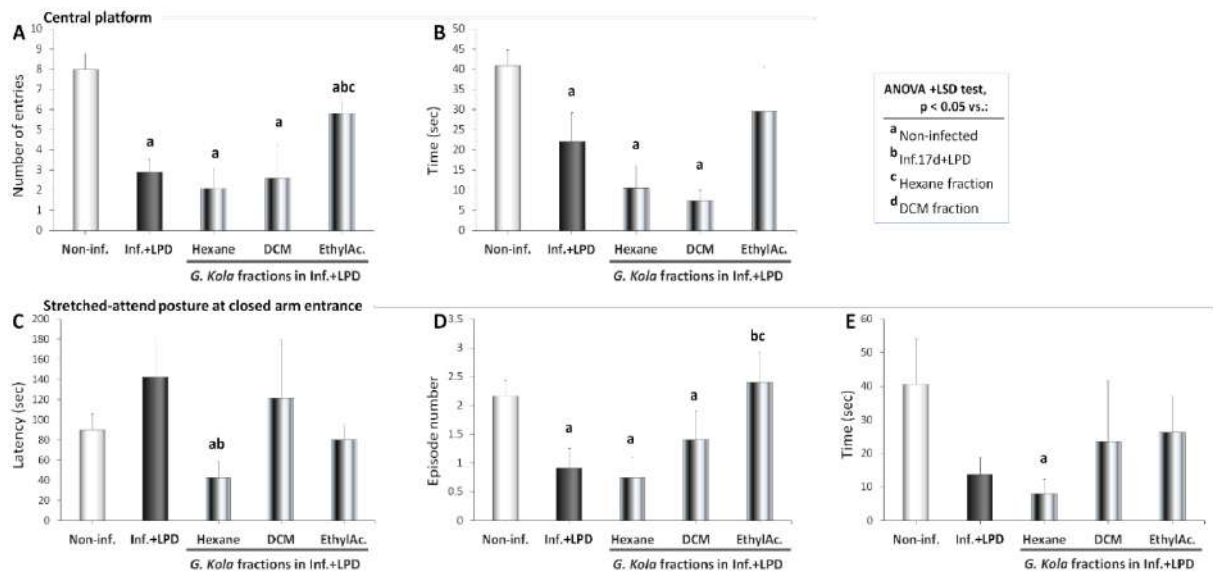


Figure 62. Centre entries and attend posture in the maze after treatment

Table XLIV. Activities around maze central platform after treatment

	LPD +Inf. 17d + <i>G. kola</i> fractions			
	LPD+Inf.17d	Hexane	Dichloromethane	Ethyl acetate
Central platform entries				
Non-inf.	3.0E-5***	9.5E-5***	0.025*	0.030*
LPD+Inf.17d		0.486	0.866	0.003**
Hex. fraction			0.794	0.004***
DCM fraction				0.120
Central platform time				
Non-inf.	0.037*	2.7E-4***	4.9E-6***	0.366
LPD+Inf.17d		0.225	0.084	0.569
Hex. fraction			0.626	0.154
DCM fraction				0.095
Latency to stretched-attend posture at closed arm entrance				
Non-inf.	0.234	0.049	0.620	0.657
LPD+Inf.17d		0.034*	0.775	0.159
Hex. fraction			0.250	0.110
DCM fraction				0.519
Number of stretched-attend posture episodes at closed arm entrance				
Non-inf.	0.009**	0.004**	0.230	0.699
LPD+Inf.17d		0.749	0.448	0.042*
Hex. fraction			0.324	0.028*
DCM fraction				0.203
Time of stretched-attend posture at closed arm entrance				
Non-inf.	0.082	0.037*	0.469	0.420
LPD+Inf.17d		0.399	0.621	0.341
Hex. fraction			0.439	0.177
DCM fraction				0.905

ANOVA+LSD test: *P<0.05; **P<0.01; ***P<0.001.

Compared to the non-infected rats, the untreated infected rats fed LPD had a significantly lower central platform time ($P = 0.037$) (figure 65B). Compared to the non-infected rats, the infected rats fed LPD treated with the hexane fraction had a significantly

lower central platform time ($P < 0.001$) (figure 65B). Compared to the non-infected rats, the infected rats fed LPD treated with the DCM fraction of the *G. kola* extract had a significantly lower central platform time ($P < 0.001$) (figure 65B).

Compared to the non-infected rats, the infected rats fed LPD treated with the hexane fraction had a significantly lower latency to stretch attend posture at closed arm entrance ($P = 0.049$) (figure 65C). Compared to the untreated infected rats fed LPD, the infected rats fed LPD treated with the hexane fraction had a significantly lower latency to stretch attend posture at closed arm entrance ($P = 0.034$) (figure 65C).

Compared to the non-infected rats, the untreated infected rats fed LPD had a significantly lower number of stretch attend posture at closed arm entrance ($P = 0.009$) (figure 65D). Compared to the non-infected rats, the infected rats fed LPD treated with the hexane fraction had a significantly lower number of stretch-attend posture at closed arm entrance ($P = 0.004$) (figure 65D). The number of stretch-attend posture at closed arm entrance of the infected rats fed LPD treated with the DCM fraction was not significantly changed compared to the non-infected rats ($P = 0.230$) (figure 65D). Compared to the untreated infected rats fed LPD, the infected rats fed LPD treated with the ethyl acetate fraction of the *G. kola* extract had a significantly higher number of stretch-attend posture at closed arm entrance ($P = 0.042$) (figure 65D). Compared to the infected rats fed LPD treated with the hexane fraction, the infected rats fed LPD treated with the ethyl acetate fraction of the *G. kola* extract had a significantly higher number of stretch-attend posture at closed arm entrance ($P = 0.028$) (figure 65D). Compared to the non-infected rats, the infected rats fed LPD treated with the hexane fraction had a significantly lower time of stretch-attend posture at closed arm entrance ($P = 0.037$) (figure 65E).

3.3.7 Parasite and immune cell count in the blood

Figure 66 shows blood smears of representative animals treated with *G. kola* extracts. Unlike LPD-fed untreated infected groups that displayed increases in white blood cell (WBC) density (figure 66B), LPD-fed infected animals treated with hexane or DCM fractions (figures 66C, D), had a decreased number of circulating *T. gondii* cysts in their blood, while ethyl acetate fraction-treated had none (figure 66E). LPD-fed infected animals treated with hexane fraction, and to a lesser extent, animals treated with DCM fraction, showed an increased WBC density figures 66C, D). Animals treated with ethyl acetate fraction had the lesser WBC density of all the infected animals (figure 66E).

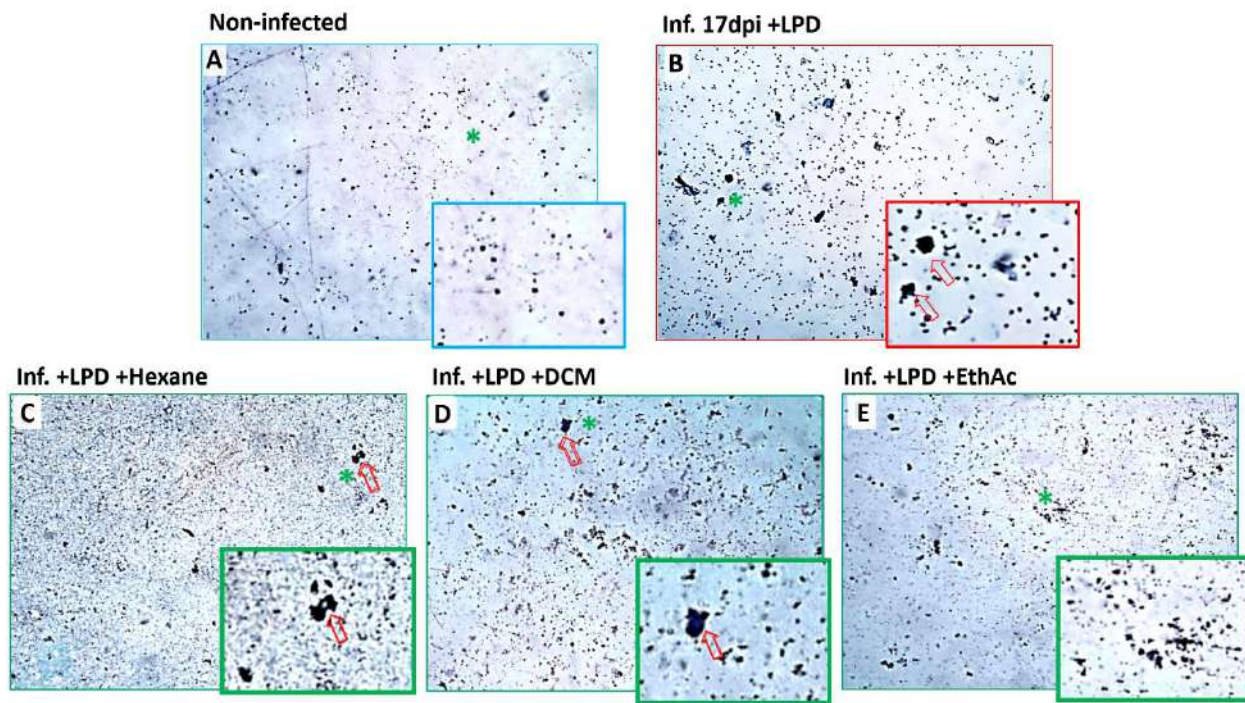


Figure 63. Blood smears of *G. kola*-treated representative treated animals

*Green asterisks: areas magnified in the insets. Red arrows: *T. gondii* cysts. Note the high number of cysts in the early stage of infection (C) but not in the terminal stage (B).*

Figure 67 shows the effect of *G. kola* fractions on parasite and white blood cell counts of infected animals, while table XLV presents the results of inter-group comparisons for statistical significance. LPD-fed infected group presented with significantly decreased cyst counts (respectively, increased tachyzoite count) (figures 67A, B and table XLV).

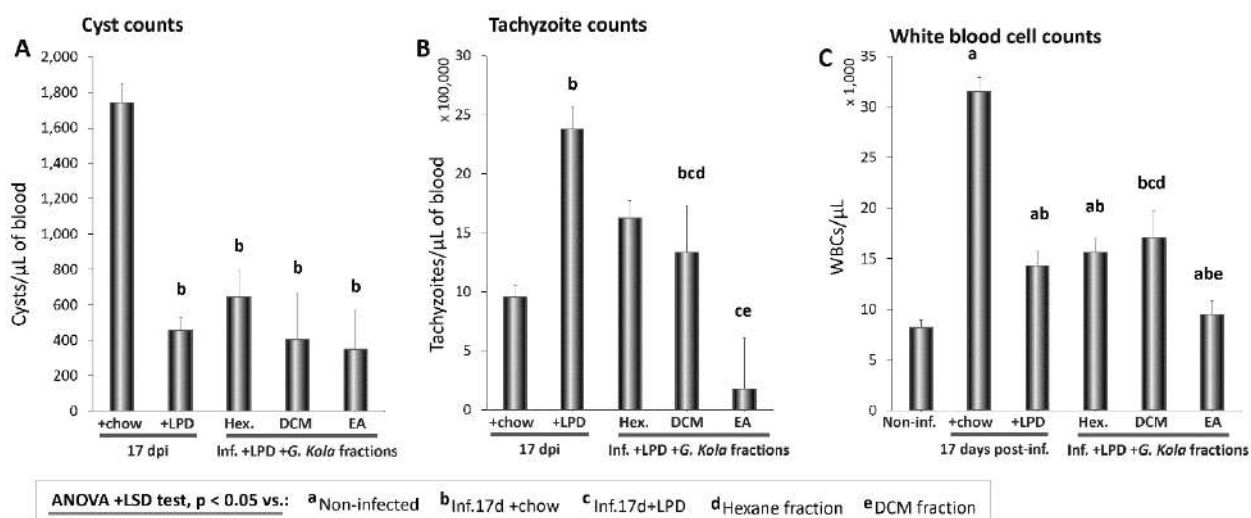


Figure 64. Blood parasite and immune cell counts of treated animals

*Blood counts of *T. gondii* cysts (A) and tachyzoites (B), and white blood cells (C). Note the higher number of white blood cells in the untreated infected group compared to the treated groups (C).*

Treatment with ethyl acetate fraction, and to a lesser extent, with DCM fraction, significantly decreased both the tachyzoite and the cyst counts compared to the untreated LPD-fed infected animals, although with a high interindividual variability (figures 67A, B).

Table XLV. Blood cell count comparisons of treated animals

	Infected 17d		Inf. +LPD + <i>G. kola</i> fractions		
	+chow	+PPD	Hex.	DCM	EthAc
Cyst counts					
Non-inf.	2.1E-8***	1.3E-4***	0.001**	0.117	0.126
+chow		7.0E-6***	2.0E-4***	2.0E-4***	0.001**
+PPD			0.298	0.662	0.862
Hex.				0.300	0.453
DCM					0.873
Tachyzoite counts					
Non-inf.	3.1E-6***	2.5E-7***	0.003**	0.278	0.006**
+chow		5.6E-5***	0.130	0.001**	0.341
+PPD			0.146	1.5E-5***	0.045*
Hex.				0.013*	0.631
DCM					0.027*
WBC counts					
Non-inf.	8.2E-8***	0.004**	0.001**	0.432	0.008**
+chow		1.3E-5***	4.0E-5***	3.4E-6***	0.001**
+PPD			0.530	0.040*	0.375
Hex.				0.014*	0.657
DCM					0.038*

The treatment with ethyl acetate fraction decreased the WBC count and restored it to levels comparable to non-infected animals, while treatment with hexane fraction (respectively, DCM fraction) did not induce change (respectively, increased) WBC counts compared to the untreated LPD-fed infected animals (figure 67C, table XLV).

3.3.8 Brain neuronal density

3.3.8.1 Brain anterior areas: cingulate cortex and medial septal nucleus

Treatment with *G. kola* extracts mitigated the neuronal loss in the anterior cingulate cortices of infected animals fed LPD (figures 68G-I).

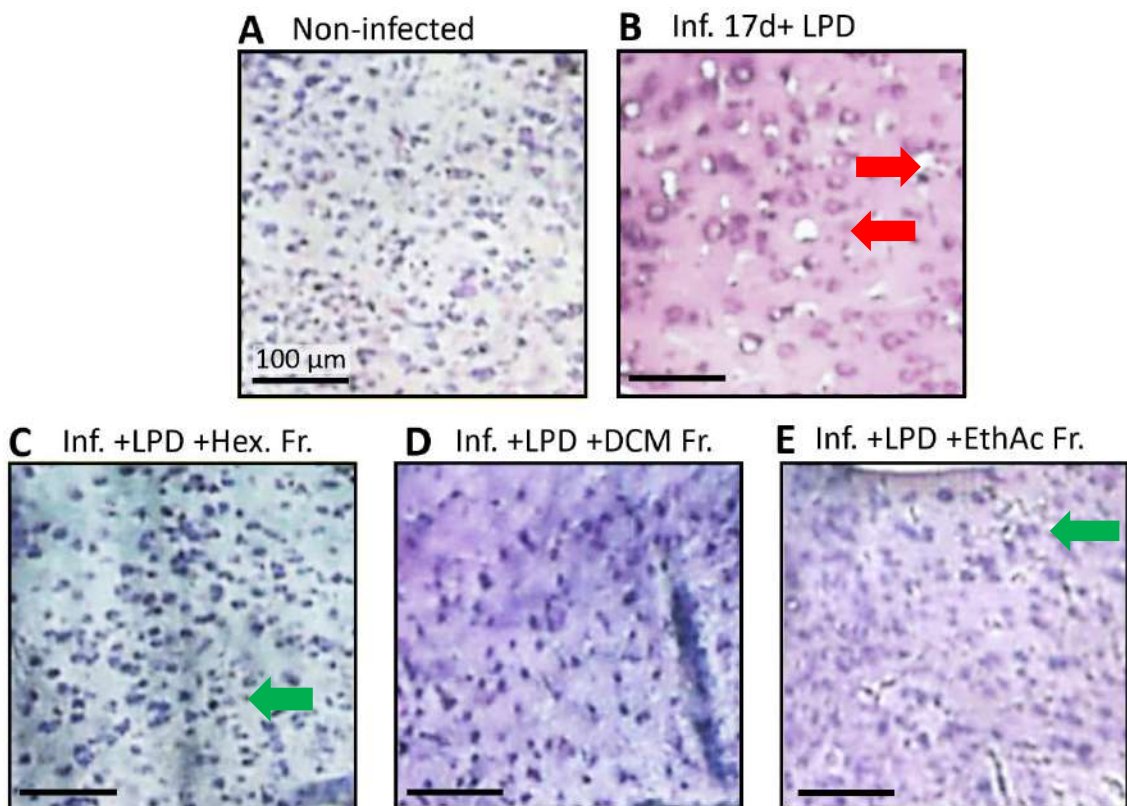


Figure 65. Anterior cingulate cortices of representative treated animals

Red arrow: Neuronal loss in LPD-fed (**B**). **Green arrow:** Prevention by the treatments (**C-E**).

Infected animals fed LPD and treated with DCM or ethyl acetate fractions of *G. kola* extract the decrease in neuronal density in the medial septal nucleus was prevented (figures 69G-I).

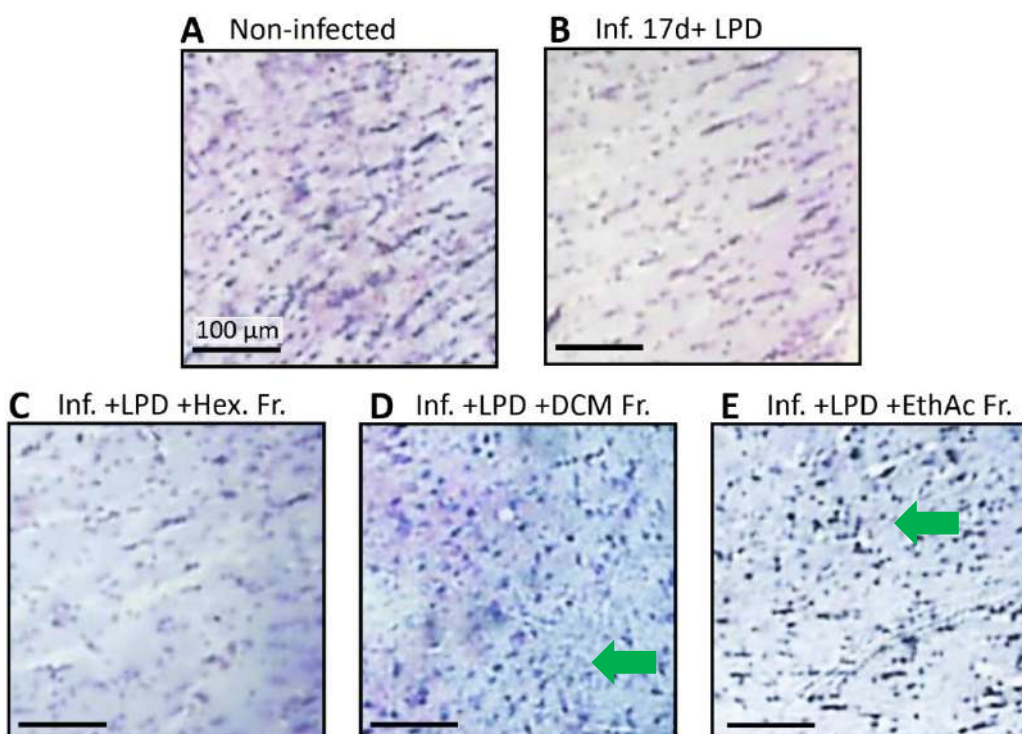


Figure 66. Medial septal nuclei of representative treated animals

Green arrow: Prevention of neuronal loss in the DCM (D) and ethyl-acetate (E) treated groups.

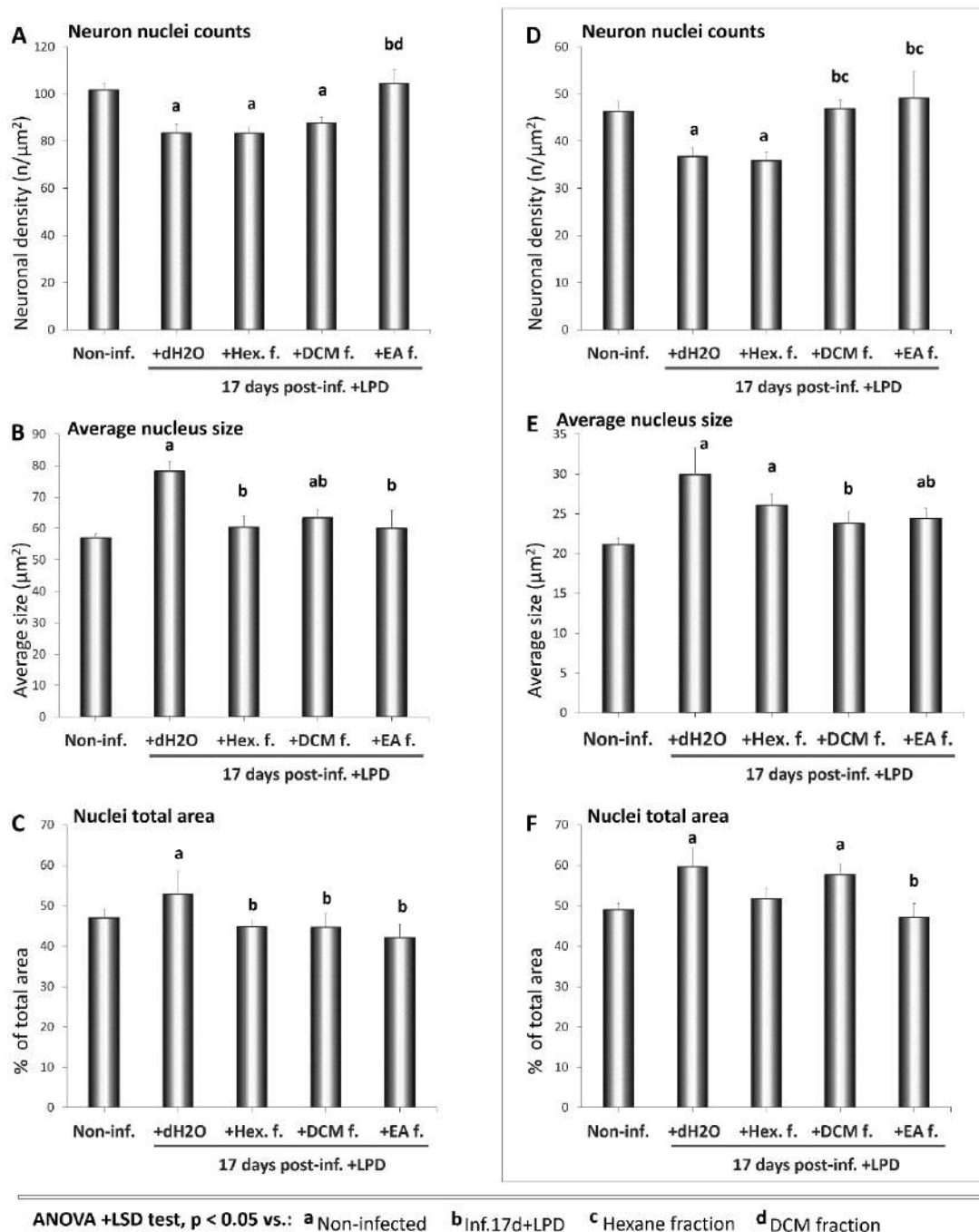


Figure 67. Average counts in brain anterior areas of treated animals

Counts in the anterior cingulate cortex (A-C) and in the medial septal nucleus (D-F).

Increases in the average nucleus size (Figure 70B, E) and in nuclei total area (figures 70C, F) were observed in the cingulate cortices and in the medial septal nuclei of untreated

LPD-fed infected animals. These alterations were prevented or mitigated by treatments with *G. kola* extract, in particular ethyl acetate fraction (figures 70A, B, D, E and table XLVI).

Table XLVI. Brain anterior area cell count comparisons of treated animals

Infected 17d		Inf.17d +LPD + <i>G. kola</i> fractions		
+Chow	+LPD	Hex.	DCM	EthylAc.
Counts in the anterior cingulate cortex				
Non-inf.	0.131	3.0E-5***	0.001**	0.016*
+Chow		1.4E-4***	0.003**	0.044*
+LPD			0.992	0.370
Hex.				0.484
DCM				0.012*
Average size of neuron nuclei in the anterior cingulate cortex				
Non-inf.	0.228	1.2E-6***	0.262	0.020*
+Chow		2.3E-5***	0.966	0.444
+LPD			0.002**	0.016*
Hex.				0.510
DCM				0.542
% area of neuron nuclei in the anterior cingulate cortex				
Non-inf.	0.377	0.036*	0.557	0.575
+Chow		4.5E-4***	0.993	0.986
+LPD			0.015*	0.021*
Hex.				0.986
DCM				0.609
Counts in the medial septal nucleus				
Non-inf.	0.375	0.002**	0.005**	0.880
+Chow		0.002**	0.003**	0.340
+LPD			0.783	0.005**
Hex.				0.007**
DCM				0.699
Average size of neuron nuclei in the medial septal nucleus				
Non-inf.	0.077***	3.9E-6***	0.002**	0.104
+Chow		7.5E-5***	0.098	0.841
+LPD			0.069	0.018*
Hex.				0.295
DCM				0.736
% area of neuron nuclei in the medial septal nucleus				
Non-inf.	0.554	0.001**	0.467	0.007**
+Chow		0.001**	0.627	0.011*
+LPD			0.080	0.657
Hex.				0.276
DCM				0.024*

3.3.8.2 Brain posterior areas: parietal cortex and lateral hypothalamus

Decreases in neuronal density in the posterior parietal cortex of LPD-fed infected rats were prevented by all *G. kola* extracts tested (figures 71G-I).

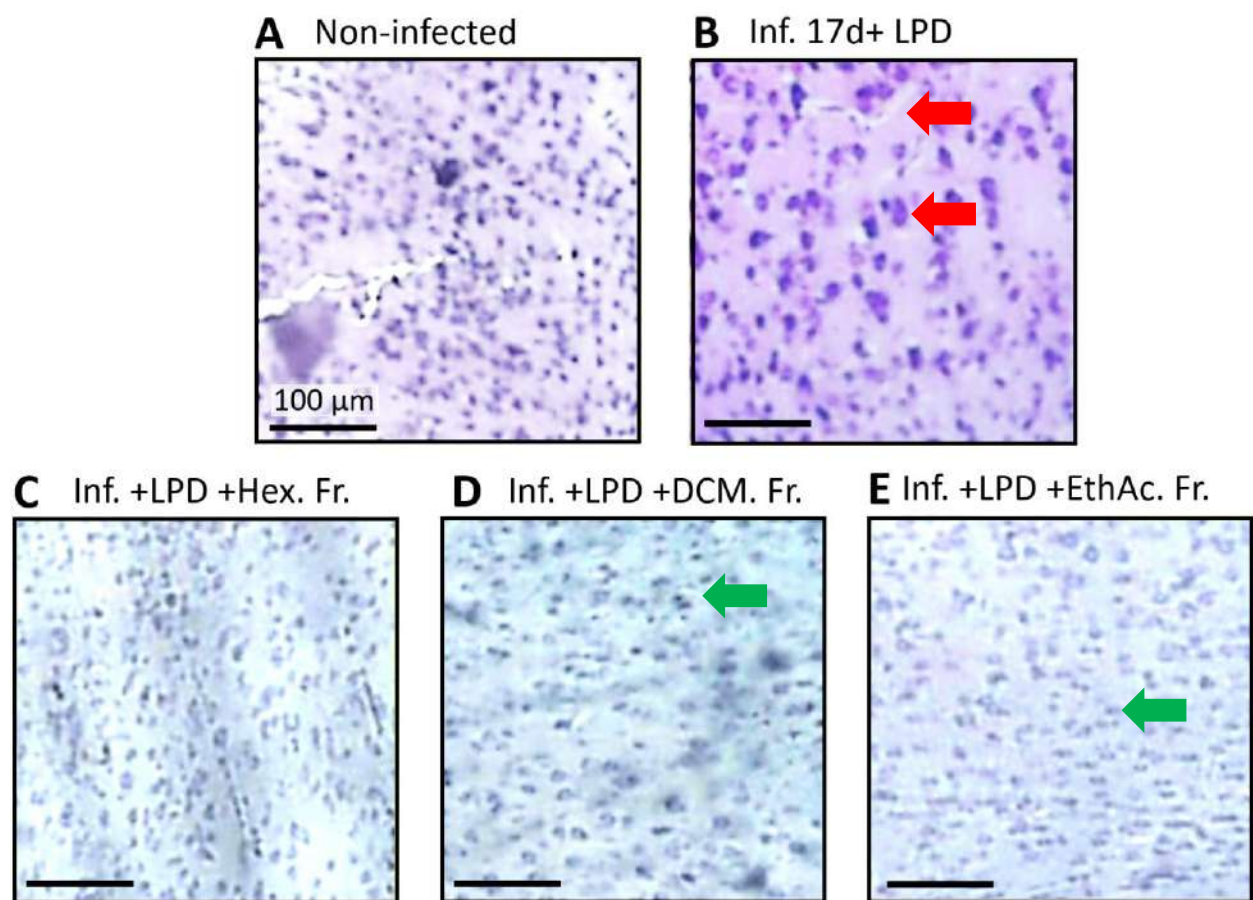


Figure 68. Posterior parietal cortices of representative treated animals

Red arrow: loss of neuron nuclei enlargement. **Green arrow:** Prevention of neuron loss in the *G. kola*-treated groups (**D-E**)

Both neuron enlargement and loss observed in LPD-fed infected animals were prevented by all *G. kola* extracts tested (figures 72G-I).

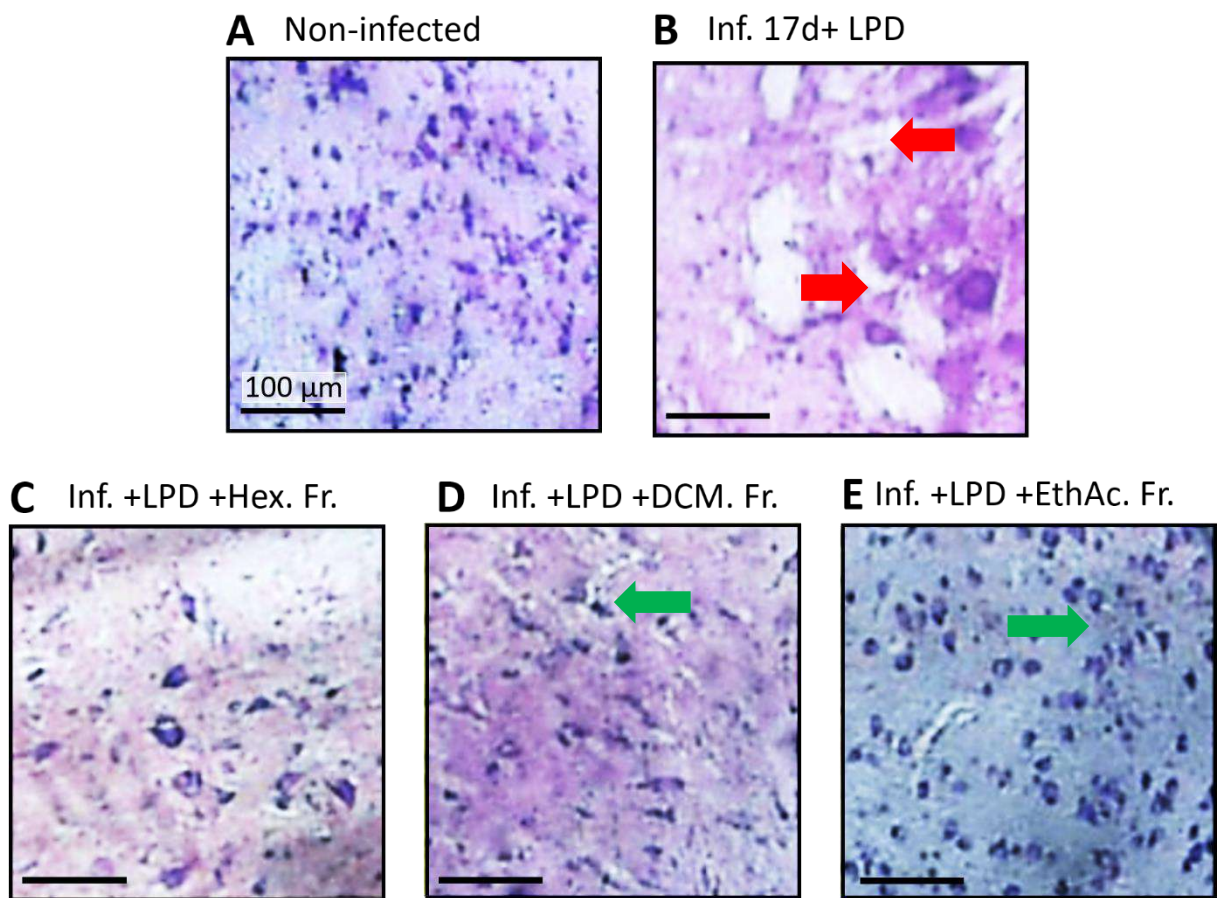
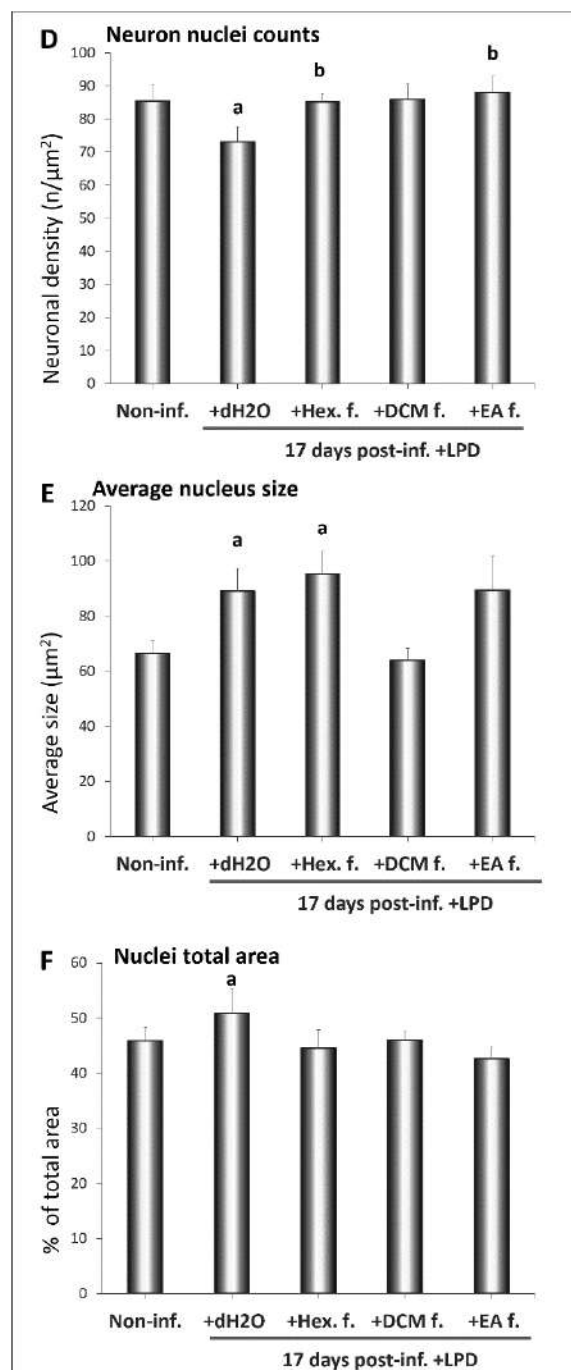
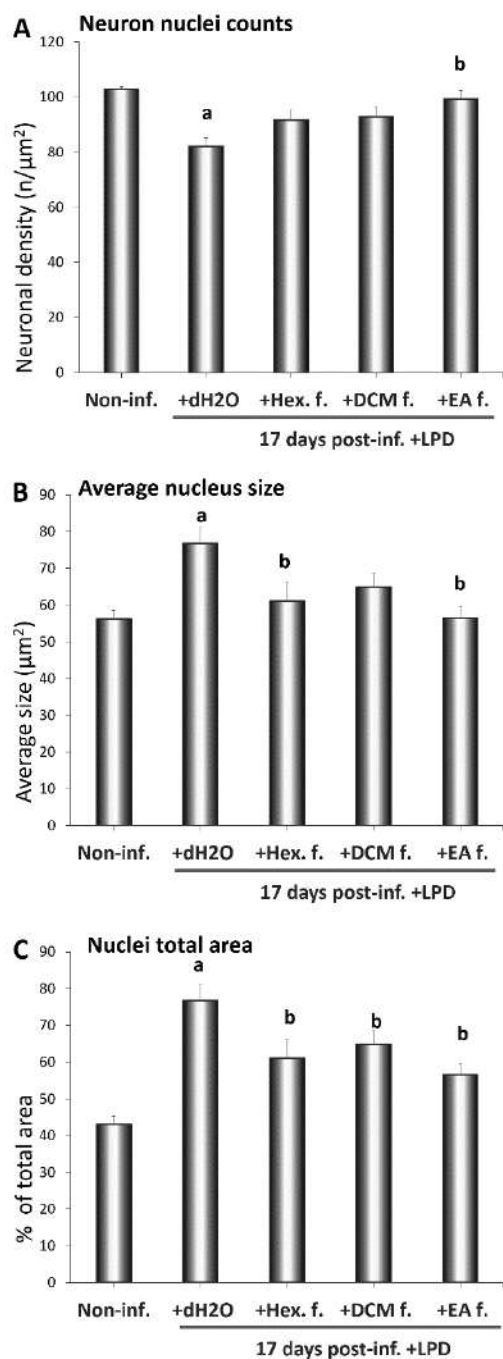


Figure 69. Lateral hypothalamic area of representative treated animals

Red arrow: loss of neuron nuclei enlargement. Green arrow: Prevention of neuron loss in the G kola-treated groups (D-E)

LPD-fed animals had significantly increased average nuclei size and nuclei total area in both the posterior parietal cortex (figures 73A-C) and the lateral hypothalamic area (figures 73D-F) (table XLIII). All these alterations were prevented or mitigated by treatments with *G. kola* extract, in particular ethyl acetate fraction (figures 73A, B, D, E and table XLVII).



ANOVA +LSD test, p < 0.05 vs.: a Non-infected b Inf. 17d+LPD c Hexane fraction d DCM fraction

Figure 70. Average counts in brain posterior areas of treated animals

Counts in the posterior parietal cortex (A-C) and lateral hypothalamic (perifornical) area (D-F).

Table XLVII. Cell count comparisons in the brain posterior areas

		Infected 17d		Inf.17d +LPD + <i>G. kola</i> fractions		
		+Chow	+LPD	Hex.	DCM	EthylAc.
Counts in the posterior parietal cortex						
Non-inf.	0.079	4.0E-6***		0.001**	0.001**	0.189
+Chow		0.001**		0.198	0.368	0.719
+LPD				0.106	0.138	0.018*
Hex.					0.834	0.148
DCM						0.176
Average size of neuron nuclei in the posterior parietal cortex						
Non-inf.	0.416	0.001**		0.217	0.067	0.951
+Chow		0.001**		0.574	0.196	0.595
+LPD				0.034*	0.199	0.031*
Hex.					0.418	0.323
DCM						0.098
% area of neuron nuclei in the posterior parietal cortex						
Non-inf.	0.871	0.028*		0.717	0.569	0.392
+Chow		0.017*		0.553	0.380	0.218
+LPD				0.028*	0.035*	0.020*
Hex.					0.793	0.578
DCM						0.734
Counts in the perifornical zone of the lateral hypothalamic area						
Non-inf.	0.616	0.028*		0.964	0.894	0.769
+Chow		0.034*		0.642	0.823	0.446
+LPD				0.011*	0.051	0.011*
Hex.					0.883	0.635
DCM						0.555
Average size of neuron nuclei in the perifornical zone of the lateral hypothalamic area						
Non-inf.	0.488	0.020*		0.011*	0.790	0.064
+Chow		0.026*		0.011*	0.402	0.076
+LPD				0.637	0.089	0.987
Hex.					0.064	0.773
DCM						0.052
% area of neuron nuclei in the perifornical zone of the lateral hypothalamic area						
Non-inf.	0.376	0.253		0.718	0.990	0.447
+Chow		0.457		0.209	0.480	0.091
+LPD				0.212	0.453	0.207
Hex.					0.746	0.658
DCM						0.240

3.3.8.3 Cerebellar areas: molecular layer and dentate nucleus

Untreated LPD-fed infected rats showed a marked decrease in neuronal density (figures 74B), unlike the groups treated with *G. kola* extracts tested where these alterations are lacking (figures 74C-E).

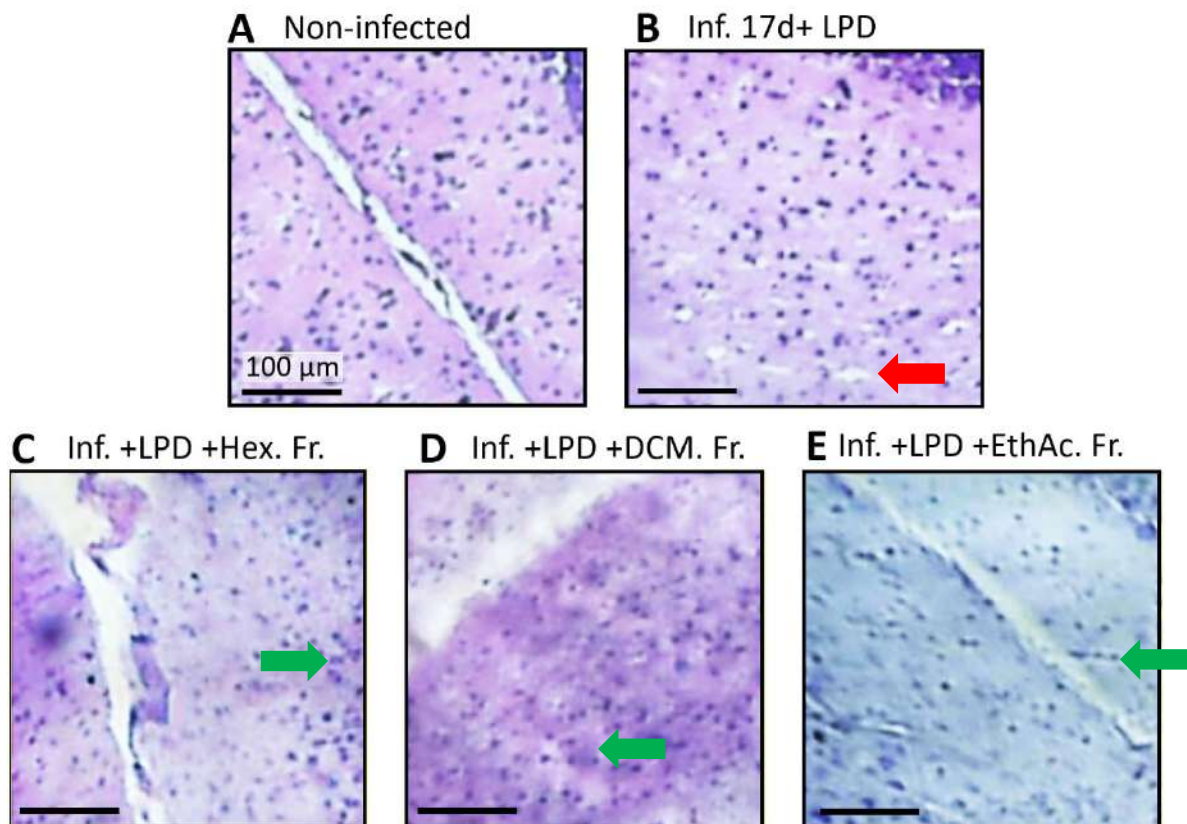


Figure 71. Molecular layer of cerebellar cortices of representative treated animals

Red arrow: neuronal loss induced by the infection (B) Green arrow: prevention by the treatments (G-I).

The alterations observed in untreated LPD-fed infected animals such as damaged nuclei were prevented or mitigated by all *G. kola* extracts tested (figures 75C-E).

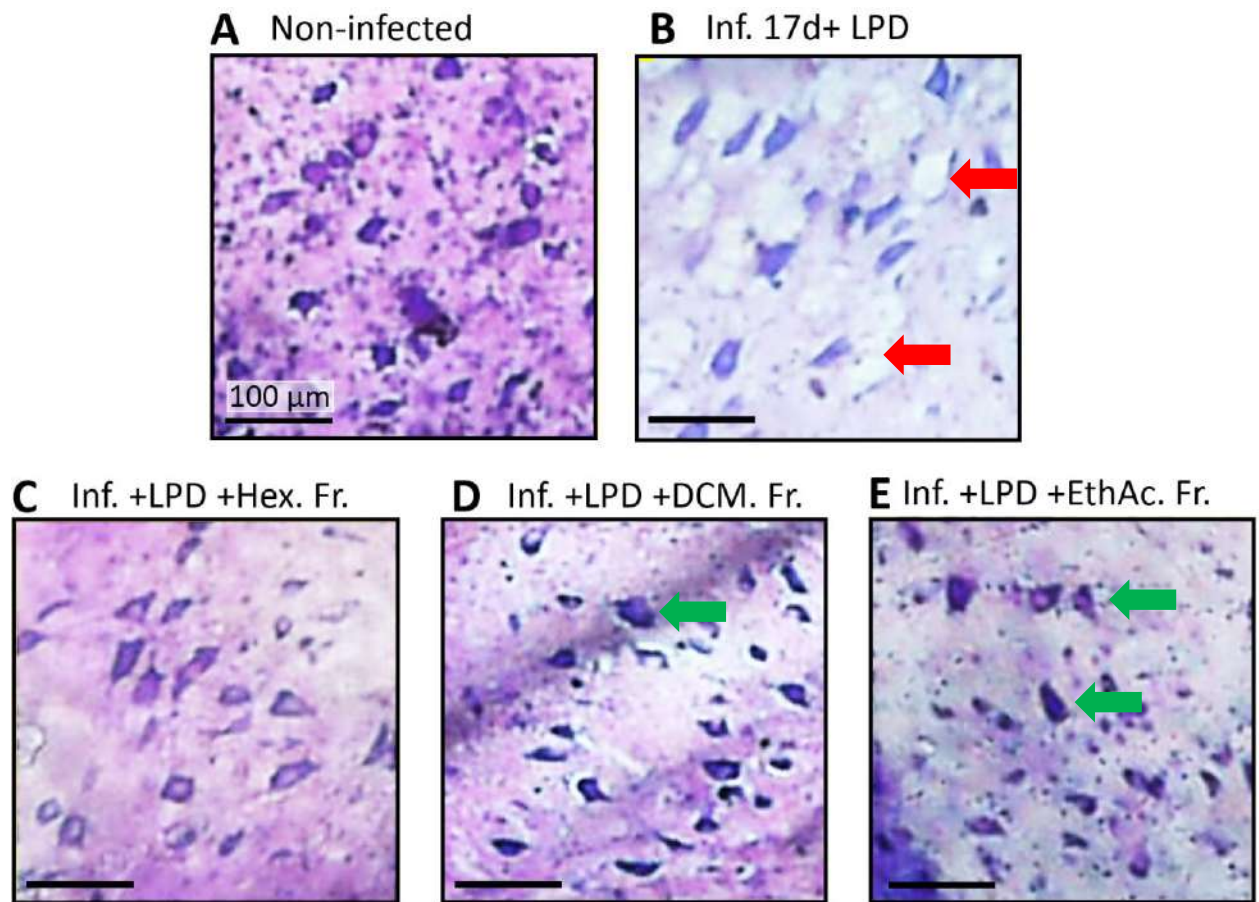


Figure 72. Micrographs of cerebellar dentate nuclei of representative animals

Red arrow: large neuron loss in LPD-fed (**B**). *Green arrow:* prevention in treated groups (**D-E**).

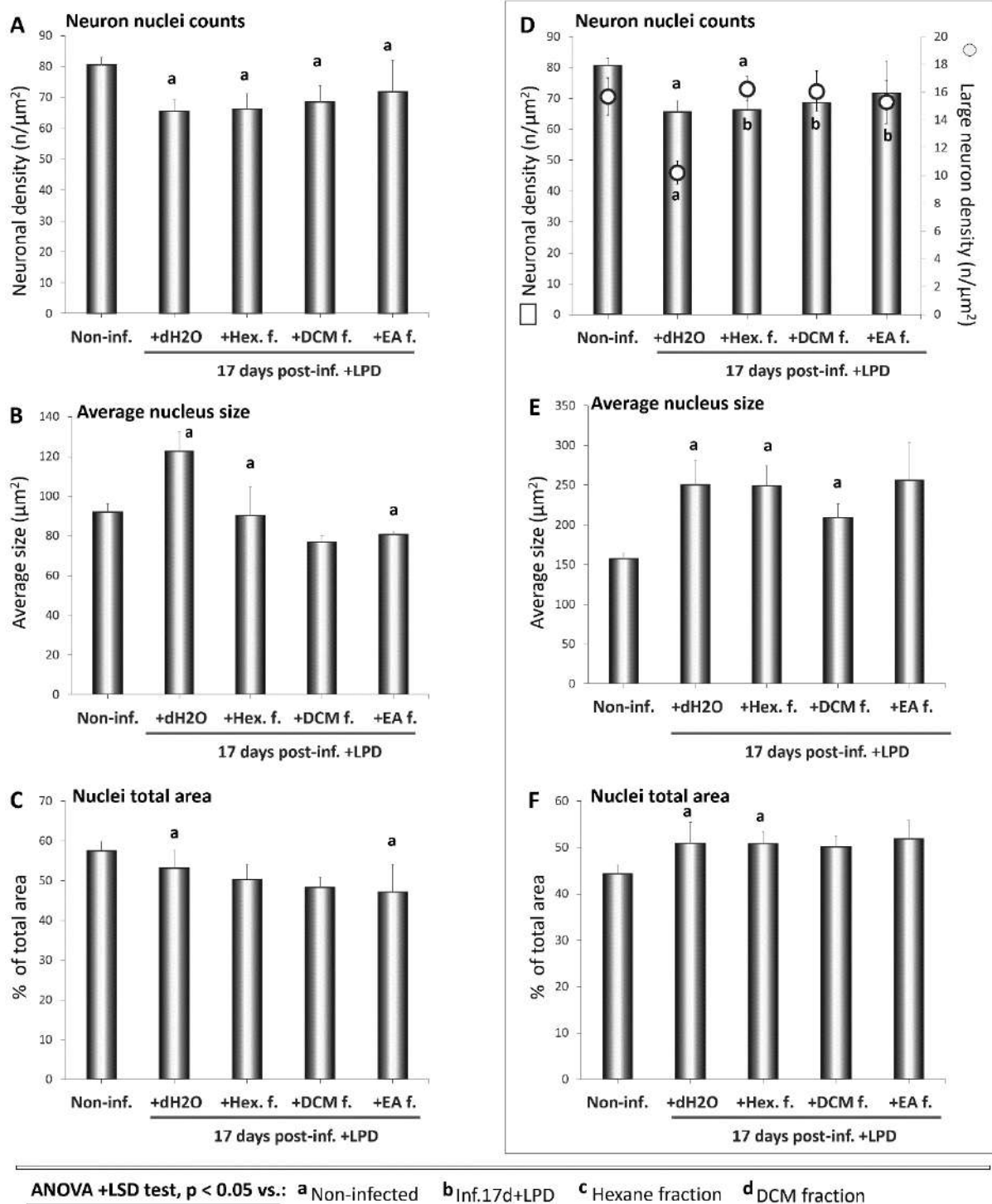


Figure 73. Average counts in cerebellar areas

Counts in the cerebellar molecular layer (A-C) and dentate nucleus (D-F).

Increases in the nuclei total area were observed in the dentate nucleus area of LPD-fed rats (figures 76C, F and table XLVIII). These alterations were prevented or mitigated by treatments with *G. kola* extract, in particular ethyl acetate fraction (figures 76A, B, D, E and table XLVIII).

Table XLVIII. Count comparisons in cerebellar areas of treated rats

Infected 17d		+LPD + <i>G. kola</i> fractions		
+Chow	+LPD	Hex.	DCM	EthylAc.
Counts in the molecular layer of the cerebellar cortex				
Non-inf.	0.305	0.007**	0.003**	0.025*
+Chow		0.001**	0.001**	0.016*
+LPD			0.923	0.742
Hex.				0.752
DCM				0.760
Average size of neuron nuclei in the molecular layer of the cerebellar cortex				
Non-inf.	0.074	0.037*	0.795	0.045*
+Chow		0.004**	0.213	0.378
+LPD			0.095	0.064
Hex.				0.088
DCM				0.501
% area of neuron nuclei in the molecular layer of the cerebellar cortex				
Non-inf.	0.870	0.325	0.110	0.043*
+Chow		0.225	0.051	0.010*
+LPD			0.632	0.458
Hex.				0.718
DCM				0.859
Counts of all neuronal nuclei in the cerebellar dentate nucleus				
Non-inf.	0.272	0.046*	0.031*	0.784
+Chow		0.012*	0.012*	0.341
+LPD			0.931	0.193
Hex.				0.138
DCM				0.268
Counts of large neurons in the cerebellar dentate nucleus				
Non-inf.	0.095	0.002**	0.765	0.890
+Chow		0.017*	0.022*	0.119
+LPD			8.4E-5***	0.003**
Hex.				0.926
DCM				0.728
Average size of neuron nuclei in the cerebellar dentate nucleus				
Non-inf.	0.066	4.5E-4***	2.2E-6***	0.002**
+Chow		0.004**	2.2E-4***	0.112
+LPD			0.978	0.285
Hex.				0.130
DCM				0.284
% area of neuron nuclei in the cerebellar dentate nucleus				
Non-inf.	0.006**	0.046*	0.033*	0.097
+Chow		0.949	0.901	0.742
+LPD			0.970	0.853
Hex.				0.850
DCM				0.689

3.3.9 Histopathological analysis

3.3.9.1 Brain

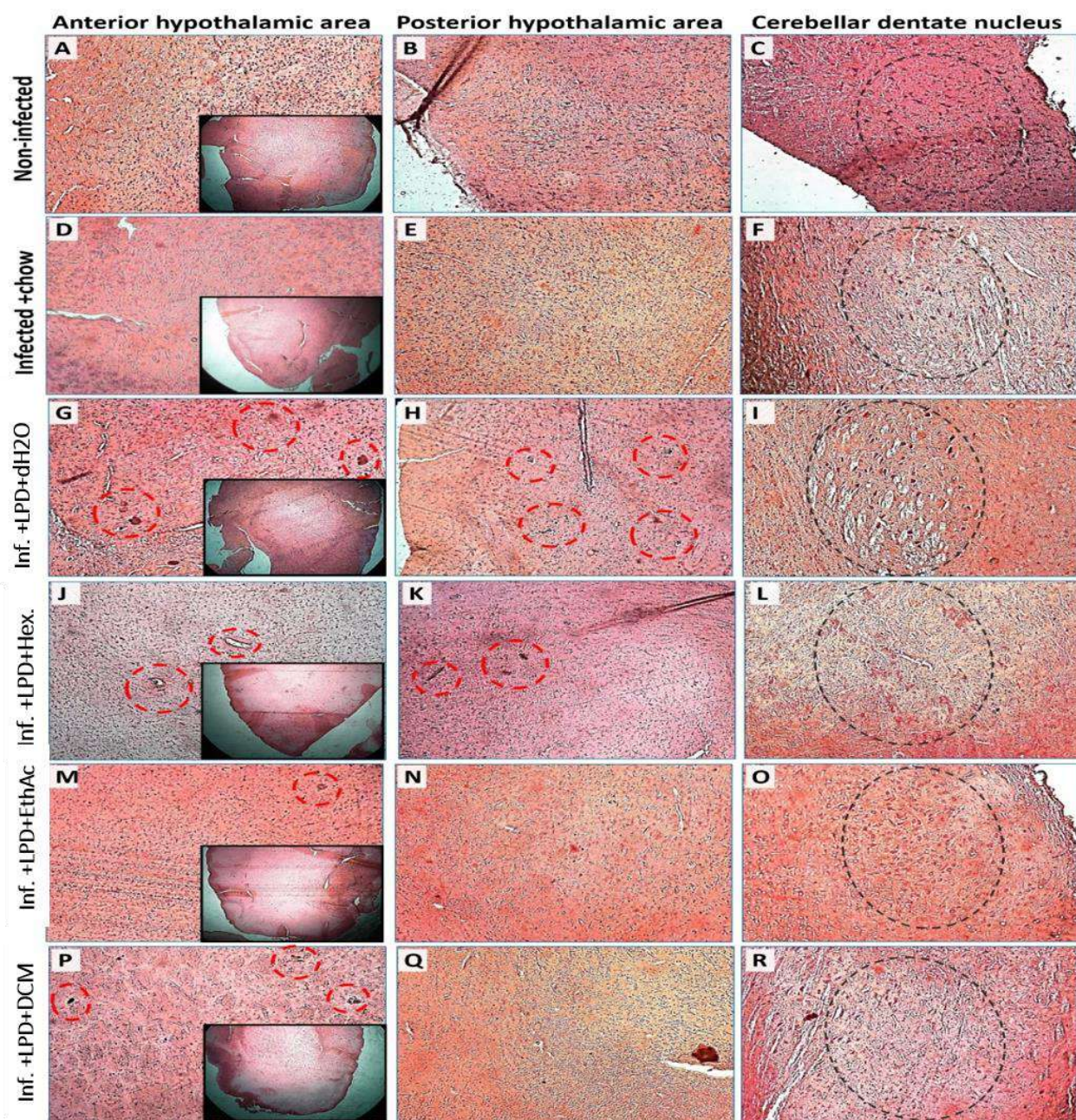


Figure 74. Micrographs of H&E stained brain sections.

Red circles: *T. gondii* infection-like lesions. **Black circles:** cerebellar dentate nucleus.

Magnification: x100. Note the prevention of neuronal loss in the treated groups.

Figure 53 presents micrographs of H&E stained brain sections in the anterior and posterior hypothalamic areas and in the cerebellar dentate nucleus of representative non-infected rat (figures 53A-C), untreated chow-fed infected rat (figures 53D-F), untreated LPD-fed infected rat (figures 53G-I) and *G kola*-treated rats (figures 53J-R). Unlike the non-infected animals (figures 53A-C), the untreated infected rats fed normal chow developed no neurotoxoplasmosis-like lesions in the anterior (figure 53D) and posterior (figure 53E) hypothalamic areas, and marked large neuron loss in the cerebellar dentate nucleus (figure

53F). While the untreated infected rats fed LPD developed neurotoxoplasmosis-like lesions in the anterior (figure 53G) and posterior (figure 53H) hypothalamic areas, and marked large neuron loss in the cerebellar dentate nucleus (figure 53I). The infected rats fed LPD treated with *G. kola* hexane or DCM fractions developed less-to-no neurotoxoplasmosis-like lesions in the anterior hypothalamic area (figures 53J, P) and the posterior hypothalamic area (figures 53K, Q), but with mitigation of large neuron loss in the cerebellar dentate nucleus (figure 53L, R). Interestingly, the infected rats fed LPD treated with ethyl acetate fraction developed few lesions in the anterior hypothalamic area (figure 53M) and no lesions in the posterior hypothalamic area (figure 53N), together with the prevention of large neuron loss in the cerebellar dentate nucleus, although large neuron shrinkage was observed (figure 63O).

3.3.9.2 Spleen and liver

Figure 54 presents micrographs of H&E-stained spleen sections of representative non-infected rat (figure 54A), untreated LPD-fed infected rat (figure 54B), and *G. kola*-treated rats (figures 54C-E). The non-infected rats presented with normal spleen tissue structures (figure 54A), unlike the untreated infected rats fed LPD which lost their spleen tissue structures, with not clearly differentiated white pulp (figure 54B). The latter animals also presented with *T. gondii* tissue cysts in the spleen (figure 54B). While white pulp was still poorly defined in LPD-fed infected animals treated with *G. kola* hexane fraction (figure 54C), almost normal spleen tissue structures were observed in their counterparts treated with ethyl acetate and DCM fractions (figures 54D, E). Cysts were not observed in animals treated with *G. kola* extracts.

Figure 55 presents micrographs of H&E stained liver sections of representative non-infected rat (figure 55A), untreated LPD-fed infected rat (figure 55B), and *G. kola*-treated rats (figures 55C-E). Unlike non-infected animals (figure 55A), untreated LPD-fed infected animals presented with *T. gondii* tissue cysts in the liver (figure 55B). These insults were not present in infected groups treated with *G. kola* (figures 55C-E).

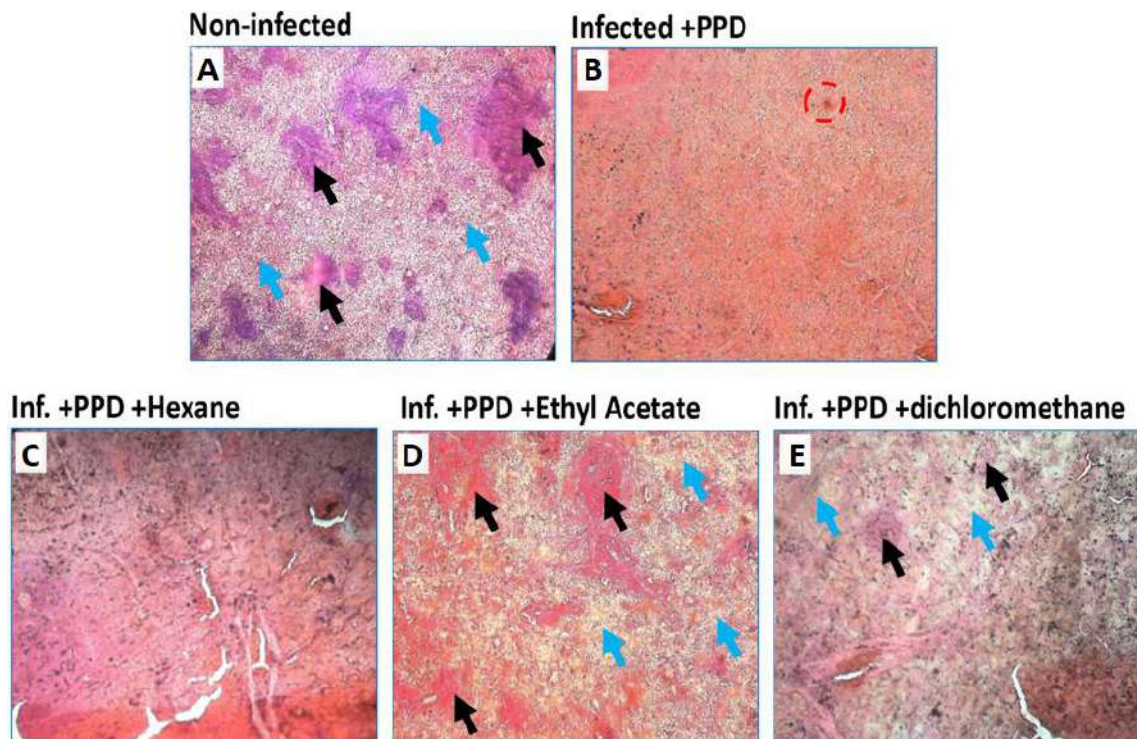


Figure 75. Micrographs of H&E stained spleen sections

Note the structure loss (black arrows: red pulp, and blue arrows: white pulp) and the tissue cysts (red circles).

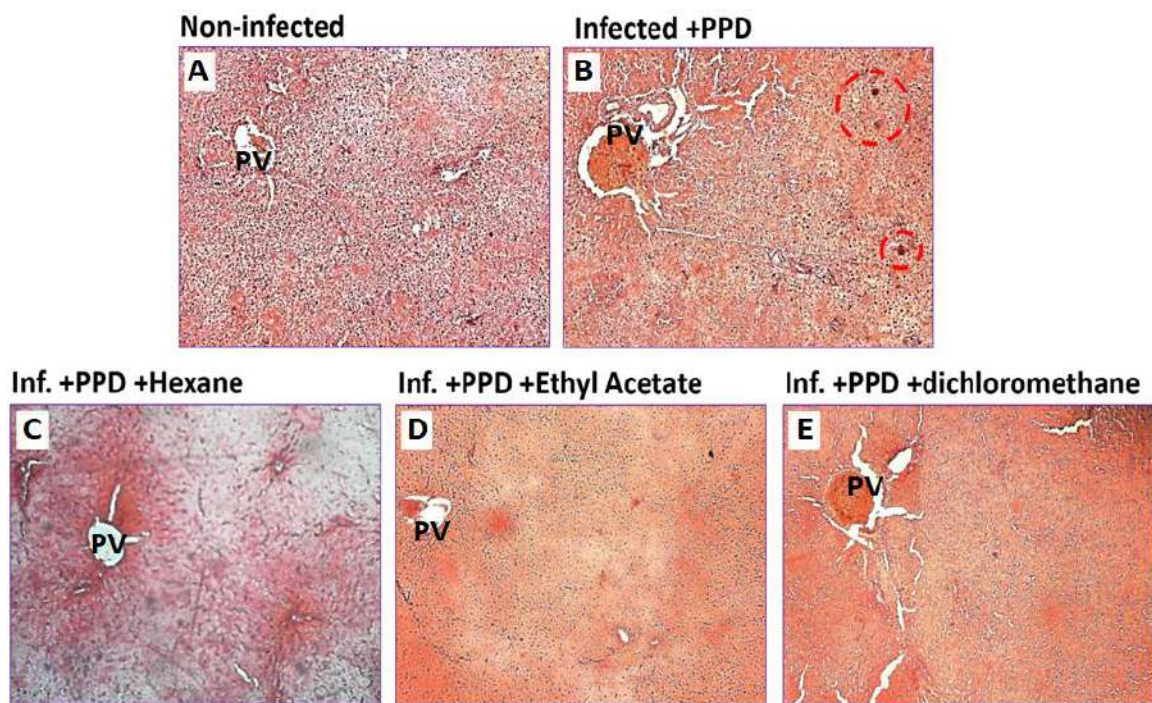


Figure 76. Micrographs of H&E stained liver sections

Note the tissue cysts in the untreated animal (red circles) (**B**) and their absence in the groups treated with *G. kola* (**C-E**). **PV:** portal vein.

3.3.10 Summary of *G. kola* potential therapeutic activities in neurotoxoplasmosis

Figure 77 summarizes the deleterious effects of *T. gondii* infection. Overall, *T. gondii* infection damaged tissues of the untreated LPD-fed infected rats but this negative impact was corrected by treating these infected rats with the different fractions of *G. kola* tested (figure 77).

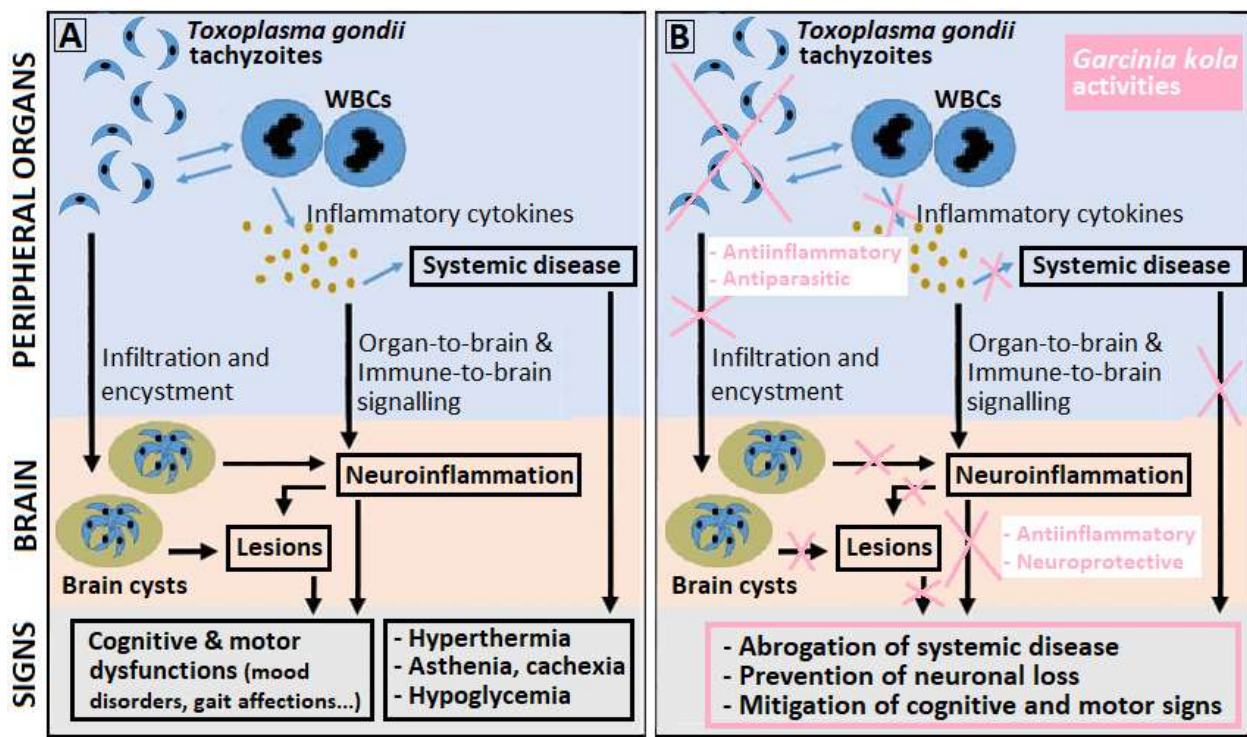


Figure 77. *Garcinia kola* therapeutic potential against neurotoxoplasmosis

A. Signs of systemic and brain disease observed in rats after infection with *Toxoplasma gondii* in this work and some driving factors hinted by the findings. **B.** Effects of *Garcinia kola* on brain and systemic disease signs observed in this work and mechanistic bases suggested by the findings.

CHAPTER IV: DISCUSSION

4.1 Chronic *T. gondii* infection in immune-competent rats

The results of our studies show marked alterations in physiological parameters and in indicators of cognitive and motor functions in late-stage *T. gondii*-infected rats compared to non-infected rats.

4.1.1 Physiological parameters

T. gondii-infected rats showed increases in body weight up to 67 dpi, although their growth was slower than that of their non-infected counterparts. Then, increasingly marked losses in body weight were observed up to 90 dpi when the animals were sacrificed. Such alterations were expected, considering that cachexia and other components of infection-associated wasting syndrome are normal signs of late-stage toxoplasmosis (248, 249). The cause of late occurrence of weight loss and other disease signs in immunocompetent laboratory animals, including neuropsychological signs, is controversial. Although these alterations are commonly attributed to systemic inflammation and reactive neuroinflammation triggered by the burden of latent tissue cysts (51, 52), a growing number of reports indicate a potential impact of environmental factors, particularly those affecting the immune system function such as hygiene and diet (250, 251). Cachexia, increased protein turnover and systemic inflammation, altered glucose metabolism is a key component of wasting syndrome (252, 253), the significantly lower blood glucose levels observed in infected rats in this series studies further support its occurrence at the late stage of *T. gondii* infection-mediated disease. Spleen mass loss also observed in infected rats in this series of studies may result from inflammatory processes, thus also indicate wasting syndrome. Small spleen is typically observed in symptomatic patients of chronic diseases with severe splenomegaly such as sickle cell disease and results from detrimental inflammatory processes in the spleen (254, 255).

4.1.2 Motor function indicators

Infected animals displayed alterations in all the motor function indicators assessed including the distances covered in the OFT arena and the EPM maze, and in gait indicators obtained using footprint analysis. Gait alterations were indicated by the tendency of the *T. gondii*-infected rats seemed to use their anterior footpads more and their heels less, particularly at the front limbs, unlike the non-infected rats. Footprint analysis is an established quantitative functional assay for the early detection of neurologic deficits (256). In our series studies, compared to non-infected rats, the infected rats also presented with significant decreases in stride and step lengths, indicating neurologic deficits (257). Stride and step length reductions are commonly observed in neurodegenerative diseases like Parkinson's disease, Huntington's disease, and their murine models (257, 258). In addition, as expected considering the stride length decrease, the speed in the EPM maze was significantly decreased in the infected rats.

Interestingly, infected rats also displayed significant decreases in the number of episodes of locomotion, in the distance covered, and in the total time spent walking in the OFT arena., as well as in the distance covered in the EPM maze. This decrease in locomotory activity can be partly explained by typical disease-related asthenia (52), but it may also suggest a decrease in rodent drive to explore novel environments termed as exploration behaviour, which would indicate anxiety-like cognitive disorders (31, 52). Furthermore, we observed decreases in the time spent active in the first minute but only in a lesser extent in the last minute, together with a decrease in the rat speed in the maze in the first minute less marked in the last minute. These observations, in particular the alterations in the first minute exploration support a decrease in the drive to explore the novel environment, hence cognitive impairment (259). In the EPM paradigm, due to their natural drive to explore novel environments, rodents tend to explore the maze faster and longer in the first minute than in the last minute, where their interest is decreased (259, 260). This may explain the less marked differences in the last minute between the infected and the non-infected rats.

4.1.3 Cognitive function indicators

Ethological tests evaluate the complex cognitive responses of laboratory animals exposed to opposing influences, such as the natural drive of rodents to explore novel environments (novelty), equivalent to sensation seeking in humans (261), and an environmental stressor such as: (i) fear to enter the central area in the open field test (OFT), based on open space anxiety (agoraphobia), a strong behavioural trait in rats and mice (262); or (ii) both height and open space for the open arms of the elevated plus maze in the EPM paradigm, exploiting rodent agoraphobia and their natural fear for heights (acrophobia) (262, 263). Healthy animals are expected to give in to their natural drive to explore in the first couple of minutes of the test, before being coerced by anxiety to avoid the stressful areas and limit their exploration to safe areas such as areas close to walls in the OFT arena or closed arms in the EPM maze (escape/avoidance responses) (260, 264). In this series of studies, unlike non-infected animals, the infected rats had a significantly higher latency time to enter the OFT arena centre and latency time to the first exploration of EPM maze open arms, suggesting a weakening of their natural drive to explore novel environments (261, 264). Also supporting this finding, the infected rats had less entries and spent less time in the EPM open arms, and most did not explore the bottom of the open arms or enter the central area of the OFT arena. Conversely, the infected animals displayed significant increases in the time spent in areas closed to walls in the arena and in the bottom of the EPM closed arms, suggesting increases in the avoidance of stressful area and in the tendency to stay close to safe walls (thigmotaxis) (31, 52). Moreover, infected rats displayed significant reductions in the distance covered in the area close to the

walls in the OFT arena, but instead, spent markedly more time in stretched-attend posture in the arena angles, an avoidance response further suggesting an increase in rat anxiety (265, 266).

On the other hand, compared to the non-infected, the infected rats showed marked decreases in the activities around the EPM central platform, a component of risk assessment and aversive state escape responses which indicate the natural hesitation of animals when choosing the arm to explore in their attempt to avoid stressors (267, 268). Such alterations included the significantly lower number of entries in the central platform of the maze and the drastic decrease in episodes of stretched-attend posture at closed arm entrance showed by the infected animals. Moreover, the infected rats had significantly lower episode numbers and spent less time in head dipping posture, in addition to a higher latency and a markedly small number of episodes of rearing on hindlimbs (sniffing) and against walls. Head dipping and sniffing behaviours are major indicators of rodent risk assessment abilities in the EPM (269, 270), and reduced rearing in a novel environment is an indicator of increased neophobia and a prodromal indicator of cognitive disorders (271). Thus, altogether these findings strongly suggest cognitive impairment, in particular, poor risk assessment and aversive state escape responses in *T. gondii*-infected rats at the late stage of the infection. Comparable observations were reported and it was proposed that the parasite would induce this behaviour, for instance through neuroinflammatory processes leading to the modulation of host glutamate and dopamine neurotransmission, to facilitate host predation and its dissemination to other hosts (17, 22, 52).

Moreover, in this series of studies, compared to the non-infected, the infected rats displayed significant decreases in both paw licking (rostral/cephalic grooming) and grooming (complex grooming sequences) episode numbers in the OFT arena, although with a high interindividual variability. This is surprising, considering that in presence of mild stressors rats reportedly express concomitant decreases in episodes of complex grooming sequences and increases in cephalic grooming episodes (272, 273). To our knowledge, this is the first report of such atypical alteration. Future studies addressing the neurobiological basis of this alteration may improve our understanding of the pathophysiology of neurotoxoplasmosis, in particular mood and other neuropsychiatric alterations (92, 274).

4.2 Abilities of diet and ovariectomy to accelerate the infection course

The results of this series of studies support the ability of low-protein diet to accelerate *T. gondii* infection course in rats to an extent comparable to late-stage infection.

4.2.1 Physiological parameters

The results of this study show significant changes in the physiological parameters and in the indicators of cognitive and motor functions in *T. gondii* infected rats compared to non-infected rat group. The *T. gondii*-infected rats fed on HFD displayed an increase in their body weight from day one to day 17 (end of experimentation) and had a straight line growth curve similar to that of the non-infected rat group this may be due to the fact that a diet rich in fats leads to weight gain hence delaying the weight loss caused by the infection caused by the parasite in its early stage (78, 79). While the infected and the ovariectomized rats group compared to the non-infected rat group lost weight as from fourth day which continued till the end of the experimentation period in a progressive manner while the infected rats group fed on LPD had a negative point of inflection at day seven and this weight lost drastically continued till the end of the experimentation period. The increase in weight lost, increased body temperature and decrease in the blood glucose level in the rats fed on LPD, which was comparable to long-term infected rats, can be a clear indication of the degree of pathogenicity of the *T. gondii* infection leading to a severe form of sustained cachexia responsible for weight loss hence leading to a drop in the blood glucose level (248, 249, 252, 253). The 17 days infected rats group fed normal chow and those fed on LPD and those infected for 90 days all produced more faecal boli compared to the non-infected rat group which is an indicative of increased anxiety and emotionality (54). The significant spleen weight loss observed in the infected rats, in particular those fed on LPD, compared to the non-infected can be due to the detrimental inflammatory processes associated with the systemic disease caused by chronic *T. gondii* infection (254, 255).

4.2.2 Cognitive and motor function indicators

In this series of studies, the gait indicators obtained using footprint analysis were altered, with the tendency of the *T. gondii*-infected rats to use their anterior footpads more and their heels less, particularly at the front limbs, unlike the non-infected rats. Moreover, compared to non-infected rats, the infected rats fed on LPD also presented with significant decreases in stride and step lengths, alike long-term infected rats, and indicating neurologic deficits (257). In addition, overall, as long-term infected animals, LPD-fed infected animals displayed alterations in all the motor function indicators and were reluctant to explore novel environment which is typical of anxiety behaviours (260, 264), both on the OFT arena and the EPM maze. More specifically, as long-term infected animals, LPD-fed infected animals displayed: (i) a decrease in total distance covered in the maze concomitantly with decreased explorations of arms, which suggest that the infected rats were not willing to explore their novel environment, possibly due to anxiety (260, 264). (ii) an increased latency of rearing episodes in response to novelty, which is considered as an early readout for neurodegenerative and cognitive disorders

(266); (iii) a higher head dipping latency, and lower head dipping number and time, which all put together are an indicator of anxiety (269, 270); (iv) a decrease in angle entries and increase in angle time that are indicative of the reluctance to exploration (267, 268); (v) a significantly increased latency of rearing episodes in the EPM and lower number of episodes of rearing on hindlimbs in the OFT, possibly indicating that they are more sensitive to acute stress which is reduced under more adverse testing conditions (269, 270); and (vi) a significantly lower latency to the first grooming episode at least partly due to *T. gondii*-mediated increase in emotional distress caused by the unfamiliar and aversive environment they were subjected to (272, 273). The occurrence of brain functional alterations alike to late-stage infection in early-stage infected animals fed on LPD suggest that environmental factors, in particular diet, may contribute to the acceleration of brain and systemic infection in immunocompetent subjects even before the persistence of tissue cysts and subsequent activation of immune response in the host brains, which was thought to be the main cause of functional alterations in the late-stage of *T. gondii* infection in rodents (34, 46) and in patients (19, 20). Thus, different mechanisms to be unravelled may drive the behavioural alterations observed here in the early stage of the disease, despite common clinical signs. Notably, also in this study, infected female rats had better cognitive and motor abilities in the OFT and to the EPM tests than their male counterparts, possibly due to the fact that male rats are reportedly more vulnerable to immunological alterations than females (275, 276). Thus, early-stage infected male rats fed LPD may constitute a good model for complications of late-stage *T. gondii* infection, particularly neurotoxoplasmosis.

4.2.3 Parasite and WBC count in the blood

Cyst, tachyzoite, and WBC counting in the blood revealed interesting information that may contribute to understanding at least the *T. gondii*-associated systemic disease in infected rats in this study. Notably, terminal-stage infected animals had the lowest cyst count and the highest tachyzoite count of all infected groups, while their WBC counts were almost normal, suggesting that tachyzoites were multiplying freely in the blood without the immune response pressure that could have forced them to encyst (15, 16). Such an occurrence could be explained by tachyzoite ability to escape the immune response as various protozoan blood form thanks to their variant surface glycoproteins (VSG) (277, 278), or did not need to hide as hosts were not able anymore to mount efficient immune responses as observed in immune deficiency cases (5-7). However, although both scenarios are not self-excluding, the results in early-stage infected animals strongly indicate that the latter is probably more likely to explain this occurrence. Notably, the early-stage infection control group (untreated early-stage chow-fed rats) had the highest cyst count, the lowest tachyzoite count, and the highest WBC count of all

untreated animals. This could have been expected as in the early stage of the infection animals were still able to mount an efficient immune response that forced tachyzoites to encyst (15, 16). In addition, HFD-fed infected animals still had high WBC and cyst counts with low tachyzoite counts compared to terminal-stage animals, suggestive of an efficient immune response (15, 16). Instead, LPD-fed and, to a lesser extent ovariectomised infected animals, presented with significantly decreased cyst counts and increased tachyzoite counts, but not very high WBC counts compared to the early-stage infection control group, suggesting poor immune responses. The well-established abilities of both undernutrition in proteins (25, 26) and menopause (29, 30) to cause serious immune function disturbances can explain these findings. Interestingly, treatment with ethyl acetate fraction, and to a lesser extent, with DCM fraction, decreased the tachyzoite counts compared to both the early-stage infection control group and the late-stage infected animals, and the cyst counts compared to the early-stage infection control group, indicating an anti-*Toxoplasma* activity against both tachyzoites and encysted forms. This result is particularly interesting as to date, no commercially available drug can eradicate *T. gondii* cysts efficiently (175, 177).

4.2.4 Brain neuronal density

The observation of Nissl-stained brain sections in the anterior, posterior, and cerebellar areas critical for cognitive and motor responses revealed the enlargement of neuron nuclei in various areas in LPD-fed infected animals, but also in the other early-stage infected groups, although to a lesser extent, while marked neuronal losses were mostly observed in LPD-fed infected animals and in terminal-stage infected animals. The areas assessed included: (i) the anterior cingulate cortex that is involved in action, emotion, and memory, with a cardinal role in the control the expression of contextual fear generalization (279, 280); (ii) the medial septal nucleus that is critical for learning and memory and which prevented sepsis-induced cognitive deficits in mice (281, 282); (iii) the posterior parietal cortex, which is an associative region comprising the primary somatosensory areas (283); (iv) the perifornical zone of the lateral hypothalamic area, which is critical for various physiological functions, including the promotion and stabilization of active-arousal and drive to eating (284, 285); (v) the cerebellar molecular layer which contains interneurons that are key elements of cerebellar network computation and behaviour (286); and (vi) the cerebellar dentate nucleus whose neuron loss account for cerebellar symptoms in various neurodegenerative disorders (287, 288). Counts of neurons confirmed these observations, with significant neuronal losses in all the areas considered in the terminal-stage infected animals, and to a lesser extent, in LPD-fed infected animals. This finding suggests that the acceleration of neurotoxoplasmosis observed in LPD-fed infected animals emerged from early neuronal loss in brain areas critical for cognitive and

motor responses as for terminal-stage infected animals. The assessment of average nucleus size and of nuclei total area revealed enlarged neurons in all early-stage infected groups and for most of the areas assessed, although particularly marked in LPD-fed infected animals. Previous studies support that neurons can alter their characteristics, including increase their nucleus size, as a response to a neurodegenerative disease in an attempt to compensate for loss of function, but such changes increase the risk of neuron's early death (289-291). Thus, it appears that neurons of *T. gondii* infected animals, in particular LPD-fed ones, would increase their size to compensate for a loss of function, whose cause is to be unravelled.

4.3 Phytochemical screening and therapeutic potential of *G. kola*

4.3.1 Phytochemical screening of the extracts tested

The qualitative phytochemical screening of the hexane, DCM and ethyl acetate fractions of *G. kola* seed had in common alkaloids, phenolic compounds and terpenoids. The ethyl acetate fraction of *G. kola* was found to contain catechic tannins which were not found in the hexane and DCM fractions. Notably, the quantitative analysis revealed the highest concentration of phenolic compounds and tannins in the ethyl acetate fraction, and of flavonoids in the hexane fraction, which was expected considering that ethyl acetate solvent has the highest polarity followed by DCM and then hexane (292, 293). These findings are comparable to previously reported phytochemical screenings of *G. kola* methanolic extract and its fractions (31, 294). Interestingly, many flavonoids with beneficial effects were previously isolated from the ethyl acetate fraction of *G. kola* methanolic extract, including kolaviron, a biflavonoid complex with reported neuroprotective, anti-inflammatory, anti-parasitic, and anti-oxidative activities (33, 215, 216). In addition, β -lactam compounds were also reported among the most common functional phytoconstituents of *G. kola* seed ethyl acetate fraction, including N,N-dimethylethanamine (31), a close molecular relative to dimethylethanamine (DMEA), an established cholinergic antidepressive agent with therapeutic potential against dyskinesia, dementia, and epilepsy (295, 296). Moreover, in addition to their well-established antimicrobial activities, some β -lactam compounds were reported neuroprotective and anti-inflammatory activities (297, 298), which probably contributed to the antiparasitic and neuroprotective activities of fractions of *G. kola* seed extracts observed in this study. Future studies performing more advanced fractionation of *G. kola* ethyl acetate fraction such as GC-MS or HPLC-MS chromatography may reveal phytocomponents with strong therapeutic potentials against both *T. gondii*-associated systemic disease and neurotoxoplasmosis.

4.3.2 Effects of extracts on physiological parameters and gait

While the untreated LPD-fed early-stage infected animals presented with a markedly lower body weight at sacrifice and a higher body temperature compared to non-treated animals, all the LPD-fed infected animals treated with *G. kola* extracts did not show any of these alterations. Notably, animals treated with *G. kola* ethyl acetate fraction in particular had values comparable to those of the non-infected animals for most of these physiological parameters. These observations suggest that treatment with *G. kola* extracts, and particularly ethyl acetate fraction, mitigated the progression of *T. gondii*-induced systemic disease, which encompasses a severe cachexia and a sustained fever (248, 253). In addition, other signs displayed by the untreated LPD-fed infected animals were prevented or mitigated in their counterparts treated with ethyl acetate fraction and, to a lesser extent, DCM fraction, including: (i) decreases in stride length, step length and step width, which are major indicator of neurologic deficits (257); (ii) the increase in faecal boli production observed in the untreated group may indicate the prevention of cognitive alterations, in particular mood disorders such as increased anxiety (54); (iii) increases in spleen and kidney weights indicating that *G. kola* extract may have prevented the detrimental inflammatory processes at the levels of these organs that drive the systemic disease associated with active *T. gondii* infection (254, 255). However, the blood glucose levels of LPD-fed infected animals remained low irrespective of the *G. kola* extracts administered. This could be partly explained by the well-established potent hypoglycaemic properties of *G. kola* (31, 215, 216).

4.3.3 Effects of extracts on cognitive and motor indicators

Untreated LPD-fed infected animals displayed decreases in the total distance covered and in the time spent exploring the OFT arena and EPM maze novel environments compared to non-infected animals, which may partly result from asthenia associated with the systemic disease (249, 253), but which are also typical signs of functional cognitive disorders, and particularly anxiety (260, 264). In addition, decreases were observed in the number of visits to the OFT arena central area and in numbers of head-dipping episodes and open arm entries in the EPM, other major indicators of anxiety (269, 270). In addition, the occurrence of a significantly lower latency to the first grooming episode in the untreated infected animals may indicate the infection also induced other mood disorders, notably, depression (272, 273). The ability of ethyl acetate fraction and, to a lesser extent, DCM fraction to prevent or delay the development of all these signs in LPD-fed infected animals in this study strongly suggest these *G. kola* extracts have potent anti-*Toxoplasma* activities with a good therapeutic potential against neurotoxoplasmosis-associated functional cognitive disorders. These activities may be explained by the previously reported potent neuroprotective activities (31-33) and antiprotozoal activities against the apicomplexans of *Plasmodium* species (34) of *G. kola* ethyl

acetate extract. Notably, other antimalarial agents were reported activities against all forms of *T. gondii* *in vitro* and trophozoites *in vivo*, including lumefantrine (174) and artemisinin derivatives artemether, artesunate, and dihydroartemisinin (189, 190), and extracts of various medicinal plants with potent activities against *P. falciparum* (202).

4.3.4 Effects of extracts on brain, spleen and liver tissues

H&E-stained cerebella observation revealed marked losses of large neurons in the dentate nucleus that confirmed the observations and counts in Nissl-stained cerebellar sections. As expected, considering the stage (17-19), the early-stage infection control group presented with a few typical neurotoxoplasmosis lesions in the anterior and posterior hypothalamic areas. These lesions, which were not observed in groups treated with *G. kola* ethyl acetate and DCM fractions, were not sufficient to explain the massive neuron loss in LPD-fed animals as proposed for terminal-stage infected animals that have numerous large persistent tissue cysts in various areas of the brain (20-22). Interestingly, although LPD-fed infected rats treated with ethyl acetate fraction did not lose large neurons in the dentate nucleus like their untreated counterparts, surviving large neuron shrinkage was observed, further supporting the presence of a physiological stress potentially causing a loss of function in early-stage LPD-fed infected rats. This early in the disease, physiological stress in the brain tissue may be due to immune-to-brain signalling as the systemic disease is strong in the week following *T. gondii* infection (15, 16). Moreover, the observation of H&E-stained spleen and liver sections from LPD-fed early-stage infected animals revealed tissue structure losses, particularly in the spleen, which support the occurrence of a severe systemic disease (254, 255). Altogether, our findings suggest that environmental factors, in particular a low-protein diet, may accelerate the systemic disease course and the development of neurotoxoplasmosis through a mechanism not-yet determined, but which as hinted by the results of this series of studies, could be a strong neuroinflammation triggered by a detrimental immune-to-brain signalling.

CHAPTER V: CONCLUSION AND PERSPECTIVES

5.1 Conclusion

The general objective of this work was to contribute to the understanding of the pathophysiology-pathogenesis of neurotoxoplasmosis and therapeutic properties of a plant extract. Three specific objectives were devised. Firstly, we aimed at evaluating the cognitive disorders associated with chronic *T. gondii* infection in the immune-competent and non-susceptible Wistar rat strain. The infection progressed with animals seemingly almost normal up to dpi 67 where cachexia was exacerbated and infection terminal stage was observed around dpi 90. Here severe disease signs and cognitive and motor alterations were observed.

Secondly, we aimed at assessing the abilities of LPD, HFD, and ovariectomy to accelerate the course of *T. gondii* infection in Wistar rats. LPD feeding induced alterations in physiological and cognitive indicators in *T. gondii*-infected rats alike to terminal stage infected animals as early as dpi 17 particularly marked in male rats, suggesting that undernutrition can lead to the development of active toxoplasmosis in non-susceptible immunocompetent animals. Histopathological analysis revealed alterations typical toxoplasmosis lesions in the brain and cell loss, tissue cysts in the liver, and structure loss in the spleen. Analysis of Nissl-stained brain sections and neuron counts revealed that while neuronal loss was common between the two, terminal stage neurons were dying keeping their normal size while the neurons of LPD-fed animals were markedly enlarged, indicating that they died during an attempt to cope with functional loss associated with the acceleration of the infection.

Thirdly, we aimed at performing the phytochemical study alongside assessing the therapeutic potential of *G. kola* extracts in *T. gondii*-infected rats fed LPD. *G. kola* ethyl acetate fraction, and to a lesser extent DCM fraction, showed potent beneficial effects by reversing or preventing physiological, motor, and cognitive alterations in LPD-fed *T. gondii* infected rats. These effects were at least partly mediated through its compounds with established neuroprotective and parasiticidal effects such as the flavonoid kolaviron. Treatment with *G. kola* ethyl acetate fraction prevented neuronal loss and mitigated neuron enlargement, while decreasing markedly the blood load in *T. gondii* tachyzoites and cysts. Hence, at the end of our work, we report that LPD-fed *T. gondii* infected rats is a potential experimental model for neurotoxoplasmosis requiring a short time for disease induction, and *G. kola* ethyl acetate fraction as a potential therapeutic agent against *T. gondii*-induced systemic or brain diseases.

5.2 Perspectives

Studies should further characterize and address the neurobiological basis of LPD-induced acceleration of infection course, considering the potential to improve our understanding of the pathophysiology of neurotoxoplasmosis and to improve our strategies aimed at decreasing the incidence of *T. gondii* infections.

More studies performing more advanced fractionation of *G. kola* ethyl acetate fraction such as GC-MS or HPLC-MS chromatography may reveal phytocomponents with strong therapeutic potentials against both *T. gondii*-associated systemic disease and neurotoxoplasmosis.

Studies aimed at developing anti-toxoplasma therapeutics from *G. kola* should be performed using the aqueous extraction of *Garcinia kola* seeds, considering the possibility to decrease an eventual toxicity, as compared to organic solvents used in the present study.

REFERENCES

1. Nadia NAC, Nino LG, Cédric Y, Raoul SNS, Christian NO, Esther DD, et al. Seroprevalence of Toxoplasma gondii IgG and IgM antibodies and associated risk factors among pregnant women consulted in three health centers in Dschang, Cameroon. *Parasite Epidemiol Control.* 2023;22:e00306.
2. Fang EE, Nyasa RB, Ndi EM, Zofou D, Kwenti TE, Lepezeu EP, et al. Investigating the risk factors for seroprevalence and the correlation between CD4+ T-cell count and humoral antibody responses to Toxoplasma gondii infection amongst HIV patients in the Bamenda Health District, Cameroon. *PloS one.* 2021;16(12):e0256947.
3. Attias M, Teixeira DE, Benchimol M, Vommaro RC, Crepaldi PH, De Souza W. The life-cycle of Toxoplasma gondii reviewed using animations. *Parasites & vectors.* 2020;13(1):588.
4. Dos Santos Silva AC, de Barros LD, Barros VMC, de Alcântara AM, Andrade MR, Garcia JL, et al. Occurrence of Atypical and New Genotypes of Toxoplasma Gondii in Free-Range Chickens Intended for Human Consumption in Brazil. *Acta parasitologica.* 2020;65(3):774-8.
5. Khalili Pour E, Riazi-Esfahani H, Ebrahimiadib N, Esteghamati VZ, Zarei M. Acquired Immunodeficiency Syndrome Presented as Atypical Ocular Toxoplasmosis. Case reports in ophthalmological medicine. 2021;2021:5512408.
6. da Cruz AB, Maia MM, Pereira IS, Taniwaki NN, Namiyama GM, Telles JPM, et al. Human extracellular vesicles and correlation with two clinical forms of toxoplasmosis. *PloS one.* 2020;15(3):e0229602.
7. Beder D, Esenkaya Taşbent F. General Features and Laboratory Diagnosis of Toxoplasma gondii Infection. *Turkiye parazitoloji dergisi.* 2020;44(2):94-101.
8. Lau A, Jain MK, Chow JY, Kitchell E, Lazarte S, Nijhawan A. Toxoplasmosis Encephalitis: A Cross-Sectional Analysis at a U.S. Safety-Net Hospital in the Late cART Era. *Journal of the International Association of Providers of AIDS Care.* 2021;20:23259582211043863.
9. Gisbert Algaba I, Verhaegen B, Murat JB, Coucke W, Mercier A, Cox E, et al. Molecular Study of Toxoplasma gondii Isolates Originating from Humans and Organic Pigs in Belgium. *Foodborne pathogens and disease.* 2020;17(5):316-21.
10. Omonijo AO, Kalinda C, Mukaratirwa S. Toxoplasma gondii Infections in Animals and Humans in Southern Africa: A Systematic Review and Meta-Analysis. *Pathogens* (Basel, Switzerland). 2022;11(2).
11. Galal L, Ajzenberg D, Hamidović A, Durieux MF, Dardé ML, Mercier A. Toxoplasma and Africa: One Parasite, Two Opposite Population Structures. *Trends in parasitology.* 2018;34(2):140-54.
12. Pekova L, Parusheva P, Mitev M, Dochev I, Naydenov C. A rare case of an HIV-seronegative patient with Toxoplasma gondii meningoencephalitis. *IDCases.* 2021;26:e01271.
13. Martinot M, Greigert V, Farnarier C, Dardé ML, Piperoglou C, Mohseni-Zadeh M, et al. Spinal cord toxoplasmosis in a young immunocompetent patient. *Infection.* 2020;48(2):299-302.
14. Minuzzi CE, Portella LP, Bräunig P, Sangioni LA, Ludwig A, Ramos LS, et al. Isolation and molecular characterization of Toxoplasma gondii from placental tissues of pregnant women who received toxoplasmosis treatment during an outbreak in southern Brazil. *PloS one.* 2020;15(1):e0228442.
15. Zhang H, Liu J, Ying Z, Li S, Wu Y, Liu Q. Toxoplasma gondii UBL-UBA shuttle proteins contribute to the degradation of ubiquitinylated proteins and are important for synchronous cell division and virulence. *FASEB journal : official publication of the Federation of American Societies for Experimental Biology.* 2020;34(10):13711-25.

16. Suzuki Y. The immune system utilizes two distinct effector mechanisms of T cells depending on two different life cycle stages of a single pathogen, *Toxoplasma gondii*, to control its cerebral infection. *Parasitology international*. 2020;76:102030.
17. Acquarone M, Poletto A, Perozzo AF, Gonçalves PFR, Panizzutti R, Menezes JRL, et al. Social preference is maintained in mice with impaired startle reflex and glutamate/D-serine imbalance induced by chronic cerebral toxoplasmosis. *Scientific reports*. 2021;11(1):14029.
18. Ma J, He JJ, Hou JL, Zhou CX, Zhang FK, Elsheikha HM, et al. Metabolomic signature of mouse cerebral cortex following *Toxoplasma gondii* infection. *Parasites & vectors*. 2019;12(1):373.
19. Meurer Y, Brito RMM, da Silva VP, Andrade JMA, Linhares SSG, Pereira Junior A, et al. *Toxoplasma gondii* infection damages the perineuronal nets in a murine model. *Memorias do Instituto Oswaldo Cruz*. 2020;115:e200007.
20. Dupont D, Lin JS, Peyron F, Akaoka H, Wallon M. Chronic *Toxoplasma gondii* infection and sleep-wake alterations in mice. *CNS neuroscience & therapeutics*. 2021;27(8):895-907.
21. Spini V, Ferreira FR, Gomes AO, Duarte RMF, Oliveira VHS, Costa NB, et al. Maternal Immune Activation with H1N1 or *Toxoplasma gondii* Antigens Induces Behavioral Impairments Associated with Mood Disorders in Rodents. *Neuropsychobiology*. 2021;80(3):234-41.
22. Ibrahim Ali M, Abdel Gawad Mousa Ismail M, Abd-Elftah Abd-Allah G, Abdel-Latif M, Mohamed Shaapan R, Salah H, et al. Toxoplasmosis in Schizophrenic Patients: Immune-diagnosis and Serum Dopamine Level. *Pakistan journal of biological sciences : PJBS*. 2020;23(9):1131-7.
23. Roe K. The link between *Toxoplasma gondii* infections and higher mortality in COVID-19 patients having schizophrenia. *European archives of psychiatry and clinical neuroscience*. 2022;272(1):167-8.
24. Abdollahi A, Razavian I, Razavian E, Ghodsian S, Almukhtar M, Marhoommirzabak E, et al. *Toxoplasma gondii* infection/exposure and the risk of brain tumors: A systematic review and meta-analysis. *Cancer epidemiology*. 2022;77:102119.
25. Alwarawrah Y, Kiernan K, MacIver NJ. Changes in Nutritional Status Impact Immune Cell Metabolism and Function. *Frontiers in immunology*. 2018;9:1055.
26. Wing EJ, Barczynski LK, Boehmer SM. Effect of acute nutritional deprivation on immune function in mice. I. Macrophages. *Immunology*. 1983;48(3):543-50.
27. Fang X, Henao-Mejia J, Henrickson SE. Obesity and immune status in children. *Curr Opin Pediatr*. 2020;32(6):805-15.
28. Kelishadi R, Roufarshbaf M, Soheili S, Payghambarzadeh F, Masjedi M. Association of Childhood Obesity and the Immune System: A Systematic Review of Reviews. *Child Obes*. 2017;13(4):332-46.
29. Monteleone P, Mascagni G, Giannini A, Genazzani AR, Simoncini T. Symptoms of menopause - global prevalence, physiology and implications. *Nat Rev Endocrinol*. 2018;14(4):199-215.
30. Gameiro C, Romao F. Changes in the immune system during menopause and aging. *Front Biosci (Elite Ed)*. 2010;2(4):1299-303.
31. Seke Etet PF, Hamza MA, El-Tahir A, Vecchio L, Osman SY, Satti GMH, et al. An Eluate of the Medicinal Plant *Garcinia kola* Displays Strong Antidiabetic and Neuroprotective Properties in Streptozotocin-Induced Diabetic Mice. *Evidence-based complementary and alternative medicine : eCAM*. 2022;2022:8708961.
32. Ahidjo N, Ngarka L, Seke Etet PF, Njamnshi WY, Nfor LN, Mengnjo MK, et al. *Garcinia kola* improves cognitive and motor function of a rat model of acute radiation syndrome in the elevated plus maze. *Brain Commun*. 2021;3(3):fcab170.
33. Farombi EO, Awogbindin IO, Owoeye O, Abah VO, Izomoh ER, Ezekiel IO. Kolaviron ameliorates behavioural deficit and injury to striatal dopaminergic terminals via

- modulation of oxidative burden, DJ-1 depletion and CD45R(+) cells infiltration in MPTP-model of Parkinson's disease. *Metabolic brain disease*. 2020;35(6):933-46.
34. Lee DH, Chu KB, Kang HJ, Lee SH, Quan FS. Previous Infection with Plasmodium berghei Confers Resistance to Toxoplasma gondii Infection in Mice. *The Korean journal of parasitology*. 2019;57(2):93-9.
35. Ogunkunle AT, Oyelakin TM, Enitan AO, Oyewole FE. A quantitative documentation of the composition of two powdered herbal formulations (antimalarial and haematinic) using ethnomedicinal information from ogbomoso, Nigeria. *Evidence-based complementary and alternative medicine : eCAM*. 2014;2014:751291.
36. Morozińska-Gogol J. The presence of Toxoplasma gondii in the terrestrial and marine environments and its importance for public health. *Ann Parasitol*. 2021;67(2):137-49.
37. Dubey JP, Lindsay DS, Speer CA. Structures of Toxoplasma gondii tachyzoites, bradyzoites, and sporozoites and biology and development of tissue cysts. *Clinical microbiology reviews*. 1998;11(2):267-99.
38. Kurne A, Ozkaya G, Karlıoguz K, Shorbagi A, Ustaçelebi S, Karabudak R, et al. [The colorful clinical spectrum of cerebral toxoplasmosis in five HIV positive cases: what comes out of Pandora's box?]. *Mikrobiyoloji bulteni*. 2006;40(1-2):85-92.
39. Melchor SJ, Ewald SE. Disease Tolerance in Toxoplasma Infection. *Frontiers in cellular and infection microbiology*. 2019;9:185.
40. Loeillet C, Mondon A, Kamche S, Curri V, Boutonnat J, Cavaillès P, et al. Toxoplasma Hypervirulence in the Rat Model Parallels Human Infection and Is Modulated by the Toxo1 Locus. *Frontiers in cellular and infection microbiology*. 2019;9:134.
41. Witola WH, Kim CY, Zhang X. Inherent Oxidative Stress in the Lewis Rat Is Associated with Resistance to Toxoplasmosis. *Infection and immunity*. 2017;85(10).
42. Kochanowsky JA, Thomas KK, Koshy AA. ROP16-Mediated Activation of STAT6 Suppresses Host Cell Reactive Oxygen Species Production, Facilitating Type III Toxoplasma gondii Growth and Survival. *mBio*. 2021;12(2).
43. Sergent V, Cautain B, Khalife J, Deslée D, Bastien P, Dao A, et al. Innate refractoriness of the Lewis rat to toxoplasmosis is a dominant trait that is intrinsic to bone marrow-derived cells. *Infection and immunity*. 2005;73(10):6990-7.
44. Kim CY, Zhang X, Witola WH. Small GTPase Immunity-Associated Proteins Mediate Resistance to Toxoplasma gondii Infection in Lewis Rat. *Infection and immunity*. 2018;86(4).
45. Dockterman J, Fee BE, Taylor GA, Coers J. Murine Irgm Paralogs Regulate Nonredundant Functions To Execute Host Defense to Toxoplasma gondii. *Infection and immunity*. 2021;89(11):e0020221.
46. Salles É M, Menezes MN, Siqueira R, Borges da Silva H, Amaral EP, Castillo-Méndez SI, et al. P2X7 receptor drives Th1 cell differentiation and controls the follicular helper T cell population to protect against Plasmodium chabaudi malaria. *PLoS pathogens*. 2017;13(8):e1006595.
47. Moreira-Souza ACA, Rangel TP, Silva S, Figliuolo VR, Savio LEB, Schmitz F, et al. Disruption of Purinergic Receptor P2X7 Signaling Increases Susceptibility to Cerebral Toxoplasmosis. *The American journal of pathology*. 2019;189(4):730-8.
48. Alsaady I, Tedford E, Alsaad M, Bristow G, Kohli S, Murray M, et al. Downregulation of the Central Noradrenergic System by Toxoplasma gondii Infection. *Infection and immunity*. 2019;87(2).
49. Tao Q, Wang X, Liu L, Ji Y, Luo Q, Du J, et al. Toxoplasma gondii Chinese I genotype Wh6 strain infection induces tau phosphorylation via activating GSK3 β and causes hippocampal neuron apoptosis. *Acta tropica*. 2020;210:105560.
50. Zhou CX, Ai K, Huang CQ, Guo JJ, Cong H, He SY, et al. miRNA and circRNA expression patterns in mouse brain during toxoplasmosis development. *BMC genomics*. 2020;21(1):46.

51. Ortiz-Guerrero G, Gonzalez-Reyes RE, de-la-Torre A, Medina-Rincón G, Nava-Mesa MO. Pathophysiological Mechanisms of Cognitive Impairment and Neurodegeneration by Toxoplasma gondii Infection. *Brain sciences*. 2020;10(6).
52. Castaño Barrios L, Da Silva Pinheiro AP, Gibaldi D, Silva AA, Machado Rodrigues ESP, Roffé E, et al. Behavioral alterations in long-term Toxoplasma gondii infection of C57BL/6 mice are associated with neuroinflammation and disruption of the blood brain barrier. *PloS one*. 2021;16(10):e0258199.
53. Prandota J, Gryglas A, Fuglewicz A, Zesławska-Faleńczyk A, Ujma-Czapska B, Szenborn L, et al. Recurrent headaches may be caused by cerebral toxoplasmosis. *World journal of clinical pediatrics*. 2014;3(3):59-68.
54. Bay-Richter C, Petersen E, Liebenberg N, Elfving B, Wegener G. Latent toxoplasmosis aggravates anxiety- and depressive-like behaviour and suggest a role of gene-environment interactions in the behavioural response to the parasite. *Behavioural brain research*. 2019;364:133-9.
55. Mouveaux T, Roger E, Gueye A, Eysert F, Huot L, Grenier-Boley B, et al. Primary brain cell infection by Toxoplasma gondii reveals the extent and dynamics of parasite differentiation and its impact on neuron biology. *Open biology*. 2021;11(10):210053.
56. Lee SH, Jung BK, Song H, Seo HG, Chai JY, Oh BM. Neuroprotective Effect of Chronic Intracranial Toxoplasma gondii Infection in a Mouse Cerebral Ischemia Model. *The Korean journal of parasitology*. 2020;58(4):461-6.
57. McGovern KE, Cabral CM, Morrison HW, Koshy AA. Aging with Toxoplasma gondii results in pathogen clearance, resolution of inflammation, and minimal consequences to learning and memory. *Scientific reports*. 2020;10(1):7979.
58. Vidal JE, Cunha MA, Kassab MJ, Dauar RF, Vasconcelos DM. First case report of eosinophilic meningitis associated with cerebral toxoplasmosis in an HIV-positive patient. *International journal of STD & AIDS*. 2020;31(6):596-9.
59. Palmer BS. Meta-analysis of three case controlled studies and an ecological study into the link between cryptogenic epilepsy and chronic toxoplasmosis infection. *Seizure*. 2007;16(8):657-63.
60. Li ZS, Huang YZ, Hu LY, Wang GS, Hua HY, Zhou YH. [Serological investigation on Toxoplasma gondii infection in patients with unknown central nervous system diseases]. Zhongguo xue xi chong bing fang zhi za zhi = Chinese journal of schistosomiasis control. 2012;24(4):375, 81.
61. Abd El-Aal NF, Saber M, Fawzy N, Ashour WR. Sero-Prevalence of Anti-Toxoplasma Gondii Antibodies among Patients with Neuropsychiatric Disorders : Epilepsy and Depression. *Journal of the Egyptian Society of Parasitology*. 2016;46(3):729-36.
62. Eraky MA, Abdel-Hady S, Abdallah KF. Seropositivity of Toxoplasma gondii and Toxocara spp. in Children with Cryptogenic Epilepsy, Benha, Egypt. *The Korean journal of parasitology*. 2016;54(3):335-8.
63. Babaie J, Sayyah M, Gharagozli K, Mostafavi E, Golkar M. Seroepidemiological study of Toxoplasma gondii infection in a population of Iranian epileptic patients. *EXCLI journal*. 2017;16:256-64.
64. Akyol A, Bicerol B, Ertug S, Ertabaklar H, Kiylioglu N. Epilepsy and seropositivity rates of Toxocara canis and Toxoplasma gondii. *Seizure*. 2007;16(3):233-7.
65. Quet F, Preux PM, Nicoletti A. Comment on "Epilepsy and seropositivity rates of Toxocara canis and Toxoplasma gondii". *Seizure*. 2008;17(3):296.
66. Ngoungou EB, Bhalla D, Nzoghe A, Dardé ML, Preux PM. Toxoplasmosis and epilepsy--systematic review and meta analysis. *PLoS neglected tropical diseases*. 2015;9(2):e0003525.
67. Uzorka JW, Arend SM. A critical assessment of the association between postnatal toxoplasmosis and epilepsy in immune-competent patients. *European journal of clinical microbiology & infectious diseases : official publication of the European Society of Clinical Microbiology*. 2017;36(7):1111-7.

68. Sadeghi M, Riahi SM, Mohammadi M, Saber V, Aghamolaie S, Moghaddam SA, et al. An updated meta-analysis of the association between Toxoplasma gondii infection and risk of epilepsy. *Transactions of the Royal Society of Tropical Medicine and Hygiene*. 2019;113(8):453-62.
69. Alvarado-Esquivel C, Rico-Almochantaf YDR, Hernández-Tinoco J, Quiñones-Canales G, Sánchez-Anguiano LF, Torres-González J, et al. Toxoplasma gondii exposure and epilepsy: A matched case-control study in a public hospital in northern Mexico. *SAGE open medicine*. 2018;6:2050312118767767.
70. Ngô HM, Zhou Y, Lorenzi H, Wang K, Kim TK, Zhou Y, et al. Toxoplasma Modulates Signature Pathways of Human Epilepsy, Neurodegeneration & Cancer. *Scientific reports*. 2017;7(1):11496.
71. Hu RS, He JJ, Elsheikha HM, Zou Y, Ehsan M, Ma QN, et al. Transcriptomic Profiling of Mouse Brain During Acute and Chronic Infections by Toxoplasma gondii Oocysts. *Frontiers in microbiology*. 2020;11:570903.
72. Zhou CX, Gao M, Han B, Cong H, Zhu XQ, Zhou HY. Quantitative Peptidomics of Mouse Brain After Infection With Cyst-Forming Toxoplasma gondii. *Frontiers in immunology*. 2021;12:681242.
73. Rostami-Mansoor S, Kalantari N, Gorgani-Firouzjaee T, Ghaffari S, Ghasemi-Kasman M. Modulation of mRNA Expression of Monoacylglycerol Lipase, Diacylglycerol Lipase and Cannabinoid Receptor-1 in Mice Experimentally Infected with *T. gondii*. *International journal of molecular and cellular medicine*. 2021;10(2):149-55.
74. Ghanbari MM, Joneidi M, Kiani B, Babaie J, Sayyah M. Cannabinoid receptors and the proconvulsant effect of toxoplasmosis in mice. *Microbial pathogenesis*. 2020;144:104204.
75. Babaie J, Sayyah M, Fard-Esfahani P, Golkar M, Gharagozli K. Contribution of dopamine neurotransmission in proconvulsant effect of Toxoplasma gondii infection in male mice. *Journal of neuroscience research*. 2017;95(10):1894-905.
76. Zhang Z, Li Y, Li H, Song X, Ma Z, Lu H, et al. Identification of Toxoplasma Gondii Tyrosine Hydroxylase (TH) Activity and Molecular Immunoprotection against Toxoplasmosis. *Vaccines*. 2020;8(2).
77. Babaie J, Sayyah M, Choopani S, Asgari T, Golkar M, Gharagozli K. Toxoplasmosis accelerates acquisition of epilepsy in rats undergoing chemical kindling. *Epilepsy research*. 2017;135:137-42.
78. Michałowicz R, Jóźwiak S, Ignatowicz R, Szwabowska-Orzeszko E. Landau-Kleffner syndrome--epileptic aphasia in children--possible role of toxoplasma gondii infection. *Acta paediatrica Hungarica*. 1988;29(3-4):337-42.
79. Muzio MR, Cascella M, Al Khalili Y. Landau Kleffner Syndrome. *StatPearls*. Treasure Island (FL): StatPearls Publishing
Copyright © 2021, StatPearls Publishing LLC.; 2021.
80. Beltrame A, Venturini S, Cricchitti G, Meroni V, Buonfrate D, Bassetti M. Recurrent seizures during acute acquired toxoplasmosis in an immunocompetent traveller returning from Africa. *Infection*. 2016;44(2):259-62.
81. Colebunders R, Mandro M, Mokili JL, Mucinya G, Mambandu G, Pfarr K, et al. Risk factors for epilepsy in Bas-Uélé Province, Democratic Republic of the Congo: a case-control study. *International journal of infectious diseases : IJID : official publication of the International Society for Infectious Diseases*. 2016;49:1-8.
82. Ae-Ngibise KA, Akpalu B, Ngugi A, Akpalu A, Agbokey F, Adjei P, et al. Prevalence and risk factors for Active Convulsive Epilepsy in Kintampo, Ghana. *The Pan African medical journal*. 2015;21:29.
83. Kamuyu G, Bottomley C, Mageto J, Lowe B, Wilkins PP, Noh JC, et al. Exposure to multiple parasites is associated with the prevalence of active convulsive epilepsy in sub-Saharan Africa. *PLoS neglected tropical diseases*. 2014;8(5):e2908.
84. Ngugi AK, Bottomley C, Kleinschmidt I, Wagner RG, Kakooza-Mwesige A, Ae-Ngibise K, et al. Prevalence of active convulsive epilepsy in sub-Saharan Africa and

- associated risk factors: cross-sectional and case-control studies. *The Lancet Neurology*. 2013;12(3):253-63.
85. Carrillo GL, Ballard VA, Glausen T, Boone Z, Teamer J, Hinkson CL, et al. Toxoplasma infection induces microglia-neuron contact and the loss of perisomatic inhibitory synapses. *Glia*. 2020;68(10):1968-86.
86. Sikorski PM, Commodaro AG, Grigg ME. A Protective and Pathogenic Role for Complement During Acute Toxoplasma gondii Infection. *Frontiers in cellular and infection microbiology*. 2021;11:634610.
87. Shinjyo N, Hikosaka K, Kido Y, Yoshida H, Norose K. Toxoplasma Infection Induces Sustained Up-Regulation of Complement Factor B and C5a Receptor in the Mouse Brain via Microglial Activation: Implication for the Alternative Complement Pathway Activation and Anaphylatoxin Signaling in Cerebral Toxoplasmosis. *Frontiers in immunology*. 2020;11:603924.
88. French T, Israel N, Düsedau HP, Tersteegen A, Steffen J, Cammann C, et al. The Immunoproteasome Subunits LMP2, LMP7 and MECL-1 Are Crucial Along the Induction of Cerebral Toxoplasmosis. *Frontiers in immunology*. 2021;12:619465.
89. Pang Y, Zhang Z, Chen Y, Cao S, Yang X, Jia H. The Nrf2 pathway is required for intracellular replication of Toxoplasma gondii in activated macrophages. *Parasite immunology*. 2019;41(5):e12621.
90. Still KM, Batista SJ, O'Brien CA, Oyesola OO, Früh SP, Webb LM, et al. Astrocytes promote a protective immune response to brain Toxoplasma gondii infection via IL-33-ST2 signaling. *PLoS pathogens*. 2020;16(10):e1009027.
91. Yin K, Xu C, Zhao G, Xie H. Epigenetic Manipulation of Psychiatric Behavioral Disorders Induced by Toxoplasma gondii. *Frontiers in cellular and infection microbiology*. 2022;12:803502.
92. Nayeri T, Sarvi S, Daryani A. Toxoplasmosis: Targeting neurotransmitter systems in psychiatric disorders. *Metabolic brain disease*. 2022;37(1):123-46.
93. Elsheikha HM, Al-Sandaqchi AT, Harun MSR, Winterton F, Altharawi A, Elsaied NA, et al. Illuminating Host-Parasite Interaction at the Cellular and Subcellular Levels with Infrared Microspectroscopy. *Cells*. 2022;11(5).
94. Li S, He B, Yang C, Yang J, Wang L, Duan X, et al. Comparative transcriptome analysis of normal and CD44-deleted mouse brain under chronic infection with Toxoplasma gondii. *Acta tropica*. 2020;210:105589.
95. Nast R, Choepak T, Lüder CGK. Epigenetic Control of IFN- γ Host Responses During Infection With Toxoplasma gondii. *Frontiers in immunology*. 2020;11:581241.
96. Jublot D, Cavaillès P, Kamche S, Francisco D, Fontinha D, Prudêncio M, et al. A Histone Deacetylase (HDAC) Inhibitor with Pleiotropic In Vitro Anti-Toxoplasma and Anti-Plasmodium Activities Controls Acute and Chronic Toxoplasma Infection in Mice. *International journal of molecular sciences*. 2022;23(6).
97. Figueiredo CA, Steffen J, Morton L, Arumugam S, Liesenfeld O, Deli MA, et al. Immune response and pathogen invasion at the choroid plexus in the onset of cerebral toxoplasmosis. *Journal of neuroinflammation*. 2022;19(1):17.
98. Ross EC, Olivera GC, Barragan A. Early passage of Toxoplasma gondii across the blood-brain barrier. *Trends in parasitology*. 2022.
99. Kongsomboonvech AK, Rodriguez F, Diep AL, Justice BM, Castallanos BE, Camejo A, et al. Naïve CD8 T cell IFN γ responses to a vacuolar antigen are regulated by an inflammasome-independent NLRP3 pathway and Toxoplasma gondii ROP5. *PLoS pathogens*. 2020;16(8):e1008327.
100. Doherty CM, Romero AD, Denkers EY. Impact of IFN- γ and CD40 signalling on Toxoplasma gondii cyst formation in differentiated Neuro-2a neuroblastoma cells. *Parasite immunology*. 2022;44(1-2):e12897.

101. Olias P, Etheridge RD, Zhang Y, Holtzman MJ, Sibley LD. Toxoplasma Effector Recruits the Mi-2/NuRD Complex to Repress STAT1 Transcription and Block IFN- γ -Dependent Gene Expression. *Cell host & microbe*. 2016;20(1):72-82.
102. Matta SK, Olias P, Huang Z, Wang Q, Park E, Yokoyama WM, et al. Toxoplasma gondii effector TgIST blocks type I interferon signaling to promote infection. *Proceedings of the National Academy of Sciences of the United States of America*. 2019;116(35):17480-91.
103. Mukhopadhyay D, Sangaré LO, Braun L, Hakimi MA, Saeij JP. Toxoplasma GRA15 limits parasite growth in IFN γ -activated fibroblasts through TRAF ubiquitin ligases. *The EMBO journal*. 2020;39(10):e103758.
104. Ihara F, Fereig RM, Himori Y, Kameyama K, Umeda K, Tanaka S, et al. Toxoplasma gondii Dense Granule Proteins 7, 14, and 15 Are Involved in Modification and Control of the Immune Response Mediated via NF- κ B Pathway. *Frontiers in immunology*. 2020;11:1709.
105. Fisch D, Clough B, Domart MC, Encheva V, Bando H, Snijders AP, et al. Human GBP1 Differentially Targets Salmonella and Toxoplasma to License Recognition of Microbial Ligands and Caspase-Mediated Death. *Cell reports*. 2020;32(6):108008.
106. Gai K, Okondo MC, Rao SD, Chui AJ, Ball DP, Johnson DC, et al. DPP8/9 inhibitors are universal activators of functional NLRP1 alleles. *Cell death & disease*. 2019;10(8):587.
107. El Saftawy EA, Shash RY, Aboulhoda BE, Arsanyos SF, Albadawi EA, Abou-Fandoud SM, et al. Insights into immunopathology and triggering of apoptosis in chronic cerebral toxoplasmosis using murine models. *Tropical biomedicine*. 2021;38(2):53-62.
108. El Saftawy EA, Amin NM, Sabry RM, El-Anwar N, Shash RY, Elsebaie EH, et al. Can Toxoplasma gondii Pave the Road for Dementia? *Journal of parasitology research*. 2020;2020:8859857.
109. Sharma V, Kaur A, Singh TG. Counteracting role of nuclear factor erythroid 2-related factor 2 pathway in Alzheimer's disease. *Biomedicine & pharmacotherapy = Biomedecine & pharmacotherapie*. 2020;129:110373.
110. Efferth T, Oesch F. The immunosuppressive activity of artemisinin-type drugs towards inflammatory and autoimmune diseases. *Medicinal research reviews*. 2021;41(6):3023-61.
111. Merritt EF, Johnson HJ, Wong ZS, Buntzman AS, Conklin AC, Cabral CM, et al. Transcriptional Profiling Suggests T Cells Cluster around Neurons Injected with Toxoplasma gondii Proteins. *mSphere*. 2020;5(5).
112. Galván Ramírez ML, Dueñas-Jiménez JM, Gutiérrez-Maldonado AF, Rodríguez Pérez LR. Effect of 17 β -Estradiol, Progesterone, and Tamoxifen on Neurons Infected with Toxoplasma gondii In Vitro. *Microorganisms*. 2021;9(10).
113. Wang J, Hou Y, Zhang L, Liu M, Zhao J, Zhang Z, et al. Estrogen Attenuates Traumatic Brain Injury by Inhibiting the Activation of Microglia and Astrocyte-Mediated Neuroinflammatory Responses. *Molecular neurobiology*. 2021;58(3):1052-61.
114. Lu Y, Sareddy GR, Wang J, Zhang Q, Tang FL, Pratap UP, et al. Neuron-Derived Estrogen Is Critical for Astrocyte Activation and Neuroprotection of the Ischemic Brain. *The Journal of neuroscience : the official journal of the Society for Neuroscience*. 2020;40(38):7355-74.
115. Azcoitia I, Santos-Galindo M, Arevalo MA, Garcia-Segura LM. Role of astroglia in the neuroplastic and neuroprotective actions of estradiol. *The European journal of neuroscience*. 2010;32(12):1995-2002.
116. Galván-Ramírez ML, Ramírez De Arellano A, Rodríguez-Pérez LR, Lopez-Pulido EI, Muñoz-Valle JF, Pereira-Suárez AL. Hormonal modulation of Toxoplasma gondii infection: Regulation of hormonal receptors and cytokine production in THP-1 cells. *Experimental parasitology*. 2019;204:107721.
117. Cabral CM, Merritt EF, Koshy AA. Three-Dimensional Reconstruction of Toxoplasma-Neuron Interactions In Situ. *Methods in molecular biology* (Clifton, NJ). 2020;2071:283-95.

118. Lima KDF, Queiroz ALG, Teixeira HS, Bonsi VM, Inada BSY, Lancellotti CLP, et al. An atypical case of neurotoxoplasmosis in immunocompetent patient. Radiology case reports. 2021;16(7):1766-9.
119. Ferra BT, Holec-Gąsior L, Gatkowska J, Dziadek B, Dzikko K, Grążlewska W, et al. The first study on the usefulness of recombinant tetravalent chimeric proteins containing fragments of SAG2, GRA1, ROP1 and AMA1 antigens in the detection of specific anti-Toxoplasma gondii antibodies in mouse and human sera. PloS one. 2019;14(6):e0217866.
120. Dard C, Swale C, Brenier-Pinchart MP, Farhat DC, Bellini V, Robert MG, et al. A brain cyst load-associated antigen is a Toxoplasma gondii biomarker for serodetection of persistent parasites and chronic infection. BMC biology. 2021;19(1):25.
121. Arranz-Solís D, Cordeiro C, Young LH, Dardé ML, Commodaro AG, Grigg ME, et al. Serotyping of Toxoplasma gondii Infection Using Peptide Membrane Arrays. Frontiers in cellular and infection microbiology. 2019;9:408.
122. Arranz-Solís D, Carvalheiro CG, Zhang ER, Grigg ME, Saeij JPJ. Toxoplasma GRA Peptide-Specific Serologic Fingerprints Discriminate Among Major Strains Causing Toxoplasmosis. Frontiers in cellular and infection microbiology. 2021;11:621738.
123. Ferra B, Holec-Gąsior L, Gatkowska J, Dziadek B, Dzikko K. Toxoplasma gondii Recombinant antigen AMA1: Diagnostic Utility of Protein Fragments for the Detection of IgG and IgM Antibodies. Pathogens (Basel, Switzerland). 2020;9(1).
124. Zhou CX, Xie SC, Li MY, Huang CQ, Zhou HY, Cong H, et al. Analysis of the serum peptidome associated with Toxoplasma gondii infection. Journal of proteomics. 2020;222:103805.
125. Cui LL, Zhou CX, Han B, Wang SS, Li SY, Xie SC, et al. Urine proteomics for profiling of mouse toxoplasmosis using liquid chromatography tandem mass spectrometry analysis. Parasites & vectors. 2021;14(1):211.
126. Rehan IF, Mahmoud ME, Salman D, Elnagar A, Salman S, Youssef M, et al. Sialylated N-glycan profile during acute and chronic infections with Toxoplasma gondii in mice. Scientific reports. 2020;10(1):3809.
127. Pena HFJ, Ferreira MN, Gennari SM, de Andrade HF, Jr., Meireles LR, Galisteo AJ, Jr. Toxoplasma gondii isolated from a Brazilian patient with rare pulmonary toxoplasmosis has a novel genotype and is closely related to Amazonian isolates. Parasitology research. 2021;120(3):1109-13.
128. Salman D, Mahmoud ME, Pumidonming W, Mairamkul T, Oohashi E, Igarashi M. Characterization of a spontaneous cyst-forming strain of Toxoplasma gondii isolated from Tokachi subprefecture in Japan. Parasitology international. 2021;80:102199.
129. Hamidović A, Etougbeh JR, Tonouhewa ABN, Galal L, Dobigny G, Houémènou G, et al. A hotspot of Toxoplasma gondii Africa 1 lineage in Benin: How new genotypes from West Africa contribute to understand the parasite genetic diversity worldwide. PLoS neglected tropical diseases. 2021;15(2):e0008980.
130. Sousa S, Castro A, Correia da Costa JM, Pereira E. Biosensor Based Immunoassay: A New Approach for Serotyping of Toxoplasma gondii. Nanomaterials (Basel, Switzerland). 2021;11(8).
131. Mévélec MN, Lakhrif Z, Dimier-Poisson I. Key Limitations and New Insights Into the Toxoplasma gondii Parasite Stage Switching for Future Vaccine Development in Human, Livestock, and Cats. Frontiers in cellular and infection microbiology. 2020;10:607198.
132. Pagheh AS, Sarvi S, Sharif M, Rezaei F, Ahmadpour E, Dodangeh S, et al. Toxoplasma gondii surface antigen 1 (SAG1) as a potential candidate to develop vaccine against toxoplasmosis: A systematic review. Comparative immunology, microbiology and infectious diseases. 2020;69:101414.
133. Foroutan M, Ghaffarifar F, Sharifi Z, Dalimi A, Jorjani O. Rhoptry antigens as Toxoplasma gondii vaccine target. Clinical and experimental vaccine research. 2019;8(1):4-26.

134. Wang JL, Liang QL, Li TT, He JJ, Bai MJ, Cao XZ, et al. Toxoplasma gondii tk11 Deletion Mutant Is a Promising Vaccine against Acute, Chronic, and Congenital Toxoplasmosis in Mice. *Journal of immunology* (Baltimore, Md : 1950). 2020;204(6):1562-70.
135. Song PX, Yao SH, Yao Y, Zhou J, Li QF, Cao YH, et al. Epitope Analysis and Efficacy Evaluation of Phosphatase 2C (PP2C) DNA Vaccine Against Toxoplasma gondii Infection. *The Journal of parasitology*. 2020;106(4):513-21.
136. Sun H, Li J, Xiao T, Huang XD, Wang LJ, Huang BC, et al. Protective immunity induced by a DNA vaccine cocktail expressing TgSAG1, TgROP2, and the genetic adjuvant HBsAg against Toxoplasma gondii infection. *Microbial pathogenesis*. 2020;147:104441.
137. Arcon N, Picchio MS, Fenoy IM, Moretta RE, Soto AS, Perrone Sibilia MD, et al. Synergistic effect of GRA7 and profilin proteins in vaccination against chronic Toxoplasma gondii infection. *Vaccine*. 2021;39(6):933-42.
138. Şahar EA, Can H, İz SG, Döşkaya AD, Kalantari-Dehaghi M, Deveci R, et al. Development of a hexavalent recombinant protein vaccine adjuvanted with Montanide ISA 50 V and determination of its protective efficacy against acute toxoplasmosis. *BMC infectious diseases*. 2020;20(1):493.
139. Zhu L, Lei Z, Xia X, Zhang Y, Chen Y, Wang B, et al. Yeast Shells Encapsulating Adjuvant AS04 as an Antigen Delivery System for a Novel Vaccine against Toxoplasma Gondii. *ACS applied materials & interfaces*. 2021;13(34):40415-28.
140. El Bissati K, Zhou Y, Paulillo SM, Raman SK, Karch CP, Reed S, et al. Engineering and characterization of a novel Self Assembling Protein for Toxoplasma peptide vaccine in HLA-A*11:01, HLA-A*02:01 and HLA-B*07:02 transgenic mice. *Scientific reports*. 2020;10(1):16984.
141. Karakavuk M, Can H, Gül A, Döşkaya AD, Alak SE, Ün C, et al. GRA8 DNA vaccine formulations protect against chronic toxoplasmosis. *Microbial pathogenesis*. 2021;158:105016.
142. Zhu Y, Xu Y, Hong L, Zhou C, Chen J. Immunization With a DNA Vaccine Encoding the Toxoplasma gondii's GRA39 Prolongs Survival and Reduce Brain Cyst Formation in a Murine Model. *Frontiers in microbiology*. 2021;12:630682.
143. Yu Z, Lu Y, Cao W, Aleem MT, Liu J, Luo J, et al. Nano DNA Vaccine Encoding Toxoplasma gondii Histone Deacetylase SIR2 Enhanced Protective Immunity in Mice. *Pharmaceutics*. 2021;13(10).
144. Li J, Galon EM, Guo H, Liu M, Li Y, Ji S, et al. PLK: Δ gra9 Live Attenuated Strain Induces Protective Immunity Against Acute and Chronic Toxoplasmosis. *Frontiers in microbiology*. 2021;12:619335.
145. Le Roux D, Djokic V, Morisse S, Chauvin C, Doré V, Lagrée AC, et al. Evaluation of immunogenicity and protection of the Mic1-3 knockout Toxoplasma gondii live attenuated strain in the feline host. *Vaccine*. 2020;38(6):1457-66.
146. Wang L, Tang D, Yang C, Yang J, Fang R. Toxoplasma gondii ADSL Knockout Provides Excellent Immune Protection against a Variety of Strains. *Vaccines*. 2020;8(1).
147. Roberts CW, McLeod R, Rice DW, Ginger M, Chance ML, Goad LJ. Fatty acid and sterol metabolism: potential antimicrobial targets in apicomplexan and trypanosomatid parasitic protozoa. *Molecular and biochemical parasitology*. 2003;126(2):129-42.
148. Kannan G, Thaprawat P, Schultz TL, Carruthers VB. Acquisition of Host Cytosolic Protein by Toxoplasma gondii Bradyzoites. *mSphere*. 2021;6(1).
149. Liang X, Cui J, Yang X, Xia N, Li Y, Zhao J, et al. Acquisition of exogenous fatty acids renders apicoplast-based biosynthesis dispensable in tachyzoites of Toxoplasma. *The Journal of biological chemistry*. 2020;295(22):7743-52.
150. Waldman BS, Schwarz D, Wadsworth MH, 2nd, Saeij JP, Shalek AK, Lourido S. Identification of a Master Regulator of Differentiation in Toxoplasma. *Cell*. 2020;180(2):359-72.e16.

151. Ricci-Azevedo R, Mendonça-Natividade FC, Santana AC, Alcoforado Diniz J, Roque-Barreira MC. Microneme Proteins 1 and 4 From *Toxoplasma gondii* Induce IL-10 Production by Macrophages Through TLR4 Endocytosis. *Frontiers in immunology*. 2021;12:655371.
152. Wang Y, Han C, Zhou R, Zhu J, Zhang F, Li J, et al. Differential expression of TgMIC1 in isolates of Chinese 1 *Toxoplasma* with different virulence. *Parasites & vectors*. 2021;14(1):253.
153. Zhang H, Yang X, Ying Z, Liu J, Liu Q. *Toxoplasma gondii* UBL-UBA Shuttle Protein DSK2s Are Important for Parasite Intracellular Replication. *International journal of molecular sciences*. 2021;22(15).
154. Albuquerque-Wendt A, Jacot D, Dos Santos Pacheco N, Seegers C, Zarnovican P, Buettner FFR, et al. C-Mannosylation of *Toxoplasma gondii* proteins promotes attachment to host cells and parasite virulence. *The Journal of biological chemistry*. 2020;295(4):1066-76.
155. Nyonda MA, Hammoudi PM, Ye S, Maire J, Marq JB, Yamamoto M, et al. *Toxoplasma gondii* GRA60 is an effector protein that modulates host cell autonomous immunity and contributes to virulence. *Cellular microbiology*. 2021;23(2):e13278.
156. Guo M, Sun J, Wang WT, Liu HY, Liu YH, Qin KR, et al. *Toxoplasma gondii* ROP17 promotes autophagy via the Bcl-2-Beclin 1 pathway. *Folia parasitologica*. 2021;68.
157. Bandini G, Agop-Nersesian C, van der Wel H, Mandalasi M, Kim HW, West CM, et al. The nucleocytosolic O-fucosyltransferase SPINDLY affects protein expression and virulence in *Toxoplasma gondii*. *The Journal of biological chemistry*. 2021;296:100039.
158. Tomita T, Mukhopadhyay D, Han B, Yakubu R, Tu V, Mayoral J, et al. *Toxoplasma gondii* Matrix Antigen 1 Is a Secreted Immunomodulatory Effector. *mBio*. 2021;12(3).
159. Guevara RB, Fox BA, Bzik DJ. A Family of *Toxoplasma gondii* Genes Related to GRA12 Regulate Cyst Burdens and Cyst Reactivation. *mSphere*. 2021;6(2).
160. Xu XP, Elsheikha HM, Liu WG, Zhang ZW, Sun LX, Liang QL, et al. The Role of Type II Fatty Acid Synthesis Enzymes FabZ, ODSCI, and ODSCII in the Pathogenesis of *Toxoplasma gondii* Infection. *Frontiers in microbiology*. 2021;12:703059.
161. Asady B, Dick CF, Ehrenman K, Sahu T, Romano JD, Coppens I. A single Na⁺-Pi cotransporter in *Toxoplasma* plays key roles in phosphate import and control of parasite osmoregulation. *PLoS pathogens*. 2020;16(12):e1009067.
162. Hamie M, Tawil N, El Hajj R, Najm R, Moodad S, Hleihel R, et al. P18 (SRS35/TgSAG4) Plays a Role in the Invasion and Virulence of *Toxoplasma gondii*. *Frontiers in immunology*. 2021;12:643292.
163. Smith D, Kannan G, Coppens I, Wang F, Nguyen HM, Cerutti A, et al. *Toxoplasma* TgATG9 is critical for autophagy and long-term persistence in tissue cysts. *eLife*. 2021;10.
164. Chen Y, Liu Q, Xue JX, Zhang MY, Geng XL, Wang Q, et al. Genome-Wide CRISPR/Cas9 Screen Identifies New Genes Critical for Defense Against Oxidant Stress in *Toxoplasma gondii*. *Frontiers in microbiology*. 2021;12:670705.
165. Leroux LP, Chaparro V, Jaramillo M. Infection by the Protozoan Parasite *Toxoplasma gondii* Inhibits Host MNK1/2-eIF4E Axis to Promote Its Survival. *Frontiers in cellular and infection microbiology*. 2020;10:488.
166. Jiang H, Zhai T, Yu Y, Li X, Gong P, Zhang X, et al. Delayed IL-12 production by macrophages during *Toxoplasma gondii* infection is regulated by miR-187. *Parasitology research*. 2020;119(3):1023-33.
167. Njiri OA, Zhang X, Zhang Y, Wu B, Jiang L, Li Q, et al. CD209 C-Type Lectins Promote Host Invasion, Dissemination, and Infection of *Toxoplasma gondii*. *Frontiers in immunology*. 2020;11:656.
168. Sikorski PM, Commodaro AG, Grigg ME. *Toxoplasma gondii* Recruits Factor H and C4b-Binding Protein to Mediate Resistance to Serum Killing and Promote Parasite Persistence in vivo. *Frontiers in immunology*. 2019;10:3105.

169. Mitra P, Deshmukh AS, Choudhury C. Molecular chaperone function of stress inducible Hsp70 is critical for intracellular multiplication of *Toxoplasma gondii*. *Biochimica et biophysica acta Molecular cell research.* 2021;1868(2):118898.
170. Zhao Y, Reyes J, Rovira-Diaz E, Fox BA, Bzik DJ, Yap GS. Cutting Edge: CD36 Mediates Phagocyte Tropism and Avirulence of *Toxoplasma gondii*. *Journal of immunology (Baltimore, Md : 1950).* 2021;207(6):1507-12.
171. Barrett MP, Kyle DE, Sibley LD, Radke JB, Tarleton RL. Protozoan persister-like cells and drug treatment failure. *Nature reviews Microbiology.* 2019;17(10):607-20.
172. Sina S, Mohammad JM, Reza S, Anita M, Soudabeh E, Hadi M. Determination of parasitic burden in the brain tissue of infected mice in acute toxoplasmosis after treatment by fluconazole combined with sulfadiazine and pyrimethamine. *European journal of medical research.* 2021;26(1):65.
173. Martynowicz J, Doggett JS, Sullivan WJ, Jr. Efficacy of Guanabenz Combination Therapy against Chronic Toxoplasmosis across Multiple Mouse Strains. *Antimicrobial agents and chemotherapy.* 2020;64(9).
174. Wang D, Xing M, El-Ashram S, Ding Y, Zhang X, Sang X, et al. Determination of lumefantrine as an effective drug against *Toxoplasma gondii* infection - in vitro and in vivo study. *Parasitology.* 2021;148(1):122-8.
175. Abou-El-Naga IF, Gomaa MM, ElAchy SN. Effect of HIV aspartyl protease inhibitors on experimental infection with a cystogenic Me49 strain of *Toxoplasma gondii*. *Pathogens and global health.* 2021;1-12.
176. Pellegrino D, Grysche R, de Oliveira ACP, Marcusso R, Correia A, Vidal JE. Efficacy and safety of trimethoprim-sulfamethoxazole in HIV-infected patients with cerebral toxoplasmosis in Brazil: a single-arm open-label clinical trial. *International journal of STD & AIDS.* 2019;30(12):1156-62.
177. Abou-El-Naga IF, Gomaa MM, ElAchy SN. Effect of HIV aspartyl protease inhibitors on experimental infection with a cystogenic Me49 strain of *Toxoplasma gondii*. *Pathogens and global health.* 2022;116(2):107-18.
178. Abou-El-Naga IF, Mogahed N. Repurposing auranofin for treatment of Experimental Cerebral Toxoplasmosis. *Acta parasitologica.* 2021;66(3):827-36.
179. Hamie M, Najm R, Deleuze-Masquefa C, Bonnet PA, Dubremetz JF, El Sabban M, et al. Imiquimod Targets Toxoplasmosis Through Modulating Host Toll-Like Receptor-MyD88 Signaling. *Frontiers in immunology.* 2021;12:629917.
180. Yan X, Han W, Jin X, Sun Y, Gao J, Yu X, et al. Study on the effect of koumiss on the intestinal microbiota of mice infected with *Toxoplasma gondii*. *Scientific reports.* 2022;12(1):1271.
181. Harun MSR, Taylor M, Zhu XQ, Elsheikha HM. Transcriptome Profiling of *Toxoplasma gondii*-Infected Human Cerebromicrovascular Endothelial Cell Response to Treatment with Monensin. *Microorganisms.* 2020;8(6).
182. FarahatAllam A, Shehab AY, Fawzy Hussein Mogahed NM, Farag HF, Elsayed Y, Abd El-Latif NF. Effect of nitazoxanide and spiramycin metronidazole combination in acute experimental toxoplasmosis. *Heliyon.* 2020;6(4):e03661.
183. Hagras NA, Mogahed N, Sheta E, Darwish AA, El-Hawary MA, Hamed MT, et al. The powerful synergistic effect of spiramycin/propolis loaded chitosan/alginate nanoparticles on acute murine toxoplasmosis. *PLoS neglected tropical diseases.* 2022;16(3):e0010268.
184. Ghosh S, Padalia J, Ngobeni R, Abendroth J, Farr L, Shirley DA, et al. Targeting Parasite-Produced Macrophage Migration Inhibitory Factor as an Antivirulence Strategy With Antibiotic-Antibody Combination to Reduce Tissue Damage. *The Journal of infectious diseases.* 2020;221(7):1185-93.
185. Nishi L, Santana PL, Evangelista FF, Beletini LF, Souza AH, Mantelo FM, et al. Rosuvastatin reduced brain parasite burden in a chronic toxoplasmosis in vivo model and influenced the neuropathological pattern of ME-49 strain. *Parasitology.* 2020;147(3):303-9.

186. Yuan W, Jia H, Tang X, Xin T, Liu X, Wang Z, et al. Tylvalosin demonstrates anti-parasitic activity and protects mice from acute toxoplasmosis. *Life sciences*. 2022;294:120373.
187. Enshaeieh M, Saadatnia G, Babaie J, Golkar M, Choopani S, Sayyah M. Valproic Acid Inhibits Chronic Toxoplasma Infection and Associated Brain Inflammation in Mice. *Antimicrobial agents and chemotherapy*. 2021;65(10):e0100321.
188. Tan S, Tong WH, Vyas A. Impact of Plant-Based Foods and Nutraceuticals on Toxoplasma gondii Cysts: Nutritional Therapy as a Viable Approach for Managing Chronic Brain Toxoplasmosis. *Frontiers in nutrition*. 2022;9:827286.
189. Zhang T, Zhang Y, Jiang N, Zhao X, Sang X, Yang N, et al. Dihydroartemisinin regulates the immune system by promotion of CD8(+) T lymphocytes and suppression of B cell responses. *Science China Life sciences*. 2020;63(5):737-49.
190. Deng H, Huang X, Jin C, Jin CM, Quan ZS. Synthesis, in vitro and in vivo biological evaluation of dihydroartemisinin derivatives with potential anti-Toxoplasma gondii agents. *Bioorganic chemistry*. 2020;94:103467.
191. Zhang RH, Jin R, Deng H, Shen QK, Quan ZS, Jin CM. Evaluation of the anti-Toxoplasma gondii Activity of Hederagenin in vitro and in vivo. *The Korean journal of parasitology*. 2021;59(3):297-301.
192. Lee J, Choi JW, Han HY, Kim WS, Song HY, Byun EB, et al. 4-Hydroxybenzaldehyde Restricts the Intracellular Growth of Toxoplasma gondii by Inducing SIRT1-Mediated Autophagy in Macrophages. *The Korean journal of parasitology*. 2020;58(1):7-14.
193. Zhang J, Si H, Lv K, Qiu Y, Sun J, Bai Y, et al. Licarin-B Exhibits Activity Against the Toxoplasma gondii RH Strain by Damaging Mitochondria and Activating Autophagy. *Frontiers in cell and developmental biology*. 2021;9:684393.
194. Leesombun A, Iijima M, Umeda K, Kondoh D, Pagmadulam B, Abdou AM, et al. Metacytofilin Is a Potent Therapeutic Drug Candidate for Toxoplasmosis. *The Journal of infectious diseases*. 2020;221(5):766-74.
195. Zhang J, Si H, Sun J, Lv K, Yan B, Li B, et al. Determination of myrislignan levels in BALB/c mouse plasma by LC-MS/MS and a comparison of its pharmacokinetics after oral and intraperitoneal administration. *BMC veterinary research*. 2021;17(1):275.
196. Bottari NB, Reichert KP, Fracasso M, Dutra A, Assmann CE, Ulrich H, et al. Neuroprotective role of resveratrol mediated by purinergic signalling in cerebral cortex of mice infected by Toxoplasma gondii. *Parasitology research*. 2020;119(9):2897-905.
197. O'Connor RM, Nepveux VF, Abenoja J, Bowden G, Reis P, Beaufshaw J, et al. A symbiotic bacterium of shipworms produces a compound with broad spectrum anti-apicomplexan activity. *PLoS pathogens*. 2020;16(5):e1008600.
198. de Assis DRR, Pimentel PMO, Dos Reis PVM, Rabelo RAN, Vitor RWA, Cordeiro MDN, et al. Tityus serrulatus (Scorpion): From the Crude Venom to the Construction of Synthetic Peptides and Their Possible Therapeutic Application Against Toxoplasma gondii Infection. *Frontiers in cellular and infection microbiology*. 2021;11:706618.
199. Tan S, Tong WH, Vyas A. Urolithin-A attenuates neurotoxoplasmosis and alters innate response towards predator odor. *Brain, behavior, & immunity - health*. 2020;8:100128.
200. Liu Y, Tang Y, Tang X, Wu M, Hou S, Liu X, et al. Anti-Toxoplasma gondii Effects of a Novel Spider Peptide XYP1 In Vitro and In Vivo. *Biomedicines*. 2021;9(8).
201. Saito H, Murata Y, Nonaka M, Kato K. Screening of a library of traditional Chinese medicines to identify compounds and extracts which inhibit Toxoplasma gondii growth. *The Journal of veterinary medical science*. 2020;82(2):184-7.
202. Banzragchgarav O, Batkhuu J, Myagmarsuren P, Battsetseg B, Battur B, Nishikawa Y. In Vitro Potently Active Anti-Plasmodium and Anti-Toxoplasma Mongolian Plant Extracts. *Acta parasitologica*. 2021.
203. Miranda NC, Araujo ECB, Justino AB, Cariaco Y, Mota CM, Costa-Nascimento LA, et al. Anti-parasitic activity of Annona muricata L. leaf ethanolic extract and its fractions

- against *Toxoplasma gondii* in vitro and in vivo. *Journal of ethnopharmacology*. 2021;273:114019.
204. Nikkhoo M, Asgari Q, Moein MR, Yaghoobi K, Gholipour A. In Vitro and In Vivo Survey of Ethyl Acetate Extract of *Acorus calamus* (Sweet Flag) Rhizome on *Toxoplasma gondii*. *Journal of parasitology research*. 2021;2021:6656023.
205. Shinjyo N, Nakayama H, Li L, Ishimaru K, Hikosaka K, Suzuki N, et al. Hypericum perforatum extract and hyperforin inhibit the growth of neurotropic parasite *Toxoplasma gondii* and infection-induced inflammatory responses of glial cells in vitro. *Journal of ethnopharmacology*. 2021;267:113525.
206. Bellini V, Swale C, Brenier-Pinchart MP, Pezier T, Georgeault S, Laurent F, et al. Target Identification of an Antimalarial Oxaborole Identifies AN13762 as an Alternative Chemotype for Targeting CPSF3 in Apicomplexan Parasites. *iScience*. 2020;23(12):101871.
207. Imhof D, Anghel N, Winzer P, Balmer V, Ramseier J, Häggeli K, et al. In vitro activity, safety and in vivo efficacy of the novel bumped kinase inhibitor BKI-1748 in non-pregnant and pregnant mice experimentally infected with *Neospora caninum* tachyzoites and *Toxoplasma gondii* oocysts. *International journal for parasitology Drugs and drug resistance*. 2021;16:90-101.
208. Elkerdany ED, Elnassery SM, Arafa FM, Zaki SA, Mady RF. In vitro effect of a novel protease inhibitor cocktail on *Toxoplasma gondii* tachyzoites. *Experimental parasitology*. 2020;219:108010.
209. Doggett JS, Schultz T, Miller AJ, Bruzual I, Pou S, Winter R, et al. Orally Bioavailable Endochin-Like Quinolone Carbonate Ester Prodrug Reduces *Toxoplasma gondii* Brain Cysts. *Antimicrobial agents and chemotherapy*. 2020;64(9).
210. Leas DA, Sanford AG, Wu J, Cal M, Kaiser M, Wittlin S, et al. Diaryl Ureas as an Antiprotozoal Chemotype. *ACS infectious diseases*. 2021;7(6):1578-83.
211. Murakoshi F, Bando H, Sugi T, Adeyemi OS, Nonaka M, Nakaya T, et al. Nullscript inhibits Cryptosporidium and *Toxoplasma* growth. *International journal for parasitology Drugs and drug resistance*. 2020;14:159-66.
212. Janetka JW, Hopper AT, Yang Z, Barks J, Dhason MS, Wang Q, et al. Optimizing Pyrazolopyrimidine Inhibitors of Calcium Dependent Protein Kinase 1 for Treatment of Acute and Chronic Toxoplasmosis. *Journal of medicinal chemistry*. 2020;63(11):6144-63.
213. Zwicker JD, Smith D, Guerra AJ, Hitchens JR, Haug N, Vander Roest S, et al. Discovery and Optimization of Triazine Nitrile Inhibitors of *Toxoplasma gondii* Cathepsin L for the Potential Treatment of Chronic Toxoplasmosis in the CNS. *ACS chemical neuroscience*. 2020;11(16):2450-63.
214. Maňourová A, Chinheya IP, Kalousová M, Ruiz-Chután JA, Okafor UC, Tchoundjeu Z, et al. Domestication Potential of *Garcinia kola* Heckel (Clusiaceae): Searching for Diversity in South Cameroon. *Plants (Basel)*. 2023;12(4).
215. Manirafasha CO, R. O.; Brooks, L. N. S.; du Plessis, S.; Aboua, G. Y.;. Potential Antioxidative Effects of Kolaviron on Reproductive Function in Streptozotocin-Induced Diabetic Wistar Rats: IntechOpen; 2019.
216. Adaramoye OA. Antidiabetic effect of kolaviron, a biflavonoid complex isolated from *Garcinia kola* seeds, in Wistar rats. *Afr Health Sci*. 2012;12(4):498-506.
217. Farombi EO, Owoeye O. Antioxidative and chemopreventive properties of *Vernonia amygdalina* and *Garcinia* biflavonoid. *Int J Environ Res Public Health*. 2011;8(6):2533-55.
218. Tauchen J, Frankova A, Manourova A, Valterova I, Lojka B, Leuner O. *Garcinia kola*: a critical review on chemistry and pharmacology of an important West African medicinal plant. *Phytochem Rev*. 2023:1-47.
219. Hussein RAE-A, A.A.;. Plants Secondary Metabolites: The Key Drivers of the Pharmacological Actions of Medicinal Plants. *Herbal Medicine*. 2018: IntechOpen; 2018. p. 61866.

220. Chomel MG-L, M.; Fernandez, C.; Gallet, C.; DesRochers, A.; Paré, D.; Plant secondary metabolites, a key driver of litter decomposition and soil nutrient cycling. *Ecology*. 2016;6(104):24.
221. Dey PK, A.; Kumar, A.; Gupta, M.; Lee, B.M.; Bhakta, T.; Analysis of alkaloids (indole alkaloids, isoquinoline alkaloids, tropane alkaloids). *Recent Advances in Natural Product Analysis*. 2020;2020:51.
222. Ernawati JM, M.; Lotulung, P.D.N.; Structure Modification of Quinine on C-9 Hydroxyl Group via Esterification Reaction. *J Pure Appl Chem Res*. 2020;209(1):7.
223. Kurek J. Introductory Chapter: Alkaloids - Their Importance in Nature and for Human Life. *Alkaloids - Their Importance in Nature and Human Life*: IntechOpen; 2019. p. 66742.
224. Nisar A. Medicinal Plants and Phenolic Compounds, Phenolic Compounds - Chemistry, Synthesis. In: IntechOpen, editor. *Diversity, Non-Conventional Industrial, Pharmaceutical and Therapeutic Applications*. 2022;2022. p. 78579.
225. Albuquerque BRH, S.A.; Oliveira, M.B.P.P.; Barros, L.; Ferreira, I.C.F.R.; Phenolic compounds: current industrial applications, limitations and future challenges. *Food Function*. 2021;18(12):15.
226. Mutha RET, A.U.; Surana, S.J.; Flavonoids as natural phenolic compounds and their role in therapeutics, an overview. *Future J Pharm Sci*. 2021;20(7):25.
227. Alotaibi BSI, M.; Buabeid, M.; Kharaba, Z.J.; Yaseen, H.S.; Murtaza, G.; Therapeutic Effects and Safe Uses of Plant-Derived Polyphenolic Compounds in Cardiovascular Diseases. *Drug Des Devel Ther*. 2021;20(15):29.
228. Schoondermark-Van de Ven EM, W.; Camps, W.; Effectiveness of spiramycin for treatment of congenital Toxoplasma gondii infection in rhesus monkeys. *Antimicrobial agents and chemotherapy*. 1994;38:7.
229. Derouin FS-H, M.; Anti-toxoplasma activities of antiretroviral drugs and interactions with pyrimethamine and sulfadiazine in vitro. *Antimicrobial agents and chemotherapy*. 2000;44:3.
230. Chamberland SK, H.A.; Current, W.L.; Comparative activity of macrolides against Toxoplasma gondii demonstrating utility of an in vitro microassay. *Antimicrobial agents and chemotherapy*. 1991;35:7.
231. Van Voorhis WC. Therapy and prophylaxis of systemic protozoan infections. *Drugs*. 1990;40(1):26.
232. Desmonts G, Daffos F, Forestier F, Capella-Pavlovsky M, Thulliez P, Chartier M. Prenatal diagnosis of congenital toxoplasmosis. *Lancet* (London, England). 1985;1(8427):500-4.
233. Beckers CJ, Roos DS, Donald RG, Luft BJ, Schwab JC, Cao Y, et al. Inhibition of cytoplasmic and organellar protein synthesis in Toxoplasma gondii. Implications for the target of macrolide antibiotics. *The Journal of clinical investigation*. 1995;95(1):367-76.
234. Dao A, Fortier B. [Evaluation of the Immulite 2000 Toxoplasma quantitative IgG et Toxoplasma IgM for the diagnosis of human toxoplasmosis]. *Ann Biol Clin (Paris)*. 2001;59(2):157-64.
235. Derouin F, Piketty C, Chastang C, Chau F, Rouveix B, Pocidalo JJ. Anti-Toxoplasma effects of dapsone alone and combined with pyrimethamine. *Antimicrobial agents and chemotherapy*. 1991;35(2):252-5.
236. Nguyen BT, Stadtsbaeder S. Comparative effects of cotrimoxazole (trimethoprim-sulphamethoxazole), pyrimethamine-sulphadiazine and spiramycin during avirulent infection with Toxoplasma gondii (Beverley strain) in mice. *Br J Pharmacol*. 1983;79(4):923-8.
237. Hindosh N, Kotala R, Nguyen K, Pintor A. Trimethoprim-Sulfamethoxazole-Induced Drug Reaction With Eosinophilia and Systemic Symptoms (DRESS) Complicated by Acute Liver Failure. *Cureus*. 2022;14(10):e30852.
238. Miranda FJ, Souza DB, Frazão-Teixeira E, Oliveira FC, Melo JC, Mariano CM, et al. Experimental infection with the Toxoplasma gondii ME-49 strain in the Brazilian BR-1 mini

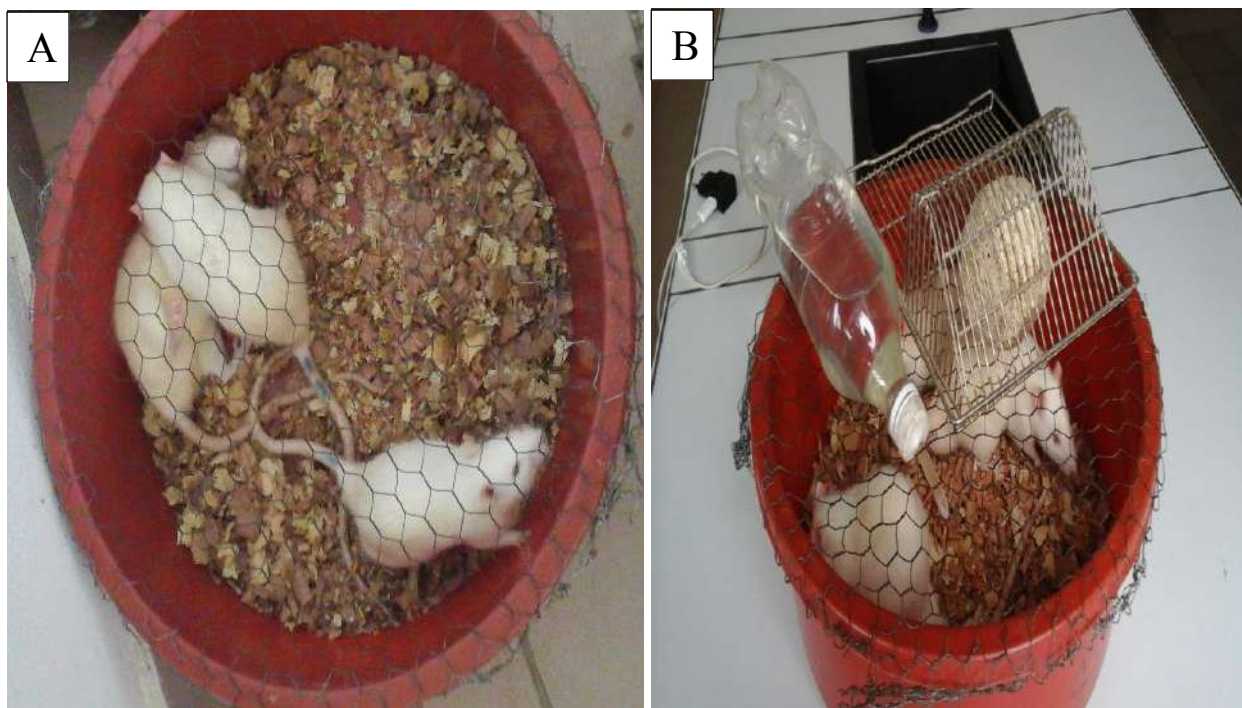
- pig is a suitable animal model for human toxoplasmosis. *Memorias do Instituto Oswaldo Cruz*. 2015;110(1):95-100.
239. Uzelac A, Klun I, Ćirković V, Djurković-Djaković O. In Vivo and In Vitro Virulence Analysis of Four Genetically Distinct *Toxoplasma gondii* Lineage III Isolates. *Microorganisms*. 2020;8(11).
240. Naik AA, Patro N, Seth P, Patro IK. Intra-generational protein malnutrition impairs temporal astrogenesis in rat brain. *Biol Open*. 2017;6(7):931-42.
241. Rodríguez-Rodríguez P, de Pablo AL, Condezo-Hoyos L, Martín-Cabrejas MA, Aguilera Y, Ruiz-Hurtado G, et al. Fetal undernutrition is associated with perinatal sex-dependent alterations in oxidative status. *J Nutr Biochem*. 2015;26(12):1650-9.
242. Seke Etet PFA, F. K.; Osman, S. Y.; Joseph, R. J.; Bushara, Y. M.; Vecchio, L.; Chijuka, J. C.; Adam, S. I. Y.; Saeed, E. M. A.; Farahna, M.; Gut Dysbiosis Clinical Indicators Associate with Body Weight Gain and Cognitive Dysfunction in High-Fat Diet-Induced Pre-obese Mice. *Journal of Diseases and Medicinal Plants*. 2016;2(3):17.
243. Djiogue S, Djiyou Djeuda AB, Seke Etet PF, Ketcha Wanda GJM, Djikem Tadah RN, Njamen D. Memory and exploratory behavior impairment in ovariectomized Wistar rats. *Behav Brain Funct*. 2018;14(1):14.
244. Iwu MM, Igoboko OA, Okunji CO, Tempesta MS. Antidiabetic and aldose reductase activities of biflavanones of *Garcinia kola*. *J Pharm Pharmacol*. 1990;42(4):290-2.
245. Zingue S, Foyet HS, Djiogue S, Ezo'o Ezo'o Y, Abaïssou HHN, Fachagbo P, et al. Effects of *Ficus umbellata* (Moraceae) Aqueous Extract and 7-Methoxycoumarin on Scopolamine-Induced Spatial Memory Impairment in Ovariectomized Wistar Rats. *Behav Neurol*. 2018;2018:5751864.
246. Mendes CS, Bartos I, Márka Z, Akay T, Márka S, Mann RS. Quantification of gait parameters in freely walking rodents. *BMC biology*. 2015;13:50.
247. Sugimoto H, Kawakami K. Low-cost Protocol of Footprint Analysis and Hanging Box Test for Mice Applied the Chronic Restraint Stress. *Journal of visualized experiments : JoVE*. 2019(143).
248. Elwell MR, Frenkel JK. Acute toxoplasmosis in hamsters and mice: measurement of pathogenicity by fever and weight loss. *Am J Vet Res*. 1984;45(12):2663-7.
249. Hatter JA, Kouche YM, Melchor SJ, Ng K, Bouley DM, Boothroyd JC, et al. Toxoplasma gondii infection triggers chronic cachexia and sustained commensal dysbiosis in mice. *PloS one*. 2018;13(10):e0204895.
250. Friesema IHM, Hofhuis A, Hoek-van Deursen D, Jansz AR, Ott A, van Hellemond JJ, et al. Risk factors for acute toxoplasmosis in the Netherlands. *Epidemiology and infection*. 2023;151:e95.
251. Singh B, Debrah LB, Acheampong G, Debrah AY. Seroprevalence and Risk Factors of *Toxoplasma gondii* Infection among Pregnant Women in Kumasi: A Cross-Sectional Study at a District-Level Hospital, Ghana. *Infect Dis Obstet Gynecol*. 2021;2021:6670219.
252. Masi T, Patel BM. Altered glucose metabolism and insulin resistance in cancer-induced cachexia: a sweet poison. *Pharmacol Rep*. 2021;73(1):17-30.
253. Delano MJ, Moldawer LL. The origins of cachexia in acute and chronic inflammatory diseases. *Nutr Clin Pract*. 2006;21(1):68-81.
254. Yildiz AE, Ariyurek MO, Karcaaltincaba M. Splenic anomalies of shape, size, and location: pictorial essay. *ScientificWorldJournal*. 2013;2013:321810.
255. Magid D, Fishman EK, Siegelman SS. Computed tomography of the spleen and liver in sickle cell disease. *AJR American journal of roentgenology*. 1984;143(2):245-9.
256. McGavern DB, Zoecklein L, Drescher KM, Rodriguez M. Quantitative assessment of neurologic deficits in a chronic progressive murine model of CNS demyelination. *Exp Neurol*. 1999;158(1):171-81.
257. Hausdorff JM. Gait dynamics in Parkinson's disease: common and distinct behavior among stride length, gait variability, and fractal-like scaling. *Chaos*. 2009;19(2):026113.

258. Carter RJ, Lione LA, Humby T, Mangiarini L, Mahal A, Bates GP, et al. Characterization of progressive motor deficits in mice transgenic for the human Huntington's disease mutation. *The Journal of neuroscience : the official journal of the Society for Neuroscience*. 1999;19(8):3248-57.
259. Navarro JF, Burón E, Martín-López M. Anxiolytic-like activity of SB-205384 in the elevated plus-maze test in mice. *Psicothema*. 2006;18(1):100-4.
260. Casarrubea M, Roy V, Sorbera F, Magnusson MS, Santangelo A, Arabo A, et al. Temporal structure of the rat's behavior in elevated plus maze test. *Behavioural brain research*. 2013;237:290-9.
261. Biedermann SV, Biedermann DG, Wenzlaff F, Kurjak T, Nouri S, Auer MK, et al. An elevated plus-maze in mixed reality for studying human anxiety-related behavior. *BMC biology*. 2017;15(1):125.
262. Ennaceur A. Open space anxiety test in rodents: the elevated platform with steep slopes. *Methods in molecular biology (Clifton, NJ)*. 2012;829:177-91.
263. Rico JL, Muñoz-Tabares LF, Lamprea MR, Hurtado-Parrado C. Diazepam Reduces Escape and Increases Closed-Arms Exploration in Gerbils After 5 min in the Elevated Plus-Maze. *Front Psychol*. 2019;10:748.
264. Arabo A, Potier C, Ollivier G, Lorivel T, Roy V. Temporal analysis of free exploration of an elevated plus-maze in mice. *J Exp Psychol Anim Learn Cogn*. 2014;40(4):457-66.
265. Holly KS, Orndorff CO, Murray TA. MATSAP: An automated analysis of stretch-attend posture in rodent behavioral experiments. *Scientific reports*. 2016;6:31286.
266. Sturman O, Germain PL, Bohacek J. Exploratory rearing: a context- and stress-sensitive behavior recorded in the open-field test. *Stress*. 2018;21(5):443-52.
267. Vuralli D, Wattiez AS, Russo AF, Bolay H. Behavioral and cognitive animal models in headache research. *The journal of headache and pain*. 2019;20(1):11.
268. Castanheira L, Ferreira MF, Sebastião AM, Telles-Correia D. Anxiety Assessment in Pre-clinical Tests and in Clinical Trials: A Critical Review. *Curr Top Med Chem*. 2018;18(19):1656-76.
269. Sengupta T, Ghosh S, Gaur TA, Nayak P. Dissimilar Anxiety-like Behavior in Prepubertal and Young Adult Female Rats on Acute Exposure to Aluminium. *Cent Nerv Syst Agents Med Chem*. 2021;21(3):187-94.
270. Rodgers RJ, Cole JC. Anxiety enhancement in the murine elevated plus maze by immediate prior exposure to social stressors. *Physiol Behav*. 1993;53(2):383-8.
271. Torres-Lista V, Parrado-Fernández C, Alvarez-Montón I, Frontiñán-Rubio J, Durán-Prado M, Peinado JR, et al. Neophobia, NQO1 and SIRT1 as premorbid and prodromal indicators of AD in 3xTg-AD mice. *Behavioural brain research*. 2014;271:140-6.
272. Veloso AG, BL; Celio, PE;. Modulation of grooming behavior in rats by different test situations. *Psychology & Neuroscience*. 2016;9(1):14.
273. Rojas-Carvajal M, Brenes JC. Acute stress differentially affects grooming subtypes and ultrasonic vocalisations in the open-field and home-cage test in rats. *Behav Processes*. 2020;176:104140.
274. Fuglewicz AJ, Piotrowski P, Stodolak A. Relationship between toxoplasmosis and schizophrenia: A review. *Adv Clin Exp Med*. 2017;26(6):1031-6.
275. El-Lakany MA, Fouda MA, El-Gowelli HM, El-Gowilly SM, El-Mas MM. Gonadal hormone receptors underlie the resistance of female rats to inflammatory and cardiovascular complications of endotoxemia. *Eur J Pharmacol*. 2018;823:41-8.
276. Klein SL, Flanagan KL. Sex differences in immune responses. *Nat Rev Immunol*. 2016;16(10):626-38.
277. Lekutis C, Ferguson DJ, Grigg ME, Camps M, Boothroyd JC. Surface antigens of Toxoplasma gondii: variations on a theme. *International journal for parasitology*. 2001;31(12):1285-92.

278. Manger ID, Hehl AB, Boothroyd JC. The surface of Toxoplasma tachyzoites is dominated by a family of glycosylphosphatidylinositol-anchored antigens related to SAG1. *Infection and immunity*. 1998;66(5):2237-44.
279. Rolls ET. The cingulate cortex and limbic systems for emotion, action, and memory. *Brain Struct Funct*. 2019;224(9):3001-18.
280. Bian XL, Qin C, Cai CY, Zhou Y, Tao Y, Lin YH, et al. Anterior Cingulate Cortex to Ventral Hippocampus Circuit Mediates Contextual Fear Generalization. *The Journal of neuroscience : the official journal of the Society for Neuroscience*. 2019;39(29):5728-39.
281. Yin L, Zhang J, Ma H, Zhang X, Fan Z, Yang Y, et al. Selective activation of cholinergic transmission from the medial septal nucleus to hippocampal pyramidal neurones improves sepsis-induced cognitive deficits in mice. *Br J Anaesth*. 2023;130(5):573-84.
282. Lee DJ, Gurkoff GG, Izadi A, Berman RF, Ekstrom AD, Muizelaar JP, et al. Medial septal nucleus theta frequency deep brain stimulation improves spatial working memory after traumatic brain injury. *J Neurotrauma*. 2013;30(2):131-9.
283. Whitlock JR. Posterior parietal cortex. *Current biology : CB*. 2017;27(14):R691-r5.
284. Tortorella S, Rodrigo-Angulo ML, Núñez A, Garzón M. Synaptic interactions between perifornical lateral hypothalamic area, locus coeruleus nucleus and the oral pontine reticular nucleus are implicated in the stage succession during sleep-wakefulness cycle. *Frontiers in neuroscience*. 2013;7:216.
285. Kumar S, Szymusiak R, Bashir T, Rai S, McGinty D, Alam MN. Effects of serotonin on perifornical-lateral hypothalamic area neurons in rat. *The European journal of neuroscience*. 2007;25(1):201-12.
286. Kim J, Augustine GJ. Molecular Layer Interneurons: Key Elements of Cerebellar Network Computation and Behavior. *Neuroscience*. 2021;462:22-35.
287. Nicholson CL, Coubes P, Poulen G. Dentate nucleus as target for deep brain stimulation in dystono-dyskinetic syndromes. *Neurochirurgie*. 2020;66(4):258-65.
288. Albert M, Barrantes-Freer A, Lohrberg M, Antel JP, Prineas JW, Palkovits M, et al. Synaptic pathology in the cerebellar dentate nucleus in chronic multiple sclerosis. *Brain Pathol*. 2017;27(6):737-47.
289. Kok FK, van Leerdam SL, de Lange ECM. Potential Mechanisms Underlying Resistance to Dementia in Non-Demented Individuals with Alzheimer's Disease Neuropathology. *J Alzheimers Dis*. 2022;87(1):51-81.
290. Dukkipati SS, Garrett TL, Elbasiouny SM. The vulnerability of spinal motoneurons and soma size plasticity in a mouse model of amyotrophic lateral sclerosis. *J Physiol*. 2018;596(9):1723-45.
291. Iacono D, O'Brien R, Resnick SM, Zonderman AB, Pletnikova O, Rudow G, et al. Neuronal hypertrophy in asymptomatic Alzheimer disease. *J Neuropathol Exp Neurol*. 2008;67(6):578-89.
292. Kurt-Celep İ, Zengin G, Uba AI, Caprioli G, Mustafa AM, Angeloni S, et al. Unraveling the chemical profile, antioxidant, enzyme inhibitory, cytotoxic potential of different extracts from *Astragalus caraganae*. *Arch Pharm (Weinheim)*. 2023;356(9):e2300263.
293. Cardona GW, Robledo S, Alzate F, Yepes AF, Hernandez C, Velez ID, et al. Antileishmanial and cytotoxic activities of four Andean plant extracts from Colombia. *Veterinary world*. 2020;13(10):2178-82.
294. Rufa'i FA, Baecker D, Mukhtar MD. Phytochemical Screening, GC-MS Analysis, and Evaluating In Vivo Antitrypanosomal Effects of a Methanolic Extract of Garcinia kola Nuts on Rats. *Antibiotics (Basel)*. 2023;12(4).
295. Kraus L, Hetsch F, Schneider UC, Radbruch H, Holtkamp M, Meier JC, et al. Dimethylethanolamine Decreases Epileptiform Activity in Acute Human Hippocampal Slices in vitro. *Front Mol Neurosci*. 2019;12:209.

296. Tammenmaa-Aho I, Asher R, Soares-Weiser K, Bergman H. Cholinergic medication for antipsychotic-induced tardive dyskinesia. *Cochrane Database Syst Rev*. 2018;3(3):Cd000207.
297. Smaga I, Fierro D, Mesa J, Filip M, Knackstedt LA. Molecular changes evoked by the beta-lactam antibiotic ceftriaxone across rodent models of substance use disorder and neurological disease. *Neuroscience and biobehavioral reviews*. 2020;115:116-30.
298. Yimer EM, Hishe HZ, Tuem KB. Repurposing of the β -Lactam Antibiotic, Ceftriaxone for Neurological Disorders: A Review. *Frontiers in neuroscience*. 2019;13:236.

ANNEXES



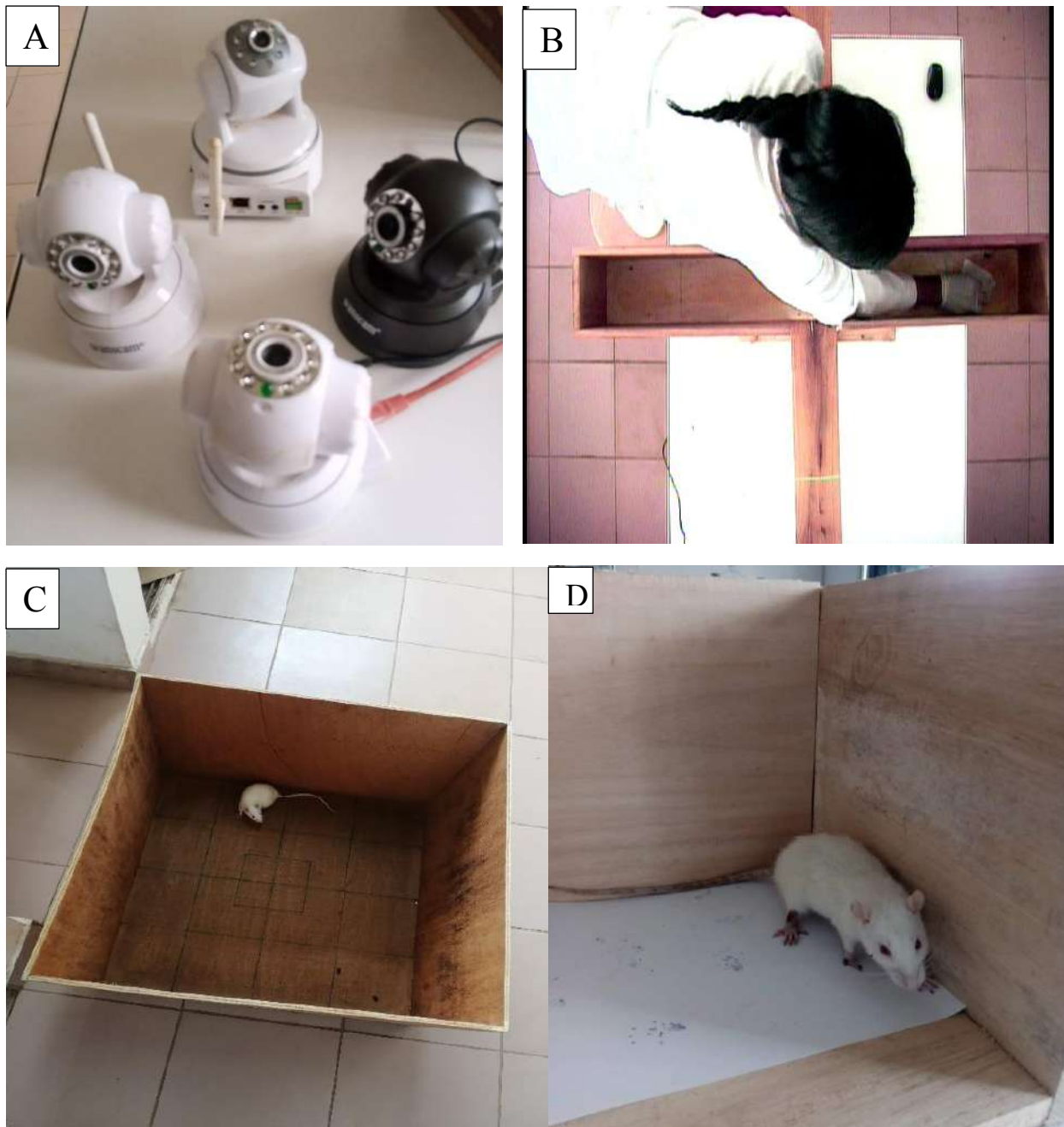
Annex 1: Wistar rats in their cages (source: present work)

A: Animals in their cage; **B:** Feeding of animals



Annex 2: Preparation of Wistar rats feed (source: present work)

A/B: Preparation of animal's feed



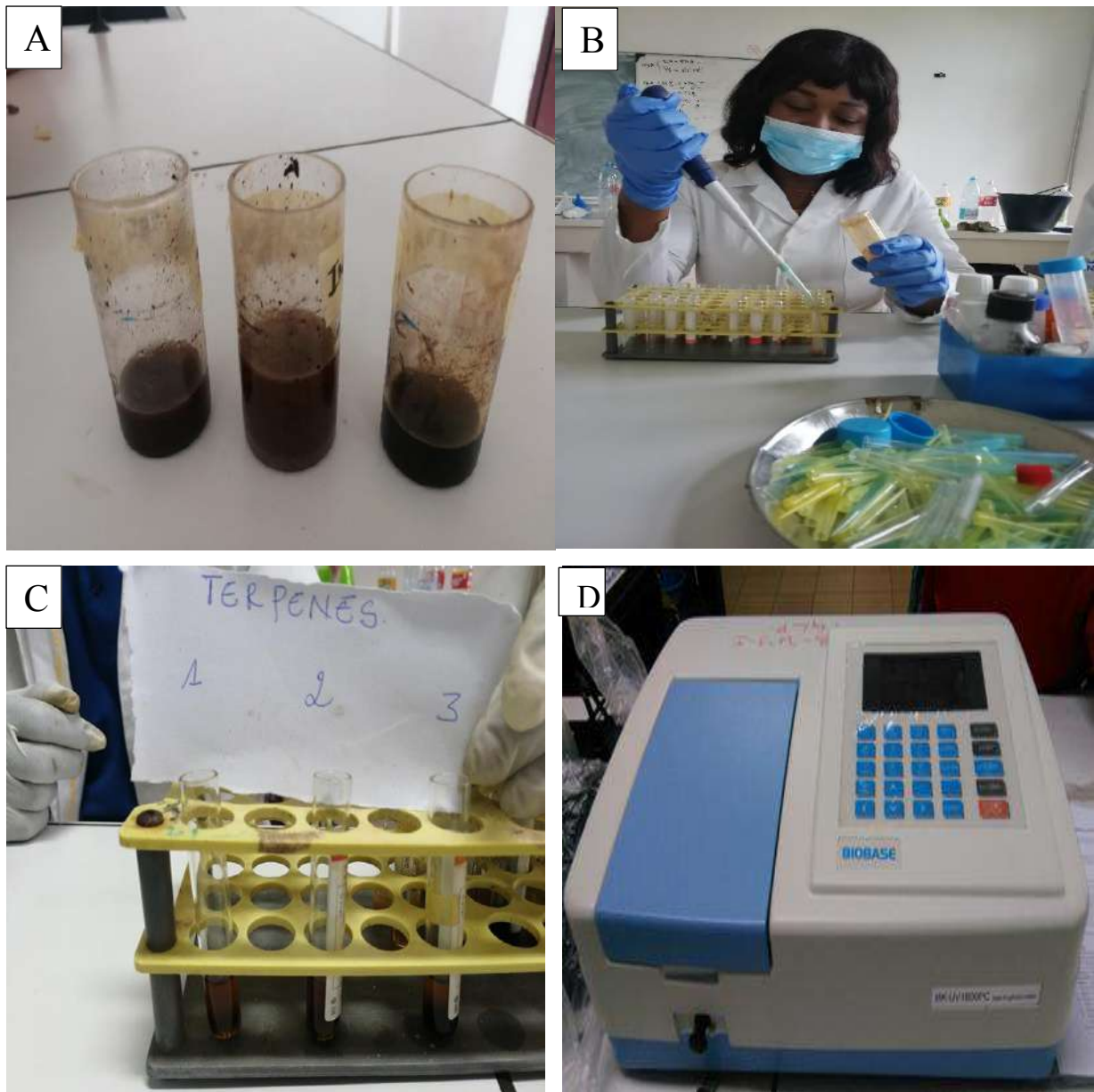
Annex 3: Ethological test setting (source: present work)

A: Infrared cameras; B: EPM process; C: OFT process; D: Foot print analysis.



Annex 4: Plant extraction (source: present work)

A: *Garcinia kola* seeds; **B:** Decantation ball; **C:** Rotatory evaporator; **D:** Soxhlet.



Annex 5: Phytochemical screening (source: present work)

A: Fractions of the methanolic extract of G.K; B/C: Qualitative analysis; D: Spectrophotometer

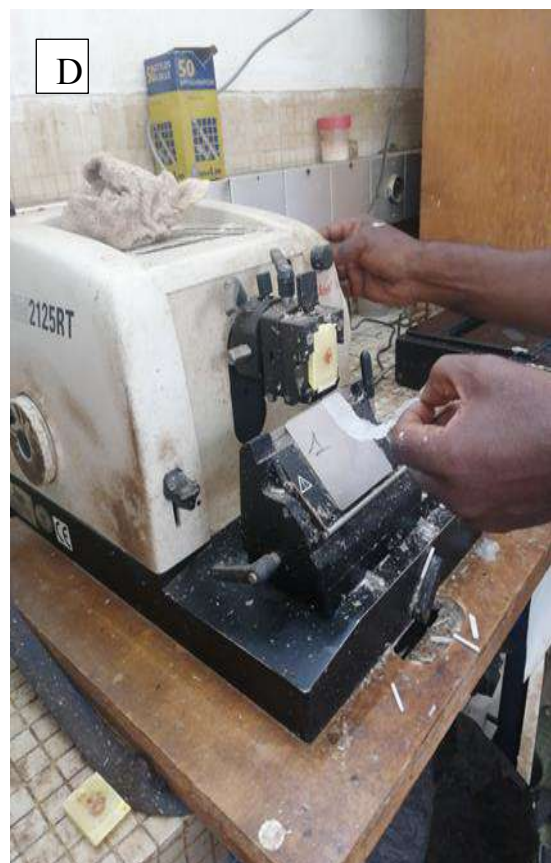
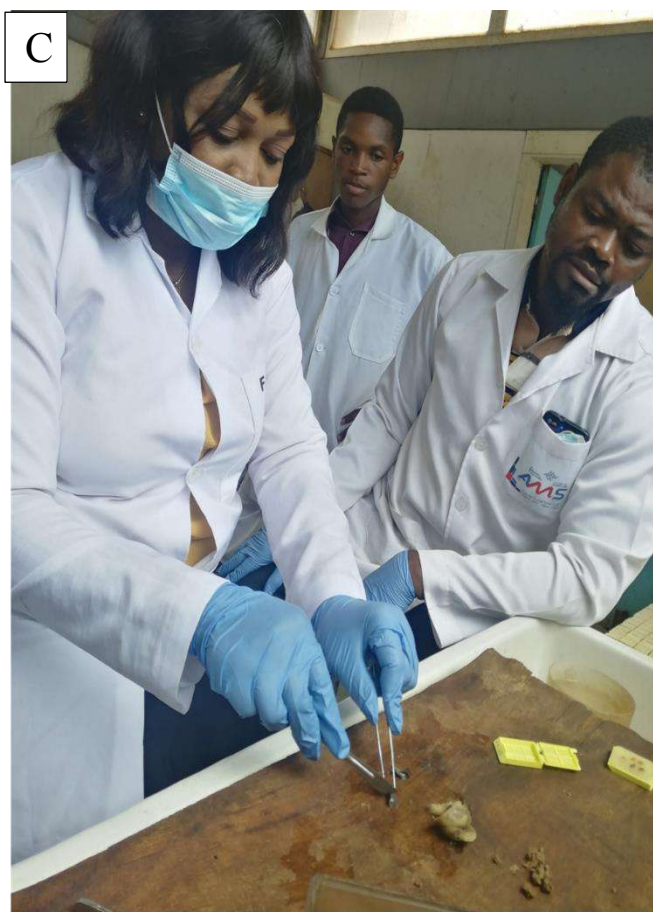
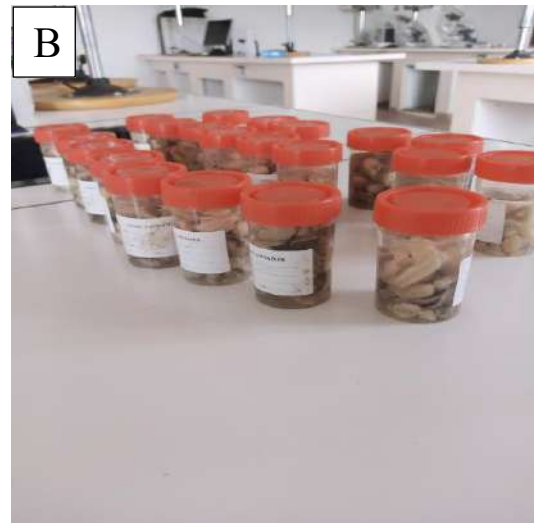


Annex 6: Animal treatment by gavage (source: present work)



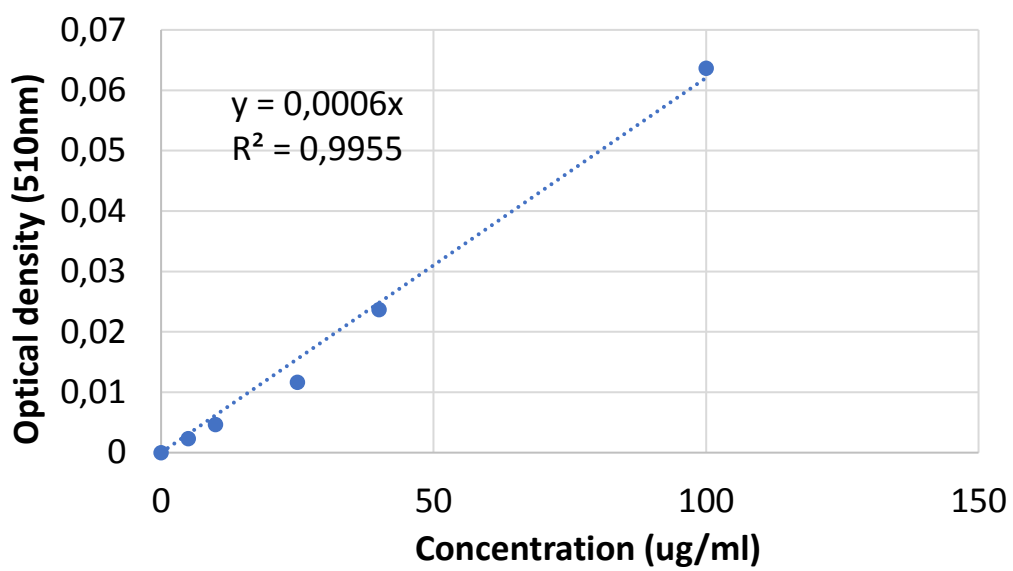
Annex 7: Rat sacrifice, blood and organ collection (source: present work)

A: Intracardiac puncture; **B:** Organs collected

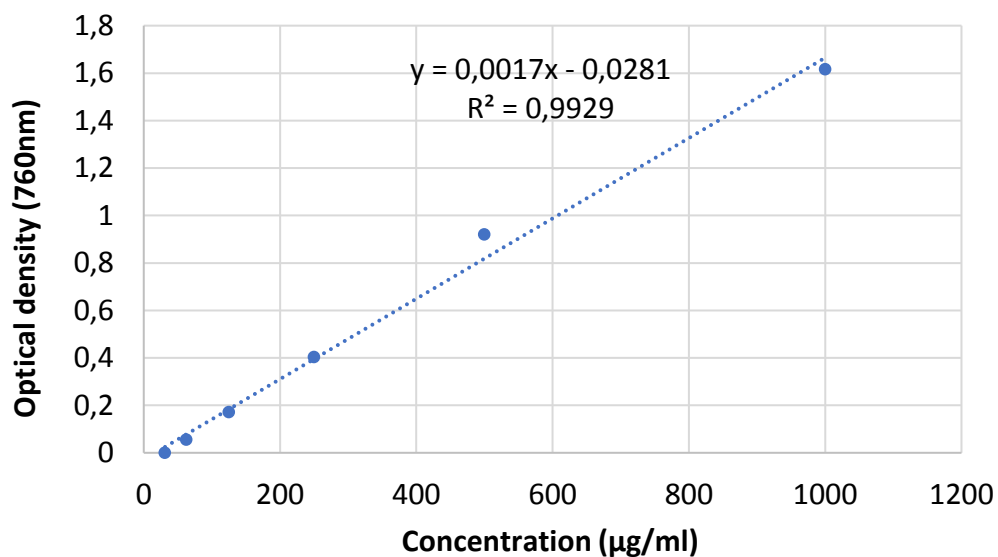


Annex 8: Histopathological analysis (source: present work)

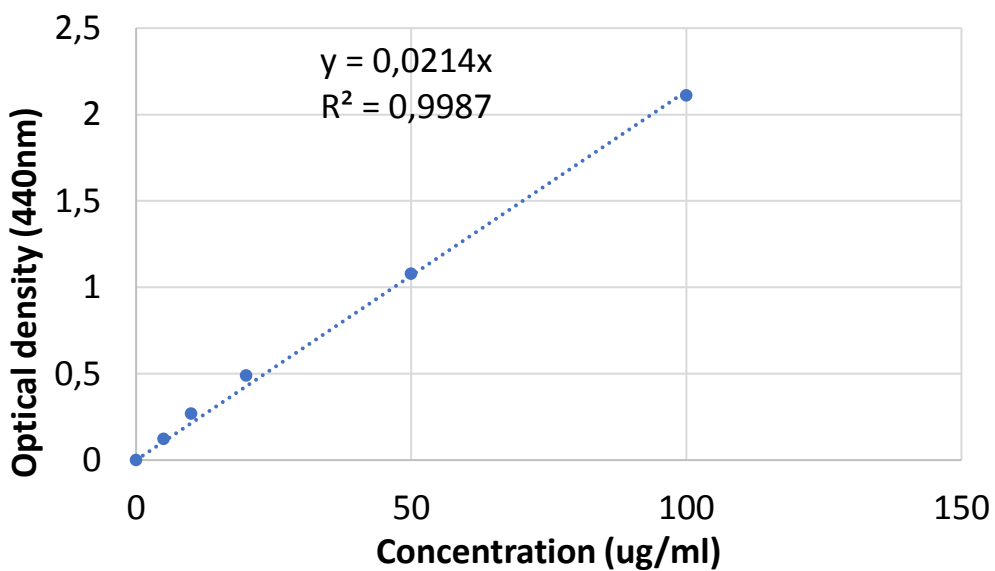
A: weighing of organs; **B:** Organ's storage; **C:** Macroscopic trimming; **D:** Microtome sectioning



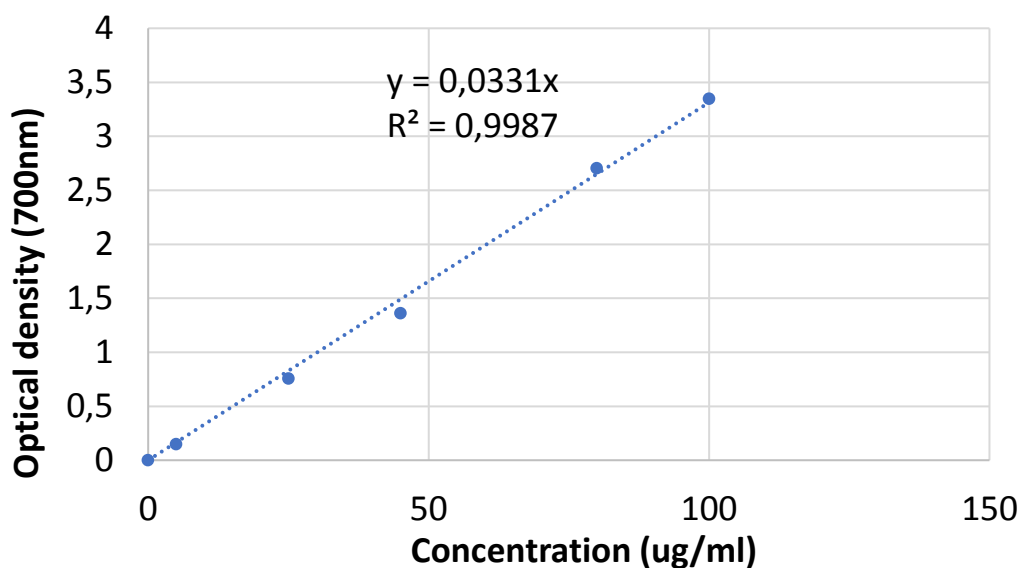
Annex 9: Standard curve for flavonoid compounds



Annex 10: Standard curve for polyphenolic compounds (gallic acid)



Annex 11: Standard curve for total flavanol content (quercetin)



Annex 12: Standard curve for total tannin content

Annex 13. Reactant calibration for flavonoid quantification

Reactants	Calibration						Blanc	Test
	1	2	3	4	5	6		
Extract 100µg/mL(mL)								0.1
Concentration in standard (µg/mL)	0	5	10	25	40	100		
Standard 100µg/µL(µL)	0	40	80	200	320	800		
Distilled water(mL)	0.8	0.760	0.720	0.600	0.480	0	0.4	0.3
NaNO ₃ , 5%(mL)	0.06	0.06	0.06	0.06	0.06	0.06	0.03	0.03
After 5 min of incubation at standard temperature								
AlCl ₃ , 10%(mL)	0.06	0.06	0.06	0.06	0.06	0.06	0.06	0.06
After 1 min of incubation at standard temperature								
NaOH 1mM(mL)	0.4	0.4	0.4	0.4	0.4	0.4	0.4	0.4
Distilled water (mL)	2	2	2	2	2	2	2	2
Shake and read the DO at 510nm								

Annex 14. Reactant calibration for flavanol quantification

Reactants	Calibration						blanc	test
	1	2	3	4	5	6		
Extract 100µg/mL(mL)								1
Concentration of standard (µg/mL)	0	5	10	20	50	100		
Standard 100 µg/mL(mL)		0.05	0.1	0.2	0.5	1.0		
Distilled water (mL)	1	0.95	0.9	0.8	0.5	0		
Ethanol AlCl ₃ , 2%(mL)	1	1	1	1	1	1	1	1
CH ₃ COONa 50g/L(mL)	1	1	1	1	1	1	1	1

After two and half hours of incubating at +20°C, read the absorbance at 440nm

Annex 15. Reactant calibration for polyphenolic compounds' quantification

Reactants	Calibration						blanc	test
	1	2	3	4	5	6		
Extract 1mg.mL(mL)								0.2
Gallic acid 1mg/mL(µL)	0	5	15	20	40	60		
Distilled water (mL)	0.2	0.195	0.185	0.180	0.160	0.140	0.2	
Folin-Ciocalteu 1/10 reagent (mL)	0.8	0.8	0.8	0.8	0.8	0.8	0.8	0.8
Na ₂ CO ₃ (mL)	2	2	2	2	2	2	2	2
Shake and keep away from sunlight for 2hours and measure the DO at 765m								

BRAIN COMMUNICATIONS

Garcinia kola improves cognitive and motor function of a rat model of acute radiation syndrome in the elevated plus maze

Nene Ahidjo,^{1,2,3} Leonard Ngarka,^{1,3,4} Paul F. Seke Etet,^{3,5,6} Wepnyu Y. Njamnshi,^{1,2,3} Leonard N. Nfor,^{1,3,4} Michel K. Mengnjo,^{1,3,4} Jonas G. Basseguin Atchou,^{1,3,7} Edmond N. Mouofo,¹ Godwin Y. Tatah,^{1,3,8} Faustin Dong A Zok,⁹ Bonaventure T. Ngadjui,¹⁰ Wilfred Ngwa¹¹ and Alfred K. Njamnshi^{1,2,3,4}

We reported recently that the elevated plus maze is a good tool for evaluating cognitive and motor functional changes in gamma-irradiated rats as a model for new drug evaluation and monitoring. The capacity of *Garcinia kola* to mitigate radiation-induced brain injury is currently unknown. We therefore assessed the effects of the neuroprotective medicinal plant *Garcinia kola*, on the cognitive and motor changes in this murine model of acute radiation syndrome. Wistar rats exposed once to an ionizing dose of Tc99m-generated Gamma radiation were treated with an ethyl acetate fraction of methanolic extract of *Garcinia kola* seeds (content of 100 mg/kg of extract) for 9 weeks. Cognitive and motor function indicators were assessed in the elevated plus maze in these animals and compared with irradiated control groups (vitamin C- and vehicle-treated groups) and the non-irradiated control rats. The irradiated control group displayed cachexia, shaggy and dirty fur, porphyrin deposits around eyes, decreased exploratory activity, reduced social interactions and a loss of thigmotaxis revealed by a marked decrease in rearing episodes and stretch attend posture episodes close to the walls of elevated plus maze closed arm, an increased central platform time, and decreases in open arm time and entries. This group further displayed a decrease in head dips and grooming episodes. Treatment with *Garcinia kola*, and in a lesser extent vitamin C, significantly prevented the body weight loss ($P < 0.001$) and mitigated the development of elevated plus maze signs of cognitive and motor affections observed in the irradiated control group ($P < 0.05$). Altogether, our data suggest for the first time that *Garcinia kola* seeds have protective properties against the development of cognitive and motor decline in the acute radiation syndrome-like context. Future studies are warranted to characterize the molecular mechanisms and neuronal networks of this action.

1 Neuroscience Laboratory, Faculty of Medicine and Biomedical Sciences, The University of Yaoundé I, Yaoundé, Cameroon

2 Brain Research Africa Initiative (BRAIN), Geneva, Switzerland

3 Brain Research Africa Initiative (BRAIN), Yaoundé, Cameroon

4 Department of Neurology, Yaoundé Central Hospital, Yaoundé, Cameroon

5 Center for Sustainable Health and Development, Garoua, Cameroon

6 Department of Physiological Sciences and Biochemistry, University of Ngaoundéré, Garoua, Cameroon

7 Department of Psychiatry, Yaoundé Military Hospital, Yaoundé, Cameroon

8 Department of Neurology, CH Saint-Nazaire, Saint-Nazaire, France

9 Radiotherapy Unit, Yaoundé General Hospital, Yaoundé, Cameroon

10 Department of Pharmacology and Traditional Medicine, Faculty of Medicine and Biomedical Sciences, The University of Yaoundé I, Yaoundé, Cameroon

11 Department of Radiation Oncology, Brigham and Women's Hospital, Dana Farber Cancer Institute, Harvard Medical School, Boston, MA, USA

Accepted June 21, 2021

© The Author(s) (2021). Published by Oxford University Press on behalf of the Guarantors of Brain.

This is an Open Access article distributed under the terms of the Creative Commons Attribution License (<http://creativecommons.org/licenses/by/4.0/>), which permits unrestricted reuse, distribution, and reproduction in any medium, provided the original work is properly cited.

Characterization of the Cognitive and Motor Changes Revealed by the Elevated Plus Maze in an Experimental Rat Model of Radiation-Induced Brain Injury

Abstract

Background: Experimental models are needed to better understand the pathophysiology of neurodegenerative diseases to develop novel therapeutics. The neuropathology and clinical signs of acute radiation syndrome resemble those of neurodegenerative conditions. We characterized elevated plus maze (EPM) indicators of cognitive and motor impairment in rats exposed to brain-damaging doses of gamma radiation to develop a model for neurological component of the acute radiation syndrome. **Materials and Methods:** Technetium 99 m was administered once through tail vein to male Wistar rats to reach an absorbed dose of Gamma radiation of 667 mGy (66.7Rad). Animal performance in the EPM was assessed every 14 days. Rats were observed for 9 weeks for the occurrence of systemic and neurological signs. Comparisons were done between irradiated and nonirradiated rats, and in each group with baseline performance. **Results:** EPM indicators of cognitive and motor impairment, anxiety, and depression were observed concomitantly and increased with the severity of acute radiation syndrome-like systemic and neurological signs. Alterations in EPM indicators appeared 3 weeks postirradiation and their severity increased with time. Notably, arm transitions and the distance covered in the maze were decreased (-56.71% and -73.62% , $P < 0.001$), as well as open arm entries and time spent in open arms (-77.78% and -76.19% , $P < 0.05$) and the indicator of thigmotaxis rearing (-92.45 , $P < 0.001$). **Conclusions:** Our results suggest that irradiated rat performance in the EPM paradigm reflects disease severity and could be used to perform both acute and subchronic pharmacological studies in acute radiation syndrome-like diseases in rats.

Keywords: Anxiety, acute radiation syndrome, cognitive dysfunction, depression, elevated plus maze, gamma rays, rats

Introduction

Although neurodegenerative and vascular brain diseases have the largest proportion of disability-adjusted life years globally and despite their rising incidence in low- and middle-income countries,^[1,2] their causative factors are still poorly understood. More investigations and experimental models are needed to better understand the neuropathophysiology of these diseases which confer risks for each other and share some common protective and risk factors.^[2-5] Furthermore, neurodegenerative and vascular brain diseases also share some neurological semiology resulting from endothelial pathology, blood-brain barrier dysfunction, neuroinflammation, and related neuronal loss.^[2-7]

Human accidental exposure to ionizing radiations may induce a neurotoxicity syndrome marked by an inflammation-mediated encephalopathy and other intractable debilitating and life-threatening pathologies shared by neurodegenerative disorders and ischemic brain diseases.^[8,9] Comparable alterations have been reported in experimental exposure to these radiations.^[4-7] In large amounts, agents-emitting gamma radiations such as the commonly used imaging agent, technetium 99 m (Tc99 m) have been reported to cause brain damage.^[10,11]

Changes in rodent exploratory behavior following experimental radiation-induced brain injury were reported in various studies using ethological tests, and particularly

This is an open access journal, and articles are distributed under the terms of the Creative Commons Attribution-NonCommercial-ShareAlike 4.0 License, which allows others to remix, tweak, and build upon the work non-commercially, as long as appropriate credit is given and the new creations are licensed under the identical terms.

For reprints contact: WIKHLPMedknow_reprints@woltersluwer.com

How to cite this article: Njamnshi AK, Ahidjo N, Ngarka L, Nfor LN, Mengnjo MK, Njamnshi WY, et al. Characterization of the cognitive and motor changes revealed by the elevated plus maze in an experimental rat model of radiation-induced brain injury. *Adv Biomed Res* 2020;9:72.

Alfred K. Njamnshi^{1,2,3},
Nene Ahidjo^{1,2,3},
Leonard Ngarka^{1,2,3,4},
Leonard N. Nfor^{1,2,3,4},
Michel K. Mengnjo^{1,2,3,4},
Wepnyu Y. Njamnshi^{1,2,3},
Jonas Guy Bassegouin Atchou^{1,2,3},
Godwin Y. Tatah^{1,2,3,4},
Louis M. Mbaku⁵,
Faustin Dong A Zok⁶,
Paul F. Seke Ete^{2,3,7,8}

¹Department of Neuroscience,
Faculty of Medicine & Biomedical Sciences, Neuroscience Laboratory,

The University of Yaoundé I,
Yaoundé, Cameroon, ²Department of

Translational Neuroscience, Brain
Research Africa Initiative (BRAIN),
Geneva, Switzerland, ³Department

of Translational Neuroscience, Brain
Research Africa Initiative (BRAIN),
Yaoundé, Cameroon, ⁴Department of

Neurology Yaoundé Central Hospital,
⁵Department of Veterinary Medicine,
Ministry of Livestock, Fisheries and

Animal Industries, ⁶Department of
Radiotherapy, Yaoundé General
Hospital, Yaoundé, ⁷Center for

Sustainable Health and Development,
⁸Department of Physiological

Sciences and Biochemistry, University

of Ngawandé, Garoua, Cameroon

Address for correspondence:
Prof. Alfred K. Njamnshi,
Faculty of Medicine & Biomedical
Sciences, Neuroscience Laboratory,
The University of Yaoundé I
and Brain Research Africa
Initiative (BRAIN), P.O. Box: 25625,
Yaoundé, Cameroon.
E-mail: alfred.njamnshi@brainafrica.org;
alfrednjamnshi@gmail.com

Received: 26 March 2020

Revised: 25 April 2020

Accepted: 10 May 2020

Published: 28 November 2020

Access this article online

Website: www.advbioresearch.net

DOI: 10.4103/abr.abr_62_20

Quick Response Code:



Annex 18. Published article 3



Therapeutic potential of *Garcinia kola* against experimental toxoplasmosis in rats

Nene Ahidjo,^{1,2} Frederic Maidawa Yaya,^{2,3} Wepnyu Y. Njamnshi,^{1,2} Judith C. Rissia-Ngo Pambe,⁴ Ethel W. Ndianteng,² Caroline N. C. Nwasike,² Christelle Kemmo,² Arnaud C. Choupo,⁵ Luc Yvan Meka'a Zang,² Anatole C. Pieme,⁵ Lorella Vecchio,^{1,3} Bonaventure T. Ngadjui,⁶ Alfred K. Njamnshi^{1,2,†} and Paul F. Seke Etet^{1,2,3,†}

† These authors contributed equally to this work.

Cerebral toxoplasmosis, the most common opportunistic infection in immunocompromised individuals, is increasingly reported in immunocompetent individuals due to mutant strains of *Toxoplasma gondii*, which, furthermore, are reported to be resistant to available treatments. We assessed the therapeutic potential of *Garcinia kola*, a medicinal plant reported to have antiplasmodial and neuroprotective properties, against experimental toxoplasmosis in rats. Severe toxoplasmosis was induced in male Wistar rats (156.7 ± 4.1 g) by injecting them with 10 million tachyzoites in suspension in 500 µl of saline (intraperitoneal), and exclusive feeding with a low-protein diet [7% protein (weight by weight)]. Then, animals were treated with hexane, dichloromethane, and ethyl acetate fractions of *Garcinia kola*. Footprints were analysed and open-field and elevated plus maze ethological tests were performed when symptoms of severe disease were observed in the infected controls. After sacrifice, blood samples were processed for Giemsa staining, organs were processed for haematoxylin and eosin staining, and brains were processed for Nissl staining and cell counting. Compared with non-infected animals, the infected control animals had significantly lower body weights (30.27%, $P = 0.001$), higher body temperatures ($P = 0.033$) during the sacrifice, together with signs of cognitive impairment and neurologic deficits such as lower open-field arena centre entries ($P < 0.001$), elevated plus maze open-arm time ($P = 0.029$) and decreased stride lengths and step widths ($P < 0.001$), as well as neuronal loss in various brain areas. The ethyl acetate fraction of *Garcinia kola* prevented or mitigated most of these signs. Our data suggest that the ethyl acetate fraction of *Garcinia kola* has therapeutic potential against cerebral toxoplasmosis.

1 Brain Research Africa Initiative (BRAIN), Yaoundé, Cameroon

2 Faculty of Medicine and Biomedical Sciences, Neuroscience Laboratory, The University of Yaoundé I, Yaoundé, Cameroon

3 Department of Physiological Sciences and Biochemistry, Faculty of Medicine and Biomedical Sciences, Center for Sustainable Health and Development, University of Garoua, Garoua, Cameroon

4 Department of Morphological Sciences and Pathological Anatomy, Faculty of Medicine and Biomedical Sciences, University of Garoua, Garoua, Cameroon

5 Faculty of Medicine and Biomedical Sciences, Laboratory of Biochemistry, University of Yaoundé I, Yaoundé, Cameroon

6 Department of Organic Chemistry, The University of Yaoundé I, Yaoundé, Cameroon

Correspondence to: Paul F. Seke Eter

Department of Physiological Sciences and Biochemistry, FMBS

University of Garoua, P.O. Box 317, Garoua, Cameroon

E-mail: paul.seke@gmail.com

Downloaded from https://academic.oup.com/braincomms/article/6/4/fca255 by guest on 11 August 2024

Received December 28, 2023. Revised June 19, 2024. Accepted August 3, 2024. Advance access publication August 6, 2024

© The Author(s) 2024. Published by Oxford University Press on behalf of the Guarantors of Brain.

This is an Open Access article distributed under the terms of the Creative Commons Attribution License (<https://creativecommons.org/licenses/by/4.0/>), which permits unrestricted reuse, distribution, and reproduction in any medium, provided the original work is properly cited.

Annex 19. Ethical clearance

UNIVERSITÉ DE YAOUNDÉ I
FACULTÉ DE MÉDECINE ET DES SCIENCES BIOMÉDICALES
COMITÉ INSTITUTIONNEL D'ÉTHIQUE DE LA RECHERCHE
Tel/ fax : 22 31-05-86 22 311224
Email: deconat/fmsb@hotmail.com
Ref. : N° 0634/UY1/FMSB/ICER/DAASR/CSD



THE UNIVERSITY OF YAOUNDE I
FACULTY OF MEDICINE AND BIOMEDICAL SCIENCES
INSTITUTIONAL ETHICAL REVIEW BOARD

08 FEV 2014

CLAIRANCE ÉTHIQUE

Le COMITÉ INSTITUTIONNEL D'ÉTHIQUE DE LA RECHERCHE (CIER) de la FMSB a examiné

La demande de la clairance éthique soumise par :

M.Mme : NENE AHIDJO

Matricule: 09M120

Travaillant sous la direction de : • Pr Njamnshi Alfred .K
• Pr Ngadjui Tchaleu Bonaventure
• Pr Seke Etet Paul .F

Concernant le projet de recherche intitulé : **Studies on the impact of diet and menopause on the course of cerebral toxoplasmosis and therapeutic potential of *Garcinia Kola* (Clusiaceae)**

Les principales observations sont les suivantes

Evaluation scientifique	
Evaluation de la convenance Institutionnelle/valeur sociale	
Equilibre des risques et des bénéfices	
Respect du consentement libre et déclaré	
Respect de la vie privée et des renseignements personnels (confidentialité) :	
Respect de la justice dans le choix des sujets	
Respect des personnes vulnérables :	
Réduction des inconvénients/optimalisation des avantages	
Gestion des compensations financières des sujets	
Gestion des conflits d'intérêt impliquant le chercheur	

Pour toutes ces raisons, le CIER émet un avis favorable sous réserve des modifications recommandées dans la grille d'évaluation scientifique.

L'équipe de recherche est responsable du respect du protocole approuvé et ne devra pas y apporter d'amendement sans avis favorable du CIER. Elle devra collaborer avec le CIER lorsque nécessaire, pour le suivi de la mise en œuvre dudit protocole. La clairance éthique peut être retirée en cas de non-respect de la réglementation ou des recommandations sus évoquées.

En foi de quoi la présente clairance éthique est délivrée pour servir et faire valoir que de droit

